



Experimental and Numerical Modelling of Vortex-Induced and Wake-Induced Vibrations of Clusters of Subsea Cylindrical Structures

Bruno Henriques Soares

A thesis submitted for the degree of
Doctor of Philosophy

February, 2023

School of Engineering
Faculty of Science, Agriculture and Engineering
Newcastle University

ABSTRACT

The Fluid-Structure Interaction phenomenon of Wake-Induced Vibrations (WIV) of groups of cylinders is studied herein. This is particularly a problem for subsea pipelines, riser systems, and other structures that may be installed in clusters. Currently, a realistic and computationally efficient model to predict WIV is lacking and, therefore, the present research focuses on the analytical and experimental modelling of Vortex-Induced Vibrations (VIV) and WIV.

Modelling of the wake flow deficit through classical boundary layer theory permits the derivation of steady wake-induced hydrodynamic forces and a computationally efficient modelling framework is introduced based on the wake oscillator concept. The model is validated with experimental results from the literature as well as experimental measurements conducted in the Wind, Wave and Current Tank at Newcastle University, for a pair of identical cylinders in the co-shedding regime, with low mass and damping ratios, and immersed in water. The experimental cylinders were attached to pendulum systems and supported by linear extension springs. Configurations tested included tandem and staggered cylinders, with a stationary or oscillating front cylinder, for a wide range of streamwise and transverse spacings.

Both the model and experimental outputs illustrate the main features of WIV that are well known from literature. Nonetheless, novelties of the work include: the proposal of an analytical model for WIV of tandem and staggered cylinder couples based on a higher order hydrodynamic force theory; derivation of the nonlinear wake stiffness concept; mapping of the response of the downstream cylinder with respect to the mechanisms of VIV and WIV for a given reduced velocity and spacing; providing measurements for the wake flow behaviour and cylinder response after a static or freely vibrating upstream cylinder; investigation of the critical effect of the mean drag force on WIV; and the effect of the inline degree-of-freedom for tandem and staggered cylinders.

The response of the downstream cylinder has been shown to be independent of the variation of d for the reduced velocity regime known as the first VIV regime; in the present study this is approximately $U_r \leq 5$, i.e. the second cylinder behaves as a single cylinder undergoing VIV. This is one of the main features of this study and has been observed for all configurations and systems tested, whether these are for a 1DOF or 2DOF, fixed-free or free-free, tandem or staggered arrangement and from experimental or numerical results. For $U_r > 5$, investigation of time series, amplitudes of vibration and oscillation frequencies led to the conclusion that, depending on d , the

second cylinder could behave within three regimes: WIV, classical VIV or a transition from WIV to VIV.

Three distinct oscillation frequency branches have been observed in the 1DOF response of the second cylinder. These are associated with three different concepts: the first cylinder vortex shedding frequency through the free-stream Strouhal law; the wake stiffness equivalent natural frequencies [12]; a wake-reduced vortex shedding frequency based on the Strouhal law which is computed using the steady wake flow velocity. They have been correlated to the mechanisms of VIV of the upstream cylinder, WIV and VIV of the downstream cylinder respectively. However, these frequency branches, although still observed, are less evident when the cylinders are also allowed to vibrate in the inline direction, as for the 2DOF numerical or experimental results.

ACKNOWLEDGEMENTS

This PhD thesis is the result of more than 4 years of total dedication. To whoever finds interest in this topic and interest in reading this piece of work, I believe you are getting to know me too as a person in some sense as this has populated my thoughts from the moment I was awake to the moment I went to sleep and at several occasions during my sleep as well.

I dedicate and thank especially my wife, Danielle Medeiros da Silva Soares, as her name should be in the title page besides mine. She has sacrificed herself as much as I have in order for us to accomplish our aim and yet she is not awarded a degree for it. Her support was emotional; financial, with her work in retail, even though she is a graduated engineer with work experience in two of the most respected companies in our mother country; and physical since she has taken care of home and personal duties for me whilst I was fixed to the computer working.

To my son, Noah, Snow and their brother(s) or sister(s), this work is for you. Not a single one of the 76310 words has been added to this thesis without your future best interests in mind. This will hopefully be more evident when you are old enough to read this. Daddy will now have a lot more time to play with you.

I thank my father, Fernando, my mother, Fatima, my sister, Gabriela, and my uncle, Antonio Soares for their love and their contribution to this work. None of this would have even started without you.

I also would like to publicly thank my supervisor Rose Norman, who has supported and guided me in completing this thesis during the time that mattered the most to me.

I would like to express my gratitude to have studied at Newcastle University. I am grateful for people I have met there and for the University for the studentship which has led to this work and publications, I hope it contributes to elevate the name of the university and city as I will always do in my trajectory. If there is one thing that I have learned from the PhD is to be resilient and I am only starting.

Special thanks go to my colleagues at Subsea 7 for the opportunity and trust placed on me even before graduating from this PhD.

I thank the few but essential friendships that have endured this PhD with me. In special I would like to thank Daniel Gama, Lucas Aguiar, Alessandro, Alexander, Markus Murray, Bruno, Alan, and Brenda.

During these 4+ years I have lost my grandparents, Ely, Daniel, Antonio, and Floripes, whilst being away from them and I also dedicate this work to my grandmother, Odete. I hope your love and our moments together stay forever in my memory.

"It is not joy that makes us grateful; it is gratitude that makes us joyful." – David Steindl-Rast.

TABLE OF CONTENTS

Chapter 1. INTRODUCTION	1
1.1. Fundamental Definitions	2
1.2. Literature Review	4
1.3. Motivation	13
1.4. Aim and Objectives of the Study	14
1.5. Novelty of the Work.....	16
1.6. Thesis Structure.....	18
Chapter 2. ANALYTICAL MODELLING OF COMBINED WIV AND VIV – 1 DEGREE- OF-FREEDOM	19
2.1. Combined VIV and WIV Modelling Assumptions	19
2.2. Wake flow modelling	21
2.3. VIV modelling and definition of the model.....	26
2.4. Calibration of Model Input Parameters.....	28
2.4.1. Calibration of 2 nd Order Wake Profile Parameters.....	29
2.4.2. Calibration of Wake Oscillator Parameters.....	35
2.5. Dynamic Response of the Downstream Cylinder.....	37
2.5.1. 1DOF WIV Amplitudes of Vibrations	38
2.5.2. Temporal Behaviour of the Downstream Cylinder	43
2.5.3. Modelling of the Wake Stiffness Concept.....	50
2.5.4. WIV Oscillation Frequencies of the Downstream Cylinder	55
2.5.5. Chapter Summary	65
Chapter 3. ANALYTICAL MODELLING OF COMBINED WIV AND VIV – 2 DEGREES OF FREEDOM.....	68
3.1. Calibration of Inline Direction Model Input Parameters	73
3.1.1. Calibration of Parameters Related to the Upstream Cylinder	74
3.1.2. Calibration of Geometric Nonlinearities	75

3.1.3. Wake Flow Parameters and Hydrodynamic Coefficients	80
3.1.4. Wake Oscillator Parameters Associated with the Downstream Cylinder .	82
3.2. Validation of Oscillation Amplitudes and Study of Dependence on Mass Ratio	87
3.3. Parametric Investigation and Discussion.....	92
3.4. Chapter Summary	105
Chapter 4. EXPERIMENTAL SETUP AND SINGLE CYLINDER TESTS	109
4.1. Wind, Wave and Current Tank	109
4.2. Experimental Rig and Pendulum System	110
4.3. Cylinder-Springs Connection Planning.....	111
4.4. WWCT Current Flow Measurements.....	113
4.5. Free Decay Tests and Spring Selection	117
4.6. Wake Deficit Flow Profile Measurements.....	119
4.7. Single Cylinder Vortex-Induced Vibrations	126
4.8. Chapter Summary	145
Chapter 5. COMBINED VIV AND WIV OF A PAIR OF CYLINDERS FOR A STATIONARY UPSTREAM CYLINDER (“FIXED-FREE” CASE)	146
5.1. Fixed-Free Experimental Setup Details.....	147
5.2. “Fixed-Free” WIV amplitudes of vibrations	148
5.3. Tandem cylinders.....	150
5.3.1. Time Series of the Displacements of the Downstream Cylinder	157
5.3.2. Plane Oscillation Trajectories of the Fixed-Free Second Cylinder	161
5.3.3. Oscillation Frequencies of a Fixed-Free Downstream Cylinder	165
5.4. Staggered cylinders.....	170
5.4.1. Amplitudes of Vibrations of the Downstream Cylinder	171
5.5. Displacement Time Series and Oscillation Trajectories	175
5.5.1. Dominant Oscillation Frequencies	184
5.6. Chapter Summary	186

Chapter 6. COMBINED VIV AND WIV OF A PAIR OF CYLINDERS FOR A DYNAMIC UPSTREAM CYLINDER (“FREE-FREE” CASE)	189
6.1. Tandem Cylinders.....	190
6.1.1. Free-Free Tandem Downstream Cylinder Amplitudes of Vibration	190
6.1.2. Free-Free Tandem Downstream Cylinder Time Series and Oscillation Trajectories	192
6.1.3. Frequencies of Oscillations of the Downstream Free-Free Tandem Cylinder	198
6.2. Staggered Cylinders	201
6.2.1. Amplitudes of Vibration of the Downstream Cylinder	202
6.2.2. Time Series of Displacements and Oscillation Trajectories.....	206
6.2.3. Dominant Frequencies of Oscillations	213
6.3. Validation of 2DOF Model with Experiments.....	214
6.4. Chapter Summary.....	217
Chapter 7. CONCLUSIONS AND RECOMMENDATIONS FOR FURTHER WORK	220
7.1. Conclusions and Contribution of the Work.....	220
REFERENCES.....	224

LIST OF FIGURES

Figure 1-1: Definition of double cylinders configurations and distances. (a) Tandem cylinders; (b) Staggered cylinders.....	3
Figure 2-1: Model of upstream and downstream tandem cylinders in a uniform free stream flow and a non-uniform wake flow, respectively.....	21
Figure 2-2: Schematic diagrams of relative flow-structure velocity vectors and associated hydrodynamic force components of upstream and downstream tandem cylinders.....	26
Figure 2-3: Comparison of numerical and experimental results of Saint-Marcoux & Blevins [43] for normalised velocity profiles across the wake behind upstream stationary and dynamic cylinders at $Re = 10^5$ for (a) $d = 4$, (b) $d = 6$, (c) $d = 12$ and (d) $d = 24$, and the associated (e) first- and (f) second-order solutions for a wake behind the oscillating cylinder with variable d	32
Figure 2-4: Comparison of numerical and experimental results for the mean wake-induced inline and transverse force coefficients across the wake behind the upstream stationary cylinder: (a, b) $d = 4$ at $Re = 19200$, (c, d) $d = 10.1$ at $Re = 22400$, and (e, f) $d = 20.2$ at $Re = 22400$	33
Figure 2-5: Comparison of normalised wake velocity profiles and wake-induced inline and crossflow force coefficients across and along the wake behind the upstream stationary (a, c, e) versus oscillating (b, d, f) cylinders with variable spacing ratio d	34
Figure 2-6: Variation of empirical wake-deficit oscillator variable (a) as a function of U_r or d , and (b) as a function of combined U_r and d	37
Figure 2-7: Comparison of response amplitude of vibrations of the downstream cylinder with varying U_r and d : (a) numerical and experimental results in fixed-free tandem cases, (b) numerical results in fixed-free vs. free-free tandem cases, with experimental results in free-free tandem and single cylinder cases.....	42
Figure 2-8: Study of the effect of mass ratio on the modelled response of the downstream cylinder and dependency on the spacing between the cylinders with $\zeta = 0.7\%$ for fixed-free (a, c, e) versus free-free (b, d, f) tandem cases: (a, b) $d = 4$, (c, d) $d = 8$ and (e, f) $d = 20$	43
Figure 2-9: Time histories of wake oscillator variables (q_1, q_2), wake deficit function (χ), wake-induced transverse force coefficient (C_{L12}) and cylinder responses (y_1, y_2) for three specified $U_r = 5, 6$ and 15 : red (black) line denotes free-free (fixed-free) tandem case with $d = 4$	45

Figure 2-10: Time histories dependency on the variation of initial spacing for two oscillating cylinders at $U_r = 6$. (a) δy . (b) χ . (c) C_{L12} . (d) y_2	48
Figure 2-11: Time histories dependency on the variation of initial spacing for two oscillating cylinders at $U_r = 10$. (a) δy . (b) χ . (c) C_{L12} . (d) y_2	49
Figure 2-12: Variation of ΔC_{L12} across the wake for fixed–free and free–free tandem cylinders with (a) $d = 4$, (b) $d = 6$, (c) $d = 8$ and (d) $d = 20$, and <i>rms</i> values of time-varying ΔC_{L12} in (e) fixed–free and (f) free–free tandem cases at specific U_r	54
Figure 2-13: Variation of dimensionless dominant frequencies of downstream cylinder responses with U_r (Re) for the fixed–free and free–free tandem cases with $d = 4$ and $d = 6$, in comparison with experimental results in fixed–free tandem cases.	55
Figure 2-14: Normalised response frequency components associated with wake oscillator variables (q_1, q_2), wake deficit variable (χ), wake-induced transverse force coefficient (C_{L12}) and transverse cylinder responses (y_1, y_2) with varying $U_r \geq 5$ in the free–free tandem case with $d = 4$	58
Figure 2-15: Variation of the dominant frequencies of crossflow oscillations of the downstream cylinder with the reduced velocity. Comparison of numerical results and experimental data for fixed-free cases. (a) $d = 4$. (b) $d = 5$. (c) $d = 6$. (d) $d = 8$. (e) $d = 10$. (f) $d = 20$	59
Figure 2-16: Numerical-experimental comparison of response amplitudes and frequencies of upstream and downstream cylinders in free–free tandem cases with $m^* = 1.343$ and $\zeta = 0.02$: (a) A_1/D , (b) A_2/D , (c) f_1/f_n , (d) f_2/f_n . A dashed line in (c) and (d) represents the $St = 0.2$ line. “Model” refers to present study in legends.	60
Figure 3-1: System sketch of a 2DOF pair of two tandem cylinders and unscaled diagram of forces exerted upon the respective cylinders.	69
Figure 3-2: Plane idealisation of the wake flow behind a cylinder. Unscaled schematic of the wake deficit, wake-induced drag and lift coefficient profiles across the wake..	69
Figure 3-3: <i>rms</i> amplitudes of vibrations of the upstream cylinder against variation of U_r . (a) displacements in the streamwise direction; (b) displacements in the crossflow direction.....	75
Figure 3-4: Dependency of amplitudes of vibrations against U_r on the geometric nonlinear parameter, α_{x2} . (a) A_{x2}/D for $d = 4$; (b) A_{y2}/D for $d = 4$; (c) A_{x2}/D for $d = 8$; (d) A_{y2}/D for $d = 8$; (e) A_{x2}/D for $d = 20$; (f) A_{y2}/D for $d = 20$	77

Figure 3-5: Dependency of amplitudes of vibrations against U_r on the geometric nonlinear parameter, α_{y2} . (a) A_{x2}/D for $d = 4$; (b) A_{y2}/D for $d = 4$; (c) A_{x2}/D for $d = 8$; (d) A_{y2}/D for $d = 8$; (e) A_{x2}/D for $d = 20$; (f) A_{y2}/D for $d = 20$ 78

Figure 3-6: Dependency of amplitudes of vibrations against U_r on the geometric nonlinear parameter, β_{x2} . (a) A_{x2}/D for $d = 4$; (b) A_{y2}/D for $d = 4$; (c) A_{x2}/D for $d = 8$; (d) A_{y2}/D for $d = 8$; (e) A_{x2}/D for $d = 20$; (f) A_{y2}/D for $d = 20$ 79

Figure 3-7: Dependency of amplitudes of vibrations against U_r on the geometric nonlinear parameter, β_{y2} . (a) A_{x2}/D for $d = 4$; (b) A_{y2}/D for $d = 4$; (c) A_{x2}/D for $d = 8$; (d) A_{y2}/D for $d = 8$; (e) A_{x2}/D for $d = 20$; (f) A_{y2}/D for $d = 20$ 80

Figure 3-8: Parametric study of the reference force coefficients and Strouhal numbers on the oscillation amplitudes of downstream cylinder against U_r in the inline direction for $d = 4$ 83

Figure 3-9: Parametric study of the reference force coefficients and Strouhal numbers on the oscillation amplitudes of downstream cylinder against U_r in the crossflow direction for $d = 4$ 84

Figure 3-10: Simplified flowchart of the optimisation algorithm based on the derivative-free unidimensional Nelder-Mead simplex scheme for minimisation of errors between model results and experimental reference data for 2DOF amplitudes of vibrations of the downstream cylinder. 85

Figure 3-11: Variation of empirical wake-deficit oscillator coefficient, Λ_{y2} , (a) as a function of U_r or d , and (b) as a function of combined U_r and d 86

Figure 3-12: Inline and crossflow *rms* oscillation amplitudes dependency on U_r for the downstream cylinder of a tandem pair of identical cylinders at different initial spacings with $m^* = 2.36$, and $\zeta = 1.55\%$. (a) A_{x2}/D for $d = 4$; (b) A_{y2}/D for $d = 4$; (c) A_{x2}/D for $d = 8$; (d) A_{y2}/D for $d = 8$; (e) A_{x2}/D for $d = 15$; (f) A_{y2}/D for $d = 15$; (g) A_{x2}/D for $d = 20$; (h) A_{y2}/D for $d = 20$ 89

Figure 3-13: Parametric study of variation of mass ratio on the amplitudes of vibrations of the downstream cylinder of the identical pair of tandem cylinders for different initial spacings. (a) A_{x2}/D for $d = 4$; (b) A_{y2}/D for $d = 4$; (c) A_{x2}/D for $d = 8$; (d) A_{y2}/D for $d = 8$; (e) A_{x2}/D for $d = 20$; (f) A_{y2}/D for $d = 20$ 91

Figure 3-14: Time series of inline response of the cylinders, inline wake variable and wake-induced drag for $d = 4$. First column: $U_r = 5$, second column: $U_r = 6$, and third column: $U_r = 15$ 93

Figure 3-15: Time series of transverse response of the cylinders, crossflow wake variable and wake-induced lift for $d = 4$. First column: $U_r = 5$, second column: $U_r = 6$, and third column: $U_r = 15$	94
Figure 3-16: Vibration trajectories of the upstream cylinder (first row) and downstream cylinder (remaining rows). First column: $U_r = 5$, second column: $U_r = 10$, third column: $U_r = 15$, and fourth column: $U_r = 20$	96
Figure 3-17: Variation of frequencies of oscillations of the pair of cylinders and wake-induced forces with U_r for $d = 4$. Legend: -- St law; -- χ St rule; -- 2St rule; -- 2χ St rule; • Model results; ■ Pereira <i>et al.</i> [24]; ▲ Armin <i>et al.</i> [25]; ◆ Jauvtis & Williamson [15]; • Assi [23].	99
Figure 3-18: Variation of frequencies of oscillations of the pair of cylinders and wake-induced forces with U_r for $d = 8$. Legend: -- St law; -- χ St rule; -- 2St rule; -- 2χ St rule; • Model results; ▲ Armin <i>et al.</i> [25].	103
Figure 3-19: Variation of frequencies of oscillations of the pair of cylinders and wake-induced forces with U_r for $d = 20$. Legend: -- St law; -- χ St rule; -- 2St rule; -- 2χ St rule; • Model results; ▲ Armin <i>et al.</i> [25].	104
Figure 4-1: Technical drawing of Newcastle University Wind, Water and Current tank: Isometric view (left-hand side); top view (middle); and rear view (right-hand side). Adapted from [68].	110
Figure 4-2: Attachment of pendulum systems to a beam over the Hydrodynamics Laboratory. View of the universal joints and mounting carriage system. Sliding carriage structure's greater length is aligned with the flow and WWCT tank. Photo taken at the single cylinder flow measurement phase with the downstream cylinder's carbon fibre tube in place.	111
Figure 4-3: Catalogue view of the (a) Bosch Rexroth grooved strut and (b) universal joint used for the cylinders' mounting systems.	111
Figure 4-4: Double frames system of the pair of cylinders (on centre). Flow direction is demarked. Downstream cylinder frame rests on top of the upstream cylinder frame. (a) CAD drawing courtesy of the Hydrodynamics Laboratory; (b) Photo of the downstream cylinder frame with spring corner mounting studs.	113
Figure 4-5: Nortek's Vectrino 3D acoustic velocimeter and mounting system. WWCT central tank current flow measurements at different depths.	115

Figure 4-6: WWCT current flow measurements at different depths. (a) varying impeller's power intensity from left to right, CPG = 5%, 10%, ..., 85%; (b) Mean value of flow velocities for the 4 depth points studied..... 116

Figure 4-7: Flume free stream velocity (m/s) depth variation (10, 25, 50, and 85 cm below water surface) at the upstream cylinder's position at $d = 4$ and CPG = 60%.116

Figure 4-8: Wake deficit measurements for the flow past an upstream static cylinder at $d = 10$. Orientation of the flow is from left to right. The two immersed components are: metal stationary cylinder (upstream) and Vectrino acoustic velocimeter (downstream)..... 121

Figure 4-9: Simplified diagram of wake flow velocity measurements behind a fixed or a 2DOF cylinder. Graphic Vectrino quantity and location of tests are merely a schematic representation and not accurate. 122

Figure 4-10: Comparison of wake flow velocity profiles behind a stationary cylinder. Legend: (a) — present study for $d = 4$ at $Re = 13500$; — Blevins [33] for $d = 4$ at $Re = 100000$; (b) — present study for $d = 10$ at $Re = 13500$; — Blevins [33] for $d = 12$ at $Re = 100000$; (c) — present study for $d = 20$ at $Re = 13500$; — Blevins [33] for $d = 24$ at $Re = 100000$ 125

Figure 4-11: Tank cross sectional wake flow velocity measurements. Flow profile after a 2DOF acrylic upstream cylinder at: (a) $d = 10$; and (b) $d = 20$. Legend: — : CPG = 55%, $U_\infty = 0.45$ m/s, $Re = 13500$; — : CPG = 50%, $U_\infty = 0.4$ m/s, $Re = 12000$; — : CPG = 40%, $U_\infty = 0.32$ m/s, $Re = 9600$; — : CPG = 30%, $U_\infty = 0.25$ m/s, $Re = 7500$; — : CPG = 20%, $U_\infty = 0.17$ m/s, $Re = 5100$; — : CPG = 10%, $U_\infty = 0.08$ m/s, $Re = 2400$ 125

Figure 4-12: Setup of VIV tests of a single cylinder. Upstream cylinder's equipment set, mounting system and location used. 127

Figure 4-13: Dependence of the amplitudes of vibrations of a single cylinder on the increasing (black dashed line) or decreasing (red dashed line) reduced velocity for $m^* = 3.75$ and $\zeta = 0.055$ (damping ratio in water). (a) Inline oscillations; (b) Crossflow oscillations. 129

Figure 4-14: Selected frame of a video recording showing the classical von Kármán alternate vortices (highlighted by red arrows) street for the 2S initial branch wake mode at $U_r = 5.5$ 131

Figure 4-15: Comparison of amplitudes of vibrations with literature studies in (a) inline direction; (b) crossflow direction. Legend: — — : Present 2DOF study for $m^* = 3.75$ and

$\zeta = 0.055$ (in water); : Pereira *et al.* [24] 2DOF study with $m^* = 2.92$ and $\zeta = 0.025$ (assumed in water); : Armin *et al.* [25] 2DOF study with $m^* = 2.36$ and $\zeta = 0.015$ (in water); : Jauvtis & Williamson [15] 2DOF study with $m^* = 6.9$ and $\zeta = 0.0015$ (assumed in air); : Assi *et al.* [11] 1DOF study with $m^* = 2.6$ and $\zeta = 0.007$ (in air); : Khalak & Williamson [74] 1DOF study with $m^* = 2.4$ and $\zeta = 0.0059$ (assumed in air)..... 132

Figure 4-16: Time evolution of displacements of the single cylinder in the streamwise direction (left-hand side column), and transverse direction (right-hand side column). $U_r = 3$: first row of subfigures; $U_r = 4$: second row of subfigures; $U_r = 6$: third row of subfigures; $U_r = 10$: fourth row of subfigures; $U_r = 15$: fifth row of subfigures; and $U_r = 20$: sixth row of subfigures..... 136

Figure 4-17: 2DOF trajectories of a single cylinder undergoing VIV for (a) $U_r = 3$; (b) $U_r = 4$; (a) $U_r = 6$; (a) $U_r = 10$; (a) $U_r = 15$; and (a) $U_r = 20$ 137

Figure 4-18: Dominant normalised frequencies of oscillations varying with the reduced velocity for the VIV of a single cylinder in a flume in the: (a) streamwise direction; (b) crossflow direction. Legend: : Strouhal law ($St = 0.2$); : Doubled Strouhal law ($2St = 0.4$); : Present 2DOF study for $m^* = 3.75$ and $\zeta = 0.055$ (in water); : Assi [23] $m^* = 1.6$ and $\zeta = 0.003$ (in air); and : Armin *et al.* [25] $m^* = 2.36$ and $\zeta = 0.015$ (in water)..... 142

Figure 5-1: Combined VIV and WIV tests of a 2DOF cylinder (on the right-hand side) downstream of a metallic cantilevered cylinder (on the left-hand side). The upstream metallic fixed cylinder is allowed to have its initial position varied along the tank length, increasing the tandem distance between the cylinders, whilst the downstream acrylic cylinder is moved transversally for staggered studies. 147

Figure 5-2: Dependence of normalised amplitudes of vibrations on the reduced velocity for a 2DOF downstream cylinder behind a static cylinder at initial spacing, $d = 4$. Caption: : increasing U_r ; : decreasing U_r 149

Figure 5-3: Dependence of normalised oscillation amplitudes of the downstream cylinder on the initial tandem spacing between the two cylinders for a fixed-free system in the (a) inline direction and (b) crossflow direction. Caption: : single cylinder; : $d = 4$; : $d = 6$; : $d = 8$; : $d = 10$; and : $d = 20$ 151

Figure 5-4: Comparison of normalised oscillation amplitudes of the downstream cylinder of fixed-free twin cylinders with reference literature studies. (a) A_{x2}/D at $d = 4$; (b) A_{y2}/D at $d = 4$; (c) A_{x2}/D at $d = 6$; (d) A_{y2}/D at $d = 6$; (e) A_{x2}/D at $d = 10$; (f) A_{y2}/D

at $d = 10$; (g) A_{x2}/D at $d = 20$; (h) A_{y2}/D at $d = 20$. Caption: \boxplus : Present results; \ominus : Assi *et al.* [11] with same d ; $\omin�$: Assi *et al.* [11] with $d_{\text{Assi}} = d + 2$; \triangle : Armin *et al.* [25]; \diamond : Pereira *et al.* [24]. 154

Figure 5-5: Temporal displacements of the downstream of a fixed-free pair of cylinders for $d = 4$. (a) x_2 at $U_r = 3$; (b) y_2 at $U_r = 3$; (c) x_2 at $U_r = 4$; (d) y_2 at $U_r = 4$; (e) x_2 at $U_r = 6$; (f) y_2 at $U_r = 6$; (g) x_2 at $U_r = 10$; (h) y_2 at $U_r = 10$; (i) x_2 at $U_r = 15$; (j) y_2 at $U_r = 15$; (k) x_2 at $U_r = 20$; and (l) y_2 at $U_r = 20$ 158

Figure 5-6: Temporal displacements of the downstream of a fixed-free pair of cylinders for $d = 10$. (a) x_2 at $U_r = 3$; (b) y_2 at $U_r = 3$; (c) x_2 at $U_r = 4$; (d) y_2 at $U_r = 4$; (e) x_2 at $U_r = 6$; (f) y_2 at $U_r = 6$; (g) x_2 at $U_r = 10$; (h) y_2 at $U_r = 10$; (i) x_2 at $U_r = 15$; (j) y_2 at $U_r = 15$; (k) x_2 at $U_r = 20$; and (l) y_2 at $U_r = 20$ 160

Figure 5-7: Temporal displacements of the downstream of a fixed-free pair of cylinders for $d = 20$. (a) x_2 at $U_r = 3$; (b) y_2 at $U_r = 3$; (c) x_2 at $U_r = 4$; (d) y_2 at $U_r = 4$; (e) x_2 at $U_r = 6$; (f) y_2 at $U_r = 6$; (g) x_2 at $U_r = 10$; (h) y_2 at $U_r = 10$; (i) x_2 at $U_r = 15$; (j) y_2 at $U_r = 15$; (k) x_2 at $U_r = 20$; and (l) y_2 at $U_r = 20$ 161

Figure 5-8: 2DOF trajectories of the downstream of a fixed-free twin bundle of cylinders undergoing WIV for $d = 4$. (a) $U_r = 3$; (b) $U_r = 4$; (c) $U_r = 6$; (d) $U_r = 10$; (e) $U_r = 15$; and (f) $U_r = 20$ 162

Figure 5-9: 2DOF trajectories of the downstream of a fixed-free twin bundle of cylinders undergoing WIV for $d = 10$. (a) $U_r = 3$; (b) $U_r = 4$; (c) $U_r = 6$; (d) $U_r = 10$; (e) $U_r = 15$; and (f) $U_r = 20$ 163

Figure 5-10: 2DOF trajectories of the downstream of a fixed-free twin bundle of cylinders undergoing WIV for $d = 20$. (a) $U_r = 3$; (b) $U_r = 4$; (c) $U_r = 6$; (d) $U_r = 10$; (e) $U_r = 15$; and (f) $U_r = 20$ 164

Figure 5-11: Initial tandem spacing dependence of the dominant normalised frequencies of oscillations for the WIV of the downstream of a pair of cylinders in a flume in the streamwise direction. Validation with reference literature studies. (a) Present results for all d ; (b) $d = 4$; (c) $d = 6$; (d) $d = 8$; (e) $d = 10$; (f) $d = 20$. Legend: $- -$: Strouhal law ($St = 0.2$); $- \cdot -$: Doubled Strouhal law ($2St = 0.4$); \circ : Present 2DOF study for $m^* = 3.75$ and $\zeta = 0.055$ (in water); \cdots : Present results for a single cylinder; \triangle : Assi [12] $m^* = 2.6$ and $\zeta = 0.007$ (in air); and \ominus : Armin *et al.* [25] $m^* = 2.36$ and $\zeta = 0.015$ (in water). 167

Figure 5-12: Initial tandem spacing dependence of the dominant normalised frequencies of oscillations for the WIV of the downstream of a pair of cylinders in a

flume in the crossflow direction. Validation with reference literature studies. (a) Present results for all d ; (b) $d = 4$; (c) $d = 6$; (d) $d = 8$; (e) $d = 10$; (f) $d = 20$. Legend: - - : Strouhal law ($St = 0.2$); - - : Doubled Strouhal law ($2St = 0.4$); \odot : Present 2DOF study for $m^* = 3.75$ and $\zeta = 0.055$ (in water); \cdots : Present results for a single cylinder; \triangle : Assi [12] $m^* = 2.6$ and $\zeta = 0.007$ (in air); and \circ : Armin *et al.* [25] $m^* = 2.36$ and $\zeta = 0.015$ (in water)..... 168

Figure 5-13: Photograph of staggered WIV tests for a flexibly mounted cylinder behind a stationary upstream cylinder..... 171

Figure 5-14: Dependence of normalised oscillation amplitudes of the downstream cylinder on the initial staggered spacing between the two cylinders for a fixed-free system with $d = 4$ in the (a) inline direction and (b) crossflow direction. Caption: - - : single cylinder; - - : tandem fixed-free cylinders at $d = 4$; \boxplus : $d = 4, T = 1$; \triangle : $d = 4, T = 2$; $*$: $d = 4, T = 3$; \ominus : $d = 4, T = 4$; and \diamond : $d = 20$ 172

Figure 5-15: Comparison of normalised oscillation amplitudes of the downstream cylinder of fixed-free staggered twin cylinders with reference literature studies. (a) A_{x2}/D at $d = 4, T = 1$; (b) A_{y2}/D at $d = 4, T = 1$; (c) A_{x2}/D at $d = 4, T = 2$; (d) A_{y2}/D at $d = 4, T = 2$; (e) A_{x2}/D at $d = 4, T = 3$; (f) A_{y2}/D at $d = 4, T = 3$. Caption: \boxplus : Present results; \triangle : Assi [23]; - - : Assi [23] tandem cylinders ($d = 4, T = 0$)..... 174

Figure 5-16: Dependence of normalised oscillation amplitudes of the downstream cylinder on the initial staggered spacing between the two cylinders for a fixed-free system with $d = 10$ in the (a) inline direction and (b) crossflow direction. Caption: - - : single cylinder; - - : tandem fixed-free cylinders at $d = 10$; \boxplus : $d = 10, T = 1$; \triangle : $d = 10, T = 2$; $*$: $d = 10, T = 3$ 175

Figure 5-17: Time series of displacements of the downstream of a fixed-free pair of cylinders for $d = 4, T = 1$. (a) x_2 at $U_r = 3$; (b) y_2 at $U_r = 3$; (c) x_2 at $U_r = 4$; (d) y_2 at $U_r = 4$; (e) x_2 at $U_r = 6$; (f) y_2 at $U_r = 6$; (g) x_2 at $U_r = 10$; (h) y_2 at $U_r = 10$; (i) x_2 at $U_r = 15$; (j) y_2 at $U_r = 15$; (k) x_2 at $U_r = 20$; and (l) y_2 at $U_r = 20$ 177

Figure 5-18: Time series of displacements of the downstream of a fixed-free pair of cylinders for $d = 4, T = 4$. (a) x_2 at $U_r = 3$; (b) y_2 at $U_r = 3$; (c) x_2 at $U_r = 4$; (d) y_2 at $U_r = 4$; (e) x_2 at $U_r = 6$; (f) y_2 at $U_r = 6$; (g) x_2 at $U_r = 10$; (h) y_2 at $U_r = 10$; (i) x_2 at $U_r = 15$; (j) y_2 at $U_r = 15$; (k) x_2 at $U_r = 20$; and (l) y_2 at $U_r = 20$ 178

Figure 5-19: Time series of displacements of the downstream of a fixed-free pair of cylinders for $d = 10, T = 1$. (a) x_2 at $U_r = 3$; (b) y_2 at $U_r = 3$; (c) x_2 at $U_r = 4$; (d) y_2 at U_r

= 4; (e) x_2 at $U_r = 6$; (f) y_2 at $U_r = 6$; (g) x_2 at $U_r = 10$; (h) y_2 at $U_r = 10$; (i) x_2 at $U_r = 15$; (j) y_2 at $U_r = 15$; (k) x_2 at $U_r = 20$; and (l) y_2 at $U_r = 20$ 179

Figure 5-20: 2DOF trajectories of the downstream of a fixed-free staggered twin bundle of cylinders undergoing WIV for $d = 4$, $T = 1$. (a) $U_r = 3$; (b) $U_r = 4$; (a) $U_r = 6$; (a) $U_r = 10$; (a) $U_r = 15$; and (a) $U_r = 20$ 181

Figure 5-21: 2DOF trajectories of the downstream of a fixed-free staggered twin bundle of cylinders undergoing WIV for $d = 4$, $T = 4$. (a) $U_r = 3$; (b) $U_r = 4$; (a) $U_r = 6$; (a) $U_r = 10$; (a) $U_r = 15$; and (a) $U_r = 20$ 183

Figure 5-22: 2DOF trajectories of the downstream of a fixed-free staggered twin bundle of cylinders undergoing WIV for $d = 10$, $T = 1$. (a) $U_r = 3$; (b) $U_r = 4$; (a) $U_r = 6$; (a) $U_r = 10$; (a) $U_r = 15$; and (a) $U_r = 20$ 184

Figure 5-23: Initial staggered spacing dependence of the dominant normalised frequencies of oscillations for the WIV of the downstream of a fixed-free pair of cylinders in a flume. Validation with reference literature studies. (a) Inline and (b) crossflow oscillation frequencies. Legend: - - : Strouhal law ($St = 0.2$); - - - : Doubled Strouhal law ($2St = 0.4$); Circles: Present 2DOF study for $m^* = 3.75$ and $\zeta = 0.055$ (in water) – blue: ($d = 4$, $T = 1$), black: ($d = 4$, $T = 2$), red: ($d = 4$, $T = 3$), green: ($d = 4$, $T = 4$), pink: ($d = 10$, $T = 1$), yellow: ($d = 10$, $T = 2$), cyan: ($d = 10$, $T = 3$); Triangles: Assi [23] $m^* = 1.6$ and $\zeta = 0.003$ (in air) – blue: ($d = 4$, $T = 1$), black: ($d = 4$, $T = 2$), red: ($d = 4$, $T = 3$)..... 185

Figure 6-1: Photograph of the free-free pair of tandem identical cylinders, frame and pendulum systems..... 189

Figure 6-2: Dependence of normalised oscillation amplitudes of the downstream cylinder on the initial tandem spacing between the two cylinders for a free-free system in the (a) inline direction and (b) crossflow direction. Caption: - - : single cylinder; free-free cylinders at \square : $d = 4$; \triangle : $d = 6$; $*$: $d = 8$; \ominus : $d = 10$; and \diamond : $d = 20$ 191

Figure 6-3: Time series of displacements of the downstream of a free-free pair of cylinders for $d = 4$. (a) x_2 at $U_r = 3$; (b) y_2 at $U_r = 3$; (c) x_2 at $U_r = 4$; (d) y_2 at $U_r = 4$; (e) x_2 at $U_r = 6$; (f) y_2 at $U_r = 6$; (g) x_2 at $U_r = 10$; (h) y_2 at $U_r = 10$; (i) x_2 at $U_r = 15$; (j) y_2 at $U_r = 15$; (k) x_2 at $U_r = 20$; and (l) y_2 at $U_r = 20$ 193

Figure 6-4: Time series of displacements of the downstream of a free-free pair of cylinders for $d = 10$. (a) x_2 at $U_r = 3$; (b) y_2 at $U_r = 3$; (c) x_2 at $U_r = 4$; (d) y_2 at $U_r = 4$;

(e) x_2 at $U_r = 6$; (f) y_2 at $U_r = 6$; (g) x_2 at $U_r = 10$; (h) y_2 at $U_r = 10$; (i) x_2 at $U_r = 15$; (j) y_2 at $U_r = 15$; (k) x_2 at $U_r = 20$; and (l) y_2 at $U_r = 20$	194
Figure 6-5: Time series of displacements of the downstream of a free-free pair of cylinders for $d = 20$. (a) x_2 at $U_r = 3$; (b) y_2 at $U_r = 3$; (c) x_2 at $U_r = 4$; (d) y_2 at $U_r = 4$; (e) x_2 at $U_r = 6$; (f) y_2 at $U_r = 6$; (g) x_2 at $U_r = 10$; (h) y_2 at $U_r = 10$; (i) x_2 at $U_r = 15$; (j) y_2 at $U_r = 15$; (k) x_2 at $U_r = 20$; and (l) y_2 at $U_r = 20$	195
Figure 6-6: 2DOF trajectories of the downstream of a free-free tandem twin bundle of cylinders undergoing WIV for $d = 4$. (a) $U_r = 3$; (b) $U_r = 4$; (a) $U_r = 6$; (a) $U_r = 10$; (a) $U_r = 15$; and (a) $U_r = 20$	196
Figure 6-7: 2DOF trajectories of the downstream of a free-free tandem twin bundle of cylinders undergoing WIV for $d = 10$. (a) $U_r = 3$; (b) $U_r = 4$; (a) $U_r = 6$; (a) $U_r = 10$; (a) $U_r = 15$; and (a) $U_r = 20$	197
Figure 6-8: 2DOF trajectories of the downstream of a free-free tandem twin bundle of cylinders undergoing WIV for $d = 20$. (a) $U_r = 3$; (b) $U_r = 4$; (a) $U_r = 6$; (a) $U_r = 10$; (a) $U_r = 15$; and (a) $U_r = 20$	198
Figure 6-9: Initial tandem spacing dependence of the dominant normalised frequencies of inline oscillations for the WIV of the downstream of a free-free pair of cylinders in a flume in the crossflow direction. Validation with reference literature studies. (a) Present results for all d ; (b) $d = 4$; (c) $d = 6$; (d) $d = 8$; (e) $d = 10$; (f) $d = 20$. Legend: - - : Strouhal law ($St = 0.2$); - - : Doubled Strouhal law ($2St = 0.4$); \circ : Present 2DOF study for $m^* = 3.75$ and $\zeta = 0.055$ (in water); \circ : Armin <i>et al.</i> [25] $m^* = 2.36$ and $\zeta = 0.015$ (in water); and Δ : Pereira <i>et al.</i> [24] 2DOF study with $m^* = 2.92$ and $\zeta = 0.025$ (assumed in water).	199
Figure 6-10: Initial tandem spacing dependence of the dominant normalised frequencies of transverse oscillations for the WIV of the downstream of a free-free pair of cylinders in a flume in the crossflow direction. Validation with reference literature studies. (a) Present results for all d ; (b) $d = 4$; (c) $d = 6$; (d) $d = 8$; (e) $d = 10$; (f) $d = 20$. Legend: - - : Strouhal law ($St = 0.2$); - - : Doubled Strouhal law ($2St = 0.4$); \circ : Present 2DOF study for $m^* = 3.75$ and $\zeta = 0.055$ (in water); \circ : Armin <i>et al.</i> [25] $m^* = 2.36$ and $\zeta = 0.015$ (in water); and Δ : Pereira <i>et al.</i> [24] 2DOF study with $m^* = 2.92$ and $\zeta = 0.025$ (assumed in water).	201
Figure 6-11: Photograph of the free-free pair of staggered identical cylinders, frame and pendulum systems.	202

Figure 6-12: Dependence of normalised oscillation amplitudes of the downstream cylinder on the initial staggered spacing between the two cylinders for a free-free system in the (a) inline direction and (b) crossflow direction. Caption: — —: single cylinder; free-free cylinders at \square : $d = 8, T = 1$; \triangle : $d = 8, T = 2$; and $*$: $d = 8, T = 3$. 204

Figure 6-13: Dependence of normalised oscillation amplitudes of the downstream cylinder on the initial staggered spacing between the two cylinders for a free-free system in the (a) inline direction and (b) crossflow direction. Caption: — —: single cylinder; free-free cylinders at \square : $d = 4, T = 1$; \triangle : $d = 8, T = 2$; $*$: $d = 12, T = 3$, and \oplus : $d = 16, T = 4$ 205

Figure 6-14: Time series of displacements of the downstream of a free-free pair of cylinders for $d = 4, T = 1$. (a) x_2 at $U_r = 3$; (b) y_2 at $U_r = 3$; (c) x_2 at $U_r = 4$; (d) y_2 at $U_r = 4$; (e) x_2 at $U_r = 6$; (f) y_2 at $U_r = 6$; (g) x_2 at $U_r = 10$; (h) y_2 at $U_r = 10$; (i) x_2 at $U_r = 15$; (j) y_2 at $U_r = 15$; (k) x_2 at $U_r = 20$; and (l) y_2 at $U_r = 20$ 207

Figure 6-15: Time series of displacements of the downstream of a free-free pair of cylinders for $d = 8, T = 2$. (a) x_2 at $U_r = 3$; (b) y_2 at $U_r = 3$; (c) x_2 at $U_r = 4$; (d) y_2 at $U_r = 4$; (e) x_2 at $U_r = 6$; (f) y_2 at $U_r = 6$; (g) x_2 at $U_r = 10$; (h) y_2 at $U_r = 10$; (i) x_2 at $U_r = 15$; (j) y_2 at $U_r = 15$; (k) x_2 at $U_r = 20$; and (l) y_2 at $U_r = 20$ 208

Figure 6-16: Time series of displacements of the downstream of a free-free pair of cylinders for $d = 12, T = 3$. (a) x_2 at $U_r = 3$; (b) y_2 at $U_r = 3$; (c) x_2 at $U_r = 4$; (d) y_2 at $U_r = 4$; (e) x_2 at $U_r = 6$; (f) y_2 at $U_r = 6$; (g) x_2 at $U_r = 10$; (h) y_2 at $U_r = 10$; (i) x_2 at $U_r = 15$; (j) y_2 at $U_r = 15$; (k) x_2 at $U_r = 20$; and (l) y_2 at $U_r = 20$ 209

Figure 6-17: 2DOF trajectories of the downstream of a free-free staggered twin bundle of cylinders undergoing WIV for $d = 4, T = 1$. (a) $U_r = 3$; (b) $U_r = 4$; (a) $U_r = 6$; (a) $U_r = 10$; (a) $U_r = 15$; and (a) $U_r = 20$ 211

Figure 6-18: 2DOF trajectories of the downstream of a free-free staggered twin bundle of cylinders undergoing WIV for $d = 8, T = 2$. (a) $U_r = 3$; (b) $U_r = 4$; (a) $U_r = 6$; (a) $U_r = 10$; (a) $U_r = 15$; and (a) $U_r = 20$ 212

Figure 6-19: 2DOF trajectories of the downstream of a free-free staggered twin bundle of cylinders undergoing WIV for $d = 12, T = 3$. (a) $U_r = 3$; (b) $U_r = 4$; (a) $U_r = 6$; (a) $U_r = 10$; (a) $U_r = 15$; and (a) $U_r = 20$ 213

Figure 6-20: Initial staggered spacing dependence of the dominant normalised frequencies of oscillations for the WIV of the downstream of a free-free pair of cylinders in a flume in the crossflow direction. (a) Inline direction; (b) Crossflow direction. Legend: — —: Strouhal law ($St = 0.2$); — —: Doubled Strouhal law ($2St =$

0.4); \circ : $d = 4V$, $T = 1$; \circ : Armin *et al.* [25] $m^* = 2.36$ and $\zeta = 0.015$ (in water); and Δ : Pereira *et al.* [24] 2DOF study with $m^* = 2.92$ and $\zeta = 0.025$ (assumed in water). ...214

Figure 7-1: Comparison of transverse oscillation amplitudes of a free-free downstream cylinder for tandem and staggered cases between numerical and experimental results. (a) Tandem cylinders and (b) staggered cylinders. Caption: symbols – experimental results; lines – numerical results. (a) blue – $d = 4$, yellow – $d = 6$; red – $d = 8$; pink – $d = 10$; green – $d = 20$; (b) blue – $d = 8$, $T = 1$, yellow – $d = 8$, $T = 2$; red – $d = 8$, $T = 3$; pink – $d = 4$, $T = 1$; green – $d = 12$, $T = 3$215

LIST OF TABLES

Table 1-1: Correlation of Thesis Chapters with objectives.	15
Table 2-1: Summary of Calibrated Wake Profile Parameters	35
Table 2-2: Summary of Calibrated Wake Oscillator Parameters.....	36
Table 4-1: Summary of free decay tests.	119
Table 4-2: Description of oscillating pendulum components and their individual masses contributing to the total oscillating mass, computation of equivalent mass of displaced fluid for an immersed length of 0.8 m of the acrylic cylinder and resulting system mass ratio.....	128

LIST OF PUBLICATIONS

Soares B, Srinil N. Modelling of wake-induced vibrations of tandem cylinders with a nonlinear wake-deficit oscillator. *Journal of Fluids and Structures*. 2021;105:103340.

Soares, B, and Srinil, N. "Capturing Wake Stiffness in Wake-Induced Vibration of Tandem Cylinders." *Proceedings of the ASME 2020 39th International Conference on Ocean, Offshore and Arctic Engineering*. Volume 6A: Ocean Engineering. Virtual, Online. August 3–7, 2020. V06AT06A011. ASME. <https://doi.org/10.1115/OMAE2020-18423>

Soares, B, and Srinil, N. "Nonlinear Wake-Induced Vibration of Downstream Cylinder in Staggered Arrangements." *Proceedings of the ASME 2021 International Mechanical Engineering Congress and Exposition*. Volume 7A: Dynamics, Vibration, and Control. Virtual, Online. November 1–5, 2021. V07AT07A032. ASME. <https://doi.org/10.1115/IMECE2021-67776>

NOMENCLATURE

c	Damping coefficient
d	Longitudinal initial spacing between the cylinders
g	Dimensionless function of lateral profile
k	Stiffness coefficient
$k_{Schlichting}$	Constant measured by Schlichting related to ε_τ
m	Cylinder mass
m^*	Mass ratio
m_a	Fluid added mass
p	Pressure
q	Wake variable transformation
s_1	First order or symmetric solution
s_2	Second order or antisymmetric solution
u, v	Components of free stream flow velocity
u_d, v_d	Components of the velocity deficit
u_2	Axial component of the wake-reduced velocity
C	Empirical quantity related to the drag measured in wake flow theory
C_a	Added mass coefficient
C_D	Sectional mean drag coefficient
C_{D0}	Reference drag coefficient based on free stream velocity
C_{D12}	Wake-induced drag coefficient
C_L	Lift coefficient
C_{L12}	Wake-induced lift coefficient
D	Cylinder external diameter
F_D	Drag force per length
F_L	Lift force per length
F_{L12}	Wake-induced lift force per length
$F_y (f_y)$	Dimensional (dimensionless) total force in the cross-flow direction

Re	Reynolds number
St	Strouhal number
T	Transverse initial spacing between the cylinders
U_r	Reduced velocity
\bar{U}	Relative velocity
U_∞	Free stream flow velocity
$X(x)$	Dimensional (dimensionless) inline displacement
$Y(y)$	Dimensional (dimensionless) cross-flow displacement
α	Coefficient of longitudinal decay of the velocity field
β	Antisymmetric solution coefficient
γ	Stall parameter
δ	Boundary layer thickness
ε, Λ	Empirical wake oscillator coefficients
ε_τ	Eddy viscosity
ζ	Damping ratio
η	Dimensionless similarity variable
λ	Coefficient of transverse decay of the velocity field
ν	Laminar kinematic viscosity
ρ_f	Fluid density
$\tau(t)$	Dimensional (dimensionless) time
χ	Wake deficit function
ω_f	Vortex shedding angular frequency
ω_n	Cylinder natural angular frequency

CHAPTER 1. INTRODUCTION

The vortex-induced vibration (VIV) phenomenon of an isolated circular cylinder has been comprehensively studied, especially since the 1960s/1970s [1, 2]. On the other hand, although there has been a recent increase of interest and popularity in the research community, one may notice that there are far fewer studies of flow around multiple circular structures. This is an industrially relevant topic due to the fact that several important structures are employed in groups, for instance in areas such as subsea engineering, mechanical engineering, Oil and Gas and innovative energy generation research.

The velocity of the disturbed wake flow behind a circular cylinder obeys a wake deficit law, while wake-induced drag and lift forces may excite the body leading to the wake induced vibration (WIV) phenomenon. Zdravkovich [3] proposed the following classification of the basic flow regime around two cylinders based on the relative position of the aft cylinder: proximity interference, wake interference, the combination of the two and no interference at all. For initially tandem cylinders with a minimum separation, the rear cylinder will be subject to wake interference. This means that the second cylinder is affected by the wake effects from the first cylinder, whereas the first cylinder behaves as a single cylinder subjected to VIV. A number of comprehensive reviews [3-5] are available for more information on flow interference and near wake flow structure.

Igarashi [6] has studied the flow patterns between tandem cylinders with the increase of the streamwise spacing. It was concluded that an increment of spacing, d , makes the cylinders turn from behaving as if they were a single elongated body, to developing a pair of stationary vortices in the gap between cylinders and finally to shedding their own wake of vortices, termed the co-shedding pattern. Moreover, below a critical spacing, complex phenomena take place and drag inversion may occur [7], i.e. the drag force becomes negative.

In contrast to the phenomenon of VIV of a single cylinder, a steady wake-induced lift force arises when the downstream cylinder oscillates away from the wake centreline. The origin of this counter-intuitive average lift force has been investigated and attributed to several sources including buoyancy due to static pressure gradient across the wake, difference in the separation points around the cylinder [8], resolved drag caused by entrainment of fluid into the wake [9] and circulation [10]. Price [10] reported that none of these hypotheses were able to fully describe the nature of the

wake-induced lift force, but rather a combination of them was most likely. More recently, Assi *et al.* [11] have shown that any description of the wake-induced force that disregards the interaction of the unsteady wake vortices is at least incomplete as they concluded the WIV mechanism is sustained by the unsteady vortex-structure interactions.

This means that the wake-induced lift force is observed to counteract the movement of the downstream cylinder as it vibrates transversely across the wake. It is always directed to the wake centreline and antisymmetric, increasing in magnitude with distance from the wake centreline up to the wake flow edges. Assi *et al.* [12] demonstrated, through their experiments for a downstream cylinder without springs, that this hydrodynamic force is capable of sustaining body oscillations even though no physical restraints (springs) were used to return the cylinder to the central position. They proposed that the C_{L12} profile across the wake behaved approximately linearly inside validity ranges. Hence, this linear behaviour that opposes the cylinder displacement was related to the role played by a spring in a dynamic system and termed the wake stiffness. An equivalent wake stiffness natural frequency was modelled and compared to their measurements. Frequency results showed that for their cylinder without springs, oscillation frequencies agreed with the wake stiffness concept, whereas vibration frequencies of the spring-mounted cylinder responded at higher frequencies but increased in the same proportion as the wake stiffness frequencies. The introduction of the wake stiffness mechanism has led to progress in the study and understanding of WIV dominant frequencies.

1.1. Fundamental Definitions

Some of the parameters and definitions that are extensively used throughout this Thesis are now defined in the following.

The reduced velocity depends on the free stream velocity, diameter of cylinder, and natural frequency of the system as follows:

$$U_r = \frac{U_\infty}{Df_n}$$

where, U_∞ is the free stream flow velocity, D is the cylinder diameter and f_n is the natural frequency of the system.

The mass ratio is defined as the ratio between the system total oscillating mass and the respective mass of displaced water:

$$m^* = \frac{m_t}{m_w}$$

The damping ratio is defined as the ratio between the system damping and the critical damping which can be derived as:

$$\zeta = \frac{c}{2m\omega_n}$$

The Strouhal number is a dimensionless quantity that describes the frequency of vortex shedding and may be defined as:

$$St = \frac{f_v D}{U_\infty}$$

where f_v is the vortex shedding frequency in Hertz.

The Reynolds number is the ratio between inertial and viscous forces in fluid dynamics and can be defined as follows:

$$Re = \frac{\rho U_\infty D}{\mu}$$

where ρ is the density of the fluid and μ is the dynamic viscosity of the fluid.

Moreover, when it comes to configurations between two cylindrical structures, the following fundamental quantities and definitions are introduced and are illustrated in Figure 1-1.

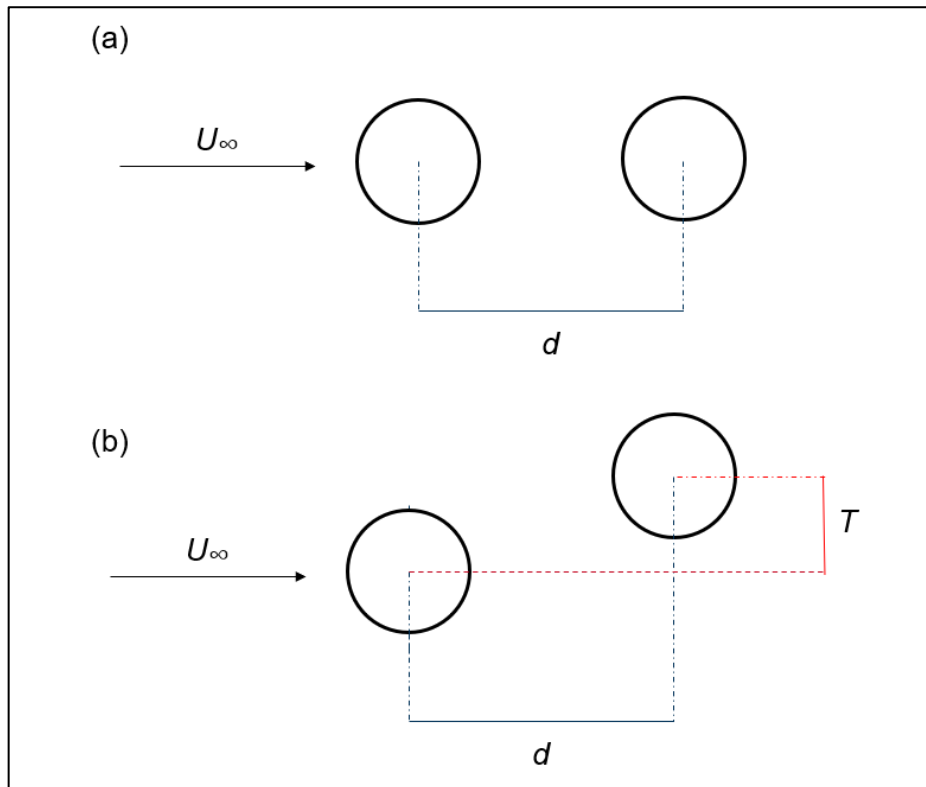


Figure 1-1: Definition of double cylinders configurations and distances. (a) Tandem cylinders; (b) Staggered cylinders.

The longitudinal spacing (d) is the centre-to-centre downstream distance between the cylinders normalised by a cylinder diameter, whilst the transverse spacing (T) is the centre-to-centre lateral offset between the cylinders normalised by a cylinder diameter.

Ultimately, a nomenclature definition that has been introduced and used throughout the present thesis is the fixed-free or free-free system. The fixed-free system is related to a system where the upstream cylinder is immobile and the downstream cylinder is allowed to vibrate. Whereas a free-free system means that both cylinders are free to move and oscillate.

1.2. Literature Review

For WIV studies focusing on the dynamic response of tandem cylinders under the co-shedding regime, selected experimental and CFD literature studies on the subject have been reviewed and are discussed in the following.

Brika and Laneville [13] performed experimental measurements in a wind tunnel for two flexible cylinders with separations equivalent to a range of 7 to 25 cylinder diameters. They concluded that the effects of the interaction from the downstream on the upstream cylinder were negligible within their studied spacing range when the coupling medium was fluid. Moreover, another interesting conclusion is that the downstream cylinder of the tandem pair could still experience WIV effects even for gap distances as far as $d = 25$, even though effects were reduced. However, their studied mass ratio was relatively high, hence yielding completely different responses from other studies.

Hover and Triantafyllou [14] studied the response of two rigid cylinders, where the first was stationary and the second one was integrated into a robotic force-feedback loop. This way, they were able to control the forces on the second cylinder and vary the natural frequency of the second cylinder to increase their reduced velocity at a constant Reynolds number (Re). The cylinders were $4.75 (d)$ diameters apart and had a low combined mass damping parameter, $m^* \zeta = 0.12$. The researchers observed rising oscillation amplitudes for the second cylinder even though the Reynolds number remained unchanged. However, their maximum reduced velocity was only what will be considered in the present study as an intermediate value. Assi *et al.* [12], through experiments with a similar force-feedback system, further analysed the effect of extending the reduced velocity range to larger values while keeping constant Reynolds numbers. Through this study, they showed that the oscillation amplitudes of the

downstream cylinder are dependent not on the reduced velocity but only on Re for the regime where WIV dominates.

So far, all of the reviewed studies focus on either fundamental aspects or on the transverse, one degree-of-freedom response of groups of tandem cylinders. However, the inclusion of an additional degree-of-freedom for the inline vibrations of the cylinders is more realistic in the sense of vibrations of real engineering structures. Moreover, it could prove to be interesting to analyse the problem of 2 degrees of freedom (DOF) WIV of cylinder clusters since there is evidence from studies of single cylinder systems under VIV that when the mass ratio is less than 6, a dramatic change occurs in the fluid-structure interaction [15]; hence, the inline freedom greatly affects the transverse responses [15]. Particularly for multiple cylinder systems, it has already been discussed that the spacing between cylinders has a large influence on the system response. This spacing between cylinders would, therefore, be dynamic over time for 2DOF systems, which highlights the importance of studying the 2DOF response of these systems.

Following this line of thought, Bao *et al.* [16] developed a CFD study of two rigid tandem cylinders, both free to vibrate in 2DOF and immersed in a constant flow. The study focused on a low $Re = 150$ which was fixed. Thus, the natural frequency of the cylinders was numerically varied for the proposed range of dimensionless reduced velocities of 3 - 12. Moreover, a parametric analysis of the ratio between natural frequencies in the inline and crossflow directions was conducted. The cylinders had low mass ratio, zero structural damping and a longitudinal spacing of 5 diameters measured from each of their centres.

Whilst the authors observed that the upstream cylinder orbit trajectories were similar to the case of an isolated cylinder, i.e., vibrating in figure-of-eight patterns; the downstream cylinder, on the other hand, would move more irregularly and occasionally asymmetrically due to the high disturbance and asymmetry in the upstream wake. For some reduced velocities and frequency ratios, the orbit of the downstream cylinder would undergo complex and presumably chaotic trajectories. In terms of maximum oscillation amplitudes, variation of the X - Y natural frequency ratios led to significant quantitative changes in the response of the first cylinder. This was true especially in the inline direction, for which the maximum amplitude was approximately five times higher for the case with a natural frequency in the inline direction twice the magnitude of the natural frequency in the transverse direction when compared to the identical

frequencies case. Furthermore, for the second cylinder the difference was not only quantitative but also qualitative. In general, when increasing the frequency ratio, the amplitude response would have fewer fluctuations. The effect of varying the natural frequency ratio for both cylinders has been shown to be greater for the cylinder response in the inline than in the crossflow directions. However, if the natural frequency ratio is assumed to have been varied through the means of modifying the natural frequency in the axial direction while controlling the orthogonal natural frequency variation to be the same in all the cases since it is associated with their reduced velocity definition; then, the relatively small difference in amplitudes of vibration for the transverse than in the inline direction could be justified.

The authors concluded that the combination of 2DOF leads to a dramatic change in the wake patterns behind the upstream cylinder, especially for the case of the natural frequency in the inline direction being twice the magnitude of the transverse direction. The oscillating drag component is the most sensitive to the variation in the natural frequency ratios, which is maximised when the inline-to-transverse natural frequency ratio is 2:1.

Yu *et al.* [17] also proposed a numerical investigation of the problem of 2DOF oscillations of two and three tandem cylinders. The governing incompressible flow equations have been described in an Arbitrary Lagrangian Eulerian (ALE) framework and computationally solved by a CFD routine. The pair of tandem cylinders were homogeneous and had similar properties to those of Bao *et al.* [16], namely zero structural damping, mass ratio of 1.27, spacing of five diameters, $Re = 150$ and - reduced velocity within a range of 2-13. Overall, their amplitude of vibration results precisely agree with the findings of Bao *et al.* [16] for the case of equal natural frequencies in both directions. Even though additional cylinders are out of context of the present study, it is interesting to highlight the conclusion of Yu *et al.* [17] that the 2DOF oscillations of three tandem cylinders are more complex than those of the tandem pair; therefore, a study of two cylinder systems should not be extrapolated to predict characteristics of systems of three cylinders.

Gao *et al.* [18] extended a similar analysis to Yu *et al.* [17] with the investigation of more centre-to-centre longitudinal spacings for three tandem cylinders including distances as close as two diameters. Within their range of studied spacings, they observed several wake flow regimes broadly associated with the single bluff body flow and co-shedding regimes. Nonetheless, the case of a tandem pair of cylinders was

used as a validation procedure for their CFD model and the spacing was limited to 5 diameters. The Reynolds number was fixed at 150 and reduced velocities of 3 - 13 were achieved through the variation of natural frequency of the cylinders. Similar mass ($m^* = 2$) and structural damping ($\zeta = 0$) ratios allowed them to compare their amplitudes of vibration and force coefficient results which coincided with the observations of Bao *et al.* [16] and Yu *et al.* [17].

Papaioannou *et al.* [19] presented a 2DOF CFD study for two tandem cylinders with three different separations of 2.5, 3.5 and 5 diameters. The Reynolds number was fixed at 160 and, therefore, the natural frequency of the identical cylinders was defined as the control parameter to vary the reduced velocity. The cylinders had a moderate mass ratio of 10 and structural damping ratio of 1%. For the spacing of 5 diameters, which is in context with the present study, the system behaves in the co-shedding flow regime which is to be defined in following sections, but mainly that means that the upstream cylinder responds similarly to a single cylinder under VIV. On the other hand, the response of the downstream cylinder is shifted towards higher values of reduced velocities and this shift is attributed to the wake-shielding effect. The authors commented that when increasing reduced velocities, higher oscillation amplitudes were observed in both inline and transverse directions. Particularly, its inline response presents two peaks at the low to intermediary reduced velocity range studied. The first peak was associated with the reduced velocity of maximum inline and transverse response of the upstream cylinder and the second peak was derived from the maximum transverse oscillation of the downstream cylinder. Furthermore, three oscillation frequency branches were mentioned; they are: the shedding frequency of the stationary tandem system, the shedding frequency of a single cylinder and the natural frequency of the system.

Prasanth and Mittal [20] conducted 2DOF CFD analysis of a similar system of a pair of tandem rigid cylinders. The cylinders were 5 diameters apart and whilst the mass ratio was 10 and they had no structural damping. The Reynolds number was fixed at 100 and reduced velocities ranged between 2 and 15 through the variation of natural frequency of the identical cylinders. As in other studies, it was found that the downstream cylinder experienced much larger oscillation amplitudes in both transverse and streamwise directions than the upstream cylinder. Moreover, perhaps owing to the zero structural damping, the response of the second cylinder was characterised by many peaks and fluctuations of amplitude with variation of reduced

velocity, which had not been observed in similar studies. However, the results conformed to other low Reynolds number studies in the sense that the maximum amplitudes of vibration were observed at intermediary reduced velocities, not too far from where the maximum amplitudes of VIV of a single cylinder normally occur; and in both directions an increase of reduced velocity lead to a decrease in oscillation amplitudes. From comparison of these and previous results, the authors concluded that the Reynolds number plays a pivotal role in the occurrence of WIV behaviour, where the response of the downstream cylinder gradually increases up to the highest reduced velocities.

The so-called WIV amplitude build-up (once called galloping [21] although there has been recent controversy around the use of this term [11]) is a response where the oscillation amplitudes of the downstream cylinder gradually increase up to the highest reduced velocities but this is absent in all the CFD studies reviewed. As mentioned by Prasanth and Mittal [20], this is due to the low Reynolds numbers of such studies. Another possible reason is that all of these studies have in common that the natural frequency is varied to excite the system of cylinders through a range of reduced velocities at a fixed flow velocity and Re . Singh and Mittal [22] demonstrated that, for the behaviour of a single cylinder, the variation of natural frequency and consequently reduced velocity at a constant Re would have no particular distinction from the contrary case where the reduced velocity is fixed whilst the Reynolds number is varied within low ranges. However, the effect of variation of natural frequency against Reynolds number is thought to influence WIV and systems with additional cylinders differently. This is because, whereas the natural frequency variation at a constant flow velocity and Re acts on one side of the equation of movement by softening or hardening the system stiffness and restoration forces, the flow velocity or, more accurately, the Reynolds number directly influences the excitation forces on the other side of the equation. For an isolated cylinder, this relative balance might make no significant difference, whilst for WIV, it may be expected that the effect of the Reynolds number alters the wake properties, such as wake deficit, width and induced hydrodynamic forces which are not relevant for a single cylinder.

Moving away from the reduced velocity and limited low Reynolds numbers of CFD studies, the review of literature experimental studies is now addressed. Assi [23] investigated the WIV of tandem and staggered cylinders experimentally, where the upstream was fixed and the downstream cylinder was elastically mounted and allowed

to vibrate in 2DOF. The second cylinder was initially located 4 diameters from the first cylinder in the streamwise direction, whereas the lateral separation could vary between 0 and 3 diameters. The Reynolds number varied from 2000 to 25000 and reduced velocities extended from approximately 1 to 12. The mass ratio of the cylinders was 1.6 and the structural damping ratio was 0.3% of the critical damping. In an attempt to maximise the response of the rear cylinder, the stiffness of the system was tuned so that the inline-to-transverse natural frequency ratio was equal to 1.9. The results showed that a WIV excitation dominant response, characterised by a gradual increase of oscillation amplitudes with increments of U_r , was observed for both streamwise and crossflow responses, especially for the tandem case, but also for the staggered cases except the one with lateral separation of 3 diameters. Indeed, it was thought that under these system conditions, when the downstream cylinder was positioned 3 diameters across the tank, it escaped the upstream wake interference zone, missing most of its direct interaction and consequently mitigating WIV. The outcome is a behaviour that closely resembles the response of an isolated cylinder, in other words, a classical VIV response. Moreover, evidence of a mechanism of wake stiffness, as defined by Assi *et al.* [12] for 1DOF, was found to occur for their tandem case and at smaller proportions for the staggered case closest to the wake centreline.

Pereira *et al.* [24] conducted towing tank experiments with two rigid tandem cylinders that were free to oscillate in 2DOF. Different centre-to-centre distances between the cylinders were tested, from 3 to 7 diameters. The reduced velocities ranged from 3 to 13 at a Reynolds number from 3000 to 30000. The structural damping ratio was 2.5%, mass ratio of the cylinders was 2.95 for the inline direction and 2.52 for the transverse dynamics, whilst the streamwise to crossflow natural frequency ratio was approximately 1.5. Emphasizing other literature evidence, they found that for all cases comprising $d \geq 3.5$, their upstream cylinder saw no effects from the presence of the downstream cylinder and behaved similarly to a single cylinder. They verified that clashing of cylinders would occur for their lowest spacing, $d = 3$, for reduced velocities as low as 8.2. Moreover, for all the other spacings, a pure WIV response of gradual amplitude of oscillation build-up, up to the largest reduced velocities was observed for both inline and crossflow displacements.

Armin *et al.* [25] presented a 2DOF experimental study of two free-free tandem cylinders in a towing tank. The spacings varied through $d = 3.5 - 20$ within a range of approximately $U_r = 2 - 22$ with 18 reduced velocity step increments corresponding to

$Re = 8.7 \times 10^3 - 5.2 \times 10^4$. Unfortunately, the comparison of results with different spacings was not always made for the exact reduced velocity point, but rather in a general curve trend. The cylinders were effectively identical with very low mass and damping ratios, $m^* = 2.36$, $\zeta = 1.5\%$ (in water). The oscillation amplitudes of the downstream cylinder were shown to largely fluctuate with the increase of reduced velocity in both inline and transverse directions and frequency results were also presented. Despite the greater oscillation amplitude variations, features observed were similar to other WIV studies, even for fixed-free studies.

Even though experiments have provided the most relevant and high-fidelity insights into the problem of WIV of pairs of cylinders, the development of an analytical modelling framework has been identified as extremely important for engineering analysis of the dynamics of groups of subsea structures. A computationally efficient and accurate model would be especially beneficial for parametric investigations and sensitivity studies, for instance, that are usually performed in full scale analyses of industry projects. Therefore, the present study proposes to fill this gap by deriving a model that would satisfy these requirements and produce results and features that may contribute to the state-of-the-art development of the subject.

For the mathematical modelling of WIV of tandem cylinders, Shiau and Yang [26] introduced one of the first reduced-order models for 1DOF combined VIV and WIV of two rigid tandem cylinders, allowed to vibrate in the cross-flow direction. The authors adopted the wake oscillator approach, consisting of introducing wake variables governed by nonlinear oscillators, in their case Rayleigh equations, known to mathematically reproduce some of the dynamic features of oscillating hydrodynamic forces for VIV of a single cylinder. Wake effects were represented as the convection time lag for the vortices to reach the second cylinder based on its distance from the first, as earlier discussed by Price and Paidoussis [27]. Facchinetti *et al.* [28] presented an alternative model for the 1DOF transverse VIV and WIV of a rigid tandem pair of cylinders. Similar to the previous study, WIV modelling was again proposed based on the convection time difference for vortices to reach the downstream cylinder and an empirical relationship was fitted to experimental data. This time, van der Pol wake oscillators were employed for hydrodynamic fluctuating coefficient modelling.

The two low-order models reviewed rely on the vortices' convection time delay assumption used for the wake oscillator initially in Shiau and Yang [29]. Even though the time lag approach has led to WIV modelling progress, some questions remain

open. For instance, if the only difference between the hydrodynamic force acting on the front and rear cylinders is that the latter is phased to account for the time it takes for the upstream vortex to reach the cylinder, then mathematically this suggests VIV and WIV forces should have the same amplitudes. However, experimental results indicate otherwise [11]. Most importantly, the mean wake-induced lift force which solely excites the second cylinder and depends on the local position within the wake flow is not observed for the leading cylinder since its oncoming flow is the free stream flow and, therefore, it could not be represented. Consequently, the wake stiffness feature would not be represented. Hence, modelling of wake effects and features such as the wake deficit and wake-induced forces could address those issues and lead to improvement of the modelling of VIV and WIV of tandem cylinders.

Looking at a different methodology, several authors have dedicated themselves to modelling wake-induced forces, more specifically the wake-induced lift force. Wu *et al.* [30] investigated the wake flow behind a circular cylinder based on the work of Huse [31] in using Schlichting's [32] solution to the steady-state boundary layer equations for a bidimensional wake. They assumed that the difference between the angles of separation on the upper and lower halves of the downstream cylinder in the wake resulted in an asymmetrical total pressure distribution which was proposed to be the source of the wake-induced lift force pointed towards the wake centre. Moreover, an iterative free streamline model was employed to calculate the wake-induced lift and drag forces and relative velocity effect was considered. The results indicated that their force modelling represents the wake-induced lift and drag forces accurately, but only within a medium range of longitudinal separations from $d = 6$ up to $d = 12$.

Blevins [33] also started from the previously mentioned boundary layer theory for the wake after a stationary circular cylinder. Asymptotic wake flow laws [32, 34, 35] were combined to yield the mean local wake flow velocity. Then, the wake-induced drag was calculated directly from the wake deficit law. Subsequently, the wake-induced hydrodynamic lift directed towards the centre of the wake was proposed following Rawlin's theory cited by Price [10]. The author then investigated the accuracy of the model for a wider range of axial spacings, i.e. $d = 3-20$ and possibly more. Hence, not only was the model validity range of spacings greater than previous studies, but especially for the lower separations which have been shown in experimental studies to be critical for the WIV of the downstream cylinder.

Blevins and Saint-Marcoux [36] proposed an extension to the previous study with a second order solution to the boundary layer theory, accounting for the case of a wake behind a vibrating cylinder. The authors commented that for $d > 2$, the wake is wider and deeper and its centre is flatter as a result of the increased drag and lateral motion of the cylinder, whereas at a larger distance, $d > 24$, the oscillating cylinder increasingly approximates the stationary cylinder classical wake profile. The authors compared their developed theory to experiments for wake velocities over a vast range of inline positions ($d = 2-50$). Good agreement was seen for most of the spacings. For as close as 2 diameters and as far as 50 diameters, inaccuracies were observed and, therefore, the validity of the model was established to be approximately $2 \leq d \leq 24$, which is promising for the present study for the mentioned reasons. Deviations for $d = 2$ are pointed out to be related to vortices being formed and separated from the extreme lateral edges of the oscillating upstream cylinder which could not be represented by the current model.

With the development and testing of a wake-induced force modelling theory, the topic now lacks an efficient model to predict the behaviour of groups of structures subjected to VIV and WIV. Thereafter, developments in the modelling of the wake field and wake-induced forces acting on the downstream cylinder are used as a foundation for the research and possible establishment of a precise modelling framework applicable to VIV and WIV of tandem cylinders throughout an extensive range of system properties, spacings and reduced velocities. The research objective is the application of van der Pol wake oscillators, as successfully employed for isolated cylinders in VIV, alongside the wake flow and wake-induced force theory to model combined VIV and WIV, in order to reproduce theory, amplitudes and modelled frequencies of vibration, including correlation to the wake stiffness and main WIV features to a higher degree of precision and reliability.

Additionally, it has been reviewed that there is a limited number of experiments studying a pair of cylinders in combined VIV and WIV, especially for cases of pairs of cylinders where both are free to vibrate in 2DOF in tandem or staggered configurations. A few studies [24, 25] are available on free-free tandem cylinder couples, however, the detail on the number of reduced velocities or spacing points considered is not ideal for calibration of the present modelling theory. On the other hand, free-free staggered cylinders have not been found in the literature. Furthermore, features such as the wake

stiffness, difference of fixed-free and free-free studies and effect of the dynamic relative mean drift between cylinders have not been discussed.

1.3. Motivation

As highlighted from the literature review, the number of studies and amount of information available for combined VIV and WIV of multiple cylinders is limited and it is a topic that still has many open questions. The study of VIV of a single cylinder is more mature and explored in the literature. However, present WIV studies report features and larger amplitudes of vibration that are only observed for multiple-cylinder dynamics and that may be critical to engineering applications. Therefore, it is not recommended to perform the analysis of a problem of groups of cylindrical structures by extrapolating models and theory from single-cylinder systems.

Specifically speaking about the combined VIV and WIV of pairs of cylindrical structures of circular cross-sections, high fidelity studies especially in the form of CFD and experimental works, are lacking for a sufficient range of cases and cylinder configurations. For instance, CFD studies presented in the literature for the dynamics of pairs of cylinders have been observed to be usually limited to $Re \leq 1000$, $U_r \leq 12$ (Re fixed with natural frequency variation) and to consider only a few cases with different spacings. Most of the reviewed CFD studies also focus on a particular characterisation of the dynamics of the two cylinders, for example on the effect of the variation of the inline-to-transverse frequency ratio, which on the one hand are extremely valuable and contribute to the general understanding of the topic, but on the other hand, provide less general information and there is a lack of sensitivity studies on parameters, such as flow velocity and spacings, that are known to vary in subsea engineering applications for example.

Experimental studies are the analysis method that is more widespread in the literature. However, groups of cylinders may differ from each other in several different ways. For instance reviewed experimental studies have been: i) for a fixed or free upstream cylinder, ii) tandem or staggered, iii) pendulum or another system, iv) for varied U_r ranges, v) for varied spacing ranges, vi) for different Reynold number ranges, vii) with equal or different natural frequencies in both directions, viii) with equal or different cylinder diameters, ix) for varied mass and damping ratios, and x) with one or two degrees-of-freedom, just to cite some possibilities. The literature review has made it clear that more studies are needed, especially for comprehensive experimental campaigns that would help to integrate the different investigations and features

observed. Experimental setups such as 2DOF staggered cylinders for a free upstream cylinder have not been studied so far and will be considered in the present study.

Moreover, no mathematical or numerical models able to represent the response of the two cylinders have been proposed in the literature prior to this study and this will also be focused on in this thesis. The proposal of a computationally efficient and robust mathematical modelling framework would be an important tool for the industry for the design and analysis of structures such as subsea pipelines, risers, umbilicals and other lines. However, such a model needs high fidelity data for calibration and validation. Therefore, the present thesis is subdivided into two parts: a) Part 1 focuses on the numerical modelling and proposal of a modelling theory for the combined VIV and WIV of a pair of cylinders and b) Part 2 is the experimental laboratory investigation of the same or similar phenomena and cases for validation with the model.

1.4. Aim and Objectives of the Study

The two main aims of this thesis are related to analytical modelling theory and experimental methodology. These are respectively a) the development, validation and establishment of a robust and computationally efficient modelling framework that has the potential to be useful for engineering analysis of multiple real subsea structures in the oil and gas or renewable energy sectors; and b) the laboratory analysis and tests of a system of a pair of cylinders making a contribution to the general understanding of the problem.

The objectives of the study could be enumerated as follows.

For the analytical modelling:

- Derivation of a model that encompasses the boundary layer theory and wake oscillator concept. Hence, a computationally efficient model not required to solve the complex Navier-Stokes equations.
- Application of the model to a 1DOF and 2DOF pair of cylinders and validation with reference experimental data.
- Verifying whether the proposed model captures the main features of WIV of multiple cylinders, e.g., the wake stiffness mechanism.

Whilst for the experimental modelling the principal objectives are:

- The design and implementation of a setup capable of reproducing a wide range of configurations of pair of cylinders.
- Measurements and analysis of the wake flow velocity profile and wake deficit downstream of a leading stationary or dynamic cylinder for different spacings.

- The comparison of WIV for a leading stationary against a leading dynamic cylinder.

Table 1-1: Correlation of Thesis Chapters with objectives.

Objective	Chapter
Derivation of a model that encompasses the boundary layer theory and wake oscillator concept. Hence, a computationally efficient model not required to solve the complex Navier-Stokes equations.	Chapter 2 & Chapter 3
Application of the model to a 1DOF and 2DOF pair of cylinders and validation with reference experimental data.	Chapter 2 & Chapter 3
Verifying whether the proposed model captures the main features of WIV of multiple cylinders, e.g. the wake stiffness mechanism.	Chapter 2 & Chapter 3
The design and implementation of a setup capable of reproducing a wide range of configurations of pair of cylinders.	Chapter 4
Measurements and analysis of the wake flow velocity profile and wake deficit downstream of a leading stationary or dynamic cylinder for different spacings.	Chapter 5 & Chapter 6
The comparison of WIV for a leading stationary against a leading dynamic cylinder.	Chapter 5 & Chapter 6

1.5. Novelty of the Work

Having reviewed the literature studies associated with the topic of WIV of tandem and staggered cylinders, a research gap associated with the lack of mathematical modelling tools for the external flow around groups of cylindrical structures in proximity has been identified. This work also contributes to the general knowledge on the topic with the experimental investigation of previously uninvestigated configurations such as the staggered pair of two 2DOF cylinders.

The novel contributions of the present study are as follows:

- 1) Derivation and proposal of a reduced order model for combined WIV and VIV of a pair of cylinders that is realistic, accurate and computationally efficient.

Recent developments in the field have derived analytical expressions for the wake-induced drag and lift forces based on the boundary layer equations. Moreover, the wake oscillator modelling theory for VIV of single cylinder systems has gained popularity over the years in the literature due to its versatility, low computational cost and capability of representing the phenomenon. Therefore, it is understood that there is a demand for the derivation of a model based on the wake oscillator idea for the representation of unsteady hydrodynamic forces, and the boundary layer theory for the prediction of steady wake-induced forces related to WIV. Equally important is assessing this against reference experimental data to determine whether such a model is able to efficiently capture WIV responses and features.

- 2) Nonlinear modelling of the wake stiffness mechanism

The idealization of the wake stiffness mechanism has been a milestone in the study of WIV. However, the wake stiffness as proposed in the literature is based on a linearization of the wake-induced lift gradient across the wake, which has a limited range of validity and may not be recommended for extremely large transverse vibrations or is unable to capture the effect of variation of spacing between the cylinders.

In the present study, the derivation of analytical expressions for the wake-induced forces, especially the hydrodynamic lift force, makes it possible to model the wake stiffness mechanism without the need for linearising the wake-induced lift force transverse gradient.

- 3) Modelling of 1DOF and 2DOF, fixed-free, free-free, tandem, and staggered systems

The modelling theory proposed herein is general with respect to the configuration of the two cylinders, respecting modelling assumptions described in Chapter 2. Ideally for a greater industry practical aspect, the proposed modelling theory should hold for a wide range of validity in terms of relative position and configuration of the pair of cylinders, which is important as these could be dynamic and vary in nature.

Comparison and validation with all these different configurations is presented with reference experimental data.

- 4) Design and construction of an experimental setup of two cylinders which covers almost every possible configuration of wake interaction for a cylinder couple undergoing WIV.

The original experimental setup used presently allows for a wider range of investigation than perhaps any other study in the literature to date and includes the study of parameters of interest including wake flow velocities after a stationary and a dynamic cylinder, tests with cylinders for a range of reduced velocities, spacings, setups with a single cylinder or double cylinders for tandem, staggered, fixed-free and free-free 2DOF cylinders. A total of 390 tests are presented for systems with double cylinders, plus benchmark single cylinder tests for increasing and decreasing reduced velocities and wake flow measurements.

The importance of this is because it permits coverage of the widest possible range of studies whilst keeping the same material, components and system properties, which is ideal for the analyses conducted.

- 5) Experimental study of double-cylinder configurations and analyses not attempted to date

This thesis reports tests for configurations that are not available in the literature so far, namely the study of staggered cylinders for two 2DOF cylinder arrangements and the comparison of WIV/VIV of the downstream cylinder after a stationary or dynamic upstream cylinder.

Each configuration will be examined in terms of amplitudes of vibration, dominant oscillation frequencies, time histories, and oscillation trajectories. This is an area that is perhaps more relevant to industry and that was missing in the majority of studies in the literature. For instance, the investigation of dominant oscillation frequencies in conjunction with other analyses has allowed for the identification of VIV, WIV, and transition regimes in Chapter 3 which may help to understand the critical cases of this fluid-structure interaction problem.

1.6. Thesis Structure

This PhD thesis is structured as follows. An introduction to the topic of combined VIV and WIV of pairs of cylinders, a literature review to identify gaps in the research and the motivation of the present work are presented in Chapter 1. Chapter 2 is dedicated to the modelling theory of 1DOF pairs of cylinders, while Chapter 3 describes the extension of the modelling theory to account for 2DOF displacements. In the experimental part of this thesis, the focus is on in-house experiments with pair of cylinders. A description of the experimental facilities and apparatus as well as a benchmark study with a single cylinder are given in Chapter 4. The results and features for the measurements of a fixed-free pair of cylinders are presented in Chapter 5, while the free-free cases are studied in Chapter 6. Finally, calibration and validation of the present modelling theory with the experiments conducted are given in Chapter 7, followed by the conclusions of this thesis in Chapter 8.

CHAPTER 2. ANALYTICAL MODELLING OF COMBINED WIV AND VIV – 1 DEGREE-OF-FREEDOM

Initially, a modelling framework is proposed to deal with the problem of combined WIV and VIV of two cylinders with only 1 degree-of-freedom (DOF). This has been done to facilitate parametric investigations, fundamental analyses and comparison or validation with 1DOF reference studies.

Therefore, derivation of the modelling theory for the case of a pair of elastically-mounted cylinders allowed to oscillate in the cross-flow direction for a steady free-stream external flow is now discussed. The tandem pair is studied for a range of downstream spacings which are always greater than a minimum critical spacing ($d \geq 4$) [7], thus both cylinders are in the co-shedding regime according to the classification of Igarashi [4]. Since the spacing studied is always larger than the critical spacing, wake-proximity interference is not accounted for. In other words, there is a unilateral influence of the first on the second cylinder through the upstream wake, but no effect on the first from the second cylinder. Therefore, the upstream cylinder is expected to behave as a single cylinder prone to be excited by the VIV mechanism, whereas the downstream cylinder is subjected to both VIV from its self-attained vortex street and WIV from the oncoming wake.

Hence, for the rear cylinder, the hydrodynamic forces may be decomposed into VIV- and WIV-associated components. This way, the steady WIV forces are modelled via the wake flow theory, while the fluctuating VIV and WIV forces are computed through the wake oscillator approach.

2.1. Combined VIV and WIV Modelling Assumptions

One of the main modelling assumptions introduced in the current study is the idea of the combination of the two phenomena: i) VIV – related to single cylinder dynamics ii) WIV – related to multiple cylinder dynamics.

In fact, both WIV and VIV have a similar origin as they are induced by vortices and wake flow. This is one of the reasons why different nomenclature has been used across some literature studies. To cite a few, the same phenomenon has been described as vortex-induced vibrations of multiple cylinders [28, 37, 38], wake-induced galloping [39] and wake-induced vibrations [40] [11]. Assi *et al.* [11] presented an interesting discussion on the nomenclature used.

More important to the present study than the preferred nomenclature used is, however, the modelling approach to the problem. Herein, the flow-induced excitation of the

downstream cylinder behind another similar upstream cylinder is modelled as a combination of WIV and VIV components, following other modelling studies in the literature [26].

For someone who observes the real phenomena of vortex shedding and flow around groups of cylinders, this assumption might feel counter intuitive. The wake flow disturbed and formed by the intrusiveness of the first cylinder is thought to engulf the second cylinder and to persist downstream of the system. In other words, an idealised separation of flow features and hydrodynamic forces as originated either from the flow surrounding the front or the rear cylinders is not realistic, despite being helpful in understanding the underlying physics. This has been remarked by Zdravkovich [41], who mentioned that vortex shedding from the upstream cylinder strongly affects and synchronises with the vortex shedding from the downstream one.

Despite the above remarks and its idealised character, the assumption of a combination of WIV and VIV components allows for the modelling of flow-induced oscillations of multiple cylinders - a problem that has a higher order of magnitude in terms of complexity - to be developed based on the advancements of single cylinder VIV modelling - a topic which is considerably more advanced to-date. The main argument supporting the validity of this core model assumption is that the WIV mechanism decays laterally and downstream of the first cylinder, just like the wake flow decays if too far across or along the wake. Therefore, just as the wake flow tends to the free stream quantities when d or T are increased, the response of a pair of cylinders originally under WIV tends to VIV when either d or T are increased, i.e. the downstream cylinder tends to respond as a single cylinder in these conditions. If this is the case, then one may expect the WIV terms to be zero or nearly zero in these circumstances and such an approach may be considered. These observations are supported by literature results, both modelling- and experimental results, and will be presented in detail in Chapter 2, Chapter 3, Chapter 5, and Chapter 6.

The benefits of this approach for the modelling of flow-induced vibration of bundles of cylindrical structures largely outweigh any drawbacks from neglecting higher order WIV-VIV coupled features that may have effects otherwise not negligible in rigorous flow characterisation studies (e.g., CFD). Nevertheless, the present study focuses mainly on the responses of structures affected by the oncoming flow, for which the calibration and validation is conducted against high fidelity reference experimental data.

2.2. Wake flow modelling

According to Schlichting [32], the application of the boundary layer equations is not restricted to regions near solid walls, but also to when two layers of fluid with different velocities meet, for instance, in the wake behind a leading cylinder resulting in WIV of a downstream cylinder, as seen in Figure 2-1.

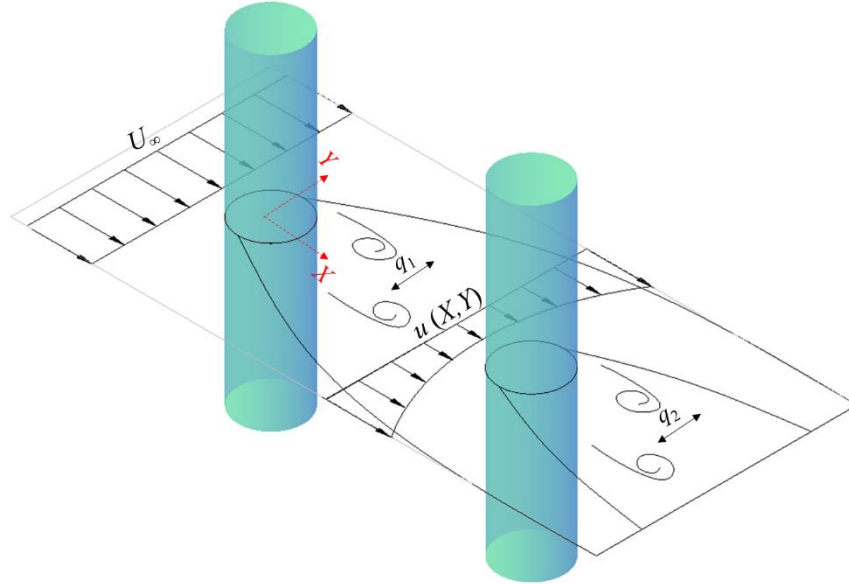


Figure 2-1: Model of upstream and downstream tandem cylinders in a uniform free stream flow and a non-uniform wake flow, respectively.

From Figure 2-1, two layers of fluid with different velocities (wake flow) downstream of each cylinder are seen and the boundary layer equations may be applied. The boundary layer theory is an asymptotic theory of the Navier-Stokes equations for high Reynolds numbers or low viscous forces [42]. The Navier-Stokes equations can be simplified by neglecting terms of relatively lower magnitude and assuming that the pressure in the wake is independent of transverse displacement, Y . For the case of a plane, steady, unidimensional outer flow, as illustrated in Figure 2-1, the boundary layer equations are [32]:

$$\frac{\partial u}{\partial X} + \frac{\partial v_2}{\partial Y} = 0; \quad (2-1)$$

$$u \frac{\partial u}{\partial X} + v_2 \frac{\partial u}{\partial Y} = -\frac{1}{\rho_f} \frac{dp}{dX} + \nu \frac{\partial^2 u}{\partial Y^2};$$

with boundary conditions: $\frac{\partial u}{\partial X} = 0$, $\frac{\partial v_2}{\partial Y} = 0$ for $Y = 0$ and $u = U_\infty$ when $Y \rightarrow \infty$, where u is the inline component of the local flow velocity in the wake, v_2 is the transverse component of the local flow velocity in the wake, U_∞ is the free stream flow velocity. In addition, a velocity profile $u(X, Y)$ must be given at an initial section, usually at $X = 0$,

where X is the inline displacement of the upstream velocity.

From Figure 2-1, it is possible to observe that the flow profile in the wake, u , is reduced due to wake-shielding from the upstream cylinder. The minimum u at a given distance X behind the first cylinder is located at the wake centreline while at the edges of the wake, $u \rightarrow U_\infty$. Therefore, there is a wake flow velocity deficit (u_d) associated with u which can be represented as:

$$u_d(X, Y) = U_\infty - u(X, Y). \quad (2-2)$$

Increasing $X \rightarrow \infty$ also causes wake effects, such as u_d , to dissipate and the flow progressively returns to undisturbed conditions. Thus, it is now possible to calculate the velocity profile in the wake, in particular at a large distance X downstream of the cylinder. Equation (2-2) can be inserted in (2-1) which becomes:

$$(u_d - U_\infty) \frac{\partial u_d}{\partial X} - v_2 \frac{\partial u_d}{\partial Y} = -\frac{1}{\rho_f} \frac{dp}{dX} - v \frac{\partial^2 u_d}{\partial Y^2}. \quad (2-3)$$

Because a sufficiently large X is considered, it can be assumed that u_d is small compared to U_∞ . This assumption simplifies the problem because quadratic terms in u_d and v_2 can be omitted and the pressure term, at least to a first approximation, is assumed to remain constant. Hence, giving:

$$U_\infty \frac{\partial u_d}{\partial X} = v \frac{\partial^2 u_d}{\partial Y^2}; \quad (2-4)$$

with boundary conditions: $Y = 0: \frac{\partial u_d}{\partial Y} = 0$ and for $Y \rightarrow \infty, u_d = 0$.

Equation (2-4) is similar to the unsteady heat conduction equation so a similar trial solution is proposed but in agreement with the power law for velocity deficit [32] [42]:

$$u_d = U_\infty \left(\frac{X}{C_{D1} D_1} \right)^{-\frac{1}{2}} g(\eta). \quad (2-5)$$

Equation (2-5) can now be reduced to an ordinary differential equation by the use of a similarity law for the function $g(\eta)$. In other words, it is assumed that velocity points at different distances downstream in the wake are similar to one another based on scaling factors. A suitable scaling factor for u is U_∞ , while for Y , the boundary layer thickness $\delta(X)$ is chosen. The similarity argument of the velocity profile can thus be written as $u/U_\infty = \chi(\eta)$ with $\eta = Y/\delta(X)$ [42].

The quantity δ is proportional to the thickness of the layer which is affected by viscous effects. Due to momentum transport considerations, $\delta^2/\nu \sim X/U_\infty$ [42], therefore, the similarity variable becomes:

$$\eta = Y \sqrt{U_\infty / \chi V}. \quad (2-6)$$

However, the wake flow behind a cylinder is, in most cases, turbulent, even in the case of comparably small Re [32]. Based on the turbulent shearing stress hypothesis, the eddy viscosity (ε_τ) can be introduced to replace the laminar kinematic viscosity (ν). Substituting in Equation (2-6) results in:

$$\eta = Y \sqrt{U_\infty / \chi \varepsilon_\tau}; \quad (2-7)$$

where, ε_τ is a constant that needs to be determined experimentally. Schlichting [32] measured the following value:

$$\varepsilon_\tau / U_\infty C_{D1} D_1 = 0.0222 = k_{Schlichting}; \quad (2-8)$$

This value was obtained for experiments with a stationary upstream cylinder generating the wake. As the focus of this study is on dynamic cylinders, an empirical parameter λ is introduced, similar to what was done by Saint-Marcoux and Blevins [43]:

$$\lambda = 1/4 k_{Schlichting} \quad (2-9)$$

Inserting the above in Equation (2-7) finally leads to:

$$\eta = Y \sqrt{\frac{4\lambda}{\chi C_{D1} D_1}}. \quad (2-10)$$

Equation (2-10) is the final definition of the similarity variable and Equations (2-2) and (2-5) can now be combined and the similarity variable and virtual kinematic viscosity definitions used, which results in:

$$U_\infty \frac{\partial}{\partial X} \left[U_\infty \left(\frac{X}{C_{D1} D_1} \right)^{-\frac{1}{2}} g(\eta) \right] = \varepsilon_\tau \frac{\partial^2}{\partial Y^2} \left[U_\infty \left(\frac{X}{C_{D1} D_1} \right)^{-\frac{1}{2}} g(\eta) \right]. \quad (2-11)$$

Now, the following ordinary differential equation can be obtained from integration of Equation (2-11):

$$g'' + \frac{1}{2} \eta g' + \frac{1}{2} g = 0; \quad (2-12)$$

where prime denotes a derivative with respect to η . Integrating Equation (2-12) yields the known solution:

$$s_1 = g(\eta) = \alpha e^{-\frac{\eta^2}{4}}; \quad (2-13)$$

This is the first symmetric solution (s_1) as referred to by Blevins and Saint-Marcoux [36]. Thus far, the mathematical formulation has been derived based on the theory of two-dimensional wake flow past a stationary cylinder. However, there are

significant differences between the wake flow after a fixed or an oscillating cylinder. In order to account for the effect of vibration of the upstream cylinder, Blevins and Saint-Marcoux [36] proposed a second solution by considering α as a function of η as follows:

$$\alpha = \beta \int_0^\eta e^{\frac{\varphi^2}{4}} d\varphi; \quad (2-14)$$

where, φ is a generic variable of integration. Substitution of Equation (2-14) back into Equations (2-12) and (2-13) results in:

$$s_2 = \beta e^{-\frac{\eta^2}{4}} \int_0^\eta e^{\frac{\varphi^2}{4}} d\varphi. \quad (2-15)$$

The second solution, s_2 , is asymmetric and the modified solution for the wake flow after a vibrating leading cylinder becomes:

$$g(\eta) = \alpha e^{-\frac{\eta^2}{4}} + \beta e^{-\frac{\eta^2}{4}} \int_0^\eta e^{\frac{\varphi^2}{4}} d\varphi. \quad (2-16)$$

Finally, combining Equations (2-2), (2-5) and (2-16) results in the expression for the wake-reduced flow velocity within the wake of a cylinder in VIV:

$$\chi(X, Y) = \frac{u(X, Y)}{U_\infty} = 1 - \left\{ \alpha \left(\frac{C_{D1} D_1}{X} \right)^{\frac{1}{2}} \left(e^{-\frac{\eta^2}{4}} + \frac{\beta}{\alpha} e^{-\frac{\eta^2}{4}} \int_0^\eta e^{\frac{\varphi^2}{4}} d\varphi \right) \right\}; \quad (2-17)$$

where constants of integration have been incorporated without loss of generality to the empirical parameters α and β which should be calibrated to experimental data. Thus, Equation (2-17) can be observed as though the velocity in the wake is the free-stream velocity modified by the wake deficit function: $\chi(X, Y) = u(X, Y)/U_\infty$.

Considering that the drag on a cylinder in a wake is proportional to the local dynamic pressure evaluated at the wake centreline [33], it becomes that:

$$C_{D12}(X, Y) = \left[\frac{u_2(X, Y)}{U_\infty} \right]^2 C_{D2}. \quad (2-18)$$

Combining Equations (2-17) and (2-18) leads to the dimensional form of the wake-induced drag coefficient:

$$C_{D12}(X, Y) = C_{D2} \left(1 - \left\{ \alpha \left(\frac{C_{D1} D_1}{X} \right)^{\frac{1}{2}} \left(e^{-\frac{\eta^2}{4}} + \frac{\beta}{\alpha} e^{-\frac{\eta^2}{4}} \int_0^\eta e^{\frac{\varphi^2}{4}} d\varphi \right) \right\} \right)^2; \quad (2-19)$$

Following Blevins [33], the wake-induced lift is assumed to be proportional to the transverse gradient of the wake-induced drag:

$$C_{L12}(X, Y) = -\frac{\partial C_{D12}(X, Y)}{\partial Y}; \quad (2-20)$$

for which the negative sign in Equation (2-20) is required so that the mean lift force is directed towards the wake centreline when the downstream cylinder is vibrating across the wake [44]. Other studies [31, 33, 36, 43] also adopted a negative sign for their lift coefficient expressions implicitly in the form of an additional empirical parameter. However, in an attempt to reduce the number of empirical inputs to the model, the minus sign has been employed explicitly in Equation (2-20).

Further developing Equation (2-20) it becomes:

$$C_{L12}(X, Y) = -4D_2\alpha \frac{\sqrt{\lambda}}{X} C_{D2} \left(1 - \left\{ \alpha \left(\frac{C_{D1}D_1}{X} \right)^{\frac{1}{2}} \left(e^{-\frac{\eta^2}{4}} + \frac{\beta}{\alpha} e^{-\frac{\eta^2}{4}} \int_0^\eta e^{\frac{\varphi^2}{4}} d\varphi \right) \right\} e^{-\frac{\eta^2}{4}} \frac{\eta}{2} - \frac{\beta}{\alpha} e^{-\frac{\eta^2}{4}} + \frac{\eta\beta}{2\alpha} \int_0^\eta e^{\frac{\varphi^2}{4}} d\varphi \right) \quad (2-21)$$

The following dimensionless coordinates are now introduced: $X/D_1 = (X_2/D_1 - X_1/D_1 + dD_1/D_1) = d$, for the case of cylinder displacements in the crossflow direction only); $Y/D_1 = (Y_2/D_1 - Y_1/D_1 + TD_1/D_1) = (y_2 - y_1 + T) = (\delta y + T)$. For which d and T are the dimensionless inline and transverse spacings between the cylinders. D_1 has been used here as the reference quantity for the dimensionless equations. This has been done because the upstream cylinder is the reference cylinder since it generates the wake that causes WIV of the downstream cylinder. Therefore, unless otherwise stated, reference quantities will refer to the first cylinder of the problem, as will be done for instance for the Re computation and for the plotted U_r in the following chapters.

It is now possible to write Equations (2-17), (2-19) and (2-21) in dimensionless forms as follows:

$$\chi(d, \delta y) = \frac{u(d, \delta y)}{U_\infty} = 1 - \left\{ \alpha \left(\frac{C_{D1}}{d} \right)^{\frac{1}{2}} \left(e^{-\frac{\eta^2}{4}} + \frac{\beta}{\alpha} e^{-\frac{\eta^2}{4}} \int_0^\eta e^{\frac{\varphi^2}{4}} d\varphi \right) \right\}; \quad (2-22)$$

$$C_{D12}(d, \delta y) = C_{D2} \left(1 - \left\{ \alpha \left(\frac{C_{D1}}{d} \right)^{\frac{1}{2}} \left(e^{-\frac{\eta^2}{4}} + \frac{\beta}{\alpha} e^{-\frac{\eta^2}{4}} \int_0^\eta e^{\frac{\varphi^2}{4}} d\varphi \right) \right\} \right)^2; \quad (2-23)$$

$$C_{L12}(d, \delta y) = -4\alpha \frac{\sqrt{\lambda}}{d} C_{D2} \left(1 - \left\{ \alpha \left(\frac{C_{D1}}{d} \right)^{\frac{1}{2}} \left(e^{-\frac{\eta^2}{4}} + \frac{\beta}{\alpha} e^{-\frac{\eta^2}{4}} \int_0^\eta e^{\frac{\varphi^2}{4}} d\varphi \right) \right\} e^{-\frac{\eta^2}{4}} \frac{\eta}{2} - \frac{\beta}{\alpha} e^{-\frac{\eta^2}{4}} + \frac{\eta\beta}{2\alpha} \int_0^\eta e^{\frac{\varphi^2}{4}} d\varphi \right) \quad (2-24)$$

The influence of the higher order solution, Equation (2-15), will be analysed and compared to the symmetric s_1 against experimental measurements in Section 2.4.1.

This will assist in the investigation on how the inclusion of a higher order solution increases the performance of the model in providing more realistic outputs.

2.3. VIV modelling and definition of the model

Based on the schematic diagram shown in Figure 2-2, the resultant force in the crossflow direction acting on the first cylinder is:

$$F_{y1} = F_{L1} \cos\theta_1 - F_{D1} \sin\theta_1. \quad (2-25)$$

Hence:

$$F_{y1} = \frac{\rho_f D_1}{2} \bar{U}_1 (C_{L1} U_\infty - C_{D1} \dot{Y}_1); \quad (2-26)$$

where \bar{U}_1 is the relative velocity defined as:

$$\bar{U}_1 = \sqrt{U_\infty^2 + \dot{Y}_1^2}. \quad (2-27)$$

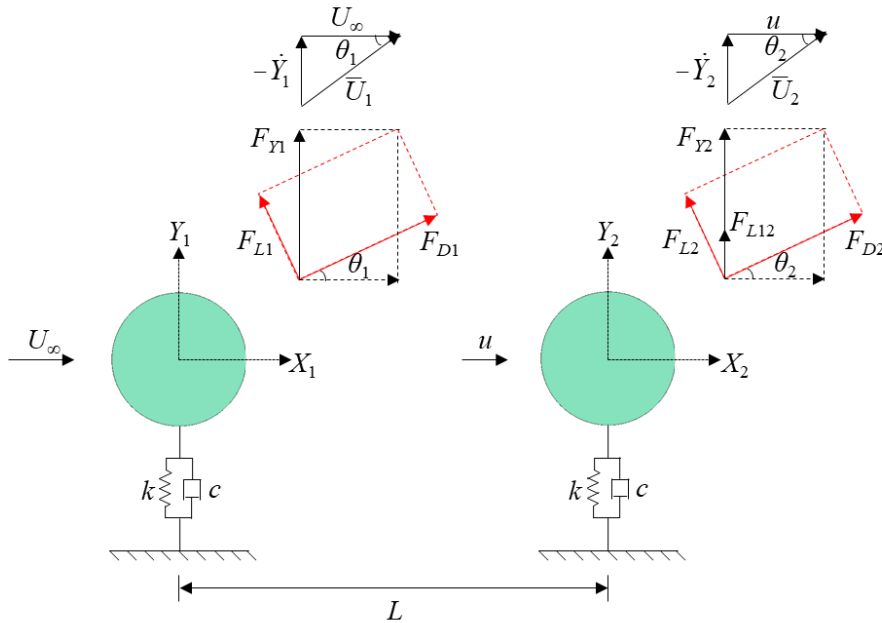


Figure 2-2: Schematic diagrams of relative flow-structure velocity vectors and associated hydrodynamic force components of upstream and downstream tandem cylinders.

Initially, the dimensionless equation of motion for the upstream cylinder is:

$$\ddot{y}_1 + 2\zeta\dot{y}_1 + y_1 = F_{y1}/((m+m_a)\omega_n^2 D); \quad (2-28)$$

where the dot denotes a derivative with respect to the dimensionless time, $t = \tau \omega_n$ (τ in seconds), the dimensionless transverse displacement is defined as $y_1 = Y_1/D$, damping ratio is $\zeta = c/(2(m+m_a)\omega_n)$ and natural frequency, $\omega_n = \sqrt{k/(m+m_a)}$.

Further elaborating the forcing term on the right-hand side of Equation (2-28) and introducing the alternative mass ratio as in [45], ($\mu = (m+m_a)/\rho D^2$):

$$F_{y1}/((m+m_a)\omega_n^2 D) = \frac{1}{2} \frac{\bar{U}_1 (C_{L1} U_\infty - C_{D1} \omega_n D \dot{y}_1)}{D^2 \omega_n^2 \mu}. \quad (2-29)$$

Introducing the reduced velocity in angular form ($U_r = 2\pi U_\infty / (\omega_n D)$), the dimensionless relative velocity (\bar{U}_1^*) can be defined as follows:

$$\bar{U}_1^* = \left(\frac{U_r^2}{4\pi^2} + \dot{y}_1^2 \right)^{1/2}. \quad (2-30)$$

Substituting back into Equation (2-29) gives:

$$\ddot{y}_1 + 2\zeta \dot{y}_1 + y_1 = \frac{\bar{U}_1^*}{2\mu} \left(\frac{C_{L1} U_r}{2\pi} - C_{D1} \dot{y}_1 \right). \quad (2-31)$$

According to Figure 2-2, the resultant transverse force on the second cylinder is:

$$F_{y2} = F_{L2} \cos\theta_2 - F_{D2} \sin\theta_2 + F_{L12}; \quad (2-32)$$

where F_{L12} is the wake-induced lift force per length. It is highlighted that in Equation (2-32), unlike other forces, F_{L12} was modelled independently from the relative flow velocity. This is justified by the fact that the wake deficit law has already been incorporated into C_{L12} , as seen in Equation (2-24), and consequently into F_{L12} . Had it been related to the relative velocity, F_{L12} would have been corrected twice for wake deficit. Therefore, F_{L12} has been related to U_∞ and is dynamic through the relative transverse position in the wake flow, δy , as shown in the following.

$$\frac{F_{L12}}{L} = \frac{1}{2} \rho_f U_\infty^2 D C_{L12}(d, \delta y). \quad (2-33)$$

Then, further expanding Equation (2-32) leads to:

$$F_{y2} = \frac{\rho_f D}{2} (\bar{U}_2 C_{L2} U_2 - \bar{U}_2 C_{D2} \dot{y}_2 + U_\infty^2 C_{L12}(d, \delta y)); \quad (2-34)$$

where, $\bar{U}_2 = \sqrt{U_2^2 + \dot{y}_2^2}$ is the downstream cylinder's relative flow velocity.

In analogy to the first cylinder, the dimensionless equation of motion for the second cylinder becomes:

$$\ddot{y}_2 + 2\zeta \dot{y}_2 + y_2 = \frac{1}{2\mu} \left(\bar{U}_2^* \frac{C_{L2} U_r \chi(d, \delta y)}{2\pi} - \bar{U}_2^* C_{D2} \dot{y}_2 + \frac{U_r^2}{4\pi^2} C_{L12}(d, \delta y) \right); \quad (2-35)$$

for which $\bar{U}_2^* = \left(\frac{\chi^2 U_r^2}{4\pi^2} + \dot{y}_2^2 \right)^{1/2}$.

After introduction of the wake variables, $q_1 = 2C_{L1}/C_{L01}$ and $q_2 = 2C_{L2}/C_{L02}$, and following the concept of wake oscillators for VIV of a single cylinder [28, 46], then the model is completed from equations (2-31) and (2-35), plus two van der Pol nonlinear

oscillator equations. The final 1DOF model in compact dimensionless form is shown below:

$$\ddot{y}_1 + \left(2\zeta + \frac{\gamma_1}{\mu}\right) \dot{y}_1 + y_1 = M_1 q_1; \quad (2-36)$$

$$\ddot{y}_2 + \left(2\zeta + \frac{\gamma_2}{\mu}\right) \dot{y}_2 + y_2 = M_2 q_2 + M_{12}; \quad (2-37)$$

$$\ddot{q}_1 + \varepsilon_1 \delta_1 (q_1^2 - 1) \dot{q}_1 + \delta_1^2 q_1 = \Lambda_1 \ddot{y}_1; \quad (2-38)$$

$$\ddot{q}_2 + \varepsilon_2 \delta_2 (q_2^2 - 1) \dot{q}_2 + \delta_2^2 q_2 = \Lambda_2 \ddot{y}_2; \quad (2-39)$$

in which: $M_1 = \bar{U}_1^* U_r C_{L01} / 8\mu\pi$; $\gamma_1 = \bar{U}_1^* C_{D1} / 2$; $M_2 = \bar{U}_2^* U_r \chi C_{L02} / 8\mu\pi$;
 $M_{12} = U_r^2 C_{L12} / 8\mu\pi^2$; $\gamma_2 = \bar{U}_2^* C_{D2} / 2$; $\delta_1 = St U_r$; $\delta_2 = St U_r \chi$; $\mu = (m + m_a) / \rho D^2$.

Having introduced all of the empirical inputs of the model, the system of dimensionless equations in Equations (2-36)-(2-39) was simultaneously solved numerically by a MATLAB algorithm based on an explicit Runge-Kutta formula, the Dormand-Prince pair [47]. The integration interval, $t = 0 - 1200$, was defined to guarantee that the dynamic response of the system fully develops, providing a reasonable data window especially for the frequency results. The cut-off dimensionless time was set up as $t = 200$, albeit the system is able to develop steady-state sooner than that. The integration step was specified by an adaptive systematic approach and the conclusion is that $t = 0.01$ is satisfactory and compatible with the resolutions of the problem.

2.4. Calibration of Model Input Parameters

As mentioned previously, the wake past a vibrating cylinder is different from that formed behind a stationary cylinder. Despite this, the boundary layer wake flow theory is usually derived for the wake of a stationary circular cylinder due to greater simplicity. However, a higher order general solution [36] has been more recently proposed with the intention to account for the displacement of the upstream cylinder in the modelling, potentially leading to improved results for the dynamics of a pair of cylinders where both are free to oscillate. Nevertheless, this comes at the expense of a greater number of input parameters to the model.

For a given set of St_1 , St_2 , C_{L01} , C_{L02} , C_{D1} and C_{D2} , the model calibration and sensitivity studies of the wake deficit (λ , α , β) and wake oscillator (ε_1 , Λ_1 , ε_2 , Λ_2) coefficients are first performed. For a tandem pair of stationary cylinders in the wake interference regime with $d > 3$, $St \leq 0.22$ [48], $C_{L01} \leq 0.6$ and $C_{L02} \leq 0.9$ [49], depending

on d and Re . As d is increased, values of St , C_{L01} and C_{L02} converge to a constant equivalent to that in a single cylinder case. Here, it is assumed that $C_{L01} = C_{L02} = 0.3$ [45] and $St_1 = St_2 = 0.2$. As for C_{D1} and C_{D2} , their amplitude-dependent values are unknown a priori, subject to a drag reduction in the wake [50] versus a drag magnification caused by VIV [51]. To avoid a time-consuming iteration process, it is assumed that $C_{D1} = 2$ [43] or $C_{D1} = 1.2$ where the upstream cylinder is freely oscillating or stationary, respectively. In all cases, $C_{D2} = 1.2$ [11] so that the calibration focus is placed on the wake deficit profile and wake oscillator coefficients.

2.4.1. Calibration of 2nd Order Wake Profile Parameters

As mentioned previously, the higher order solution consists of $s_1 + s_2$, Equation (2-16). The downstream cylinder response is coupled with the wake velocity profile $\chi(d, \delta y)$ behind the upstream cylinder which may be fixed (“fixed-free” case) or oscillating (“free-free” case). As $\chi(d, \delta y)$ comprises the first order (s_1) and second order (s_2) solutions, it is worth understanding their individual solution contributions to the predicted wake profiles in comparison with experimental data. Their effect is such that both the input empirical parameters, α and β , govern the in-line deficit velocity decay profile whereas λ governs the lateral wake width. Only s_1 is considered in the fixed-free tandem case whereas both s_1 and s_2 are considered in the free-free tandem case.

Without a downstream cylinder in this first instance, δy is referred to as the location of the measured mean wake velocity with respect to the fixed or moving centreline of the single cylinder. This is in the range of $-3 \leq \delta y \leq 3$. A calibration procedure is carried out with the aim of capturing qualitative features of the widened and flattened wake profiles, through minimising errors between numerical results and experimental data. By performing a numerical tuning in individual $d = 4, 6, 12$ and 24 cases, it has been deduced that the optimal functions are $\lambda = 0.74d^{0.61}$ and $\alpha = 0.53d^{0.17}$ in the oscillating cylinder case, whereas the optimal coefficients are $\lambda = 5.5$ and $\alpha = 0.7$ in the stationary cylinder case for all d . These coefficients are employed for the symmetric s_1 profile. For s_2 , the tuning process yields $\beta = -0.15$ for $\eta > 0$, $\beta = 0$ at $\eta = 0$, and $\beta = 0.15$ for $\eta < 0$, such that the shape function s_2 and the combined s_1 and s_2 profiles behind an oscillating cylinder become symmetric as experimentally observed [36]. Alternatively, the $|s_2|$ condition may be imposed as in Saint-Marcoux and Blevins [43].

The channel flow experiment of Saint-Marcoux and Blevins [43] resulted in measured time-averaged wake velocity profiles behind both stationary and oscillating

cylinders in a uniform flow at $Re = 10^5$ which were used for calibration of the wake deficit coefficients (λ , α , β). The results are shown in Figure 2-3.

It is important to highlight that the experimental data used for the vibrating pair was obtained for a forced system which produced controlled vibrations of 1.25 diameter amplitudes for the upstream cylinder.

The downstream cylinder of the tandem pair is at an initial position $\delta y = 0$. However, once the cylinder starts oscillating due to the hydrodynamic forces, it may spend more time at staggered positions than at the equilibrium position. The wake-induced forces are well-known to vary across the wake, with the F_{D12} profile being symmetric and F_{L12} antisymmetric [10, 49], therefore, calibration and validation of the model regarding the cross-wake profiles of C_{D12} and C_{L12} are important and presented in Figure 2-4. The profile of C_{D12} , as shown in Figure 2-4a,c,e, is directly derived from χ in Figure 2-3. However, whilst χ tends to $\chi = 1$, i.e. the wake velocity tends to the free stream velocity at the edges of the wake, $C_{D12} \rightarrow C_{D02}$ out of the wake. For $d = 4$, the minimum C_{D12} recorded by experiments at $\delta y = 0$ is about 0.50 (Figure 2-4a), whereas the $s_1 + s_2$ minimum C_{D12} is 2.78% lower. For $d = 10.1$, the minimum C_{D12} recorded by experiments at $\delta y = 0$ is about 0.63 (Figure 2-4c), whereas the $s_1 + s_2$ minimum C_{D12} is 1.12% higher. For a much larger spacing of $d = 20.2$, when wake effects have diminished considerably, the minimum C_{D12} recorded by experiments at $\delta y = 0$ is about 0.80 (Figure 2-4e), whereas the $s_1 + s_2$ minimum C_{D12} is 6.76% lower. The wake width and edge of wake features from the $s_1 + s_2$ solution are also comparable. On the other hand, s_1 results fail to capture the wake breadth.

When it comes to C_{L12} , Figure 2-4 b, d and f, results from $s_1 + s_2$ agree with the experiments for the maximum and minimum amplitudes of the antisymmetric peaks. This will be seen to be especially important in Section 2.5.4 as it is related to the wake stiffness concept to be introduced and adopted for identification of WIV frequencies. Model $s_1 + s_2$ results present a steep slope each side of the wake near $\delta y = 0$ that is only exhibited for lower spacings, $d < 4$ as in Cooper [52]. Even though this effect is negligible, a possible explanation for why this is not reflected in the experiments for similar, higher spacings is related to the fact that the two sets of experimental data with similar Re used for comparison have been measured for static cylinders, while the modelling approach has oscillating cylinders which are scarce in experimental data.

The reference drag coefficients on the first and second cylinders are defined as $C_{D01}=2$ and $C_{D02}=1.2$ respectively. These constants are within the range which is

normally estimated and used in the literature [33, 36, 53, 54]. In the present study, $C_{D01} = 2$ has been tuned based on a better agreement to the experimental data. However, thorough investigation of the model and parameters led to the value of $C_{D02} = 1.2$. The current proposal of C_{D02} becomes clearer to justify if Figure 2-4e is analysed. It can be seen that if C_{D12} measurements are followed out of the wake ($|T| > 3$), its value tends to approximately 1.2.

For additional investigation of s_1 against $s_1 + s_2$ in terms of the way the increase of d and wake decay affect the wake in its entirety, χ , C_{D12} and C_{L12} fields with variation of lateral and longitudinal spacings are presented in Figure 2-5. The disturbed flow boundaries are clearly observed in Figure 2-5a-b and it is possible to estimate the modelled wake width, recalling its definition as being limited within the region for which $\chi < 1$ ($u \leq 0.99U_\infty$). Moreover, it is possible to confirm that the wake breadth grows as the wake spreads downstream, as mentioned previously, and that the model captures such a feature. Physically, this happens either through viscous effects or entrainment in the absence of external turbulence [55].

Figure 2-5 confirms that the model reproduces the main WIV features. For instance, the mean C_{L12} is anti-symmetric across the wake. It is zero for a thin line at the wake centreline ($T = 0$), negative when $\partial C_{D12}/\partial T$ is positive and vice versa. In other words, C_{L12} will always be pointing towards the wake centreline as the cylinder is displaced from the initial tandem position, which agrees with the literature [10]. Further downstream, but still inside the wake zone, it is possible to verify that wake shielding effects weaken and the system slowly tends to undisturbed flow characteristics, i.e., free-stream velocity ($\chi \approx 1$), reference drag ($C_{D12} \approx C_{D2}$) and zero mean wake lift coefficients ($C_{L12} \approx 0$). Another interesting feature is observed for C_{D12} as d increases and wake width extends, where the drag and lift profiles become flatter and larger, with increased separation between C_{L12} negative and positive peaks, as in literature observations [5].

There are two minimum and maximum C_{L12} peaks off the wake centreline where C_{D12} is minimum, and these peaks shift laterally as d is increased. At $d = 4$, the peak $C_{L12} \approx 0.66$ occurs at about $\delta y \pm 0.80$ behind the fixed cylinder (Figure 2-5e) whereas the peak $C_{L12} \approx 0.42$ occurs at about $\delta y \pm 1.54$ behind the oscillating cylinder (Figure 2-5f). This highlights a greater reduction and variation range of C_{L12} due to the upstream cylinder motion in accordance with the wake profile calibration in Figure 2-3.

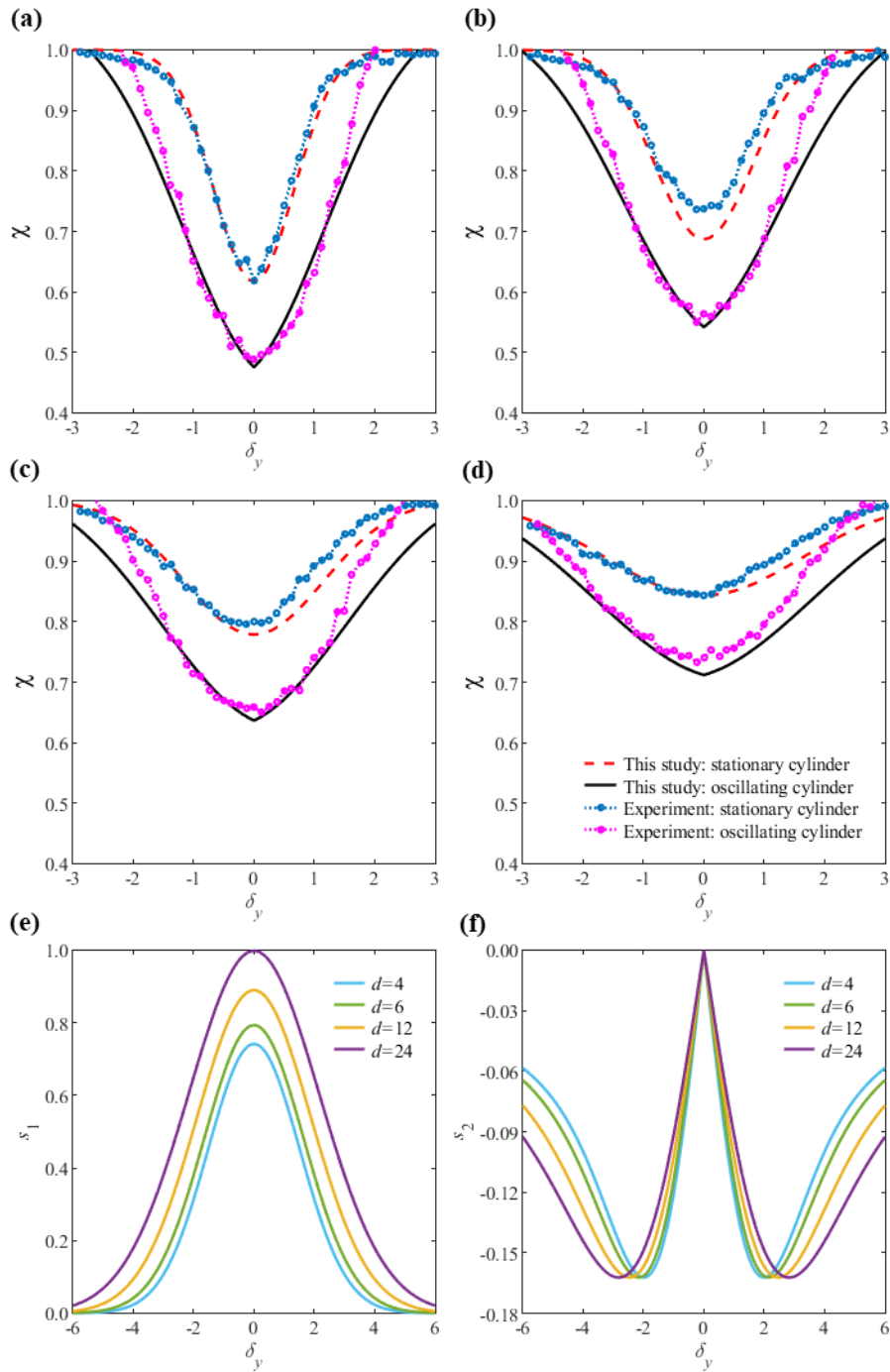


Figure 2-3: Comparison of numerical and experimental results of Saint-Marcoux & Blevins [43] for normalised velocity profiles across the wake behind upstream stationary and dynamic cylinders at $Re = 10^5$ for (a) $d = 4$, (b) $d = 6$, (c) $d = 12$ and (d) $d = 24$, and the associated (e) first- and (f) second-order solutions for a wake behind the oscillating cylinder with variable d .

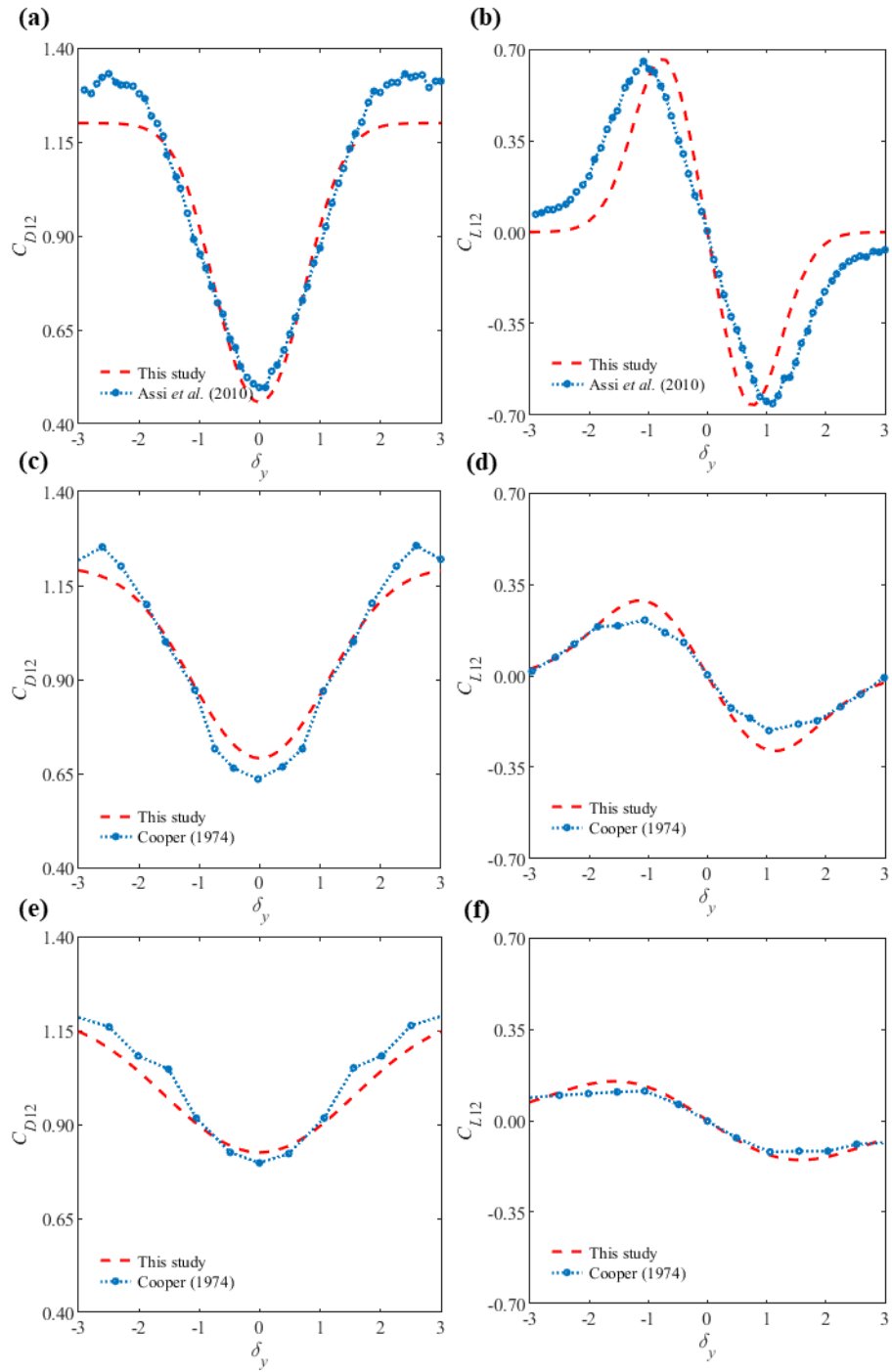


Figure 2-4: Comparison of numerical and experimental results for the mean wake-induced inline and transverse force coefficients across the wake behind the upstream stationary cylinder: (a, b) $d = 4$ at $Re = 19200$, (c, d) $d = 10.1$ at $Re = 22400$, and (e, f) $d = 20.2$ at $Re = 22400$.

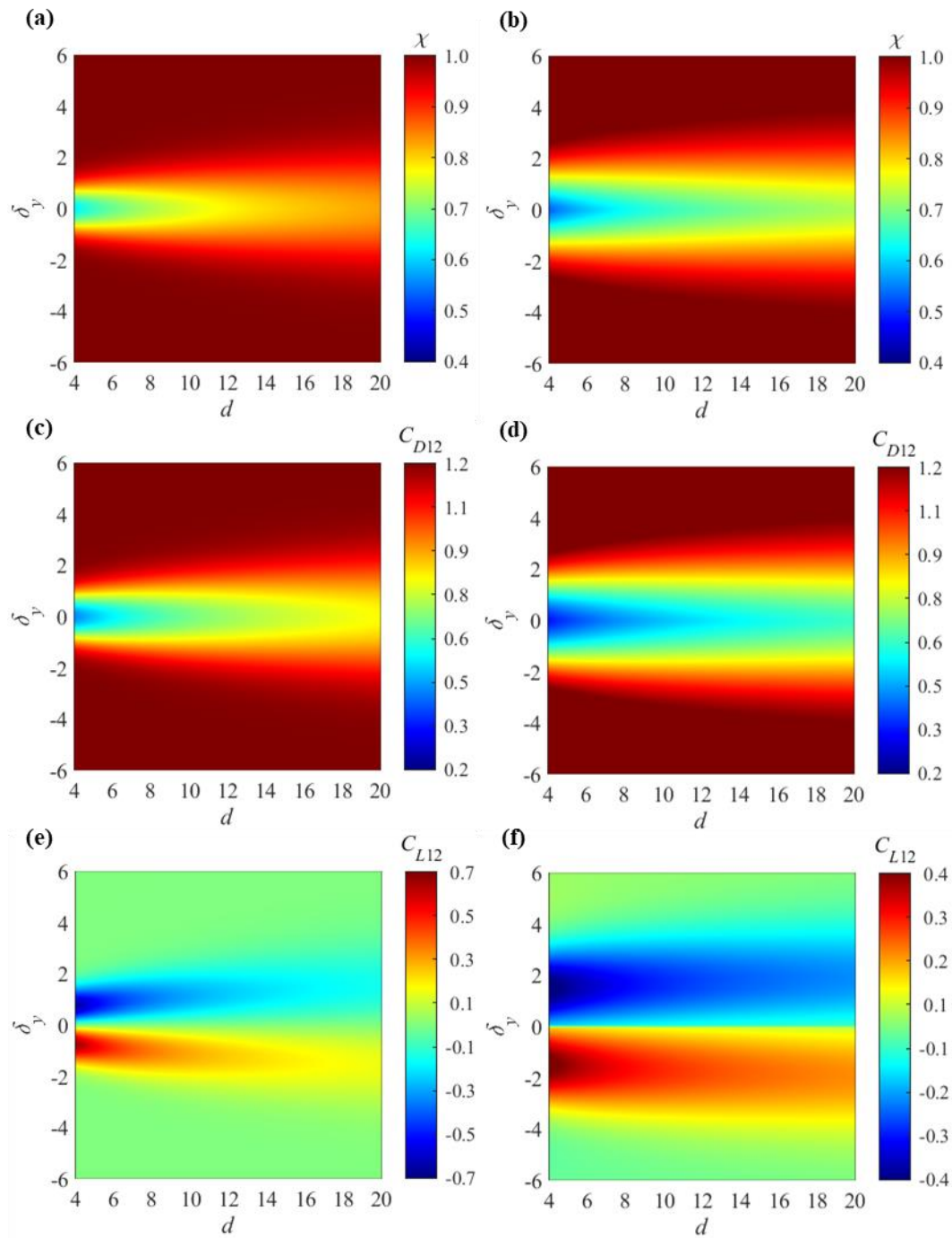


Figure 2-5: Comparison of normalised wake velocity profiles and wake-induced inline and crossflow force coefficients across and along the wake behind the upstream stationary (a, c, e) versus oscillating (b, d, f) cylinders with variable spacing ratio d .

For a summary of calibrated wake profile parameters refer to Table 2-1.

Table 2-1: Summary of Calibrated Wake Profile Parameters

Parameter		Value
α	Fixed-Free	0.7
	Free-Free	$0.53d^{0.17}$
β	Fixed-Free	N/A
	Free-Free	± 0.15
λ	Fixed-Free	5.5
	Free-Free	$0.74d^{0.61}$
C_{D01}		2.0
C_{D02}		1.2

2.4.2. Calibration of Wake Oscillator Parameters

The wake oscillator empirical input parameters (ε_1 , ε_2 , Λ_1 and Λ_2) were calibrated with experiments and the modelled dynamic responses are presented for a range of cylinder spacings, system properties and input parameters. Figure 2-6 illustrates the calibration routine of the mentioned parameters. Initially, constant values have been proposed for the wake oscillator parameters associated with the first cylinder and with the damping term of the second cylinder, $\varepsilon_1 = 0.011$, $\varepsilon_2 = 0.1$ and $\Lambda_1 = 10$. The experimental data of Assi *et al.* [11] for $m^* = 2.6$ and $\zeta = 0.7\%$ is used as reference for $d = 4, 5, 6, 8, 10$ and 20 .

One of the conclusions drawn from the analysis of Figure 2-5 is that the wake-induced forces depend on d . Moreover, analysis of sensitivity studies has identified that Λ_2 is an input parameter that is directly related to the magnitude of oscillation amplitudes. It has been observed that the amplitudes of vibration of the second cylinder for every spacing are similar to the amplitudes of the first cylinder for up to approximately $U_r = 5$. As it will be detailed, this is due to the initial VIV [11, 12, 56]. For this reason, a constant value of $\Lambda_2 = 25$ is used for all spacings for $U_r \leq 5$.

On the other hand, when $U_r > 5$, using the reported amplitudes of vibration from Assi *et al.* [11] as reference data, optimum Λ_2 value points that would lead to comparable model results were obtained through the Nelder-Mead derivative-free method [57] for minimisation of the errors between model outputs and the experimental reference data for a given U_r point, where the error tolerance was defined as 0.1%. As

a result, 33 optimal Λ_2 values were obtained for 33 U_r points from 5.75 to 29.75 with an equal increment of 0.75 for each of the six spacings, $d = 4, 5, 6, 8, 10$ and 20 .

Subsequently, a sixth-order polynomial function was fitted to emulate the 33 optimal Λ_2 points. Instead of having one sixth-order polynomial function for each of the six spacings, it is proposed that a multiplication factor could be applied to a reference spacing polynomial function in order to predict the other spacings. In this case, it was found that $d = 5$ is the reference spacing which, when multiplied by given constants, would mimic the other spacings' optimum Λ_2 trend with increased precision. Multiplication factors for each spacing between 1.1 and 0.54 for $d = 4$ and $d = 20$ respectively have been calibrated through adaptive analysis and an exponential function fitted. In summary, the function of $\Lambda_2(U_r, d)$ is a combination of an exponential function of d and a sixth-order polynomial function of U_r/Re , as follows:

$$\Lambda_2 = (3.206e^{-0.450d} + 1.163e^{-0.025d})[(43.59U_r^2 - 626U_r + 2669)/(U_r^2 - 5.29U_r + 19.82)] \quad (2-40)$$

Each exponential or polynomial function is plotted in Figure 2-6a and the combined functions are plotted in Figure 2-6b with contour isolines of Λ_2 values, for the range of $5 < U_r \leq 30$ ($0.4 \times 10^4 < Re \leq 2.3 \times 10^4$) and $4 \leq d \leq 20$. In Figure 2-6a, Λ_2 decreases as d is increased. In contrast, as U_r is increased, Λ_2 initially decreases for $U_r < 9$ and then increases for $U_r > 9$. This suggests that the polynomial function captures a VIV-to-WIV transition feature around a narrow range of $5 < U_r < 10$ whereas the exponential function contributes to the prediction of WIV feature. The combined functions in Figure 2-6b provide the best-fit predictions of response amplitudes obtained by the present model.

For a summary of calibrated wake oscillator parameters refer to Table 2-2.

Table 2-2: Summary of Calibrated Wake Oscillator Parameters

Parameter	Value
ϵ_1	0.011
ϵ_2	0.1
Λ_1	10
Λ_2	$(3.206e^{-0.450d} + 1.163e^{-0.025d})[(43.59U_r^2 - 626U_r + 2669)/(U_r^2 - 5.29U_r + 19.82)]$

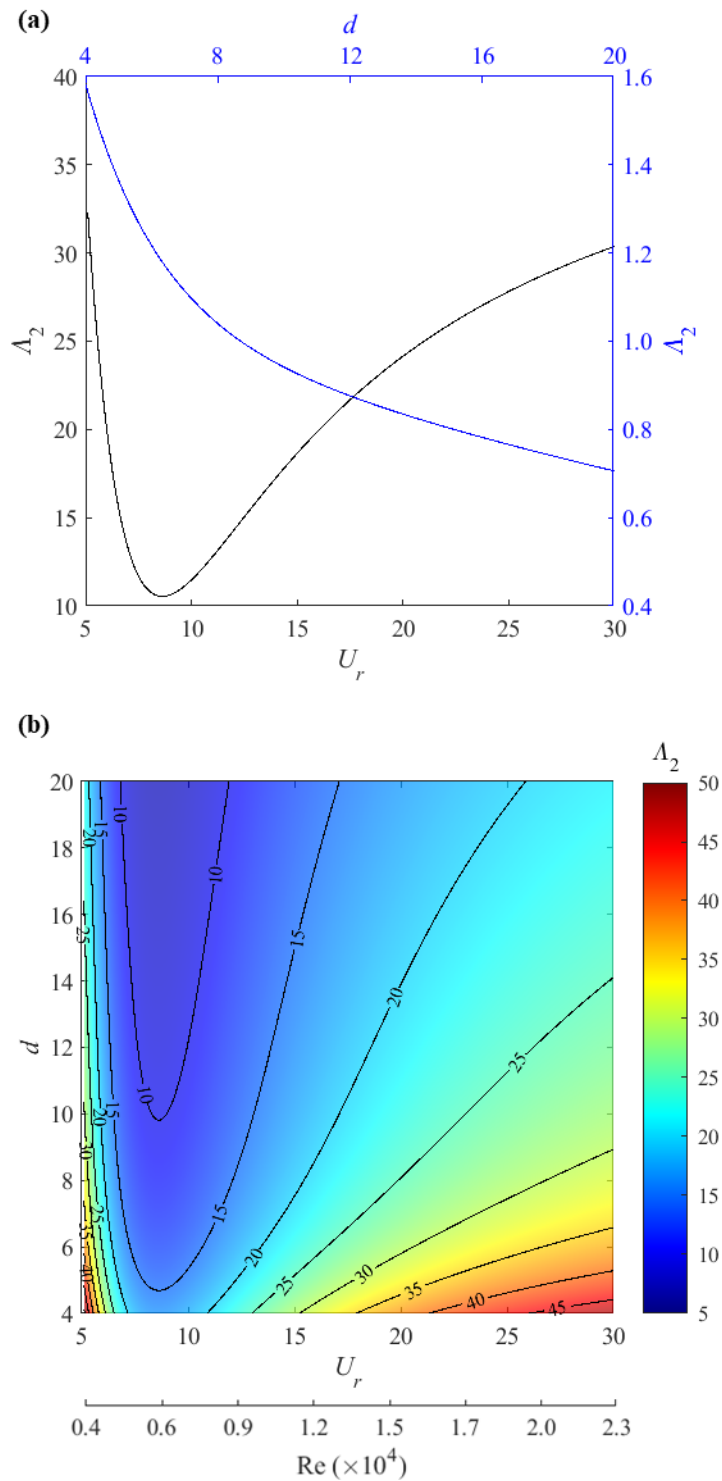


Figure 2-6: Variation of empirical wake-deficit oscillator variable (a) as a function of U_r or d , and (b) as a function of combined U_r and d .

2.5. Dynamic Response of the Downstream Cylinder

As previously discussed, the minimum separation between the tandem cylinders is always greater than or equal to $4D$. This ensures that both cylinders can fully develop their vortex streets. The co-shedding regime, associated with configurations that possess a d greater than the critical spacing, entails that the forces on the front cylinder

are similar to those on a single cylinder [21], i.e. the first cylinder behaves as an isolated cylinder subjected to VIV, since it is not affected by the second cylinder. The dynamic response of one cylinder under classical VIV has been widely studied and for this reason the focus is now on the more complex 1DOF response of the downstream cylinder only and not of the upstream cylinder.

Having calibrated the proposed model with high fidelity experimental data and having obtained the optimal input parameters for the fixed-free and free-free cases, attention is now focused on the results of the computational solution of the model and its capability to predict the main features of the involved phenomena, including oscillation amplitudes and frequencies and time histories.

2.5.1. 1DOF WIV Amplitudes of Vibrations

Figure 2-7 presents comparisons of numerical and experimental response amplitudes per diameter of the downstream cylinder (A_2/D) in fixed-free (2-7a) and free-free (2-7b) tandem cases based on the calibrated coefficients and functions (λ , α , β , ε_2 , Λ_2). For the upstream cylinder response undergoing VIV in free-free tandem cases, $\varepsilon_1 = 0.011$ and $\Lambda_1 = 8.5$ are used based on calibration of response amplitudes with the experimental data of Assi *et al.* [11] for a single cylinder with the same $m^* = 2.6$ and $\xi = 0.007$ in a uniform flow. This single cylinder case is equivalent to the downstream isolated cylinder with a very large spacing whose results, represented by A_2/D ($\approx A_1/D$), are shown in Figure 2-7b. Note that A_2/D is numerically obtained by calculating a root-mean-squared displacement and then multiplying the resulting value by $\sqrt{2}$. This numerical estimation is consistent with the post-processing method in Assi *et al.* [11]. Recent CFD results of Lin *et al.* [58] with the same $m^* = 2.6$, $\xi = 0.007$ and $d = 4$ are also compared in Figure 2-7a and b. Further, for $2 < U_r < 15$, experimental A_2/D results in free-free tandem cases from Assi [59] with $m^* = 1.92$, $\xi = 0.007$, $2 \times 10^3 \leq \text{Re} \leq 1.2 \times 10^4$, $d = 4, 5$ and 5.6 , and those of Pereira *et al.* [24] with $m^* = 2.52$ for the downstream cylinder and $m^* = 2.95$ for upstream cylinder, $\xi = 0.025$, $3 \times 10^3 \leq \text{Re} \leq 3 \times 10^4$ and $d = 4$ are presented in Figure 2-7b.

For the fixed-free tandem cases in Figure 2-7a, numerical and experimental results agree that the A_2/D response builds up as $U_r > 0$ and attains a resonance peak of $A_2/D \approx 0.8$ at $U_r \approx 5$, in all d cases. This is associated with a pure VIV resonance of the downstream cylinder. For a single cylinder with $m^*\xi \approx 0.013$ [56] or 0.014 [60], similar to the present $m^*\xi = 0.0182$, the peak $A_2/D \approx 0.9$ has been experimentally reported. For small spacings of $d = 4$ to 6 , A_2/D responses in Figure 2-7a first slightly

decrease in a transitional $5 < U_r < 8$ range where VIV is evolving to WIV, after which a galloping-like WIV feature occurs with A_2/D growing almost monotonically when further increasing U_r . CFD results agree well with numerical predictions and experimental results where the minimum $d = 4$ case shows the highest growth rate of A_2/D achieving the maximum value at the maximum $U_r = 30$ ($Re = 2.3 \times 10^4$). For the moderate spacing of $d = 8$, a plateau response feature is revealed such that A_2/D appears to be relatively sustained with a value of about 0.8 on average for $U_r > 5$. As d is further increased to 10, the lower A_2/D branch reappears in the range of $5 < U_r < 15$ after which a moderate amplitude of about 0.4 persists throughout the remaining higher U_r range. Finally, the response resembles the VIV behaviour with a small-amplitude ($A_2/D \approx 0.1$) lower branch prevailing when $U_r > 10$ for the highest $d = 20$ where the upstream wake interference effect becomes less significant. For such a large spacing, the downstream cylinder is nearly dependent on the free stream flow. Overall, the present model captures VIV and three WIV qualitative features of the downstream cylinder exhibiting (i) a growing response for a low d , (ii) a plateau response for an intermediate d , and (iii) a VIV-like response for a high d , with acceptable amplitude comparisons vs. experimental data.

Figure 2-7b shows comparisons of numerically predicted A_2/D results for fixed-free vs. free-free tandem cases with $m^* = 2.6$ and $\xi = 0.007$ for a representative $d = 4, 8$ or 20 and $2 < U_r < 20$. Results reveal greater WIV amplitudes in free-free tandem cases, suggesting the effect of upstream cylinder response and associated δy on the hydrodynamic force and downstream response prediction.

However, both fixed-free and free-free tandem cylinders exhibit similar numerical WIV features with large vibration amplitudes which are also shown by results of Assi [59] and Pereira *et al.* [24]. CFD results in the free-free tandem case with the same $m^*\zeta$ and $d = 4$ from Lin *et al.* [58] agree well with the numerical prediction, with the increasing response trend and comparable amplitudes for a limited range of $6 \leq U_r \leq 8.9$ ($6750 \leq Re \leq 10^4$). Overall, experimental and numerical responses reveal some amplitude discrepancies, and these are attributed to differences in the system parameters (m^*, ζ, Re, U_r, d) since wake oscillators have been calibrated in fixed-free tandem cases with the results of Assi *et al.* [11]. A re-tuning with results of Assi [59] and Pereira *et al.* [24] could be performed, but this task could be repeated indefinitely and is particular to a certain d, m^*, ζ, Re and U_r range and that is ignoring the fact that some of the two-cylinder properties may be dissimilar (e.g., Pereira *et al.* [24]).

Moreover, amplitudes of vibration after the initial VIV regime are slightly different for a system with a marginally larger separation, $d = 6$ shown in Figure 2-7. Now, the oscillation amplitudes do not grow as rapidly. Instead, experimental amplitudes of vibration slowly increase with U_r , almost sustaining the same level of A_2/D of the first VIV peak at $U_r \sim 5$. On the other hand, modelled results slightly contrast with this amplitude plateau. Moreover, when amplitudes of vibration of a much wider spaced system, $d = 20$ in Figure 2-7 are analysed, a totally different regime of amplitude response is observed. In fact, the complete A_2/D curve resembles that of classical VIV. Therefore, it is postulated that the evolution of d from the minimum $d = 4$ to the maximum studied $d = 20$, by gradually going over each of the four systems in Figure 2-7, results in three different regimes of response of the downstream cylinder: a) a build-up regime of A_2/D leading to the largest oscillation amplitudes for a low d , as observed in Figure 2-7a and b; b) a transitional regime of A_2/D for which amplitudes of vibration are sustained or almost at a constant level, for instance, for $d = 6$ in Figure 2-7; and c) VIV-like response regime for large spacings as in Figure 2-7, $d = 20$.

The build-up of amplitude or the WIV regime is observed for low spacings, where an upward high-amplitude branch develops after transition from the first VIV peak ($U_r > 5$). It results in significantly higher amplitudes than pure VIV and it is assumed to be directly related to the WIV mechanism. This relationship will be further explored in Section 2.5.4 where the frequency domain of the response of the rear cylinder will be analysed to support this assumption.

The VIV amplitude regime occurs for large spacings because, in the limiting case, the second cylinder is so far downstream of the first cylinder that vortices and wake flow diffuse so that the flow downstream returns to free-stream conditions ($u = U_\infty$ at $T = 0$). Thus, each of the separate cylinders would be expected to behave as single cylinders only subject to VIV, i.e. the amplitude response consists of a lock-in region with large oscillation amplitudes and desynchronization with U_r increase that results in low A_2/D .

The transitional amplitude regime from WIV happens for intermediate spacings and is responsible for a switch from WIV to VIV response regimes and excitation mechanisms. If a scenario is imagined for which the rear cylinder is sufficiently far from the front cylinder, but not so far as to avoid the wake from completely dissipating ($u_2 \leq 0.99U_\infty$ at $T = 0$), then wake effects may be modest, but not insignificant. Hence, it is reasonable to assume that the response of the second cylinder may consist of a

combination between WIV rising amplitudes of vibration and VIV classical lock-in and desynchronization response. It is postulated that this occurs for $d > 6$ in Figure 2-7 and, from the experimental point of view, this is observed in the amplitudes of oscillations for $d = 8-20$ in the study of Assi *et al.* [11].

In summary, the dynamic response of the downstream cylinder for every spacing consists of the first VIV peak ($U_r \approx 5$) and after that, increasing U_r provokes a transition to WIV amplitude build up, pure VIV or a combination of the two, depending on d for a given system. As it will be explained in the following section, these are not only branches of amplitude of vibrations, but it is proposed that they are three response regimes based on observation and that these regimes govern how the second cylinder behaves, being reflected in forces and frequencies of the system. Further investigation was conducted and, as it will be detailed in the following study of dominant oscillation frequencies, these regimes may be associated with three different mechanisms interacting in the dynamics of a pair of cylinders.

Based on the calibrated wake profile and wake oscillators, Figure 2-8 displays the predicted response contours of the downstream cylinder with contours of amplitude values (A_2/D) in the case of varying m^* and U_r (Re) for a fixed $\zeta = 0.007$. Three spacing cases with $d = 4$ (Figure 2-8a, b), $d = 8$ (Figure 2-8c, d) and $d = 20$ (Figure 2-8e, f) are considered, comparing between fixed–free (Figure 2-8a, c, e) and free–free tandem (Figure 2-8b, d, f) cases. It can be seen that the model is capable of predicting a realistic trend of the downstream cylinder dynamics for which A_2/D increases with decreasing m^* and d . For the minimum $d = 4$, the WIV response feature appears in all m^* cases with a maximum A_2/D reaching a value of almost 2 for $m^* = 1$ and $U_r = 30$ in both tandem cases. The free vibration of the upstream cylinder affects the patterns and ranges of contour lines depending on the m^* - U_r combination (see, e.g., Figure 2-8b vs. a). For the intermediate $d = 8$, the plateau response feature, which is noticed in the lower $m^* < 3.5$ range, disappears in the higher $m^* > 3.5$ range in the fixed–free tandem case. This $m^* \approx 3.5$ threshold is shifted to a higher $m^* = 5$ in the free–free tandem case widening the WIV excitation. For the high spacing of $d = 20$, the general VIV-like resonance feature with a small $A_2/D \approx 0.2$ in a high U_r range becomes a plateau response when decreasing m^* towards the neutrally buoyant condition ($m^* = 1$) such that the maximum A_2/D is increased to 0.4 in the fixed–free tandem case and 0.6 in the free–free tandem case. Overall prediction results in Figure 2-8 highlight the

combined effects of d , U_r (Re), m^* and the upstream response in both qualitative and quantitative behaviours of the downstream cylinder undergoing WIV.

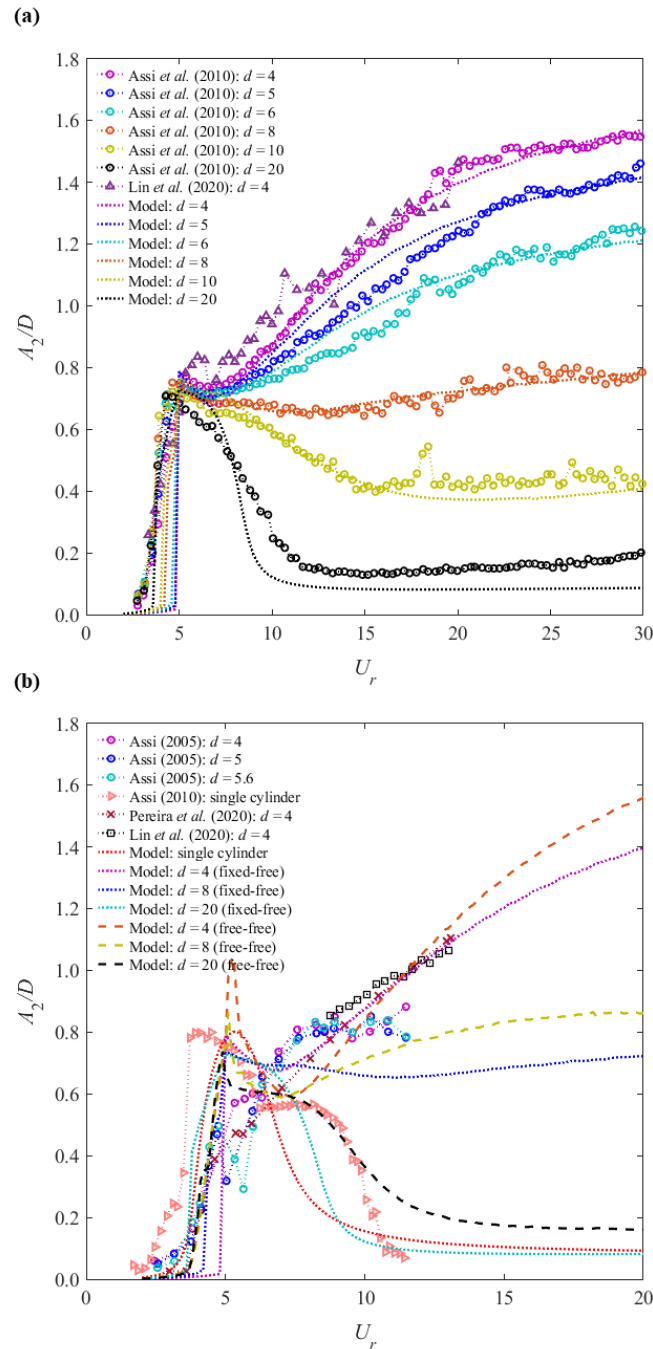


Figure 2-7: Comparison of response amplitude of vibrations of the downstream cylinder with varying U_r and d : (a) numerical and experimental results in fixed-free tandem cases, (b) numerical results in fixed-free vs. free-free tandem cases, with experimental results in free-free tandem and single cylinder cases.

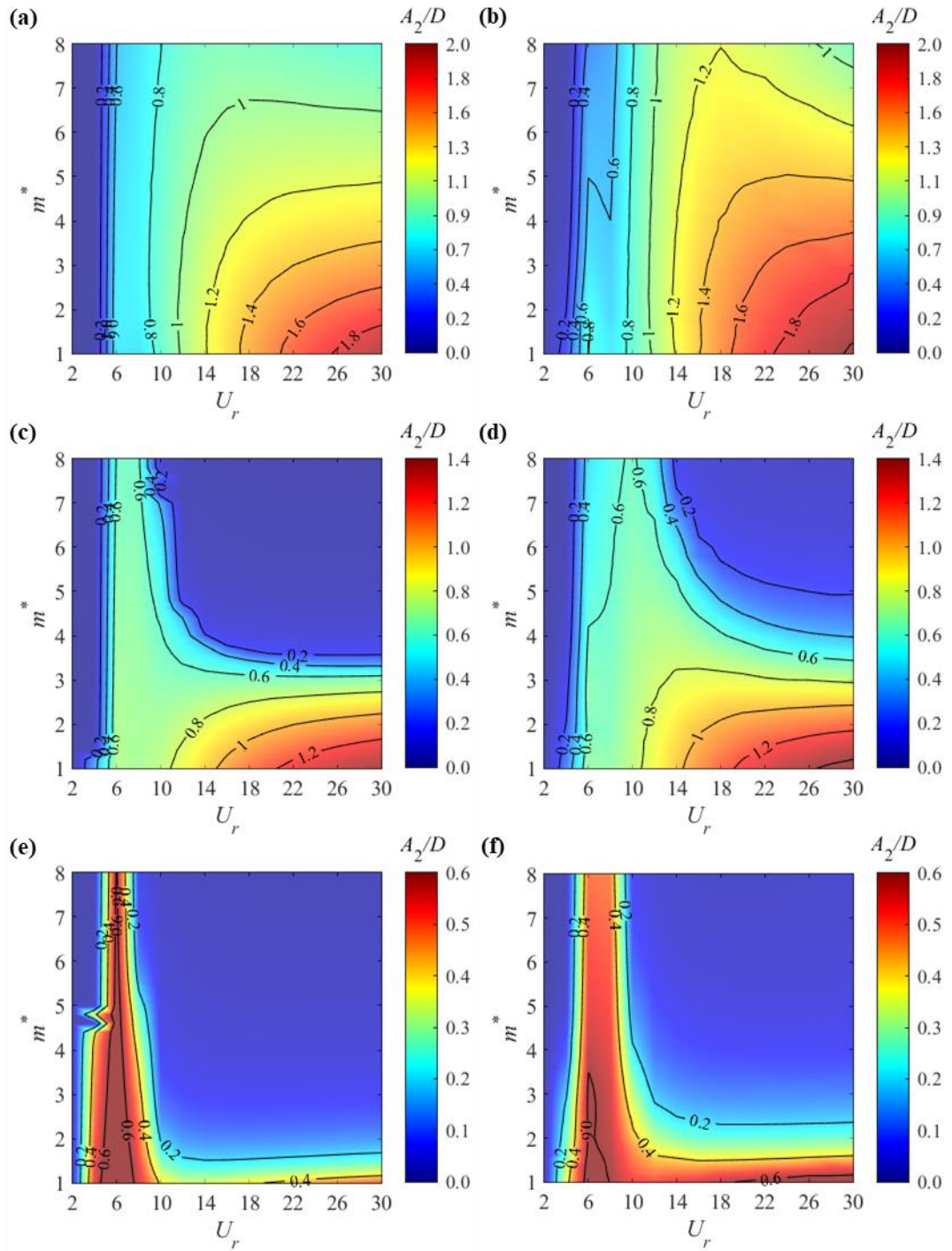


Figure 2-8: Study of the effect of mass ratio on the modelled response of the downstream cylinder and dependency on the spacing between the cylinders with $\zeta = 0.7\%$ for fixed-free (a, c, e) versus free-free (b, d, f) tandem cases: (a, b) $d = 4$, (c, d) $d = 8$ and (e, f) $d = 20$.

2.5.2. Temporal Behaviour of the Downstream Cylinder

Three particular U_r cases for $d = 4$ have been selected for investigation and dimensionless time histories in the range of $t = 0-200$ for q_1 , y_1 , χ , C_{L12} , q_2 and y_2 are presented in Figure 2-9 for $U_r = 5, 6$ and 15 demonstrating VIV, VIV-to-WIV transition and WIV features of the downstream cylinder, respectively.

The reduced velocity cases of $U_r = 5$ and 6 have been selected, despite their small difference, because this reduced velocity range has been identified as a sensitive area for the system. As it has been explained in Section 2.5.1, the first VIV regime is observed for the lowest reduced velocities up to approximately $U_r = 5$. Therefore, refining the study for $U_r = 5$ and 6, for instance, may reveal interesting points.

Even though the behaviour of the first cylinder is not the main interest of the present study, its wake variable, q_1 and its transverse displacement component, y_1 , are plotted as reference and comparison in the first two rows of Figure 2-9 respectively.

Initially, it is observed that q_1 and y_1 behave in similar ways one to another. This may be explained as the two variables are strongly coupled, as is evident from Equations (2-36) and (2-38). However, even though q_1 and y_1 are qualitatively similar, with trends and response behaviours that are alike, on the other hand they are quantitatively distant, where the magnitude of q_1 is one order higher than for y_1 . It is seen that q_1 is significantly larger than y_1 for each of the three cases investigated. This is also expected as q_1 is a wake variable forcedly related to the transverse hydrodynamic force acting on the first cylinder, which is damped before opposing the inertia of the body.

Moving on to analysing the wake-induced properties and quantities related to the dynamics of the downstream cylinder, fixed-free results (black line) have been compared to the free-free results (red line). Regarding the wake deficit variable, χ , one may notice that fixed-free values are on average greater than the corresponding free-free values for all three U_r points. Moreover, whilst the fixed-free response is relatively organised, the free-free configuration behaves in a contrasting manner. This is true not only for χ but also for the remaining variables of interest for $d = 4$ and all three U_r cases.

Additionally, a greater average wake flow velocity, as observed for the fixed-free pair of cylinders (greater χ), generates a larger wake-induced lift coefficient. On the other hand, magnitudes of q_2 are almost the same for both fixed-free and free-free schemes, although q_2 exhibits amplitude modulation for the free-free case.

Despite both C_{L12} and q_2 , which are related to the forcing terms in Equations (2-37) and (2-39), being greater for the fixed-free configuration than for the free-free case, amplitudes of transverse vibrations of the downstream cylinder show a different trend, where y_2 is greater for the second cylinder at least for $U_r = 5$. This is understood to be related to the point of transition after the first VIV regime, i.e. VIV to WIV mechanism transition, as previously discussed. This is also seen in Figure 2-7 for

which the fixed-free downstream cylinder transitions to WIV for a lower reduced velocity than the free-free corresponding system. The average difference for y_2 is almost negligible with the increase of $U_r = 15$ as seen from Figure 2-9.

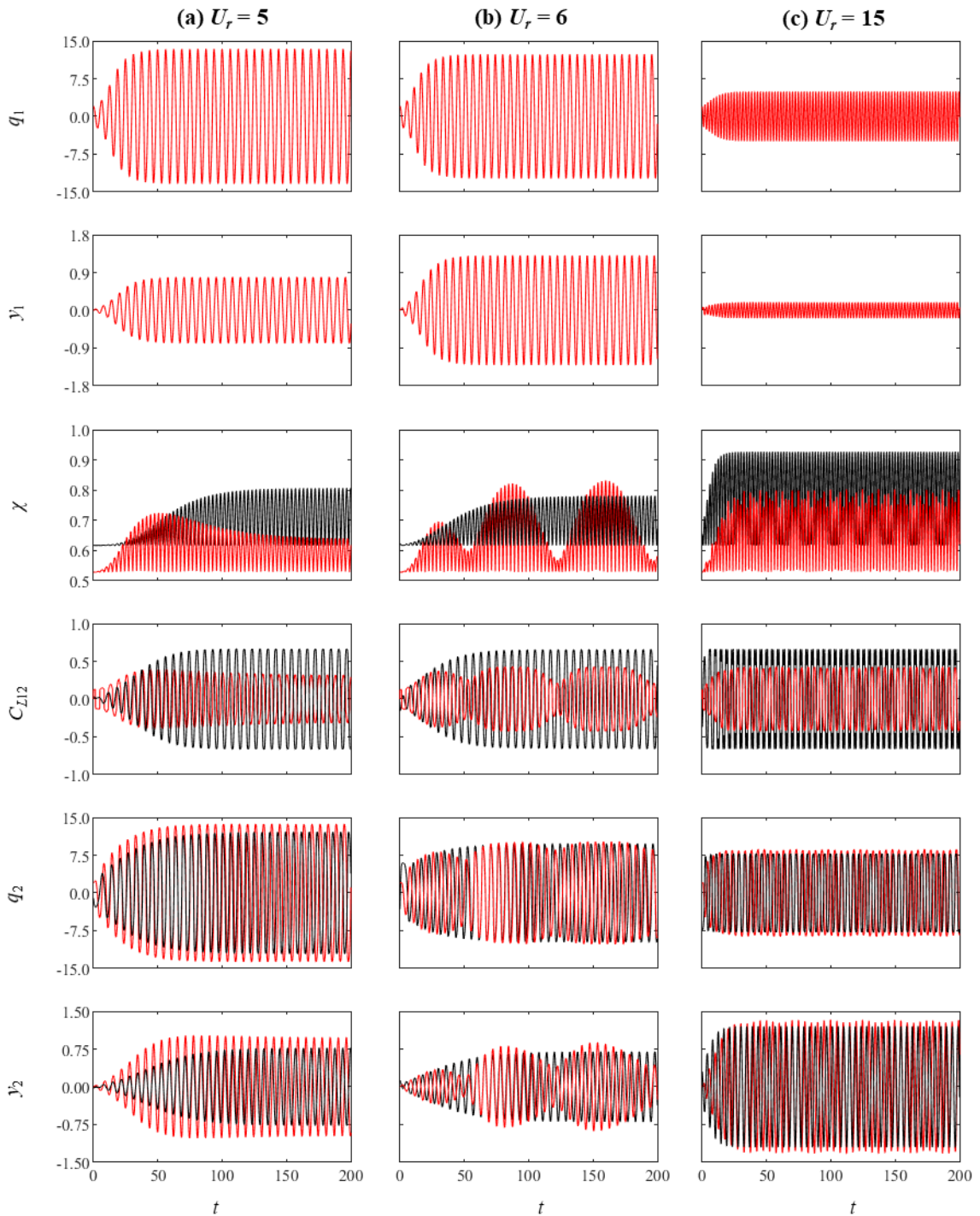


Figure 2-9: Time histories of wake oscillator variables (q_1 , q_2), wake deficit function (χ), wake-induced transverse force coefficient (C_{L12}) and cylinder responses (y_1 , y_2) for three specified $U_r = 5, 6$ and 15 : red (black) line denotes free-free (fixed-free) tandem case with $d = 4$.

Qualitatively, the time series of transverse displacements of the rear cylinder, y_2 , are not dissimilar to the wake variable, q_2 , as it happens to be for the first cylinder (y_1

and q_1). In fact, y_2 appears to be the result of a combination of q_2 and C_{L12} as could be noticed from Equation (2-39).

In conclusion, the response of the downstream cylinder is regular and well-behaved for $U_r = 5$ and similar to the upstream cylinder for both fixed-free and free-free studies. When the reduced velocity is further increased to $U_r = 6$, amplitude modulation and additional frequencies are seen. This suggests that additional mechanisms start to interact within the system. It is proposed that this is a region that the transition VIV-WIV occurs, which is in agreement with literature studies [11]. For higher reduced velocities, herein at about $U_r = 15$, the magnitude of oscillations of the downstream cylinder is considerably larger than for an upstream cylinder. This is also observed in literature studies [11, 12] and in Figure 2-7. Moreover, for all U_r cases it is worth recalling that the minimum or time-averaged value of χ in the free-free tandem case is lower than that in the fixed-free tandem case because of the greater influence of the upstream cylinder oscillation and the resulting greater δy variation on the wake shielding and spreading as shown in Figure 2-3. In Figure 2-9, all the crossflow responses of upstream and downstream cylinders have zero mean components since the two cylinders initially start from a tandem configuration aligned with the wake centreline. The zero-mean y_2 responses are further confirmed in Figure 2-10 and Figure 2-11 with variation d from 4 to 20. Despite the relative transverse positions ($\pm\delta y$ in Figure 2-10a and Figure 2-11a) during the oscillations across the wake resulting in the modified inline (Figure 2-10b and Figure 2-11b) and transverse (Figure 2-10c and Figure 2-11c) forces, the transverse load acts upon the downstream cylinder in the opposite inward direction ($\pm C_{L12}$) towards the wake centreline. These model predictions are in qualitative agreement with experimental observations (e.g., Bokaian and Geoola [39]).

The dependency of instantaneous cylinder responses on the initial spacing is also highlighted in Figure 2-10 and Figure 2-11. The four contour subplots of Figure 2-10 show that the general time-varying trends of δy , χ , C_{L12} , y_2 are disturbed by a visual trend that is seen as amplitude modulations. This agrees with what has been observed in Figure 2-9 for y_2 . Therefore, amplitude modulations for $U_r = 6$ are observed for the full range $d = 4 - 20$.

Previously, it has been shown that the responses even for the downstream cylinder are regular for $U_r = 5$ whilst the transverse response of the upstream cylinder is mostly regular, independent of U_r (Figure 2-9). Hence, it is inferred that the amplitude

modulation in the time series of $\bar{\delta}_y$ presented in Figure 2-10 and Figure 2-11 should be related to y_2 and not y_1 .

The fact that amplitude modulations of y_2 are still observed for $d = 20$, even if with a lower proportion, is interesting as it suggests that WIV is still present even for such a large spacing, $d = 20$. This suggestion comes from the difference between time-varying responses of y_1 (Figure 2-9) and y_2 for $d = 20$ (Figure 2-10), indicating that the downstream cylinder is still affected by WIV as it has not yet fully returned to behaving as a single cylinder.

Moreover, the d -evolution of time histories are displayed in Figure 2-11 for $U_r = 10$. This time, a higher degree of irregularity is observed in the responses linked to the downstream cylinder and a greater variation is observed with increase of d . This is also seen in Figure 2-7 for a high reduced velocity. For a high U_r , variation of spacing greatly influences the system, where the downstream cylinder may have a build-up of oscillation amplitudes or be returning to single-cylinder dynamics.

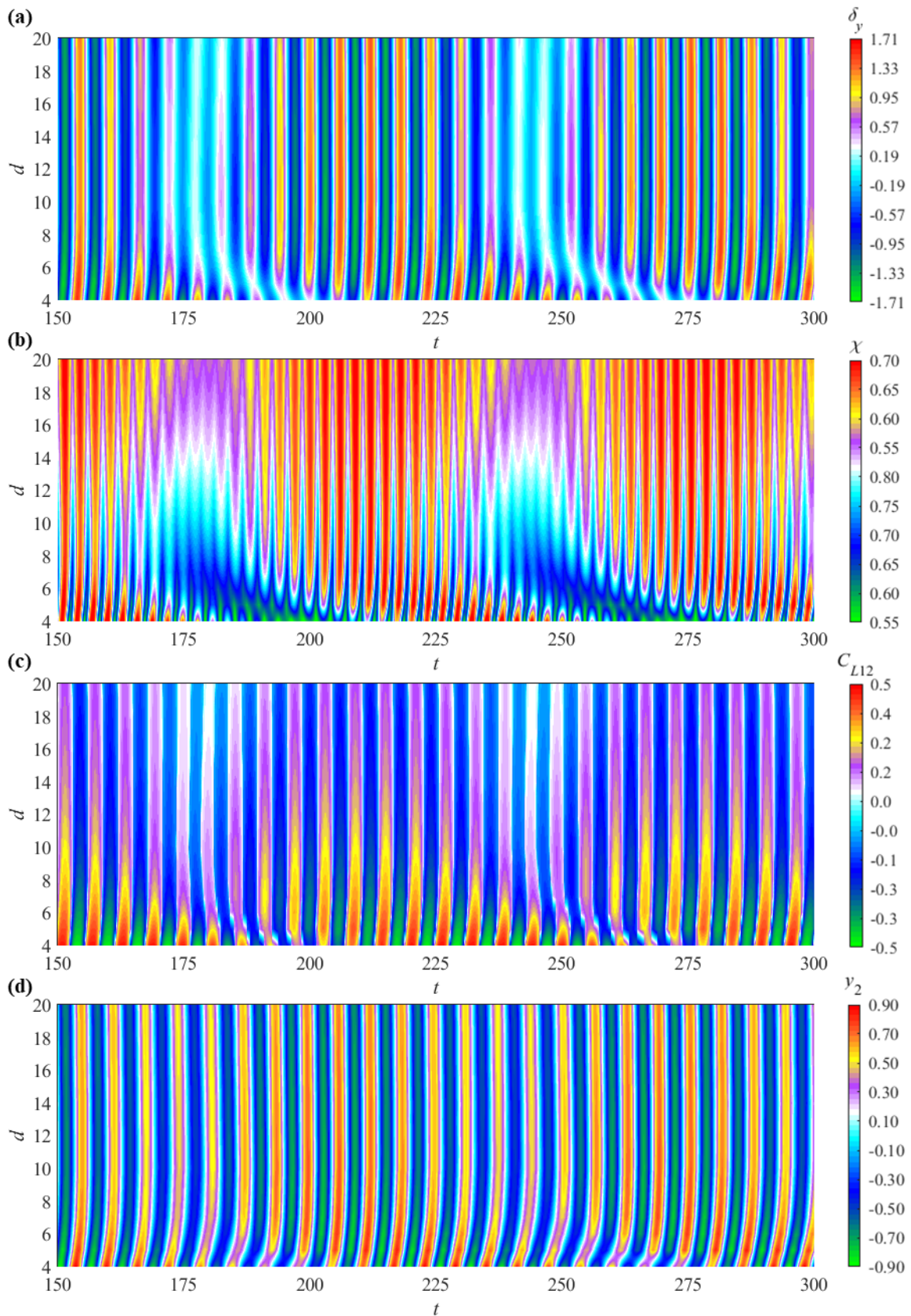


Figure 2-10: Time histories dependency on the variation of initial spacing for two oscillating cylinders at $U_r = 6$. (a) δ_y . (b) χ . (c) C_{L12} . (d) y_2 .

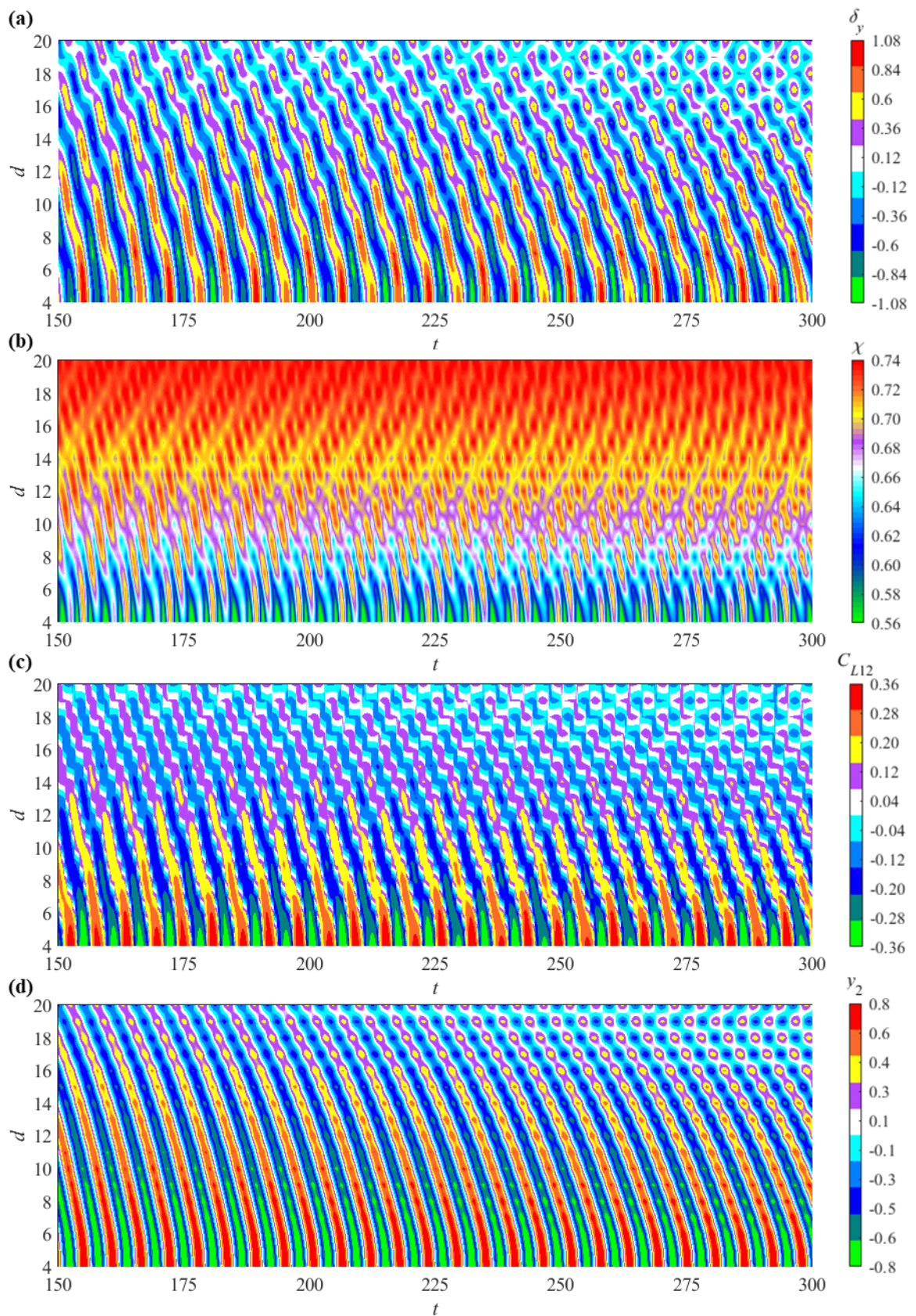


Figure 2-11: Time histories dependency on the variation of initial spacing for two oscillating cylinders at $U_r = 10$. (a) δ_y . (b) χ . (c) C_{L12} . (d) y_2 .

2.5.3. Modelling of the Wake Stiffness Concept

Prior to the analysis of oscillation frequencies of the second cylinder, it is important to introduce the concept of the wake stiffness [12], given its importance in identifying WIV frequencies as will be discussed later.

Assi *et al.* [12] conducted experiments for tandem cylinders with an unsupported rear cylinder. Interestingly, they proved that their downstream cylinder still developed oscillatory motion in the crossflow direction even without the restoring force from springs. In fact, amplitudes of vibration for the second cylinder, without springs, were comparable to the case with springs, apart from the first VIV regime within $U_r \leq 5$ which disappeared, as expected from the removal of the springs (k) and consequently VIV excitation frequency would not lock-in to the natural frequency given its relationship with the stiffness of the system.

The observation that the cylinder sustained vibrations even without springs instead of just drifting away from the initial position indicates that somehow another restoring force acts on the cylinder. The authors concluded that it is the steady wake-induced lift force which plays the role of a hydrodynamic balancing force. The mean C_{L12} is always directed towards the wake centreline and, thus, exercises a restoring action on the vibrating downstream cylinder. It has been proposed that the C_{L12} profile across the wake, similar to the stiffness of a spring, behaves approximately linearly between its maximum and minimum antisymmetric peaks, around $-1 \leq T \leq 1$ (for low spacings), as seen in Figure 2-4 for example. Therefore, the slope $\partial C_{L12}/\partial T$ may be approximated to $\Delta C_{L12}/\Delta T$ within the nominal linear region and is defined as the wake stiffness.

However, not only does the steady C_{L12} depend on the transverse position across the wake, but also it depends on d . It is observed that for a low d , C_{L12} is larger, and its antisymmetric peaks are situated closer to the wake centreline ($T = 0$) in a way that its behaviour may be effectively simplified and considered linear. On the other hand, increasing d leads to a decrease of the mean C_{L12} and disperses the antisymmetric peaks away from the wake centreline. Hence, in order for the linear approximation employed in the wake stiffness concept to remain valid or acceptable, it should account for $C_{L12}(d, T)$. Thus, following Assi *et al.* [12], the equivalent natural frequency associated with the wake stiffness is:

$$f_w = \frac{1}{2\pi} \frac{U_\infty}{D} \sqrt{\frac{2 \partial C_{L12}/\partial T}{\pi (m^* + C_a)}} \quad (2-41)$$

Thereafter, $\partial C_{L12}/\partial T$ can be analytically derived based on the function of C_{L12} in Equation (2-24) as:

$$\frac{\partial C_{L12}(d, T)}{\partial T} = \frac{\partial C_{L12}(d, \delta y)}{\partial \delta y} = - \frac{8\lambda C_{D2}}{d^{3/2} C_{D1}^{1/2}} \left[\left(\frac{C_{D1}}{d} \right)^{1/2} \left\{ \alpha \frac{\eta}{2} e^{-\frac{\eta^2}{4}} + \beta \frac{\eta}{2} e^{-\frac{\eta^2}{4}} \int_0^\eta e^{\frac{\varphi^2}{4} d \varphi} - \beta \right\} \right] \left[\alpha \frac{\eta}{2} e^{-\frac{\eta^2}{4}} - \beta \left\{ 1 - \frac{\eta}{2} e^{-\frac{\eta^2}{4}} \int_0^\eta e^{\frac{\varphi^2}{4} d \varphi} \right\} \right] + \left[\chi \left(\frac{\alpha}{4} (2 - \eta^2) e^{-\frac{\eta^2}{4}} + \frac{\beta}{2} \left\{ e^{-\frac{\eta^2}{4}} \int_0^\eta e^{\frac{\varphi^2}{4} d \varphi} - \frac{\eta^2}{2} e^{-\frac{\eta^2}{4}} \int_0^\eta e^{\frac{\varphi^2}{4} d \varphi} + \eta \right\} \right) \right] \quad (2-42)$$

In contrast to Assi *et al.* [12] who employed a constant gradient $\partial C_{L12}/\partial T \approx \Delta C_{L12}/\Delta T = 0.65$ within the limited linear range of C_{L12} across the wake within $-1 \leq y_2 \leq 1$ at $d = 4$ for the fixed-free tandem system, Equation (2-41) which is nonlinear and has been introduced to parametrically capture (i) the dynamic effects of δy in the system, (ii) the higher-order nonlinear effect of cylinder response when $|y_2| > 1$, (iii) the influence of Re when varying U_∞ (U_r and χU_r), (iv) the dependence of the wake stiffness with spacing d , and (v) a more general approach for the wake flow behind an oscillating as well as a static upstream cylinder.

For a given range of $-3 \leq \delta y \leq 3$, results of ΔC_{L12} based on Equation (2-41) are shown in Figure 2-12a-d for $d = 4, 6, 8$ and 20 , respectively, by comparing fixed-free and free-free tandem cases depending on the associated wake profiles (Figure 2-3).

For the simulated cases of real oscillations of the tandem cylinders for both fixed-free and free-free cases, the behaviour of ΔC_{L12} has been analysed for three different reduced velocities throughout the complete range of spacings considered and results have been plotted in Figure 2-12 (e,f). For all three examined reduced velocities, ΔC_{L12} diminishes with increase of d , although this trend is considerably intensified for the fixed-free cases compared to the case where both cylinders are free to vibrate. This indicates that the fixed-free ΔC_{L12} is more dependent on the spacing than its free-free equivalent, as is also reflected in Figure 2-12 (a-d).

In terms of U_r variation, it is observed that both fixed-free and free-free cases are weakly dependent on U_r and consequently Re within the ranges considered. In fact, the two highest U_r curves in Figure 2-12 (e,f) are quite similar. For both fixed-free and free-free configurations, ΔC_{L12} curves for $U_r = 15$ and 20 start off at a lower value for $d = 4$ than the $U_r = 6$ curve, whereas this feature is reversed when d is increased to 20 . Indeed, ΔC_{L12} behaves smoothly for $U_r = 6$ and less so for the other two U_r cases analysed. An explanation for that comes from the study of amplitudes of vibration of

the cylinders. For $U_r = 6$, the downstream cylinder behaves similarly for every spacing considered as it is within the first VIV peak. This has been demonstrated in Figure 2-7. On the other hand, larger $U_r = 15$ and 20 cases show a strong dependency between the response of the second cylinder and the spacing. Depending on the spacing range the downstream cylinder could be oscillating mainly in the WIV regime which would lead to large amplitudes of vibration, or it could be excited prominently by VIV yielding lower oscillation amplitudes.

In conclusion, the gradient ΔC_{L12} depends greatly on the spacing between the cylinders, especially for the fixed-free but also for the free-free case. However, U_r and Re do not seem to contribute to considerable variation of ΔC_{L12} within the ranges of study. The dependency on d is clearly reflected onto the wake stiffness equivalent frequencies, even though at lower proportions than for ΔC_{L12} .

It can be seen that the maximum ΔC_{L12} takes place along the wake centreline ($\delta y = 0$) in all tandem cases because of a sudden change in C_{L12} from being positive ($\delta y < 0$) to negative ($\delta y > 0$), as shown in Figure 2-4. The maximum ΔC_{L12} decreases as d is increased from 4 (Figure 2-12a) to 20 (Figure 2-12d) since the wake flow effect is reduced for such a large spacing between the cylinders. For $d = 4, 6$ and 8 , the maximum ΔC_{L12} for the fixed-free tandem case is greater than the corresponding free-free because the wake shielding effect is centred around the centreline, whereas the wake flow spreads laterally (for greater T extremities) due to the motion of the upstream cylinder leading to a shift in C_{L12} peaks and, in turn, a reduction of C_{L12} gradients. However, for the higher $d = 20$ the relative motion between the cylinders decreases and, as seen in Figure 2-7, the downstream cylinder has its oscillation amplitudes greatly reduced, behaving almost the same as the upstream cylinder. Towards the maximum dual C_{L12} values off the centreline ($\delta y > 0$ and $\delta y < 0$), there are corresponding equal peaks of ΔC_{L12} , depending on d , on the wake flow thickness (boundaries) and whether the upstream cylinder oscillates.

For all d , C_{L12} peaks in the free-free tandem case occur at greater $|\delta y|$ locations. The off-centreline ΔC_{L12} peak values in the fixed-free tandem case are greater than those in the free-free case for the low $d = 4$. However, the values of the former case become comparable to and lower than the latter ones for the intermediate $d = 8$ and high $d = 20$, respectively. Overall results in Figure 2-12a-d highlight the dependence of the gradient ΔC_{L12} and consequently of the wake stiffness concept, on the cylinder relative position δy , the upstream cylinder's response and d .

At $d = 4$ and $|y_2| = 1$ (or $|\delta y| = 1$ as $y_1 = 0$), Figure 2-12a predicts, based on Equation (41), that $\Delta C_{L12} \approx 0.6$ which is comparable to the approximation $\Delta C_{L12} \approx 0.65$ suggested by Assi *et al.* [12]. For free vibrations of tandem cylinders, it is also worthwhile predicting the time-averaged wake stiffness by accounting for unsteadiness of the relative transverse cylinder positions, δy , during their oscillations (e.g., Figure 2-10a and Figure 2-11a through Equation (2-41)). For a given $U_r = 6, 15$ and 20 , Figure 2-12e-f present the variation of the root-mean-squared ΔC_{L12} versus d in the fixed-free and free-free tandem cases, respectively. In all cases, it is seen that the averaged wake stiffness value is inversely proportional to d since wake flow effects lose energy with d . The fixed-free tandem case shows a greater range of ΔC_{L12} variation (from 0.85 to 0.14) because of the greater δy dependence as shown in Figure 2-12a-d. For a given d , ΔC_{L12} changes slightly at the higher $U_r = 15$ and 20 ,

reflecting the similarity in δy variation ($-1 \leq \delta y \leq 1$) associated with a WIV response (see, e.g., Figure 2-11a). The invariance of ΔC_{L12} within the present Re (U_r) range has also been observed in Assi *et al.* [12]. However, there is a transition around $d = 8$ where ΔC_{L12} reveals both the U_r (equivalently Re) and d dependence: ΔC_{L12} at $U_r = 6$ is greater than for $U_r = 15$ and 20 when $d < 8$, whereas the former becomes smaller when $d > 8$. This transition coincides with the change in the downstream response behaviour from experiencing VIV ($U_r < 10$) to WIV ($U_r > 10$), and with the prediction that the two tandem cylinders experience the greater δy unsteadiness ($-1.7 \leq \delta y \leq 1.7$) in a lower U_r range as depicted in Figure 2-10a.

Having introduced the wake stiffness concept, frequencies of oscillation will be investigated and Equation (2-41) will be employed for correlation with the WIV mechanism. It is believed that the wake stiffness frequencies are closely related to the frequencies of the WIV mechanism due to its connection to the wake-induced lift coefficient and due to the fact that for a downstream cylinder to oscillate without springs, as demonstrated by Assi *et al.* [12], then WIV must be the dominant regime, since there is no mean lift force associated with VIV. Therefore, a cylinder under pure VIV would be expected to be displaced from an initial to a final position and not oscillate around the initial position.

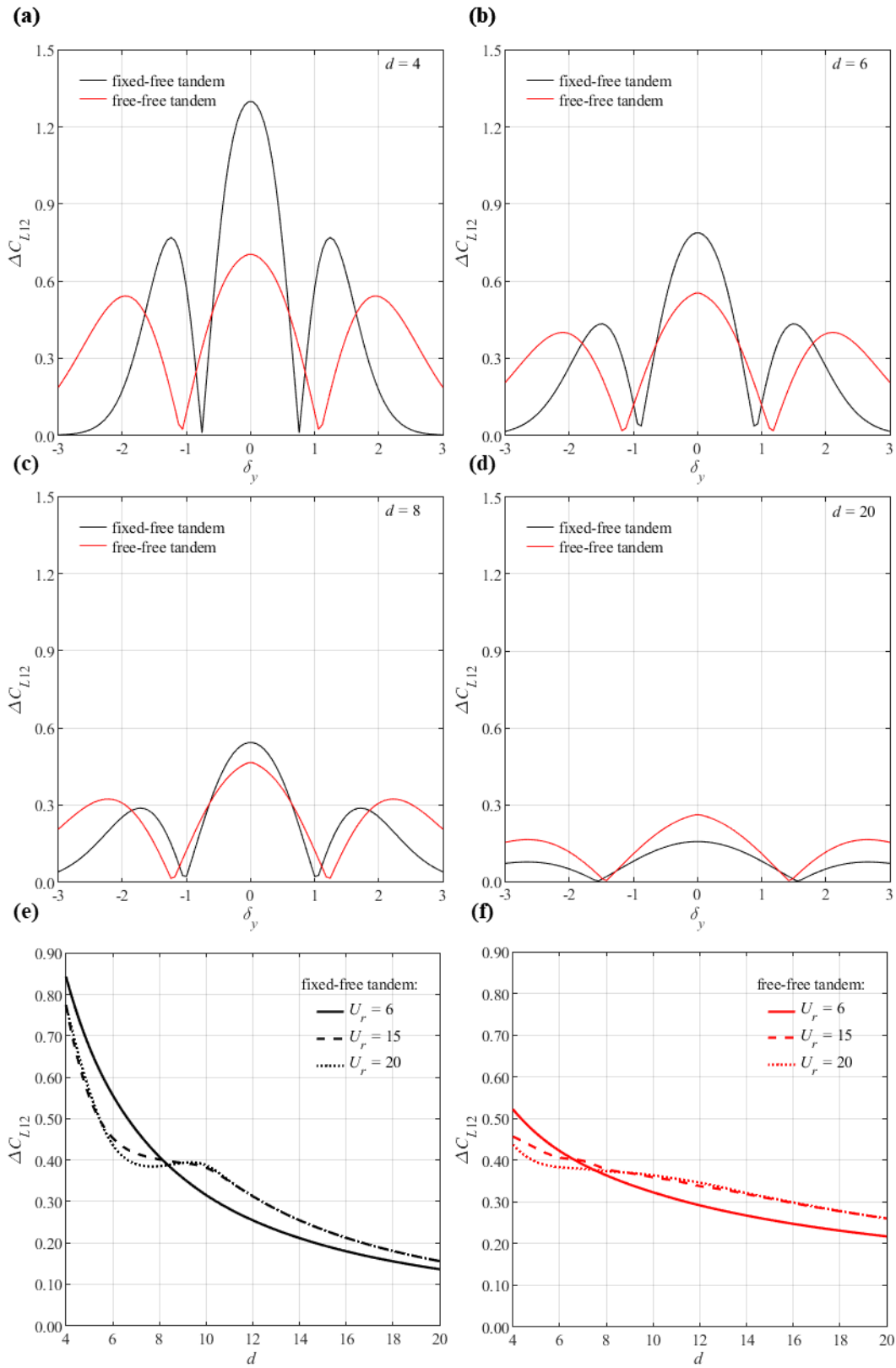


Figure 2-12: Variation of ΔC_{L12} across the wake for fixed-free and free-free tandem cylinders with (a) $d = 4$, (b) $d = 6$, (c) $d = 8$ and (d) $d = 20$, and rms values of time-varying ΔC_{L12} in (e) fixed-free and (f) free-free tandem cases at specific U_r .

2.5.4. WIV Oscillation Frequencies of the Downstream Cylinder

Analysis of dimensionless frequencies of oscillation of the downstream cylinder is presented in Figure 2-13 at $d = 4$ and 8 for fixed-free and free-free numerical results. A fast Fourier transform algorithm has been applied to convert the time series of y_2 to the frequency domain after removal of the first 200 seconds of simulation to ensure the analysis of the steady-state response, and the dominant frequency has been determined for each U_r .

Reference wake stiffness equivalent frequencies have been added to Figure 2-13. The blue dotted-lines represent the modelled wake stiffness frequencies, whereas the red dashed line is associated with the experimental frequencies in the study of Assi *et al.* [12].

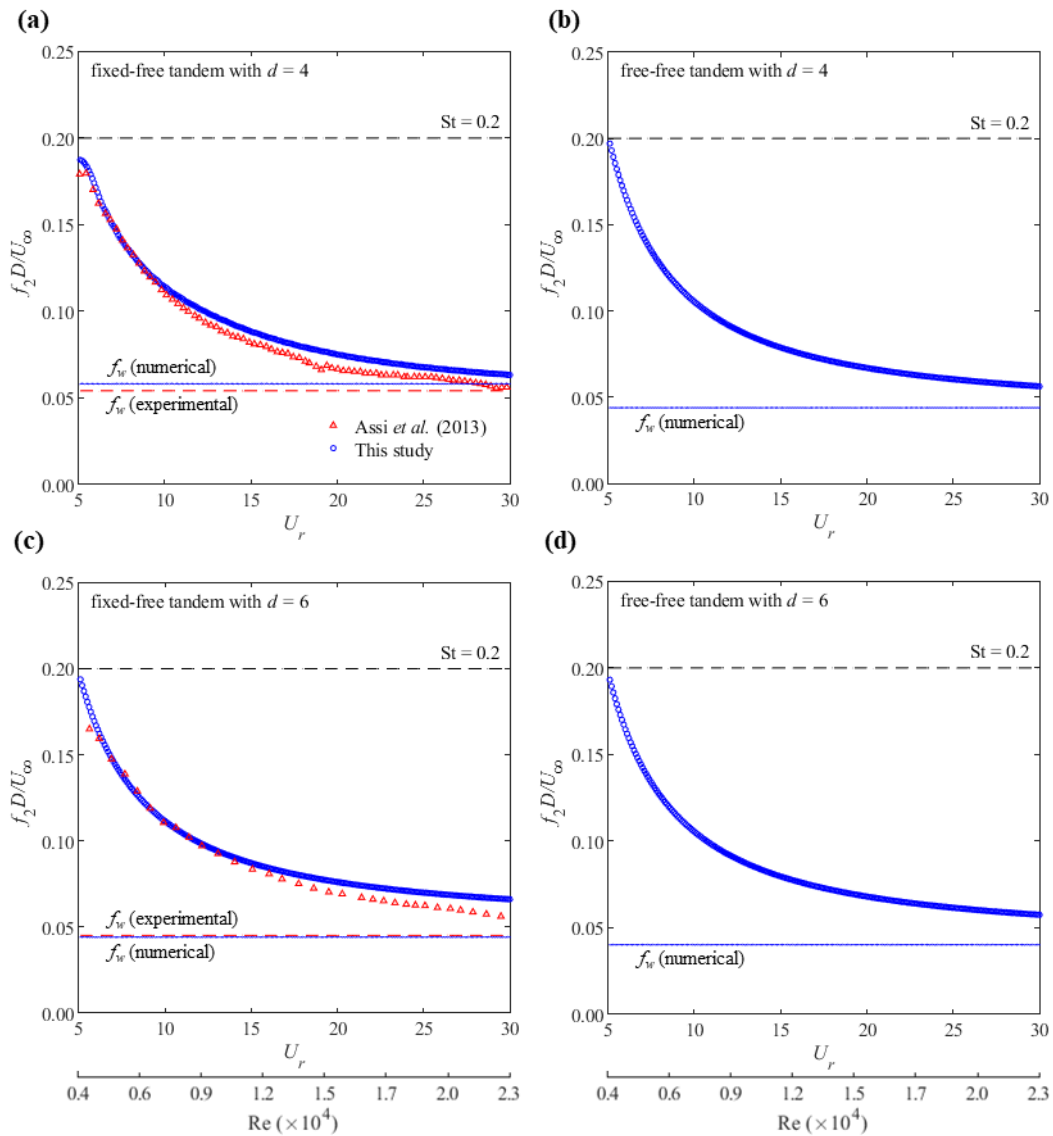


Figure 2-13: Variation of dimensionless dominant frequencies of downstream cylinder responses with U_r (Re) for the fixed-free and free-free tandem cases with $d = 4$ and $d = 6$, in comparison with experimental results in fixed-free tandem cases.

Model outputs agree reasonably well with experimental data for fixed-free cases and especially for the lower spacings. Whilst experimental oscillation frequencies barely change from $d=4$ to $d=6$ and tend to the experimental wake stiffness frequency values, numerical results exhibit a similar tendency for $d=4$. However, numerical results diverge from numerical wake stiffness equivalent frequencies for $d=6$. Nevertheless, the experimental and modelled wake stiffness lines diverge only for $d=4$. This is due to the largest vibration amplitudes (Figure 2-7) that are seen for systems with $d=4$ which may exceed the approximately linear wake stiffness region within about $-1 \leq \delta y \leq 1$, as previously discussed. This way, the linear approximation used for the computation of the experimental wake stiffness (red dashed line) in Figure 2-13 may not suffice. Also, a similar discrepancy is observed between fixed-free and free-free results for the modelled wake stiffness lines based on Equation (2-41). This discrepancy is also understood to be related to the greater δy , a consequence of the vibration of the upstream cylinder and, once again, the downstream cylinder may vibrate out of the approximately linear region. Finally, the effect of spacing increase is negligible at least for a jump from $d=4$ to $d=6$ for the wake stiffness computation, as similarly concluded by Assi *et al.* [12].

Unfortunately, owing to the lack of comparable experimental data, it has not been possible to compare the present free-free 1DOF results. However, in terms of dominant frequencies for $U_r > 5$, they are qualitatively and quantitatively similar to the fixed-free cases.

The power spectral density (PSD) results for the free-free tandem case with varying $U_r \geq 5$ are plotted in Figure 2-14. The PSD has also been obtained by applying the Fast Fourier Transform (FFT) to convert from the time domain, from $t = 200-1200$, to the frequency domain. The PSD results of Figure 2-14 are useful to demonstrate over which frequency band the system vibrates with more energy, hence it highlights the dominant frequencies for every U_r . Moreover, oscillation frequencies have been normalised with respect to the cylinder natural frequency, f_n , for each dynamic variable considered.

For the initial analysis of the variables associated with the upstream cylinder, y_1 and q_1 , it is seen that both wake variable and transverse displacements vibrate with similar frequencies for every U_r studied in Figure 2-14. This agrees with the conclusions from Figure 2-9, where y_1 and q_1 are seen to behave qualitatively similarly. Also, normalised frequencies of oscillation are equal to one for $U_r = 5$, due to the VIV feature

of lock-in, meaning that the oscillation frequency of the first cylinder is equal to the natural frequency of the system. Overall, the responses linked to the first cylinder are monotonic and correspond to literature observations [15].

On the other hand, properties associated with the wake flow dynamics, C_{L12} , χ , respond at different frequencies. Dynamics of χ and C_{L12} are multi-frequency and the main frequency of χ is twice the predominant frequency of C_{L12} . In fact, it is suggested that the main frequencies of χ and C_{L12} are intertwined and associated to y_1 and y_2 through δy in their formulations in Equations (2-22) and (2-24) from which it is concluded that the only dynamic variable is δy , whilst all other terms are time-independent. Indeed, it is clear from Figure 2-14 that the oscillation frequencies of C_{L12} are a combination of the frequencies of y_1 and y_2 .

However, a question still remains: why are vibration frequencies of the wake deficit variable χ , and therefore the wake flow velocity spatial fluctuation frequencies, twice the frequencies of C_{L12} , y_2 and q_2 ? To answer this question Figure 2-3 is recalled – a single cycle of cylinder transverse oscillation (zero-mean) across the wake through negative and positive transverse positions actually results in two cycles of χ oscillations around its non-zero mean value and is supported by the minimum wake flow velocity. This way, frequencies of χ are still solely connected to δy , however, with twice its frequency spectrum.

Furthermore, analysis of the dependency of spacing on the dominant oscillation frequencies of the downstream cylinder leads to similar observations, as seen in Figure 2-15 for fixed-free systems and Figure 2-16 for free-free systems.

Before concentrating on analysing the oscillation frequencies of the second cylinder for $d = 4, 6, 8, 10$ and 20 , it is important to detail the three interacting excitation mechanisms. For the prior analysis of amplitudes of vibration, three frequency branches were identified that have been proposed to be related to three different mechanisms in the intricate dynamics of double cylinders. So far, only two of these mechanisms have been discussed: VIV and WIV. However, the two wake vortices excite VIV differently due to the difference in oncoming flow velocity, i.e., while the upstream cylinder vortex shedding frequency is derived from U_∞ , the downstream cylinder vortex shedding frequency is based on $u = \chi U_\infty$.

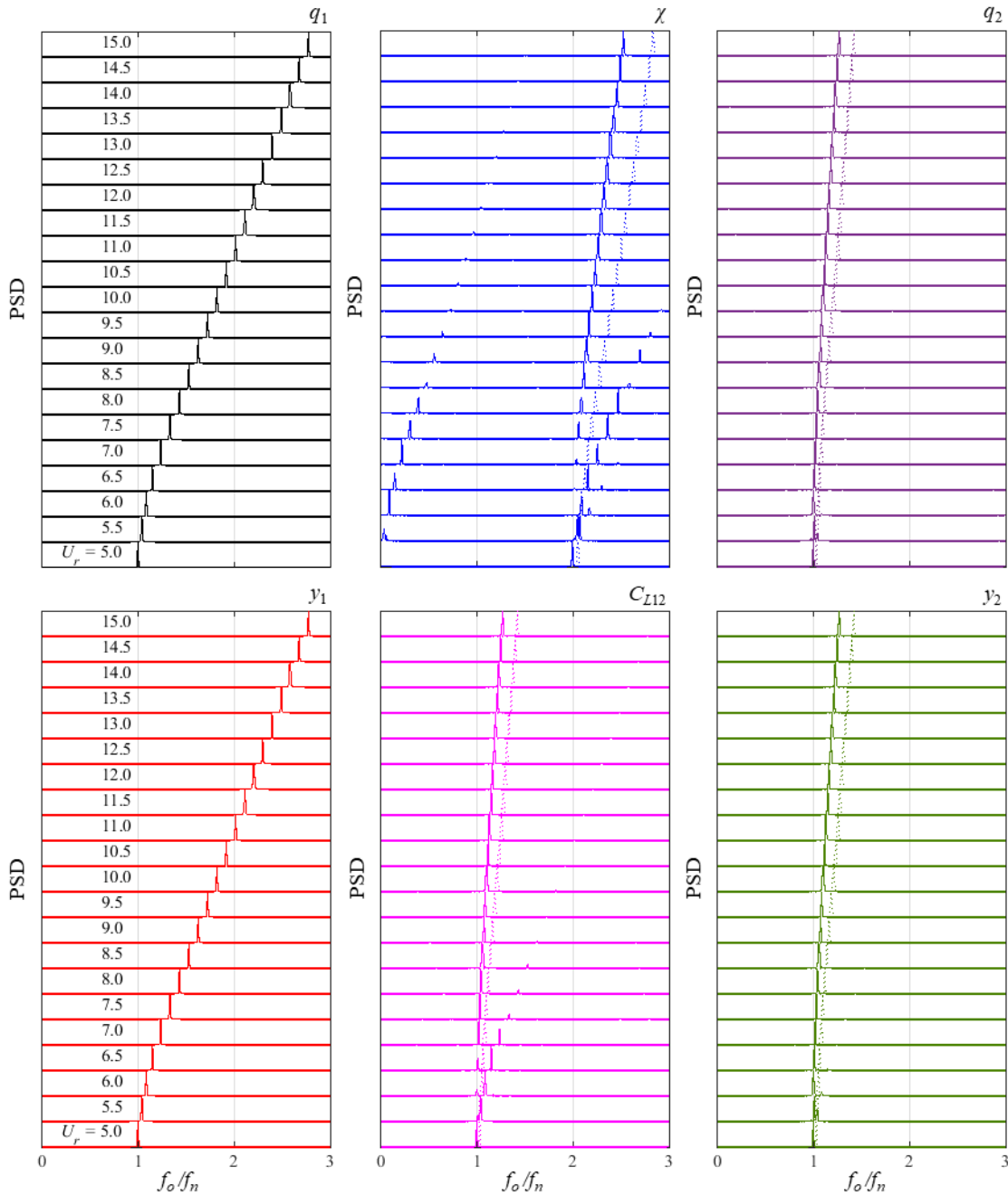


Figure 2-14: Normalised response frequency components associated with wake oscillator variables (q_1 , q_2), wake deficit variable (χ), wake-induced transverse force coefficient (C_{L12}) and transverse cylinder responses (y_1 , y_2) with varying $U_r \geq 5$ in the free-free tandem case with $d = 4$.

Hence, it is proposed that the three frequency branches of the downstream cylinder are: i) classical VIV, ii) VIV frequency of the downstream cylinder and iii) a lower-frequency branch associated with WIV.

The first frequency branch (VIV) is derived from the upstream wake of vortices. The upstream cylinder which is responsible for the wake in the gap of the two cylinders is under VIV. Therefore, the frequency of this cylinder is impinged on the wake.

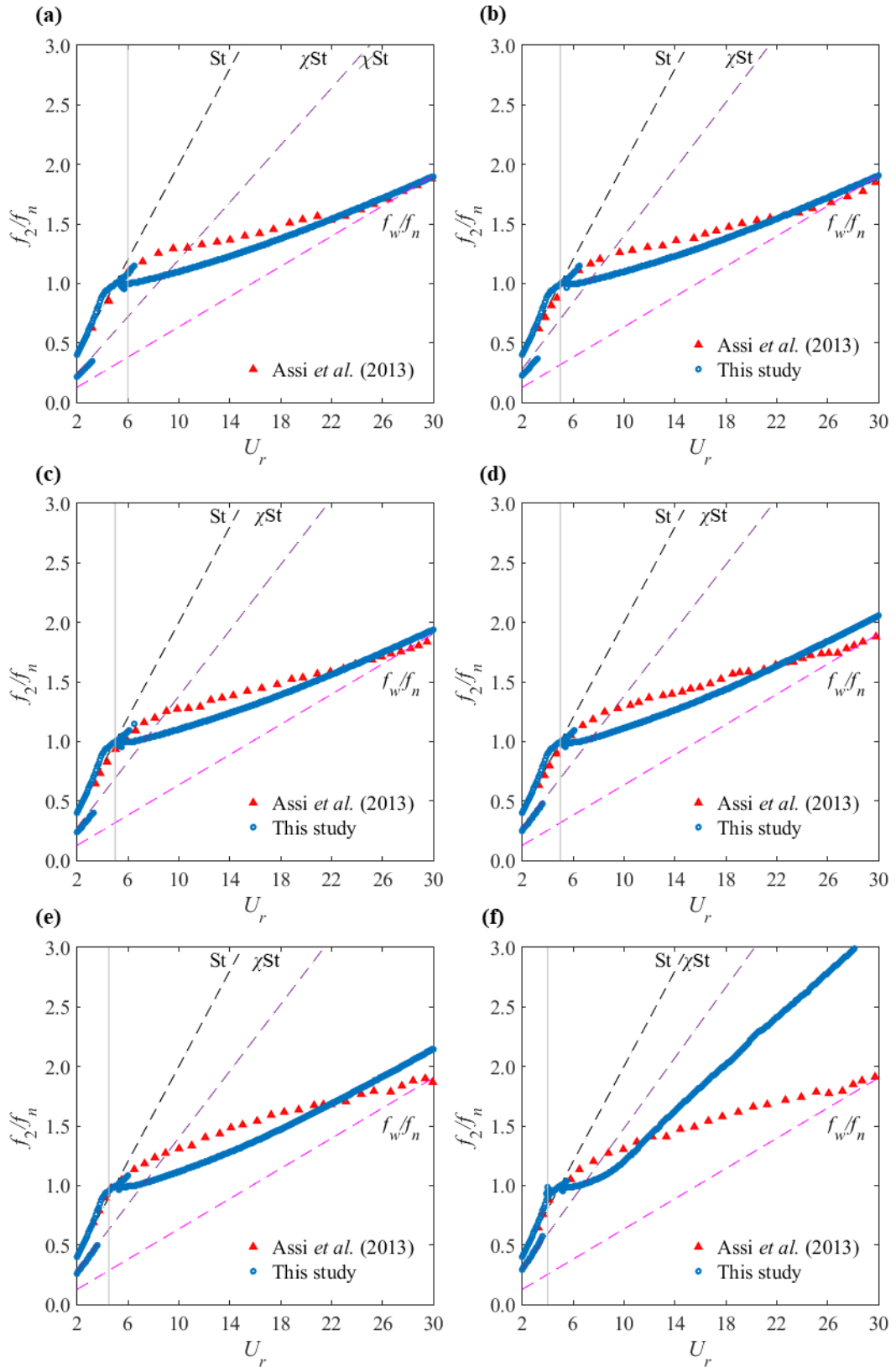


Figure 2-15: Variation of the dominant frequencies of crossflow oscillations of the downstream cylinder with the reduced velocity. Comparison of numerical results and experimental data for fixed-free cases. (a) $d = 4$. (b) $d = 5$. (c) $d = 6$. (d) $d = 8$. (e) $d = 10$. (f) $d = 20$.

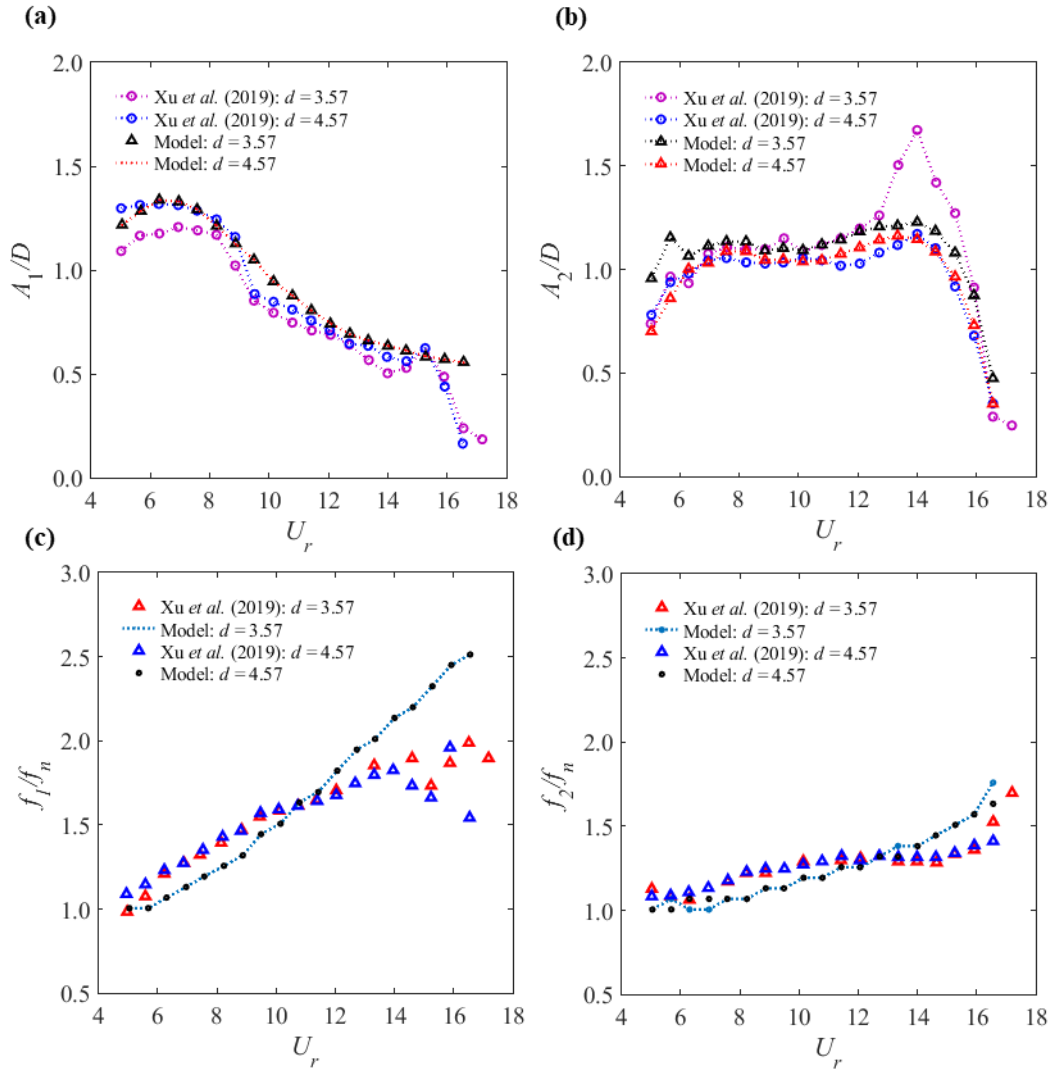


Figure 2-16: Numerical-experimental comparison of response amplitudes and frequencies of upstream and downstream cylinders in free-free tandem cases with $m^* = 1.343$ and $\zeta = 0.02$: (a) A_1/D , (b) A_2/D , (c) f_1/f_n , (d) f_2/f_n . A dashed line in (c) and (d) represents the $St = 0.2$ line. “Model” refers to present study in legends.

The leading cylinder shields the undisturbed upstream flow and shedding vortices, but in the meantime, it is also laterally displaced in VIV. Thus, vortices are shed from the moving cylinder at different positions as time goes by. The result is that every wake measure is dynamic and depends on the dynamics of both cylinders, or more importantly on their relative time dependent position, translated mathematically by δy in Section 2.2. The frequencies associated with this mechanism are clearly identified following the black-dashed Strouhal line in Figure 2-15. One may observe this frequency branch in the downstream cylinder frequency response for any d in Figure 2-15b-f as equivalent to the frequencies of the upstream cylinder shown in Figure 2-15a for $U_r < 8$.

The second frequency branch is attributed to VIV of the downstream cylinder caused by the downstream wake of vortices. The principal wake is the wake in the gap between the cylinders. However, the system is in the co-shedding regime, as previously mentioned, so that $d \geq 4$. In other words, both cylinders shed vortices and interact with their trailing wake flow. Since the downstream cylinder is subjected to combined VIV and WIV, physical separation between the two phenomena is difficult if not impossible, thus, a theoretical mental exercise is proposed for which the vortices and the associated unsteadiness from the upstream wake are temporarily disregarded but not the steady wake deficit; an idea similar to the interesting shear flow experiments conducted by Assi *et al.* [11]. This way, the second cylinder will still experience a mean wake-reduced flow velocity in the wake and if the Reynolds number is sufficiently high, which will lead to vortex shedding and VIV by the same phenomena as for the upstream cylinder. With that in mind, a reduced Strouhal law was computed based on the local wake-reduced flow velocity and was represented by the purple-dashed lines in Figure 2-15. It is well known that the VIV vortex shedding frequency can be estimated by the Strouhal law up to the point of lock-in and, hence, the lower frequency branch seen from Figure 2-15b-f following the reduced Strouhal relationship for $U_r < 5$ is attributed to VIV of the second cylinder. It is important to highlight that, in practice, it is likely that the second wake interacts and is modified by the oncoming upstream wake vortices which consequently may alter the response and oscillation frequencies of the downstream cylinder, but the reduced Strouhal law seems to satisfactorily represent a frequency branch of the rear cylinder for the model predictions.

The third highlighted frequency content is linked to WIV of the second cylinder. When the downstream cylinder is transversely displaced and leaves the tandem initial position, an opposing C_{L12} starts to act on the cylinder in an attempt to restore it back to the wake centreline ($T = 0$). The relationship between WIV frequencies and the wake stiffness associated natural frequency has then been established. Therefore, Equation (2-41) is computed and depicted in Figure 2-15 by the dashed pink line.

To summarise, three frequency components have been identified for the aft cylinder and it is argued that these frequencies are due to VIV of the first cylinder reflected on the upstream wake, VIV of the second cylinder and WIV on the downstream cylinder. Nonetheless, an interesting point can be drawn from experiments with a fixed first cylinder, for which VIV frequencies are also observed. In fact, there is no VIV of the first cylinder as it is fixed. However, it is still shedding vortices

with the same frequency as the Strouhal law is fundamentally derived exactly for a stationary body. As mentioned, the upstream cylinder in VIV conforms to the Strouhal law up to approximately $U_r \leq 4$, when it enters lock-in. Then, for a low U_r the excitation source is the vortex shedding from the upstream cylinder, whereas for post lock-in reduced velocities for systems with a dynamic first cylinder, it is the oscillation frequency of the first cylinder through δy .

Moreover, Figure 2-15 shows that two frequency contents follow the free-stream and the wake-reduced Strouhal frequencies for $U_r < 5$. As mentioned, these were related to the vortex shedding frequency of the leading cylinder and VIV of the trailing cylinder respectively. The WIV frequency branch is not seen for this U_r zone because this phenomenon is believed to only start to act and prevail after the so-called VIV first peak, as mentioned before, where the second cylinder behaves similarly to the VIV of a single cylinder until $U_r \sim 5$. Therefore, analysis of frequency results in Figure 2-15 helps to support the understanding that WIV is a relevant mechanism only after a minimum U_r due to the lack of correlation to the wake stiffness curve, whereas VIV is present even for a lower U_r . PSD of the frequencies of Figure 2-15 led to the conclusion that VIV is the predominant mechanism working on the system for the low U_r regime which extends itself until the VIV amplitude peak.

When U_r is increased, it was observed that for approximately $4 < U_r < 8$, the first cylinder enters lock-in and vibrates with its largest recorded amplitudes. Its maximum amplitudes of vibration, as cited previously, are seen for $U_r \sim 5$. However, Figure 2-15 reveals additional frequency peaks for $U_r \sim 5$ or reduced velocities slightly above. It is argued that this frequency branch, that consolidates itself and becomes the prevailing frequency content until the end of the U_r range studied, is a result of the combined interaction of WIV and VIV on the downstream cylinder depending on d . It is highlighted that this frequency branch is the only y_2 oscillation frequency for most of the d values investigated. WIV and VIV mechanisms are absolute in their influence over the system, as the upstream wake is now being displaced with minimal amplitudes because the upstream cylinder is past the lock-in regime (VIV). Subdivision between the intermediary and high U_r domain for a given d is related to predominance of one mechanism over the other, WIV or VIV.

Hence, it is proposed that the low U_r region is delimited from the minimum U_r shown until the first VIV peak ($U_r \sim 5$ for the current system), the intermediary U_r zone begins at the VIV-WIV transition point immediately after the first VIV peak up to the

point where VIV - originated from the downstream cylinder's own vortex shedding - overcomes the WIV mechanism and, finally, the high U_r regime is when VIV dominates. It is stressed that this subdivision in the three U_r regions depends on d , m^* , ζ and on Re. For instance, for an established system with m^* , ζ and fixed Re range, it is expected that d variation leads to a larger intermediate or high U_r region or different transition points. As a matter of fact, one may consider it is possible to have intermediate U_r ranges from $U_r \sim 5$ up to $U_r > 30$, such a case is represented for $d = 4$ in Figure 2-15a, or to have limited or no intermediate U_r regime as exemplified by $d = 20$ in Figure 2-15f.

Furthermore, WIV is reported to dominate in the dynamics of the second cylinder after the first VIV peak, $U_r > 5$. For a given system, variation of d results in more robust or weakened upstream vortices and WIV mechanism, controlling whether the body will respond in WIV, VIV or transitional regimes. These 3 oscillation amplitude regimes are important in analysing the frequency response of the downstream cylinder.

For a lower d , Figure 2-15a-c, it has been shown that the cylinder experiences a build-up of amplitudes of vibration and consequently WIV is the dominant mechanism, dictating the only frequency branch observed for $U_r > 8$ and up to the highest U_r studied, as concluded from the observation that the modelled frequencies rise with U_r in the same proportion as the wake stiffness line. However, for moderate spacings, Figure 2-15d-f the three U_r region divisions become clearer. Assi *et al.* [11] have shown that intermediary spacings trigger sustained amplitudes of vibration, i.e. a transition between typical WIV amplitude build-up and VIV of a single cylinder responses. It is observed that, once again, WIV prevails after the VIV peak ($U_r \sim 5$) as the frequency curve evolves similarly to the wake stiffness concept for $d = 8$ and 10. Although, at some turning point, the modelled oscillation frequency curve switches and becomes almost parallel to the reduced Strouhal purple-dashed line in Figure 2-15. This is a possible model indication that self-attained VIV is now competing within the system and becoming the dominating mechanism in the complex multiple wakes-cylinder interaction. This characterises the beginning of the third or high U_r region. Therefore, the frequency plots could be subdivided in three zones according to the dominant phenomenon working on the system: VIV associated with the first cylinder, WIV and VIV associated with the second cylinder, related to the low, intermediate and high U_r regions in that order.

Vibration frequencies for a rear cylinder at $d = 20$ are shown in Figure 2-15f. The cylinders are so far away that the downstream cylinder experiences an almost pure

VIV response as seen from comparison to Figure 2-15a. However, it is seen that the wake effects have not ceased completely, and the second cylinder is not acting as a typical isolated cylinder. For instance, i) the Strouhal lines have not merged yet, i.e. free-stream Strouhal \neq wake-reduced Strouhal, ii) the frequency peaks are shifted but following the reduced Strouhal law and iii) there is still a small but noticeable intermediate frequency zone for which modelled frequencies increase with U_r variation in the same slope as the wake stiffness line.

Modelled vibrating frequencies of the second cylinder are relatively accurate and agree with the experiments for a pair of cylinders at $d = 4$ with small discrepancies for the highest reduced velocities. A vertical line is used to indicate the approximate U_r for which transition from the initial VIV regime occurs. It has been discussed that the downstream cylinder responds in pure VIV for lower reduced velocities and transition to WIV happens for $U_r \sim 5$ for $d = 4$. As seen previously, the classical VIV response for a low U_r is common for every studied spacing so a vertical line indicating the end of the initial VIV regime is also provided for $d \geq 6$.

Modelled dominant oscillation frequencies agree with the dominant experimental frequencies with increase of U_r until the moment the model frequencies shift and start to increase at a steeper gradient. It is proposed that this slope change is due to the dominant transition from the WIV mechanism to the VIV mechanism. The vibration frequencies of the second cylinder for the intermediate U_r range at any d follow the experimental measurements with reasonable accuracy. It has been seen that the model frequencies for a spring-mounted downstream cylinder increase with U_r with similar slope to the wake stiffness line, apparently only differing by a constant related to the spring stiffness. However, at an intermediary/high U_r transition point the frequency gradient unlocks from the wake stiffness line (WIV) and locks to the wake-reduced Strouhal law (VIV). It is proposed that this indicates a change of the dominant mechanism exciting the rear cylinder. In other words, WIV is the dominant mechanism for intermediate U_r , while co-shedding VIV is the dominant excitation source for the high U_r region.

The dynamic transverse response of a couple of tandem free-free cylinders with different system properties has been simulated and compared to the results of Xu *et al.* [61] Even though the separation between the cylinders is comparable to other free-free 1DOF studies in the literature [58] [59], in the study of Xu *et al.* [61] the variation of amplitude of the downstream cylinder's vibration with U_r shows an interestingly

distinct trend. Perhaps, associated with the difference in system properties and Re or the use of virtual-spring damping devices, these qualitative differences in response trends require a new calibration of the model empirical parameters related to the damping and hydrodynamic force acting on the modelled system in order to accurately represent the experimental features.

For validation of the free-free results, the model has been simulated for the same reduced velocities and compared with the results of Xu *et al.* [61] in Figure 2-16 by adopting the following input parameters $\varepsilon_1 = 0.01$, $\Lambda_1 = 19$, $\varepsilon_2 = 0.035$, $\Lambda_2 = (-0.0152 U_r^4 + 0.4046 U_r^3 - 5.477 U_r^2 + 30.76 U_r - 47.45)$.

Amplitudes of vibration of the upstream cylinder show that whilst experiment results are slightly different between $d = 3.57$ and $d = 4.57$, model outputs remain unchanged given the model assumption that the first cylinder is not affected by the second. This assumption is expected to hold in the wake interference regime for $d \geq 4$, as commented previously. Despite, $d = 3.57$ being slightly lower than this minimum range of validity, the model results agree with the experimental results.

In the comparison of vibration amplitudes of the downstream cylinder, the model is capable of representing the features shown by the reference data with some degree of precision for most of the U_r domain, especially for $d = 4.57$. However, a region of larger amplitudes of vibration at $U_r = 12-16$ is not captured by the model for $d = 3.57$. This can be related to one of the modelling assumptions that considers $d \geq 4$.

Frequency results analysis show that comparison of results for the upstream cylinder is satisfactory for the initial VIV branch all the way to the lock-in upper branch. As widely reported, wake oscillator models show a limitation in mimicking the lower branch oscillation frequencies, in the present case occurring at $U_r > 11$. Nevertheless, WIV frequencies of oscillation of the downstream cylinder conform well to the experimental data for the whole range of reduced velocities.

2.5.5. Chapter Summary

The present chapter focused on the modelling of combined VIV and WIV of a tandem pair of cylinders. Initially, the wake flow was investigated through the boundary layer theory. In order to account for the oscillation of the first cylinder, which is responsible for the wake flow that leads to WIV of the second cylinder, a second order solution has been investigated. Comparison to experimental data has led to the conclusion that the higher order solution improves the model's ability to represent the problem, most importantly for amplitudes of vibration at the first VIV peak for lower

spacings and decaying wake effects for high U_r and d .

In this way, a model has been developed and adopted to simulate the tandem pair of cylinders in various configurations of d , U_r , m^* and ζ . Results reveal that the model can satisfactorily reproduce wake property measurements and dynamic outputs in time and frequency domains. Frequencies and amplitudes of vibration of the rear cylinder have been validated with experiments and have been seen to agree with experimental measurements for the WIV regime, for which oscillation amplitudes are the largest and increase progressively with U_r . Additionally, the model shows the asymptotic response of VIV for increasingly larger spacings, in other words, if $d \rightarrow \infty$, then the two cylinders act as isolated cylinders under classical VIV.

The response of the downstream cylinder for every studied d exhibits similar features for approximately $U_r \leq 5$, i.e. the second cylinder behaves as a single cylinder in VIV. This is due to the initial VIV regime, which conforms to experimental data. Thus, oscillation amplitudes of both cylinders are similar until approximately $U_r = 5$.

For $U_r > 5$, examination of time series, amplitudes of vibration and oscillation frequencies has led to the conclusion that, depending on d , the second cylinder could behave within three regimes: WIV, classical VIV or a transition from WIV to VIV.

Three distinct oscillation frequency branches have been observed in the 1DOF response of the second cylinder. These are associated with three different concepts: the first cylinder vortex shedding frequency through the free-stream Strouhal law; the wake stiffness equivalent natural frequencies [12]; a wake-reduced vortex shedding frequency based on the Strouhal law which is computed using the steady wake flow velocity. They have been correlated to the mechanisms of VIV of the upstream cylinder, WIV and VIV of the downstream cylinder respectively. It has been discussed that the upstream wake after a dynamic rather than a static first cylinder is more complex, resulting in a relatively stronger coupling of the second cylinder to the first. In other words, wake properties including wake-induced hydrodynamic forces and consequently the response of the downstream cylinder are affected by the VIV of the upstream cylinder. Furthermore, the study of the frequency branches associated with VIV of the second cylinder and WIV led to identification of the previously mentioned response excitation mechanisms.

It has been concluded that the two wakes of vortices are interacting with the downstream cylinder so WIV and VIV coexist. Whilst U_r governs the dominant excitation mechanism acting on the second cylinder, d dictates the response regime,

whether it is WIV, VIV or WIV-VIV transition and this is reflected on the amplitudes and frequencies of vibration. For low spacings, $d \leq 6$, amplitudes of vibration build-up with the increase in U_r and this has been defined as the WIV regime. For $6 < d < 10$, WIV-VIV transition occurs where the two mechanisms interact more evenly resulting in a plateau of amplitudes of vibration after the first VIV peak for the full range of studied U_r . Lastly with further increase of d the downstream cylinder gradually resembles a single cylinder in classical VIV. These d regime boundary points have been discussed to depend on m^* and ζ .

The response regime framework study is relevant because it allows one to anticipate whether the downstream cylinder will respond more vigorously or moderately with the increase of flow velocity. For instance, for a design engineering study it would be beneficial to avoid $d < 10$ for an equivalent m^* and ζ system, as the downstream cylinder would maintain oscillation amplitude levels similar to classical VIV lock-in over a much wider range of U_r or alternatively build-up amplitudes of vibration in classical WIV for $d \leq 6$.

These are the initial observations and conclusions from the modelling work conducted thus far for the problem of 1DOF tandem cylinders. The next logical step is to propose an extension to this model to consider a more general 2DOF problem. This is addressed in the following chapter and will facilitate the analyses and discussions about the features observed for a 1DOF system, more specifically the response frequencies and regimes of the downstream cylinder under VIV and WIV.

CHAPTER 3. ANALYTICAL MODELLING OF COMBINED WIV AND VIV – 2 DEGREES OF FREEDOM

A 2DOF reduced-order model is now proposed to represent the underlying physics of the problem inspired and extending the 1DOF modelling framework presented in Chapter 2.

To do that, two rigid cylinders are idealised as mass-spring-damper systems and the flow is initially assumed constant and laminar outside of the wake-shielding effects of the cylinders. Three-dimensional effects are not considered. An outline of the modelled system is illustrated in Figure 3-1.

The intrusive presence of the cylinders, which are initially at rest, modifies the once inviscid flow. Furthermore, the significant difference of flow velocities between the layers of disturbed and undisturbed fluid allows the problem to be addressed through the boundary layer theory perspective following other studies [31, 33, 34, 42] as discussed in Chapter 2.

Therefore, it is assumed that the wake flow velocities at different locations within the wake obey a mathematical similarity in the sense that they are related to each other and can be mapped onto one another by a suitable mathematical function. In this way, the wake flow velocity can be understood as a wake deficit function applied to the steady, free stream velocity and the similarity law may be written as:

$$u(X, Y) = \chi(X, Y) U_{\infty}, \quad (3-1)$$

for which the wake deficit function and the wake flow velocity are dependent on the local relative position within the wake. In the longitudinal direction, the deficit is greater the closer to the generating cylinder and in the lateral direction, it is greater at the wake centreline, rapidly decreasing towards the edges of the wake as it can be seen in Figure 3-2.

in which x and y are non-dimensional relative displacements between the cylinders. Thereafter, through the assumption of similarity, the partial differential boundary layer equations can be reduced to ordinary differential equations and after introduction of a dimensionless transformation variable for the turbulent wake $\eta(X, Y) = Y \sqrt{4\lambda X D C_{D1}}$ [33, 42, 62], then:

$$u(\eta) = \chi(\eta) U_{\infty}, \quad (3-2)$$

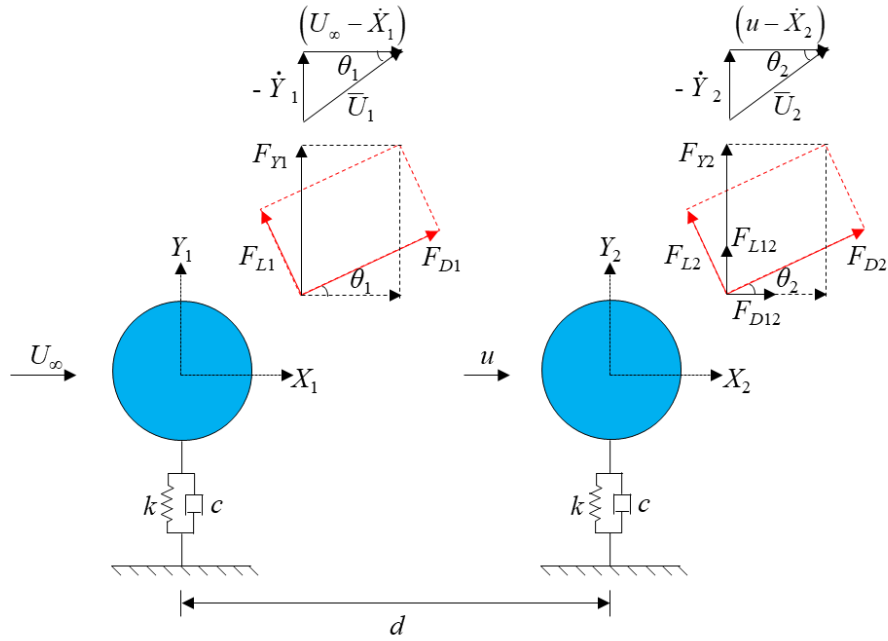


Figure 3-1: System sketch of a 2DOF pair of two tandem cylinders and unscaled diagram of forces exerted upon the respective cylinders.

From Figure 3-1, the time-varying relative spacing between the cylinders is defined as:

$$X = (X_2 - X_1) + d; \quad Y = (Y_2 - Y_1) + T$$

$$x = X/D; \quad y = Y/D$$

$$x = (x_2 - x_1) + d = \delta x + d; \quad y = (y_2 - y_1) + T = \delta y + T$$

where C_{D1} is the reference drag coefficient for the upstream cylinder, D is the cylinder diameter and λ is an empirical parameter related to the eddy viscosity which may be obtained experimentally as in Schlichting [32].

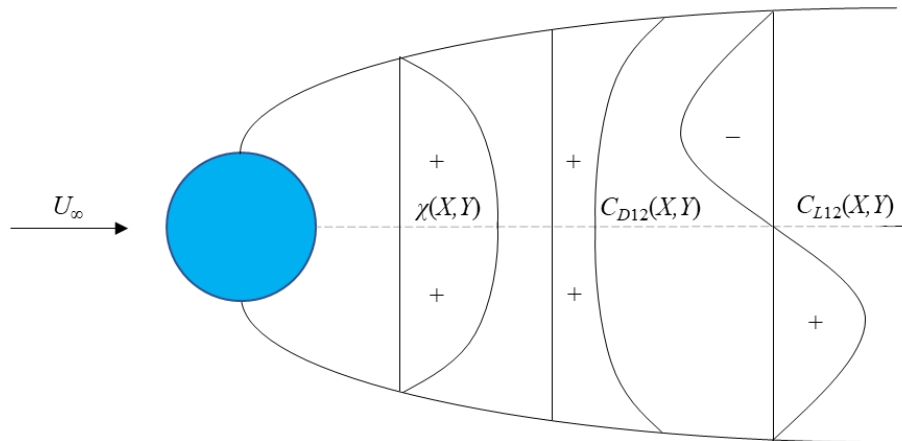


Figure 3-2: Plane idealisation of the wake flow behind a cylinder. Unscaled schematic of the wake deficit, wake-induced drag and lift coefficient profiles across the wake.

Thereafter, the following wake deficit function for 2DOF cylinders, considering the higher order theory of Blevins and Saint-Marcoux [36] for the wake flow behind a

moving upstream cylinder, is derived from repeated direct integrations of the reduced boundary layer equations which yield:

$$\chi(x,y) = \frac{u(x,y)}{U_\infty} = 1 - \left\{ \alpha \left(\frac{C_{D1}}{\delta x + d} \right)^{\frac{1}{2}} \left(e^{-\frac{\eta^2}{4}} + \frac{\beta}{\alpha} e^{-\frac{\eta^2}{4}} \int_0^\eta e^{\frac{\varphi^2}{4}} d\varphi \right) \right\}; \quad (3-3)$$

where α and β are constants of integration and φ is a generic integration variable. Derivation of these equations has been discussed in Chapter 2.

Subsequently, the steady components of wake-induced drag and lift can be modelled according to Blevins [33]. Intuitively, the direct relationship between hydrodynamic drag and flow velocity out of the wake is still valid for the wake flow. Thus, the wake-induced drag per unit length can be written as follows:

$$F_{D12} = \frac{1}{2} \rho U_\infty^2 D C_{D12} = \frac{1}{2} \rho U_\infty^2 D [u^2(x,y)/U_\infty^2] C_{D2}, \quad (3-4)$$

where C_{D2} is the reference drag for the second cylinder and ρ is the fluid density. The wake-induced drag coefficient can then be rewritten as:

$$C_{D12}(x,y) = \chi(x,y)^2 C_{D2}$$

$$C_{D12}(x,y) = C_{D2} \left(1 - \left\{ \alpha \left(\frac{C_{D1}}{(\delta x + d)} \right)^{\frac{1}{2}} \left(e^{-\frac{\eta^2}{4}} + \frac{\beta}{\alpha} e^{-\frac{\eta^2}{4}} \int_0^\eta e^{\frac{\varphi^2}{4}} d\varphi \right) \right\} \right)^2 \quad (3-5)$$

The wake flow velocity and the wake-induced drag force have a symmetric wake profile, which is not the case for the wake-induced lift force. As it can be observed from Figure 3-2, the wake lift profile is antisymmetric, it is negative for $Y > 0$ and vice versa. In other words, the wake lift always opposes the displacement of a downstream cylinder and always points to the wake centreline.

Blevins [33] proposed that the wake-induced lift coefficient is proportional to the negative transverse gradient of C_{D12} :

$$C_{L12}(x,y) = -\frac{\partial C_{D12}(x,y)}{\partial y},$$

$$C_{L12}(x,y) = -4\alpha \frac{\sqrt{\lambda}}{(\delta x + d)} C_{D2} \left(1 - \left\{ \alpha \left(\frac{C_{D1}}{(\delta x + d)} \right)^{\frac{1}{2}} \left(e^{-\frac{\eta^2}{4}} + \frac{\beta}{\alpha} e^{-\frac{\eta^2}{4}} \int_0^\eta e^{\frac{\varphi^2}{4}} d\varphi \right) \right\} \right) e^{-\frac{\eta^2}{4}} \frac{\eta}{2} - \frac{\beta}{\alpha} e^{-\frac{\eta^2}{4}} + \frac{\eta\beta}{2\alpha} \int_0^\eta e^{\frac{\varphi^2}{4}} d\varphi \quad (3-6)$$

Therefore, wake properties and hydrodynamic forces (Equations (3-3), (3-5), and (3-6)) are clearly dependent on the local position, as illustrated by Figure 3-2.

Equations (3-5) and (3-6) are expressions for the steady wake-induced hydrodynamic force coefficients associated with the WIV mechanism. The unsteady force components and the combined effect of the VIV mechanism will be investigated through the wake oscillator approach.

According to Figure 3-1, the equations of motion of the two cylinders may be written as:

$$\begin{aligned} m\ddot{x}_i + c\dot{x}_i + kx_i &= F_x \\ m\ddot{y}_i + c\dot{y}_i + ky_i &= F_y \end{aligned}$$

where m is the total mass accounting for the structural and the hydrodynamic added mass, the dot represents differentiation with respect to time, τ (in seconds), and subscript $i = 1, 2$ symbolises the first or second cylinder respectively. Further division by m and introduction of the dimensionless time, $t = \tau\omega_n$, leads to:

$$\begin{aligned} \ddot{x}_i + 2\zeta\dot{x}_i + x_i &= F_x/(\omega_n^2 m) \\ \ddot{y}_i + 2\zeta\dot{y}_i + y_i &= F_y/(\omega_n^2 m) \end{aligned}$$

where the dot denotes differentiation with respect to the dimensionless time, t , the structural damping ratio, $\zeta = c/(2m\omega_n)$ and ω_n is the angular natural frequency of the identical cylinders.

Furthermore, the nonlinear spring expansion of Zanganeh and Srinil [63] has been incorporated into the present model motivated by improvements in capturing features of 2DOF modelling in problems of single cylinders, such as figure-of-8 trajectories and lower branch of oscillation amplitudes. Details on the expansion procedure and derivation of equations can be found in Chapter 2. The resulting structural nonlinear equations of motion are as follows.

$$\begin{aligned} \ddot{x}_i + 2\zeta\dot{x}_i + (x_i + \alpha_{xi}x_i^3 + \beta_{xi}x_iy_i^2) &= F_x/(\omega_n^2 m) \\ \ddot{y}_i + 2\zeta\dot{y}_i + (y_i + \alpha_{yi}y_i^3 + \beta_{yi}y_ix_i^2) &= F_y/(\omega_n^2 m) \end{aligned} \quad (3-7)$$

in which α and β are empirical parameters related to the cubic geometric nonlinearities [63].

The hydrodynamic forces in each direction can be summed to yield the total force, as seen in Figure 3-1, and can be expressed as:

$$\begin{aligned} F_{X1} &= F_{D1}\cos\theta_1 - F_{L1}\sin\theta_1 = \frac{1}{2}\rho D\bar{U}_1^2(C_{D1}\cos\theta_1 - C_{L1}\sin\theta_1) \\ F_{Y1} &= F_{L1}\cos\theta_1 + F_{D1}\sin\theta_1 = \frac{1}{2}\rho D\bar{U}_1^2(C_{L1}\cos\theta_1 + C_{D1}\sin\theta_1) \end{aligned} \quad (3-8)$$

$$\bar{U}_1 = \sqrt{(U_\infty - \dot{x}_1)^2 + \dot{y}_1^2}$$

$$F_{X2} = F_{D12} + F_{D2} \cos \theta_2 + F_{L2} \sin \theta_2 = \frac{1}{2} \rho D U_\infty^2 C_{D12}(x, y) + \frac{1}{2} \rho D \bar{U}_2^2 (C_{D2} \cos \theta_2 + C_{L2} \sin \theta_2)$$

$$F_{Y2} = F_{L12} + F_{L2} \cos \theta_2 - F_{D2} \sin \theta_2 = \frac{1}{2} \rho D U_\infty^2 C_{L12}(x, y) + \frac{1}{2} \rho D \bar{U}_2^2 (C_{L2} \cos \theta_2 - C_{D2} \sin \theta_2)$$

$$\bar{U}_2 = \sqrt{(u - \dot{x}_2)^2 + \dot{y}_2^2} = \sqrt{(\chi(x, y) U_\infty - \dot{x}_2)^2 + \dot{y}_2^2}$$

$$\cos \theta_1 = (U_\infty - \dot{x}_1) / \bar{U}_1, \quad \sin \theta_1 = \dot{y}_1 / \bar{U}_1, \quad \cos \theta_2 = (u - \dot{x}_2) / \bar{U}_2, \quad \sin \theta_2 = \dot{y}_2 / \bar{U}_2$$

The total drag coefficients of each of the cylinders may be decomposed into steady and unsteady components, defined as:

$$C_{Di} = C_{D0i} + C_{Di}^{fl}$$

The lift coefficient associated with vortex shedding (C_{L2}) does not have a time-averaged component, unlike the wake-induced lift coefficient, which is spatially dependent.

As previously mentioned, nonlinear van der Pol oscillators are adopted to represent the fluctuating hydrodynamic coefficients, following the wake oscillator approach as in Facchinetti *et al.* [45]. The relationship between the wake variables (p_i, q_i) and the unsteady force coefficients can be mathematically expressed in the following.

$$\begin{aligned} p_i &= 2C_{Di}^{fl} / C_{D0i} \\ q_i &= 2C_{Li} / C_{L0i} \end{aligned} \quad (3-9)$$

Finally, Equations (3.7), (3.8), and (3-9) can be combined in dimensionless forms alongside the van der Pol wake oscillator equations to lead to the final form of the nonlinear 2DOF model, a system of eight equations:

$$\begin{aligned} \ddot{x}_1 + \left(2\zeta + \frac{(C_{D01} + 0.5C_{D01}^{fl} p_1)}{2\mu} \bar{U}_1 \right) \dot{x}_1 + (x_1 + \alpha_{x1} x_1^3 + \beta_{x1} x_1 y_1^2) &= \\ = \left(\bar{U}_1 \left[\frac{U_r}{8\pi\mu} (C_{D01} + 0.5C_{D01}^{fl} p_1) + \frac{C_{L01}}{4\mu} q_1 \dot{y}_1 \right] \right) & \quad (3-10) \\ \ddot{y}_1 + \left(2\zeta + \frac{(C_{D01} + 0.5C_{D01}^{fl} p_1)}{2\mu} \bar{U}_1 \right) \dot{y}_1 + (y_1 + \alpha_{y1} y_1^3 + \beta_{y1} y_1 x_1^2) &= \end{aligned}$$

$$\begin{aligned}
&= \left(\bar{U}_1 \left[\frac{U_r}{8\pi\mu} C_{L01} q_1 (C_{D01} + 0.5C_{D01}^{fl} p_1) - \frac{C_{L01}}{4\mu} q_1 \dot{x}_1 \right] \right) \\
&\quad \ddot{p}_1 + 2\varepsilon_{x1} (StU_r) (p_1^2 - 1) \dot{p}_1 + 4(StU_r)^2 p_1 = \Lambda_{x1} \ddot{x}_1 \\
&\quad \ddot{q}_1 + 2\varepsilon_{y1} (StU_r) (q_1^2 - 1) \dot{q}_1 + 4(StU_r)^2 q_1 = \Lambda_{y1} \ddot{y}_1 \\
\dot{x}_2 + \left(2\zeta + \frac{(C_{D01} + 0.5C_{D01}^{fl} p_2)}{2\mu} \bar{U}_2 \right) \dot{x}_2 + (x_2 + \alpha_{x2} x_2^3 + \beta_{x2} x_2 y_2^2) = \\
&= \frac{U_r^2 C_{D12}(x,y)}{8\pi^2\mu} + \left(\bar{U}_2 \left[\frac{U_r}{8\pi\mu} (C_{D02} + 0.5C_{D02}^{fl} p_2) + \frac{C_{L02}}{4\mu} q_2 \dot{y}_2 \right] \right) \\
\dot{y}_2 + \left(2\zeta + \frac{(C_{D02} + 0.5C_{D02}^{fl} p_2)}{2\mu} \bar{U}_2 \right) \dot{y}_2 + (y_2 + \alpha_{y2} y_2^3 + \beta_{y2} y_2 x_2^2) = \\
&= \frac{U_r^2 C_{L12}(x,y)}{8\pi^2\mu} + \left(\bar{U}_2 \left[\frac{U_r}{8\pi\mu} C_{L02} q_2 - \frac{C_{L02}}{4\mu} q_2 \dot{x}_2 \right] \right) \\
&\quad \ddot{p}_2 + 2\varepsilon_{x2} (StU_r) (p_2^2 - 1) \dot{p}_2 + 4(StU_r)^2 p_2 = \Lambda_{x2} \ddot{x}_2 \\
&\quad \ddot{q}_2 + 2\varepsilon_{y2} (StU_r) (q_2^2 - 1) \dot{q}_2 + 4(StU_r)^2 q_2 = \Lambda_{y2} \ddot{y}_2
\end{aligned}$$

The derivation of the equations above has been conducted similarly to the 1DOF study in Chapter 2, with the extension of the model to account for displacements in the inline direction.

3.1. Calibration of Inline Direction Model Input Parameters

The model equations derived in the previous section encompass a set of empirical inputs associated with: i) wake flow theory, ii) wake oscillator theory and iii) geometric nonlinearities. These will now be calibrated based on the theory of minimisation of errors between the model results and recently published experimental results of the dynamics of two tandem cylinders in a towing tank [25]. Moreover, a sensitivity study of reference hydrodynamic coefficients will also be analysed.

Model equations, as defined in Equation (3-10), have been coded into a Matlab algorithm. An order reduction change of variables of the form $z = \dot{x}_1$, $\dot{z} = \ddot{x}_1$ has been implemented to transform the second order ordinary differential equations (ODEs) to first order ODEs – a requirement of the inbuilt Matlab 4th/5th order Runge-Kutta solver, ode45. In computational form the variables have been assigned as follows:

$$z(1) = \dot{x}_1, z(9) = \dot{x}_2$$

$$z(2) = \ddot{x}_1, z(10) = \ddot{x}_2$$

$$z(3) = \dot{p}_1, z(11) = \dot{p}_2$$

$$z(4) = \ddot{p}_1, z(12) = \ddot{p}_2$$

$$z(5)=\dot{y}_1, z(13)=\dot{y}_2$$

$$z(6)=\ddot{y}_1, z(14)=\ddot{y}_2$$

$$z(7)=\dot{q}_1, z(15)=\dot{q}_2$$

$$z(8)=\ddot{q}_1, z(16)=\ddot{q}_2$$

where z is a 1×16 column vector with no physical meaning in this context.

After convergence studies, the time span of simulations has been identified as 1200 s with time steps of 0.01 s. Therefore, 120,000 data points have been recorded for each U_r , d and additional control parameters as required. Regarding initial conditions, at $t = 0$, the cylinder is considered to be stationary ($x_1=x_2=\dot{x}_1=\dot{x}_2=y_1=y_2=\dot{y}_1=\dot{y}_2=0$) and subject to the limit cycle amplitude of the van der Pol oscillators ($p_1=p_2=q_1=q_2=2; \dot{p}_1=\dot{p}_2=\dot{q}_1=\dot{q}_2=0$) as similarly done in Chapter 2. The transient-free responses in the range of $200 < t \leq 1200$ are then post-processed and analysed for both upstream and downstream cylinders as presented in the following section.

3.1.1. Calibration of Parameters Related to the Upstream Cylinder

As previously mentioned, the focus of the present study is on the co-shedding regime. This requires that the initial inline position between the cylinders is greater than a minimum critical spacing, in this case, considering a safety margin, $d \geq 4$ is assumed. Related studies [11, 12, 24, 25, 58, 62] have all reported that for this d range, whilst the downstream cylinder may be deeply affected by wake interference caused by the upstream cylinder, yielding WIV, there is no such feedback from the rear to the front cylinder. Therefore, the first cylinder behaves as a single cylinder, unaffected by the presence of the second cylinder. With that in mind, it is reasonable to address the calibration of the empirical parameters related to the upstream cylinder as a first step.

Calibration of the wake oscillator parameters, ε_{x1} , ε_{y1} , Λ_{x1} and Λ_{y1} , was conducted initially for the VIV results of the leading cylinder. The topic of 2DOF VIV of a single cylinder has been studied extensively and many studies have applied van der Pol wake oscillators to that problem [45, 64]. Particularly, based on the proposed empirical parameters of Srinil *et al.* [46], but accounting for different system properties and Reynolds numbers, the following values have been defined, $\varepsilon_{x1} = \varepsilon_{y1} = 0.003$ and $\Lambda_{x1} = \Lambda_{y1} = 9$.

The comparison between model amplitudes of vibration, calculated as the *rms* of time varying displacements as in Armin *et al.* [25], is presented in Figure 3-3 for the

upstream cylinder. Initially, it can be observed that the model captures the initial inline (A_{x2}) peak at very low reduced velocities, $U_r < 4$. This is likely to be associated with the inline vibration mode, as has been reported by Jauvtis and Williamson [15]. For higher reduced velocities, the modelled system agrees with the experimental results within the initial and upper branches for the maximum oscillation amplitudes for both inline and crossflow directions.

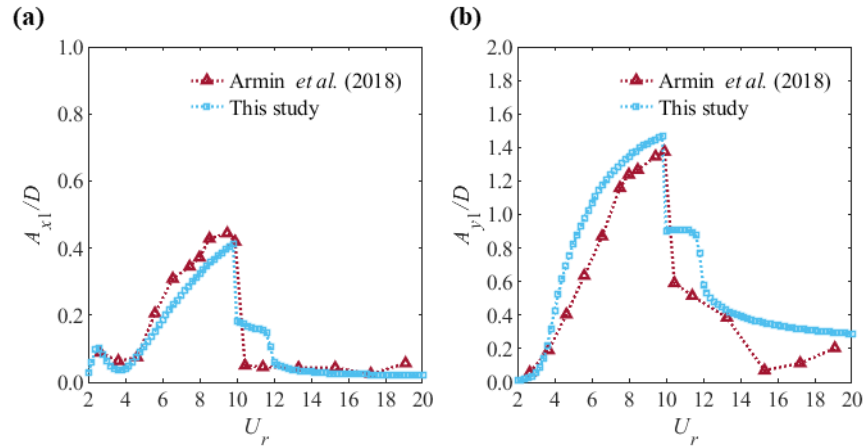


Figure 3-3: *rms* amplitudes of vibrations of the upstream cylinder against variation of U_r . (a) displacements in the streamwise direction; (b) displacements in the crossflow direction.

Moreover, features of the upper-to-lower branch drop in amplitudes of responses are well represented in the two directions. However, the model yields slightly greater amplitudes of vibration for the lower branch regime ($10 < U_r < 12$). Even though the reference measurements of Armin *et al.* [25] do not show such an evident lower branch of VIV responses, it is interesting to observe this feature reflected on the model results, since many 2DOF VIV studies of isolated cylinders of low mass ratio have shown similar trends [15, 51]. This feature is directly related to the incorporation of structural geometric nonlinearities [63] into the modelling theory as discussed previously. Overall, oscillation amplitudes of the upstream cylinder are satisfactorily captured by the model in both directions.

3.1.2. Calibration of Geometric Nonlinearities

Following the calibration of the wake oscillator empirical parameters associated with the upstream cylinder, the focus is now on the calibration of input parameters for the downstream cylinder. Initially, a parametric investigation of the geometric nonlinear empirical parameters is conducted.

All four parameters related to the downstream cylinder have been varied from 0 to 2, as similarly performed by Srinil and Zanganeh [63] in their VIV modelling of a

single cylinder. The results for the sensitivity study of the parameters are presented in Figure 3-4 to Figure 3-7 for inline and transverse amplitudes of vibration at three initial spacing configurations, namely $d = 4, 8$ and 20 .

It is possible to observe that, for $d = 4$, the maximum A_{x2}/D , reaching approximately 70% of a diameter, occurs in a range of approximately $0.5 > \alpha_{x2} > 1.1$ and at intermediary reduced velocities, whilst A_{y2}/D generally tends to increase with U_r up to values close to 2 diameters for all non-zero α_{x2} values. It is important to highlight that the response of the second cylinder is different when α_{x2} is zero than when it is non-zero for most of the spacings. For the cases of $d = 8, 20$, the response of the rear cylinder is mostly resonant (lock-in), in the sense that there is a range of intermediate reduced velocities that leads to the greatest oscillation amplitudes, whereas out of this domain (larger U_r) the amplitudes of vibration are greatly reduced. Variation of α_{x2} for these larger separation setups seems to affect the lower branch more than the lock-in zone.

Similarly, parametric analysis of α_{y2} is presented in Figure 3-5. Variation of α_{y2} leads to the largest amplitudes of vibration, reaching values close to $A_{x2}/D = 1$ and $A_{y2}/D = 3$ respectively. This is due to the relationship between α_{y2} and the cubic value of the transverse oscillation amplitudes, as demonstrated by Equation (3-10), which are normally known to be larger than the inline amplitudes. Overall, values of $\alpha_{y2} > 0.6$ result in smoother numerical response amplitudes.

Thereafter, the increment of β_{x2} from 0 to 2 is presented in Figure 3-6 and it is shown to increase inline amplitudes of vibration, whilst transverse oscillation amplitudes remain mostly unaffected. This is an interesting feature that can be useful in the calibration of the model. Indeed, it will be discussed in the following that β_{x2} is the only parameter changed from reference values of the literature.

Finally, the results of the parametric study of β_{y2} are presented in Figure 3-7. It is seen that lower values of β_{y2} tend to enlarge amplitudes of vibration in both directions (x_2 and y_2) and variation of this parameter appears to cause fluctuations of cylinder response in general.

The structural model nonlinearities have been considered to improve the present modelling theory. These are specifically relevant to the 2DOF modelling given that previous studies have demonstrated the capability of this modelling approach in better predicting the inline-to-crossflow frequency ratio and the lower branch of oscillation amplitudes of a single cylinder undergoing VIV [46, 63, 65]. In the following section,

the investigation considers whether the higher order structural parameters contribute to the modelling representation of 2DOF systems of multiple cylinders.

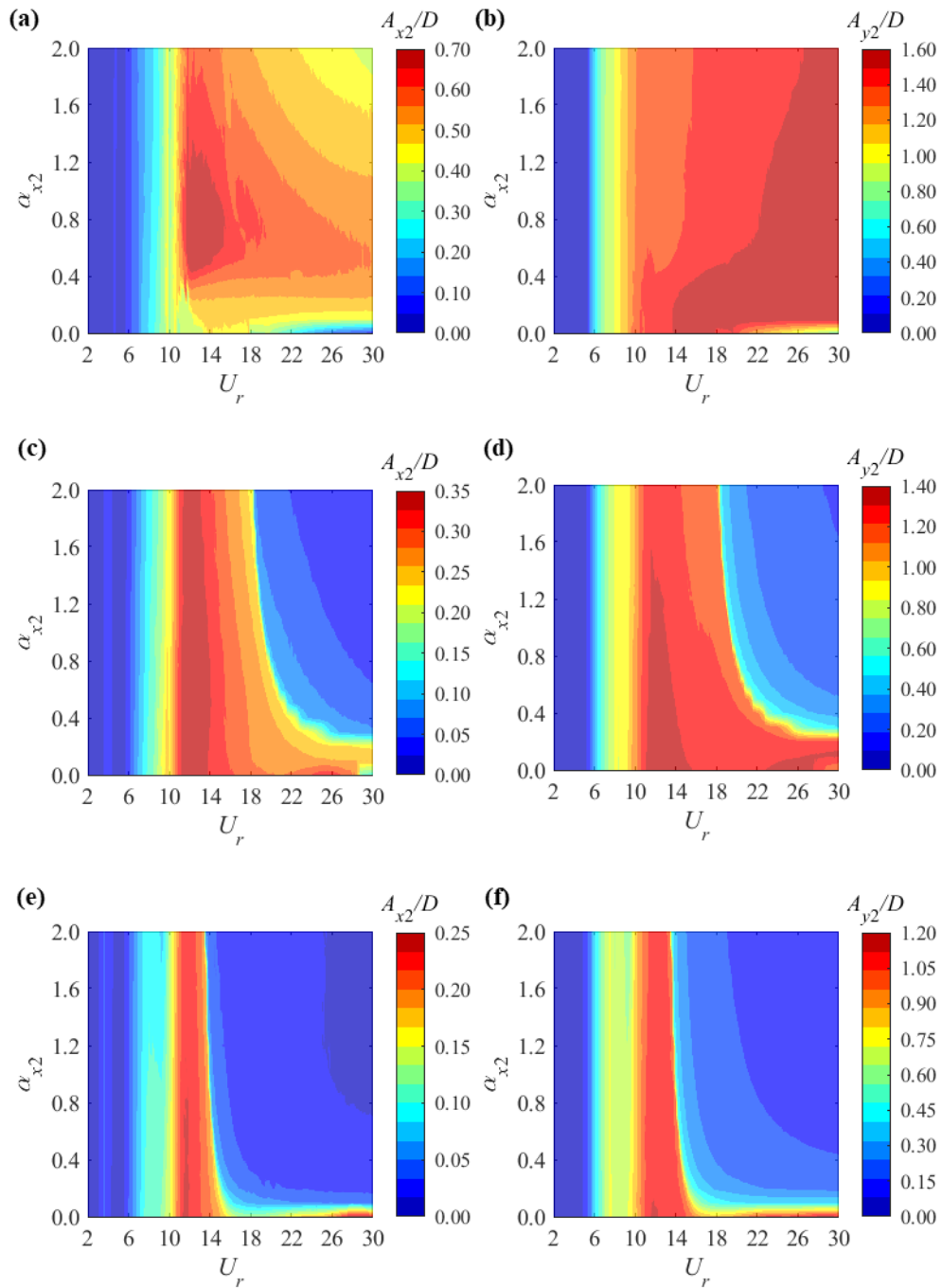


Figure 3-4: Dependency of amplitudes of vibrations against U_r on the geometric nonlinear parameter, α_{x2} . (a) A_{x2}/D for $d = 4$; (b) A_{y2}/D for $d = 4$; (c) A_{x2}/D for $d = 8$; (d) A_{y2}/D for $d = 8$; (e) A_{x2}/D for $d = 20$; (f) A_{y2}/D for $d = 20$.

The empirical parameters have been defined as $\alpha_{x2} = \alpha_{y2} = \beta_{y2} = 0.7$, following Zanganeh and Srinil [63], however, based on the parametric studies conducted and previously discussed, it is proposed that $\beta_{x2} = 2$. This is justified by the larger inline amplitudes reported for WIV in the literature [23, 25, 31].

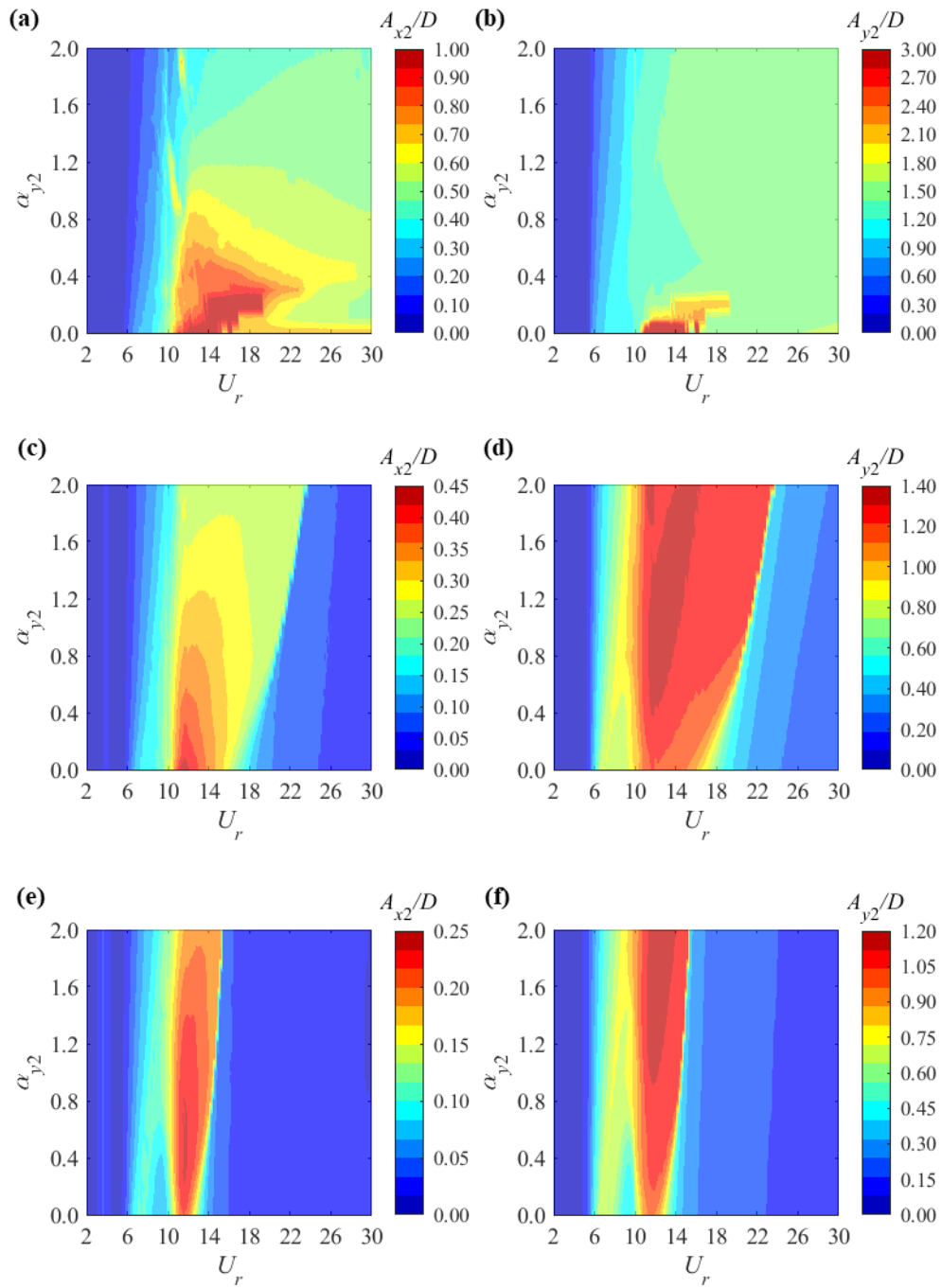


Figure 3-5: Dependency of amplitudes of vibrations against U_r on the geometric nonlinear parameter, α_{y2} . (a) A_{x2}/D for $d = 4$; (b) A_{y2}/D for $d = 4$; (c) A_{x2}/D for $d = 8$; (d) A_{y2}/D for $d = 8$; (e) A_{x2}/D for $d = 20$; (f) A_{y2}/D for $d = 20$.

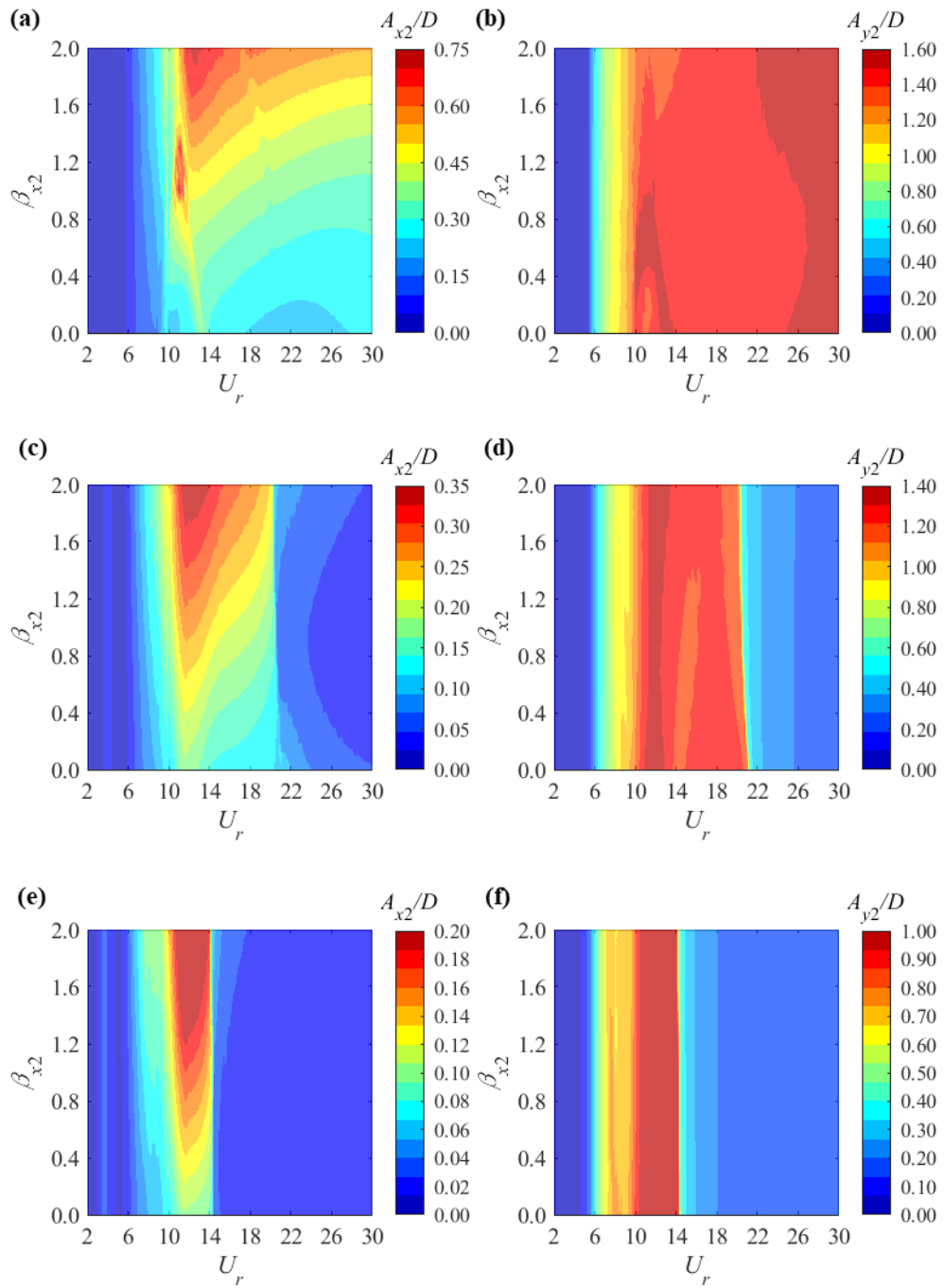


Figure 3-6: Dependency of amplitudes of vibrations against U_r on the geometric nonlinear parameter, β_{x2} . (a) A_{x2}/D for $d = 4$; (b) A_{y2}/D for $d = 4$; (c) A_{x2}/D for $d = 8$; (d) A_{y2}/D for $d = 8$; (e) A_{x2}/D for $d = 20$; (f) A_{y2}/D for $d = 20$.

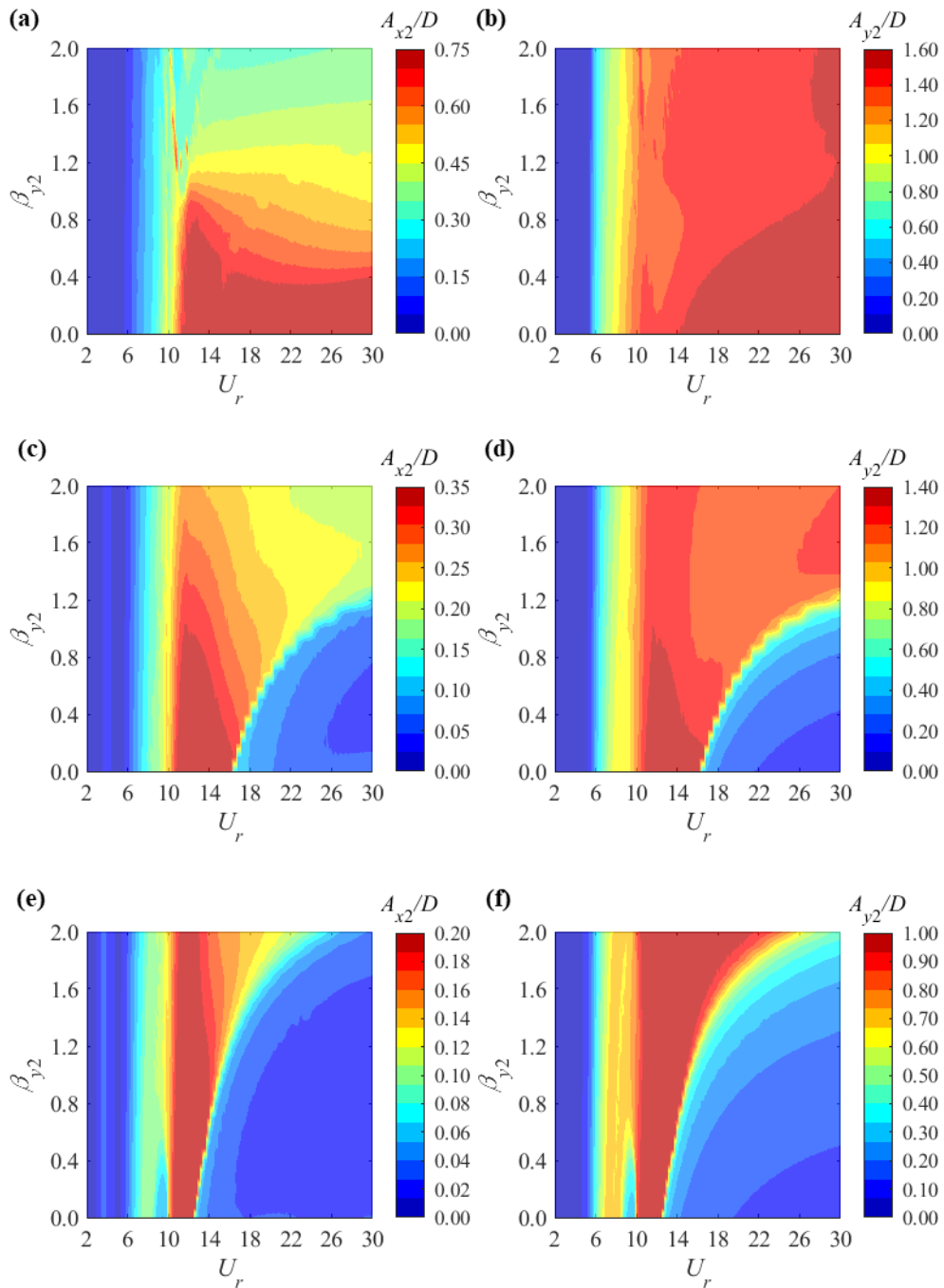


Figure 3-7: Dependency of amplitudes of vibrations against U_r on the geometric nonlinear parameter, β_{y2} . (a) A_{x2}/D for $d = 4$; (b) A_{y2}/D for $d = 4$; (c) A_{x2}/D for $d = 8$; (d) A_{y2}/D for $d = 8$; (e) A_{x2}/D for $d = 20$; (f) A_{y2}/D for $d = 20$.

3.1.3. Wake Flow Parameters and Hydrodynamic Coefficients

Modelling of the system excitation hydrodynamic forces and the wake deficit flow acting on the downstream cylinder are highly dependent on the definition of hydrodynamic reference coefficients and wake flow empirical parameters respectively. Regarding the latter, wake flow parameters will be calibrated taking in consideration

the length and width of the wake flow and their dependence on the spacing, d , which in 1DOF discussed in Chapter 2 would not vary with time. The parameters herein are adapted for the time-varying displacement in the inline direction and are assumed as $\lambda = 0.74(\delta x + d)^{0.61}$, $\alpha = 0.53(\delta x + d)^{0.17}$, $\beta = -0.15$ for $\eta > 0$, $\beta = 0$ at $\eta = 0$, and $\beta = 0.15$ for $\eta < 0$.

Similarly, the hydrodynamic reference coefficients and Strouhal numbers are based on previous studies and experimental measurements. In summary, $C_{D1} = 2.0$, $C_{D2} = 1.2$, $C_{D1}^{fl} = 0.2$, $C_{D2}^{fl} = 0.2$, $C_{L1} = 0.3$, $St_1 = 0.2$ and $St_2 = 0.2$ [36, 45, 48]. The exception is that $C_{L2} = 0.6$ is now considered as suggested by the experiments of Alam *et al.* [49].

Since there is not a consensus and these values may have small variations from study to study, it is important to understand how the reference hydrodynamic coefficients and Strouhal numbers affect the 2DOF behaviour of the downstream cylinder. This is presented in Figure 3-8 and Figure 3-9.

Overall, it is possible to observe that the reference parameters related to the upstream cylinder, C_{L1} , C_{D1} , St_1 and C_{D1}^{fl} mostly do not affect the XY response of the downstream cylinder significantly. However, when these parameters do influence the behaviour of the rear cylinder, this occurs mainly at the first VIV peak. The first VIV peak is a known feature of two tandem cylinders dynamics (within the co-shedding regime), where the downstream cylinder behaves as a single cylinder solely undergoing VIV for low reduced velocities, as discussed by Assi *et al.* [11] and on Chapter 2. Therefore, the fact that the model is sensitive to these parameters within the first VIV regime is interesting and expected. Even though some of these parameters are directly presented in the wake flow equations of the second cylinder, e.g., C_{D1} features in Equations (3-3), (3-5), and (3-6), upon further model investigation, it has been determined that the mentioned small change of response outputs of the downstream cylinder with variation of parameters of the upstream cylinder is predominantly given indirectly through δx and δy .

On the other hand, variation of reference parameters associated with the second cylinder, namely C_{L2} , C_{D2} , St_2 , greatly modifies the oscillation amplitudes of the downstream cylinder. Changes in C_{L2} within the range of values studied lead to the greatest effect on A_{y2}/D , as expected since the lift force acts in the y direction as seen in Figure 3-1, but interestingly, a similar feature also occurs for A_{x2}/D . Such an observation suggests that the inline response of the downstream cylinder is heavily

dependent on the crossflow response. This has been reported and is well known for the problem of single cylinder VIV [66], so is interesting to also observe for WIV.

In terms of the mean drag coefficient, it is observed that C_{D2} is inversely proportional to A_{y2}/D . Hence, increments in C_{D2} result in lower amplitudes of vibration, but obviously a larger mean drag displacement of the downstream cylinder. The Strouhal number, being directly linked to the damping term in Equations (3-10), is also inversely proportional to the response amplitudes, although affecting A_{x2}/D significantly more than A_{y2}/D . This is possibly due to the fact that the inline frequency (and Strouhal number) is doubled as shown in Equations (3-10), which should affect the *rms* amplitude of cylinder displacements, A_{x2}/D . Lastly, one may notice that the model is insensitive to variation of C_{D2}^{fl} , as similarly demonstrated for C_{D1}^{fl} .

3.1.4. Wake Oscillator Parameters Associated with the Downstream Cylinder

Analogous to what has been done for the upstream cylinder in Section 3.1.1, the calibration of the last set of empirical parameters, which are associated with the wake oscillator in the equations of the downstream cylinder, Λ_{x2} , Λ_{y2} , ε_{x2} and ε_{y2} , is now addressed.

Optimisation methods are once again employed to minimise the errors between the predicted amplitudes of responses and the experimental results of Armin *et al.* [25] in both directions.

Moreover, a simplified schematic of the optimisation procedure based on the Nelder-Mead simplex algorithm [57] for the unidimensional calibration of the empirical parameter Λ_{y2} is presented in Figure 3-10. In practice, at each algorithm iteration, the model is evaluated and errors compared and reduced. The error tolerance has been set up as 0.1% difference between the model results and experimental reference data, which is averaged for the two directions. The other stopping criteria are: i) stop when the maximum number of model evaluations is 2000, ii) stop when the value of the calibration parameter is varied more than 0.001, but the function (integration of model equations) does not change more than 0.001. Usually, the optimisation procedure would stop due to either reaching the expected precision of 0.1%, which led to the best comparison, or due to criterion ii), meaning that at a certain point, further looking to optimise Λ_{y2} would neither effectively improve nor deteriorate the comparison between model and reference experiments.

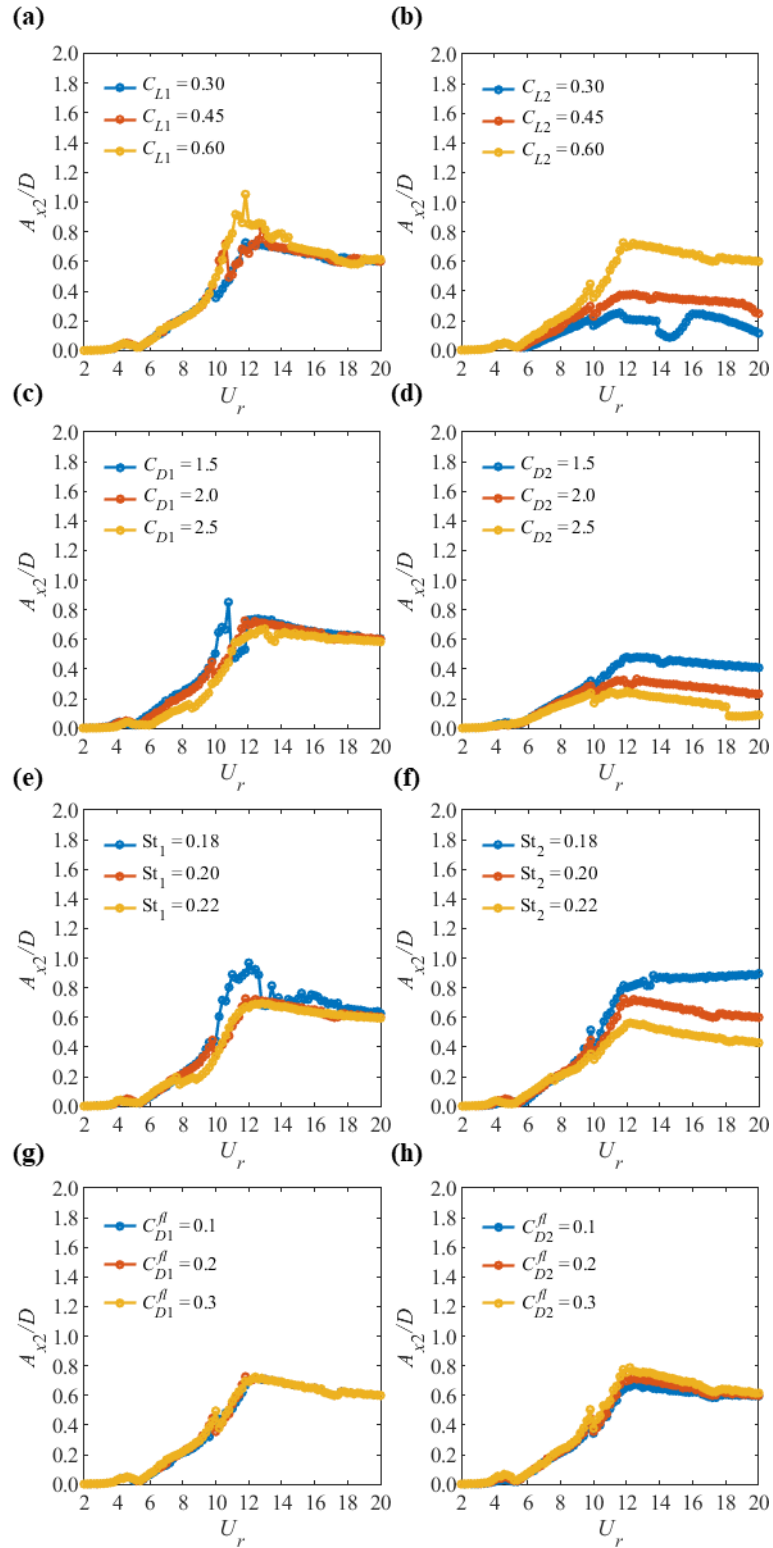


Figure 3-8: Parametric study of the reference force coefficients and Strouhal numbers on the oscillation amplitudes of downstream cylinder against U_r in the inline direction for $d = 4$.

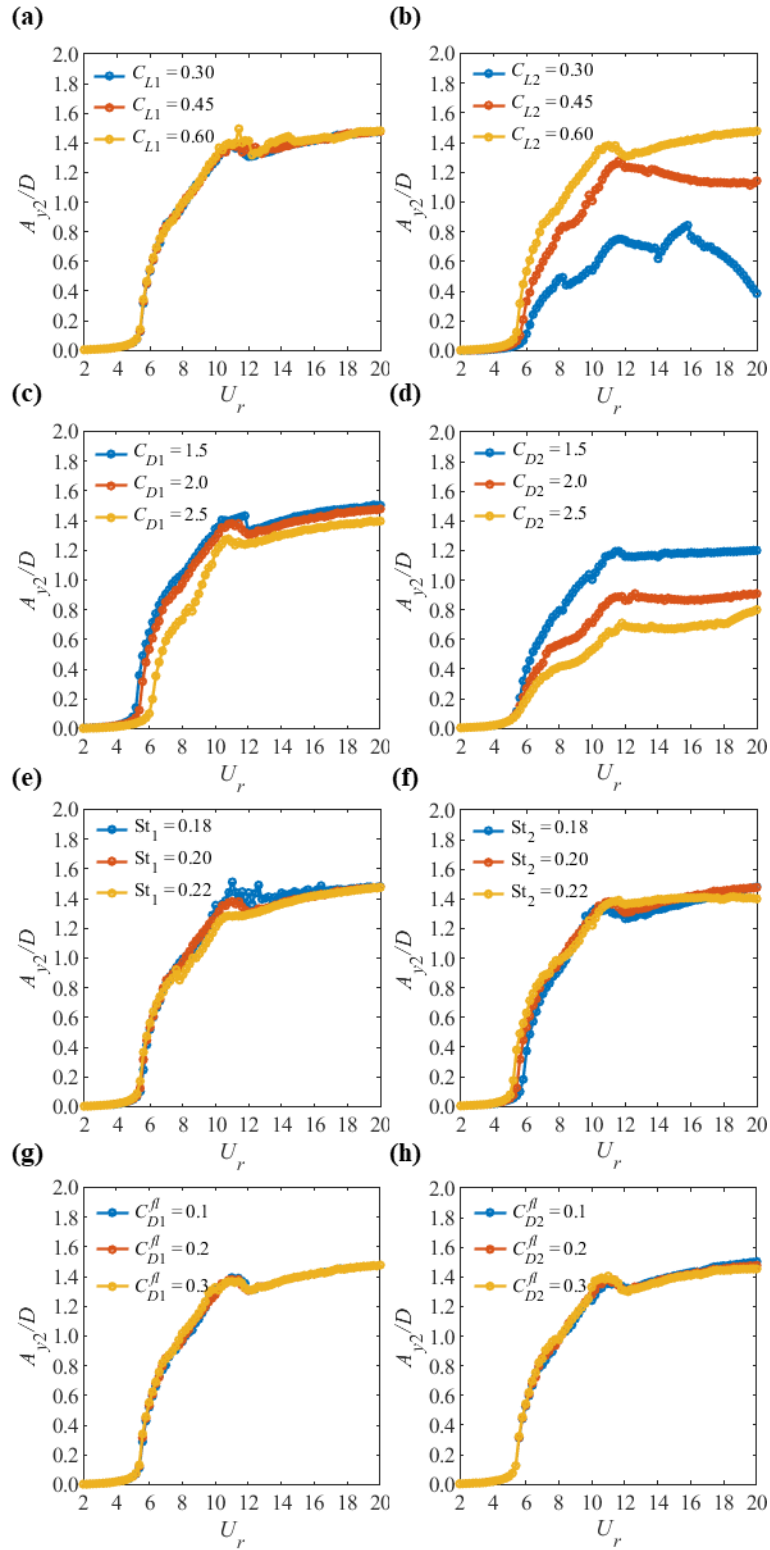


Figure 3-9: Parametric study of the reference force coefficients and Strouhal numbers on the oscillation amplitudes of downstream cylinder against U_r in the crossflow direction for $d = 4$.

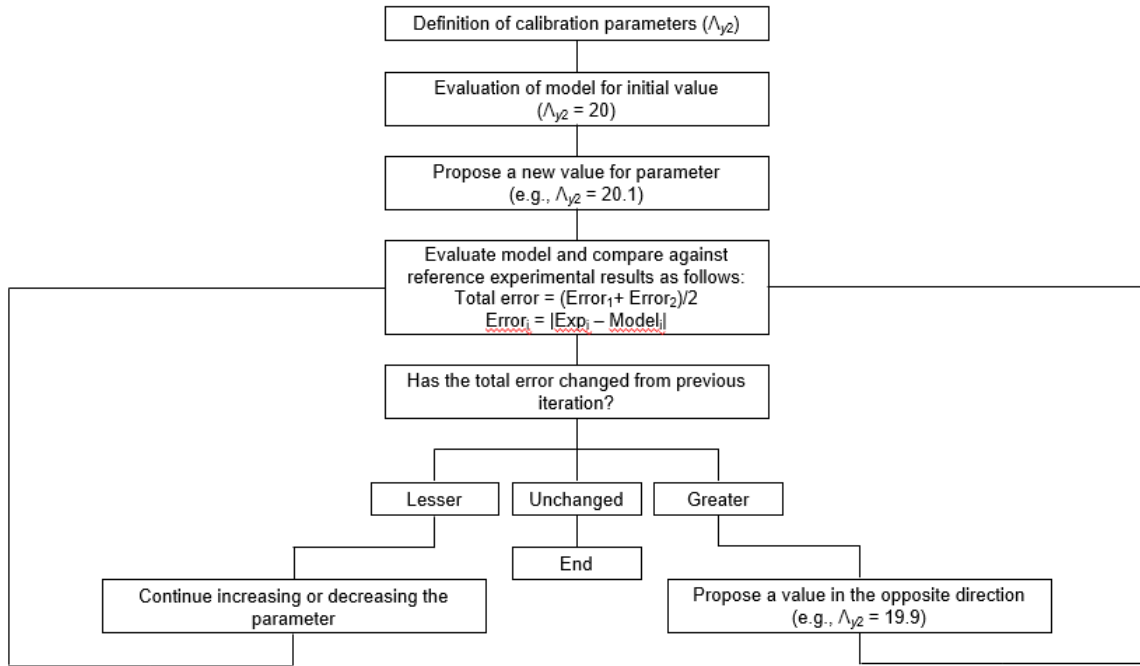


Figure 3-10: Simplified flowchart of the optimisation algorithm based on the derivative-free unidimensional Nelder-Mead simplex scheme for minimisation of errors between model results and experimental reference data for 2DOF amplitudes of vibrations of the downstream cylinder.

Optimisation can be a powerful mathematical tool when applied to empirical or semi-empirical models. However, it is not an intrusive technique in the sense that it cannot change the model structure. Nevertheless, the procedure has been applied to the model and compared to the reference experimental data for each U_r and d , yielding an overall good comparison and capturing the most important features of WIV.

Therefore, for each of the 91 U_r points and five initial spacings ($d = 4, 6, 8, 10$ and 20) considered, the algorithm returned an optimum Λ_{y2} , totalling 455 values. Through nonlinear regression, five curves have been generated to approximate the trend of the 91 optimal points of Λ_{y2} . Thus, it has been concluded that the type of function that provided the best curve fitting was a rational of third over second order polynomials, resulting in five rational functions – one for each spacing. Subsequently, it has been observed that these five functions would qualitatively resemble each other to a degree. From this observation, it was possible to select a reference polynomial function ($d = 8$) from the five and calibrate a function of spacing that would lead to improved results, while satisfying a more general model. This way, $\Lambda_{y2}(U_r, d)$ has been established as a combination of a function of spacing and a function of U_r as follows:

$$\Lambda_{y2}(U_r, d) = \left(\frac{0.97d^2 - 15.6d + 79.99}{d^2 - 11.34d + 42.63} \right) \left\{ \frac{0.09U_r^3 + 2.24U_r^2 - 67.02U_r + 373.7}{U_r^2 - 21.05U_r + 114.2} \right\} \quad (3-11)$$

These individual functions of d and U_r and their final combined form (Equation (3-11)) have been plotted in Figure 3-11.

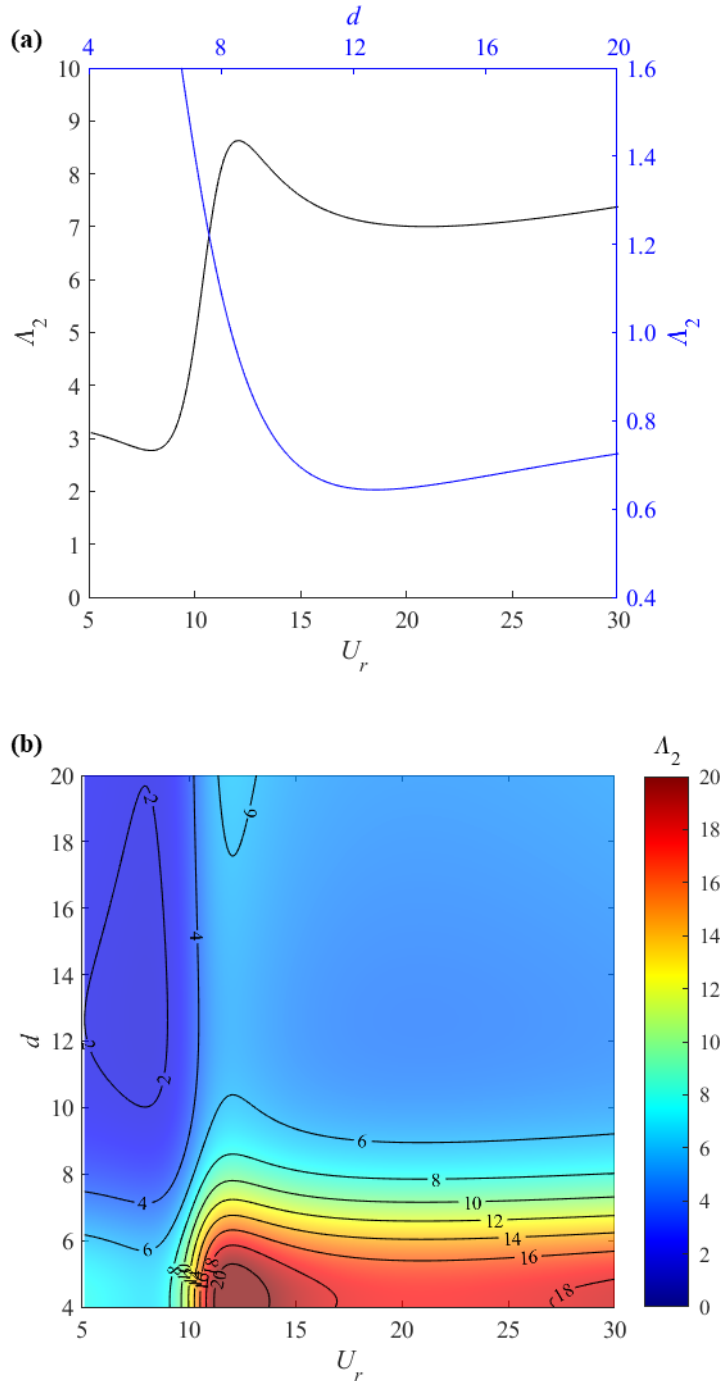


Figure 3-11: Variation of empirical wake-deficit oscillator coefficient, Λ_{y2} , (a) as a function of U_r or d , and (b) as a function of combined U_r and d .

Initially, it can be observed that the individual function of U_r presents some similarities to WIV oscillation amplitude curves against U_r , as it will be detailed in Section 3.3. This is expected as Λ_{y2} is directly related to the excitation force acting on the downstream cylinder. The individual function of d is highest for low spacings and rapidly decreases with increasing increments of separation distance between the cylinders within the WIV-dominated zone ($d < 10$). For higher spacings, the function reaches a plateau as the downstream cylinder starts to return to single cylinder behaviour. The final version of the function, plotted against U_r and d in Figure 3-11, clearly demonstrates the well-known decay of hydrodynamic forces acting on the downstream cylinder once the initial separation of cylinders increases. The maximum Λ_{y2} is approximately 20.

Finally, $\epsilon_{y2} = 0.1$ has been obtained from an initial sensitivity study of the model. Given the negligible sensitivity of model XY response to variations in ϵ_{x2} and Λ_{x2} , for simplicity they are considered equal to their y -associated counterparts.

3.2. Validation of Oscillation Amplitudes and Study of Dependence on Mass Ratio

Using the same numerical scheme previously mentioned along with the newly defined input empirical parameters, the model was simulated and validated against the results of Armin *et al.* [25]. It is important to note that very few studies are available on 2DOF vibrations of two tandem cylinders. To the best of knowledge, most similar studies to date [23, 24] [16-18, 20, 37] have been reviewed and compared to the model predictions. However, most of these results significantly differ in terms of Reynolds number, mass and damping properties, distance of cylinders, configurations, reduced velocities, and features discussed. Therefore, considering two cylinders free to oscillate in 2DOF and a more detailed investigation in terms of spacings and reduced velocities, the experimental tests of Armin *et al.* [25] have been used as reference data. Results are presented in Figure 3-12.

Comparison of oscillation amplitudes in both directions has been conducted for the spacings of $d = 4, 8, 15$ and 20 . Initially, it can be seen that both experimental and numerical results exhibit considerably more amplitude fluctuations than a similar 1DOF system. This greater response variation may be attributed to the effect that the dynamic relative spacing ($\delta x + d$) has on the downstream cylinder. The dynamic relative spacing is a combination of three factors: i) the initial centre-to-centre separation between the cylinders in the streamwise direction, ii) the instantaneous relative difference between

mean drifts of both cylinders caused by the mean hydrodynamic drag forces and iii) the instantaneous relative difference of vibration amplitudes of both cylinders in the inline direction. The relative importance of each of these three factors on the present study are in order. The initial centre-to-centre separation (i) is $d \geq 4$, the instantaneous relative difference between mean drifts of both cylinders (ii) can reach a maximum of approximately $d = 2$ as seen in trajectories of oscillations; and the instantaneous relative difference of vibration amplitudes between both cylinders can reach a maximum of approximately $d = 1$ ($x_1 + x_2$) as seen in the analysis of inline amplitudes of vibrations. Therefore, all these factors may strongly influence the behaviour regime of the rear cylinder and may lead to a greater degree of disorder in the responses.

For $d = 4$, as seen in Figure 3-12a-b, both A_{x2}/D and A_{y2}/D reflect a behaviour predominantly governed by WIV, as discussed in Chapter 2, in the sense that the oscillation amplitudes are non-resonant and continue to rise with increase of reduced velocities up to the largest U_r studied. However, for 2DOF this happens in terms of general trends since the fluctuations lead to local peaks of amplitudes. Nevertheless, the WIV-dominant trend of XY response amplitudes increases with U_r .

Large amplitudes of vibration are not restricted to the lock-in condition, as in the problem of VIV of single cylinders. Whilst WIV of the downstream cylinder does lead to a greater absolute maximum A_{y2}/D for high U_r than VIV of only one cylinder, the greatest change comes for A_{x2}/D , which is more than doubled (for $d = 4$) for flow-induced vibrations of two cylinders, when compared to flow-induced vibrations of an isolated cylinder with similar mass and damping properties, as in the study of Jauvtis and Williamson [15].

For $d = 8$, as shown in Figure 3-12c-d, the same general trend of a WIV-dominant response is observed, although considerably milder than for $d = 4$. This observation contrasts with previous 1DOF studies [11] and with the results of Chapter 2, that have shown that the second cylinder would start to behave in a combined WIV-VIV for $d = 8$, resulting in a plateau of amplitudes of vibration with increase of U_r . To understand why the results of 2DOF systems at $d = 8$ still behave in a WIV-dominant manner with progressive magnification of oscillation amplitudes with the increase of U_r , the instantaneous model cylinder displacements are analysed.

The mean drift of the first cylinder averaged across $U_r \geq 10$ is approximately 1.2 diameters, while for the second cylinder it is about 0.8 diameter for $d = 8$. This is expected given that the mean drift is a direct product of the hydrodynamic drag which

is reduced for the wake flow acting on the downstream cylinder. In conclusion, this makes the two cylinders closer.

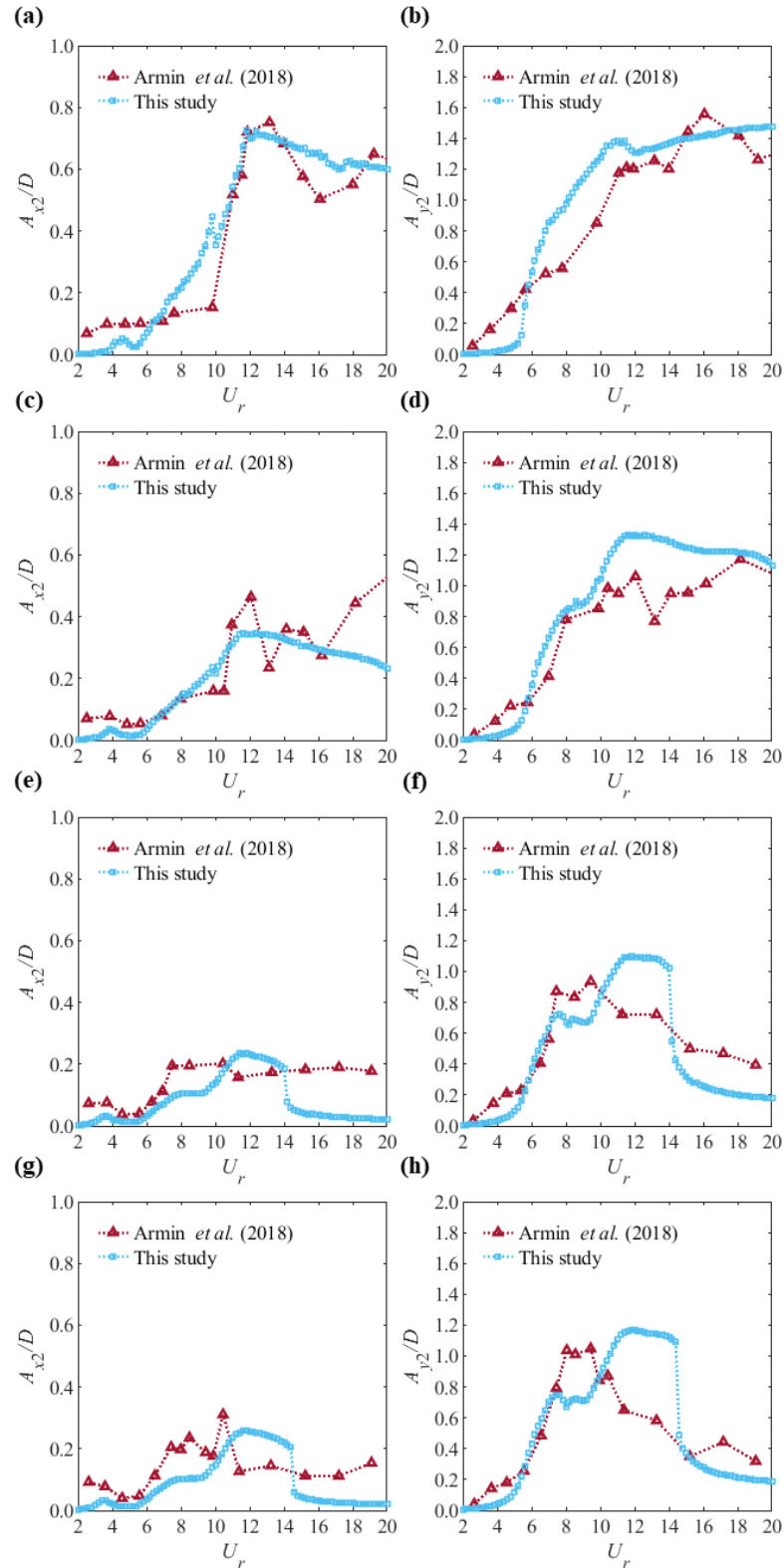


Figure 3-12: Inline and crossflow *rms* oscillation amplitudes dependency on U_r for the downstream cylinder of a tandem pair of identical cylinders at different initial spacings with $m^* = 2.36$, and $\zeta = 1.55\%$. (a) A_{x2}/D for $d = 4$; (b) A_{y2}/D for $d = 4$; (c) A_{x2}/D for $d = 8$; (d) A_{y2}/D for $d = 8$; (e) A_{x2}/D for $d = 15$; (f) A_{y2}/D for $d = 15$; (g) A_{x2}/D for $d = 20$; (h) A_{y2}/D for $d = 20$.

Furthermore, if it is considered that the two cylinders do not always vibrate with the same frequency, as indicated by other studies [58] and Chapter 2, and may oscillate towards each other at given times, this can be up to one further diameter closer. Therefore, a two-cylinder scheme with an initial $d = 8$ may in reality be vibrating a lot closer to each other than thought. This suggests that for 2DOF systems, the downstream cylinder may oscillate in a WIV-dominant regime even for larger initial separations yielding larger amplitudes of vibrations, due to the dynamic relative movement of the two cylinders.

The response amplitudes for $d = 15$ and $d = 20$ are quite comparable to each other. These responses amplitudes resemble that of a single cylinder undergoing VIV as also remarked by previous studies [11]. For these high initial spacings, the model is able to represent the resonant or lock-in peak, even though it occurs at slightly higher reduced velocities. After the lock-in peak, the desynchronisation is well represented for A_{y2}/D , whereas experimental results for A_{x2}/D seem to remain stable, which is interesting and possibly related to the previously mentioned fluctuations, but this has not been observed in other studies or model results and, thus, needs to be further investigated.

Overall, the calibrated model captures the XY amplitude response of the downstream cylinder qualitatively and quantitatively for most of the U_r range, especially for the lowest initial separation of the cylinders. More importantly, it provides relevant information at a relatively very low computational cost. This has allowed for the analysis of instantaneous dynamic relative streamwise position of the downstream cylinder and will allow further investigation of time and frequency domain analyses in the following section.

Furthermore, a parametric investigation of the mass ratio effect on the inline and crossflow vibrations of the downstream cylinder has been conducted and is presented in Figure 3-13. It is important to remember that the variation of mass ratio is done for both cylinders, preserving the concept of flow-induced vibrations of two identical cylinders.

In general, it is possible to observe that lower mass ratio systems experience a wider range of U_r that leads to larger oscillation amplitudes for both A_{x2}/D and A_{y2}/D . For this kind of system, typically $m^* \leq 3$, a WIV-dominant response regime is seen (depending on damping ratio and Re), where amplitudes of vibration continue to increase up to the highest reduced velocities. On the other hand, larger mass ratios

result in a narrower band of large oscillations and a response dominated by VIV, more in line with what is observed for single cylinders.

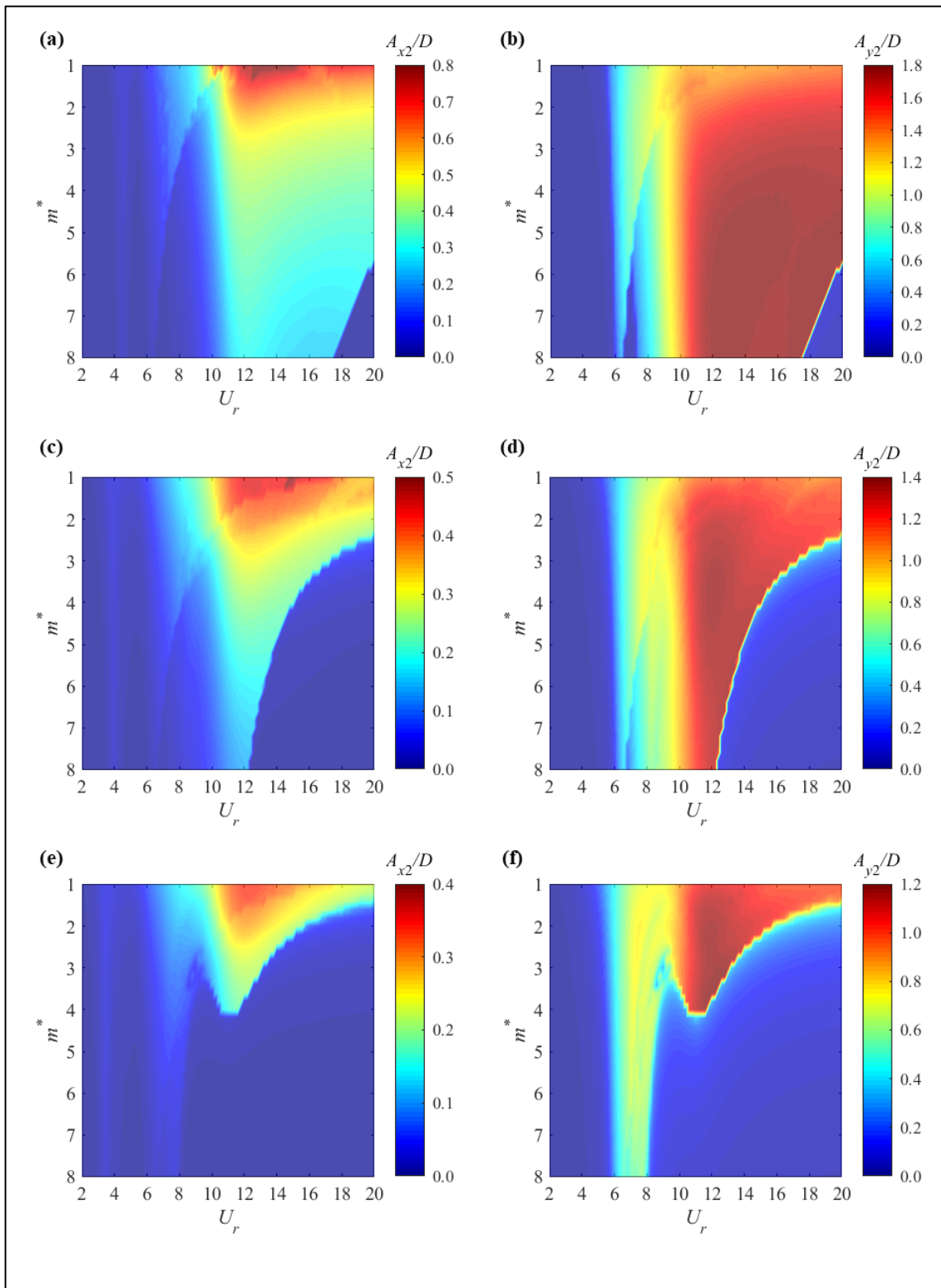


Figure 3-13: Parametric study of variation of mass ratio on the amplitudes of vibrations of the downstream cylinder of the identical pair of tandem cylinders for different initial spacings. (a) A_{x2}/D for $d = 4$; (b) A_{y2}/D for $d = 4$; (c) A_{x2}/D for $d = 8$; (d) A_{y2}/D for $d = 8$; (e) A_{x2}/D for $d = 20$; (f) A_{y2}/D for $d = 20$.

Whilst lower mass ratio systems demonstrate the maximum and wider range of A_{x2}/D , which is in agreement with the literature on VIV [15] and what has been seen in Chapter 2 for 1DOF WIV. However, the addition of the degree of freedom in the inline direction has changed that. One may observe that the maximum A_{y2}/D does not necessarily occur for the lowest studied mass ratios. This finding should be further investigated experimentally to ascertain whether this is a feature of 2DOF WIV systems or merely a model fluctuation of responses as seen and explained before.

3.3. Parametric Investigation and Discussion

Based on the previously developed model and calibration procedure, parametric model simulations were performed and results examined in terms of oscillation trajectories, time histories and frequency domain analyses.

The time evolutions of x_1 , C_{D12} , p_2 and x_2 have been evaluated for $d = 4$ and three reduced velocities, specifically: $U_r = 5, 6$ and 15 , and are presented in Figure 3-14. The leading cylinder is always initially displaced a certain static distance before oscillating. This mean drift, as it has been referred to previously, is due to the hydrodynamic steady drag force and it increases with U_r . As it has been considered in the modelling assumptions that the upstream cylinder behaves as a single cylinder, it is expected that the dynamic displacement of the front cylinder achieves its maximum amplitudes in the resonant or lock-in condition for intermediary reduced velocities. For $U_r = 15$, which is past the known lock-in regime, the oscillation amplitudes are substantially reduced.

Furthermore, the time series of C_{D12} show a distinctive response pattern that is not observed for the other studied parameters. As it has been shown by other studies [10, 49] the wake-induced drag coefficient is minimum at the wake centreline, therefore, the rear cylinder of a tandem pair, when allowed to vibrate across and along the wake flow is subject to the mostly one-sided oscillations that are viewed in Figure 3-14, where the bottom limit of the oscillation cycle of C_{D12} is the minimum wake centreline value. An increase of reduced velocity to $U_r = 15$, suggests a more disordered temporal behaviour, which, as it will be shown later, is related to additional excitation frequency contents.

Moving on to analyse the time histories of the wake variable, p_2 , it can be seen that it always has zero mean values unlike the other parameters presented in Figure 3-14. This occurs due to the modelling definition of p_2 that states that it is a wake variable created to represent the unsteady vortex-induced drag force component,

which if time averaged is equal to zero. It is observed that p_2 increases with U_r for $d = 4$, which is likely related to the WIV build-up of model oscillation amplitude regime discussed in the previous section.

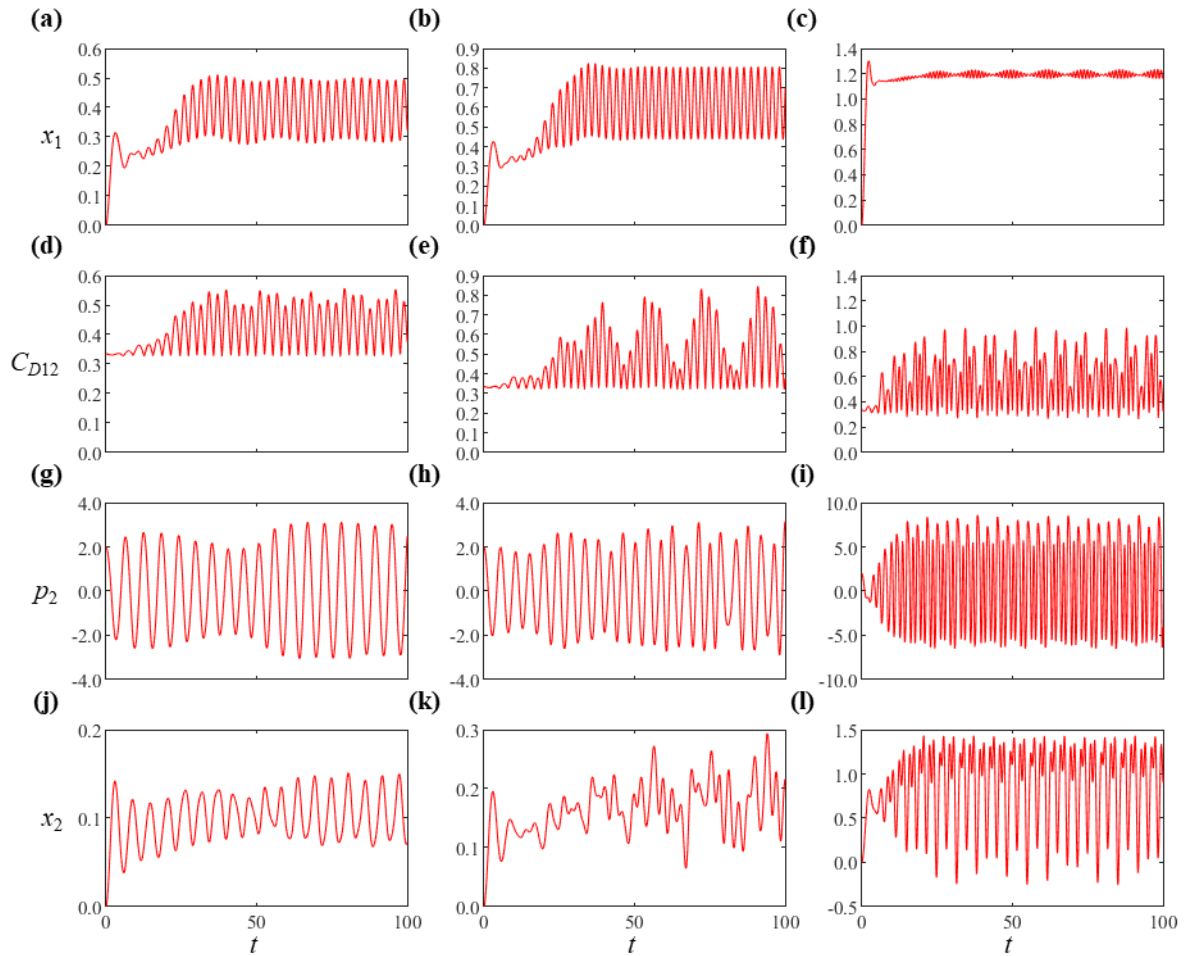


Figure 3-14: Time series of inline response of the cylinders, inline wake variable and wake-induced drag for $d = 4$. First column: $U_r = 5$, second column: $U_r = 6$, and third column: $U_r = 15$.

Finally, the displacement of the downstream cylinder in the streamwise direction is affected by all of the other three parameters through δx , wake flow and wake oscillator equations respectively. The steady hydrodynamic drag force also causes a mean drift of the second cylinder which is smaller than for the first cylinder. This is attributed to the wake deficit and wake-reduced drag force that acts on the downstream cylinder. One may notice that x_2 may behave quite irregularly for $U_r = 6$ and 15 . In fact, the response of x_2 depends on the other parameters which do not behave similarly as discussed.

Interestingly, as well as a high frequency vibration justified by the model definition where the drag force excites the system with double the frequency of the lift force, a lower frequency x_2 oscillation content may also be observed. This is perhaps more

clearly seen for $U_r = 15$, where an oscillation envelope of greater mean drift, lower amplitudes of vibration and apparently twice the frequency is noticeable from the time series. A similar feature is also observed in the time series of experimental tests by Armin *et al.* [25] in the form of an oscillating mean x_2 . Moreover, a likely related feature is also seen for p_2 for the same reduced velocity. This will be investigated in more detail in the following frequency analyses.

The time variation study of the transverse displacement of the cylinders and directly related parameters has also been conducted and is shown in Figure 3-15. From the time series of y_1 , it can be observed that the response is predominantly monoharmonic and resonant, achieving the greatest amplitudes within the lock-in regime, i.e., for intermediary reduced velocities. Increasing U_r past these limits, specifically $U_r = 15$, leads to desynchronisation from $f_{y1}/f_n = 1$ and consequently lower amplitudes of vibration.

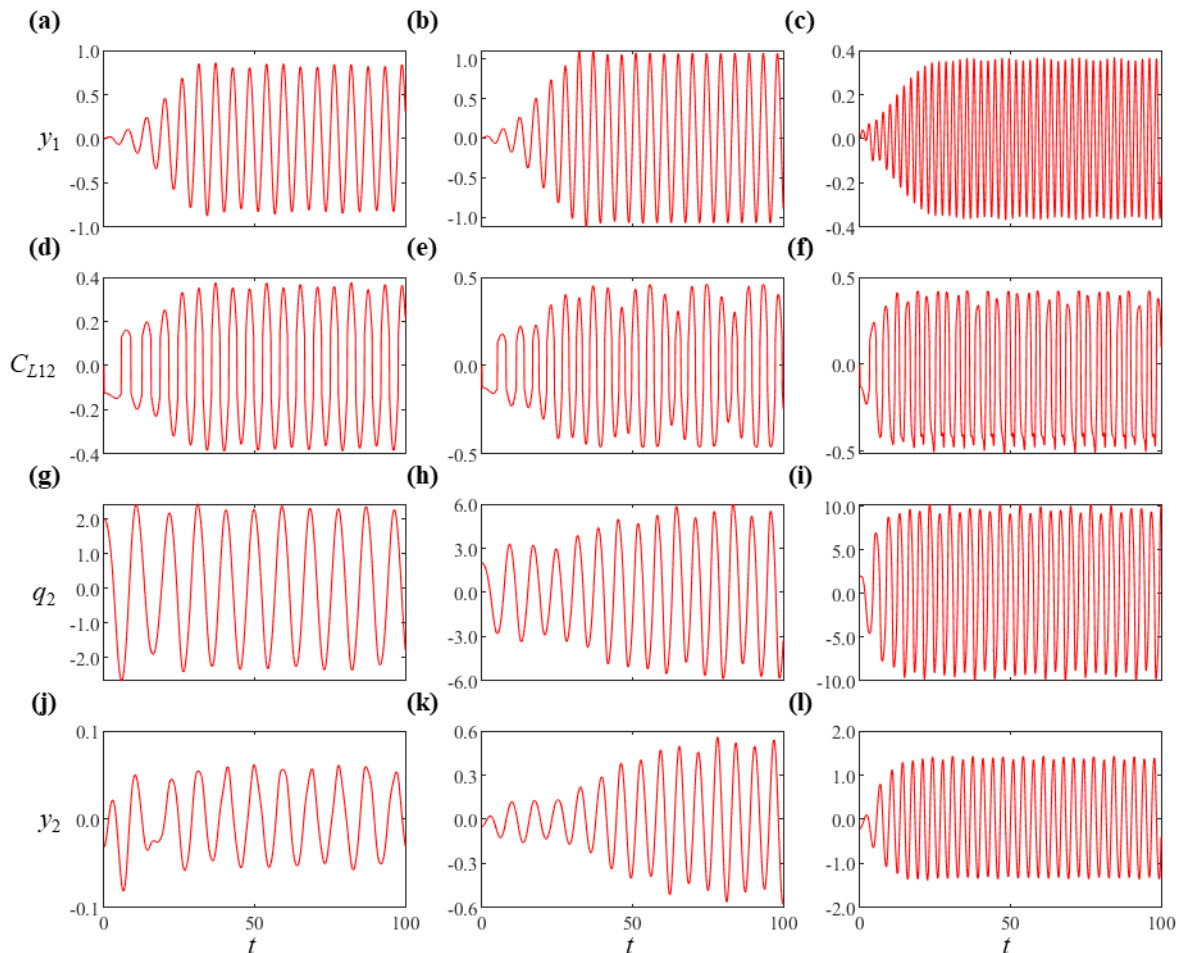


Figure 3-15: Time series of transverse response of the cylinders, crossflow wake variable and wake-induced lift for $d = 4$. First column: $U_r = 5$, second column: $U_r = 6$, and third column: $U_r = 15$.

The temporal behaviour of C_{L12} is also studied where amplitude modulations can be seen for given reduced velocities, which is a possible indication of more than one vibration frequency. The wake-induced lift coefficient does not appear to change significantly in amplitude with increments of U_r for $d = 4$, which is the opposite of what is seen for the wake variable q_2 . This q_2 behaviour is analogous to what has been previously remarked for p_2 . Furthermore, the transverse displacement of the front cylinder, y_2 , is well-behaved and noticeably more organised than the corresponding inline displacement. There is a leap in y_2 amplitude magnitudes in the comparison between $U_r = 6$ and $U_r = 15$. This is a clear example of a WIV-dominant response, where amplitudes are not resonant, but instead increase progressively with the increment of reduced velocities.

In general terms, it has been demonstrated how the inline response of the downstream cylinder may be more irregular than its respective transverse displacement. Thus, it is important to understand how the instantaneous 2DOF trajectories of the cylinders develop with time. These have been plotted in Figure 3-16 for $d = 4, 8$ and 15 for four reduced velocities cases each.

Initially, the oscillation trajectories of the front cylinder are presented for reference. The first cylinder mainly vibrates in figure-of-8 orbits, moving from elongated figures-of-8 to clearer shapes and then to non-repeatable 8-patterns with the increase of U_r . This feature indicates that the cylinder undergoes one oscillation cycle in the y direction, while conducting two cycles in the x direction, hence, the frequency ratio between the inline and the transverse directions is 2:1. This observation is in agreement with extensive literature data on VIV for a single cylinder [15, 23]. It is worth remembering that as far as the model is concerned, the upstream cylinder behaves as an isolated cylinder and is independent of d due to the modelling assumptions.

On the other hand, the response of the downstream cylinder is heavily dependent on d , Re and other parameters due to WIV [4, 11]. It has been demonstrated in Chapter 2 that the 1DOF response of the rear cylinder of a pair in the co-shedding regime past the first VIV peak ($U_r > 5$ in their study) is a combination of wake flow and vortex-structure interactions originating from the disturbed upstream flow (WIV) and its own vortex shedding (VIV). According to the authors, $d = 4$ is a primary example of a WIV-dominated regime of the second cylinder.

From the plane trajectories of the rear cylinder for $d = 4$, it can be seen that an unrepeated figure-of-8 pattern is observed for $U_r = 5$ near the first VIV regime as

explained by previous studies [11] as well as on Chapter 2 and that the increment of reduced velocity turns the cylinder's orbit into a shape that resembles a half-moon, hence with an inline-to-transverse oscillation frequency ratio more closely associated to a 1:1 ratio than to a 2:1 ratio.

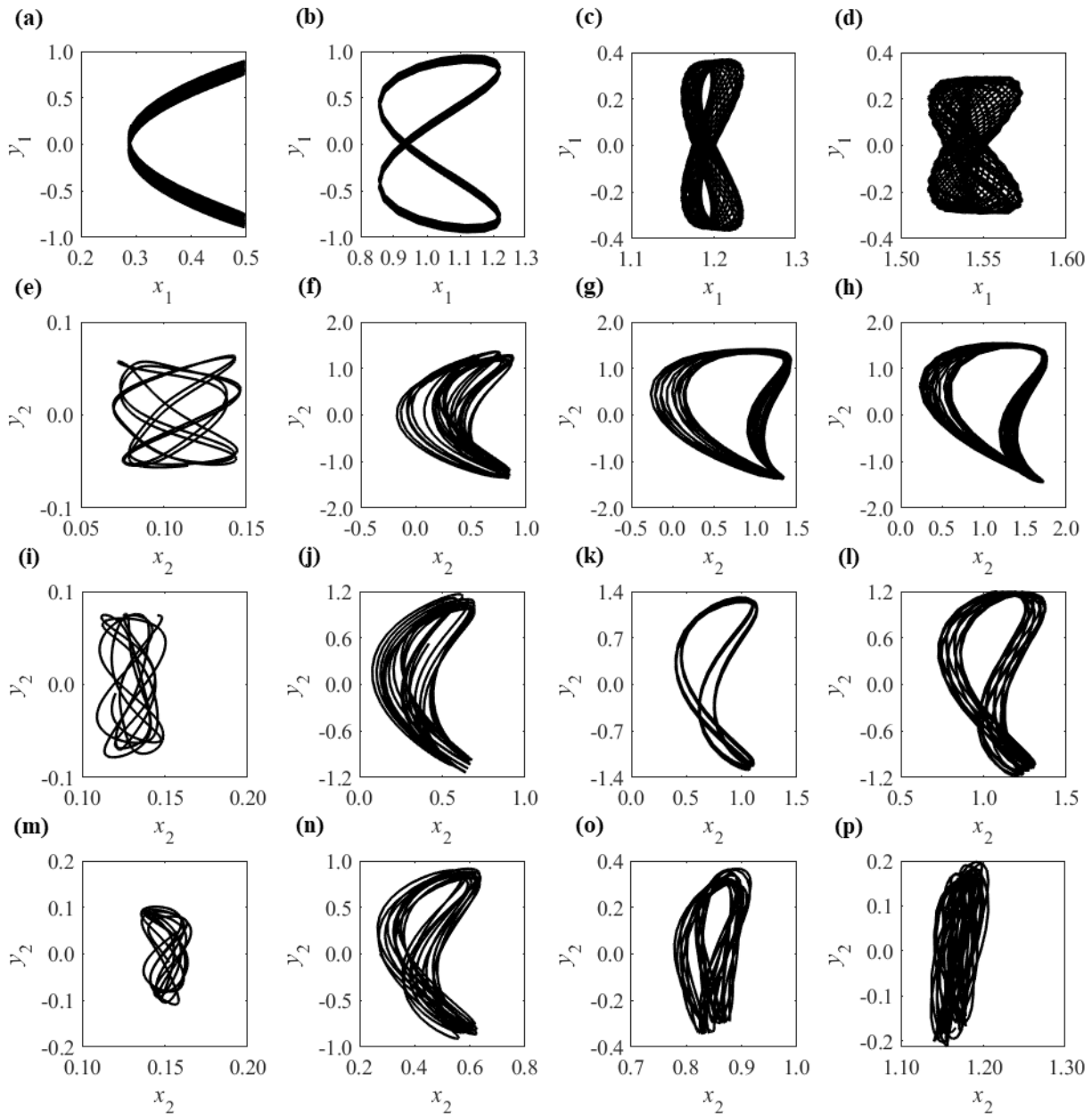


Figure 3-16: Vibration trajectories of the upstream cylinder (first row) and downstream cylinder (remaining rows). First column: $U_r = 5$, second column: $U_r = 10$, third column: $U_r = 15$, and fourth column: $U_r = 20$.

The half-moon-like shape is visibly symmetric for $U_r = 10$ and becomes asymmetrically greater towards the upper side of the wake flow for $U_r = 15$ and 20 . Nevertheless, cylinder trajectories appear to be returning to an asymmetric figure-of-8 for $U_r > 20$. It has been previously demonstrated from the time series investigation that

this asymmetry in the response of the downstream cylinder for WIV-dominated regimes is principally related to the multi-frequency inline response of the cylinder.

It is also relevant to highlight that for $U_r = 15$, during the elapsed time the downstream cylinder vibrates in the negative direction towards the upstream cylinder for up to approximately $-0.5 D$. Whereas, the upstream cylinder drifts and oscillates up to approximately $1.2 D$ towards the rear cylinder. If added this is an approximately $1.7 D$ closer and remembering that the initial spacing of $d = 4$ is measured centre-to-centre, then the cylinders may only be separated by $1.3 D$ at a given time, which may pose a risk of collision if the situation further escalates.

With the increase of initial spacing between the cylinders, there is a transition of WIV-VIV excitation mechanism and it can be seen from Figure 3-16. that the trajectories start to take the form of figures-of-8 once again, thus with an inline oscillation frequency twice the value of the transverse component. It is now clear to see that the mean drift of the downstream cylinder is reduced due to the reduced wake-induced drag that acts on it when compared to the first cylinder. This reinforces the idea that the real instantaneous spacing between the cylinders is lower than the initial spacing, which could mean that WIV and larger amplitude vibrations may be observed even for larger initial cylinder separations for 2DOF systems as suggested previously.

In order to further investigate these features, results are now analysed in the frequency domain and presented in Figure 3-17, Figure 3-18, and Figure 3-19, where predominant frequencies have been plotted against U_r for $d = 4, 8$ and 20 respectively.

Initially, oscillation frequencies of the upstream cylinder have been compared against the experimental results of the 2DOF single cylinder system of Jauvtis and Williamson [15] and the 2DOF tandem pair of cylinders system of Armin *et al.* [25] and Pereira *et al.* [24]. It is important to note that only the latter study has been compared in terms of inline vibration frequencies, since these are not available for the single cylinder study nor have the different f_{x2}/f_n trends and features of Armin *et al.* [25] been discussed by the authors.

As previously mentioned, one of the principal model assumptions considered in Chapter 2 is that the first cylinder is not affected by the second cylinder in any way, which means that the upstream cylinder is modelled as a single cylinder. Moreover, it is well-known in the topic of single cylinder VIV that the cylinder initially oscillates at the vortex shedding frequency governed by the Strouhal number. With an increase of reduced velocity, the excitation and cylinder vibration frequency synchronise with the

natural frequency of the system, in what is called the lock-in regime, leading to the largest amplitudes of vibration that a single cylinder under VIV can normally achieve.

It is seen from Figure 3-17a,b that modelled frequencies of vibration follow the Strouhal line (f_{y1}/f_n) and the doubled Strouhal line (f_{x1}/f_n) as expected for approximately $U_r < 4$. Nonetheless, one may observe that the reference experimental measurements do not follow the $St_1 = 0.2$ (transverse direction) nor the $2St_1 = 0.4$ (inline direction) lines, but rather follow a trend of lower frequencies. Considering that they generally should follow the Strouhal law for low reduced velocities as previously mentioned, a possible explanation is that the experimental Strouhal number was different, although unfortunately it has not been measured or presented in the comparison studies.

The adoption of $St_1 = St_2 = 0.2$ has been considered based on previous studies [45]. However, this is not a consensus. For instance, Norberg [67] has reviewed the variation of the Strouhal number especially with Re and, more recently, Srinil *et al.* [46] have proposed a function to account for the Strouhal dependency on the Reynolds number. In that sense, the present model is as good as its input parameter allows, and for $St_1 = St_2 = 0.2$, and oscillation frequencies agree with such values for $U_r < 4$.

As the reduced velocity is increased, whilst experimental transverse oscillation frequencies lock-in to the natural frequency, $f_{y1}/f_n = 1$, for a range of intermediary U_r , the predicted model frequencies continue to follow the Strouhal line. The inline oscillation frequencies mostly follow the doubled Strouhal line as expected. One may observe that frequency results in the two directions occasionally leap for both model and experimental outputs and this may occur especially in the lock-in regime, approximately $4 < U_r < 10$. Physically, this is likely to be associated with vortex shedding wake mode transitions [15].

The frequencies are mostly singular with the exception of cases of very high reduced velocities where two relevant inline frequencies of vibration are observed. Overall, the modelled upstream cylinder vibrates according to the Strouhal law for most of the U_r cases, while the experiments vibrate at slightly lower frequencies and do not follow the Strouhal rule during or after lock-in. However, the 2:1 inline-to-crossflow frequency ratio has been preserved and the model produces realistic figure-of-8 trajectories for the leading cylinder and represents its amplitudes of vibration with good agreement to the experiments in terms of branches of responses and general features.

The observations and findings above shed light on the modelled behaviour of the upstream cylinder, but most importantly these will assist in the novel analysis of the

downstream cylinder response and the phenomenon of 2DOF WIV which will be investigated in the following.

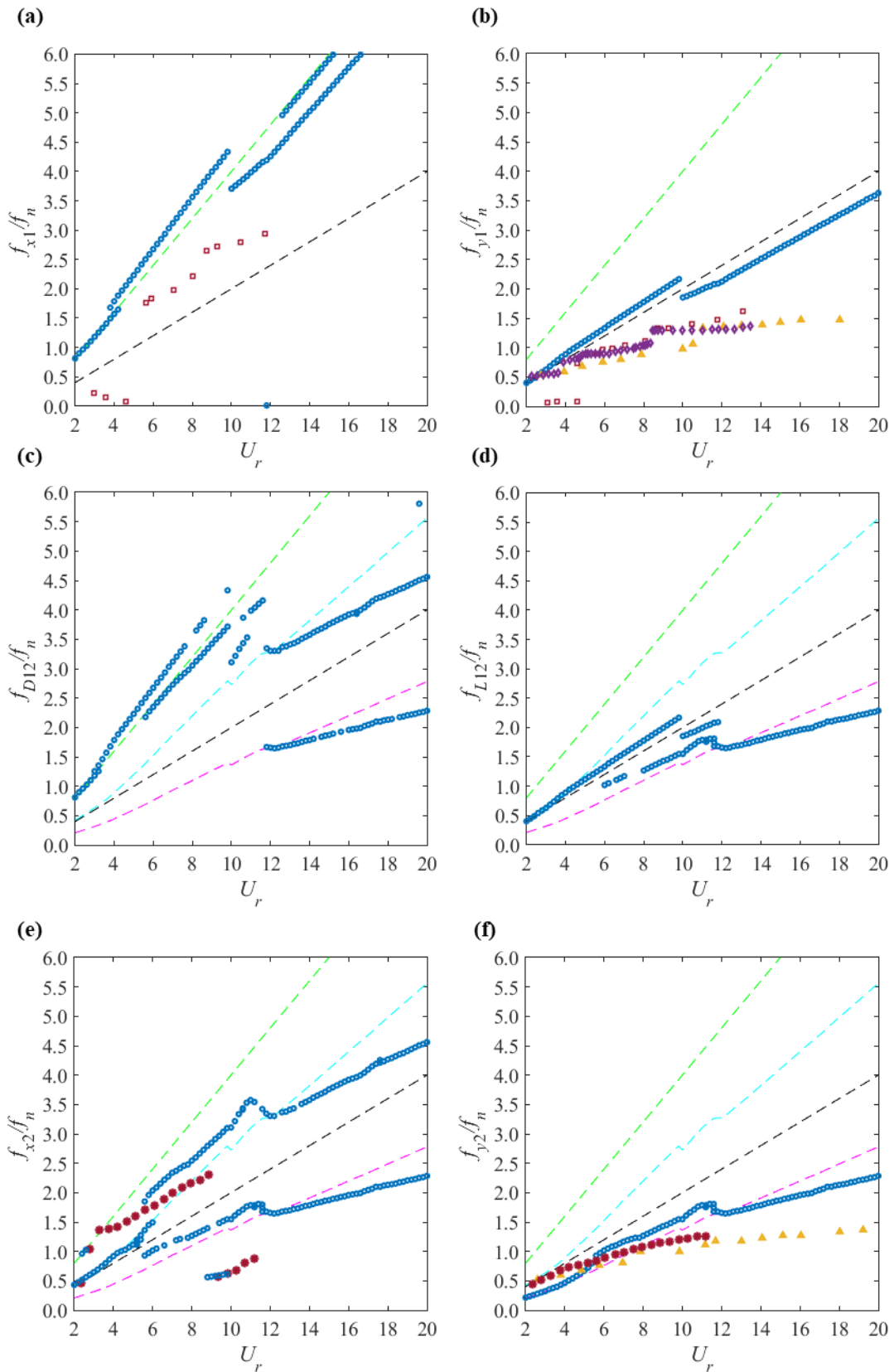


Figure 3-17: Variation of frequencies of oscillations of the pair of cylinders and wake-induced forces with U_r for $d = 4$. Legend: -- St law; -- χ St rule; -- 2St rule; -- 2χ St rule; • Model results; ■ Pereira *et al.* [24]; ▲ Armin *et al.* [25]; ◆ Jauvtis & Williamson [15]; • Assi [23].

It is observed from Figure 3-17 that C_{D12} , C_{L12} and x_2 behave in a multifrequency response for most of the reduced velocities at $d = 4$. Hence, the initial focus is addressed to the analysis of y_2 results. In analogy to the dependency that has been observed between the first cylinder results and the Strouhal rule, frequencies of transverse vibrations of the downstream cylinder mostly follow the wake reduced Strouhal line, χSt , as introduced in Chapter 2. The χSt line has been evaluated according to the average value of χ for a given U_r . Clearly, the mean χ value varies moderately with U_r as $\bar{\delta}x$ and $\bar{\delta}y$ change and this explains why the wake reduced Strouhal line is not completely straight, as in the original Strouhal law.

Within a range of approximately $6 < U_r < 12$, the predominant frequencies of y_2 clearly lock to a slightly higher frequency branch near the natural frequency of the system, $f_{y2}/f_n = 1$. Previous 1DOF studies have shown that this is a range dominated by the VIV excitation mechanism and it has been defined as the first VIV regime or peak [11, 12]. Those studies have concluded that the downstream cylinder responds as an isolated cylinder under classical VIV for low reduced velocities. It is observed that frequencies unlock and return to following the wake reduced Strouhal law for $U_r > 12$. Nevertheless, this apparent synchronisation of f_{y2} to the natural frequency, even though not a perfect constant line at $f_{y2}/f_n = 1$ - which is possibly caused by the WIV mechanism that starts to strengthen and dominate for intermediary reduced velocities - together with the conclusions of the previously mentioned studies suggest that the first VIV peak regime is also observed for 2DOF systems.

On the other hand, f_{y2}/f_n experimental frequencies of vibration are observed very close to the original $St_2 = 0.2$ line for the lowest U_r . Further increment of reduced velocity leads to a greater wake deficit relevance and causes the oscillation frequencies to switch to a gradient that is more aligned with the wake reduced Strouhal concept. At lock-in range, previously estimated within approximately $6 < U_r < 12$, experimental frequencies of vibration are observed close to $f_{y2}/f_n = 1$. The trend of experimental f_{y2}/f_n for post lock-in reduced velocities, $U_r > 12$, increases with a moderate slope until the largest reduced velocities. Even though modelled oscillation frequencies are still mostly governed by the wake reduced Strouhal line, model frequency predictions for the downstream cylinder exhibit a higher degree of fidelity to the experimental results than the respective upstream cylinder comparison. In other words, the frequencies of oscillations of the downstream cylinder (f_2/f_n) are more loyally

represented by the model than the frequencies of oscillations of the upstream cylinder (f_1/f_n).

With these findings in mind, the multifrequency response of other parameters may now be analysed. Frequencies of vibration of the downstream cylinder in the streamwise direction are now studied. From a first glance at the model results in Figure 3-17, it becomes evident that the lower f_{x2}/f_n frequency branch is related to f_{y2}/f_n for $U_r > 6$. Thus, it is concluded that the inline unsteady displacement of the downstream cylinder is directly affected by the transverse oscillation, which is a possible explanation for the 1:1 inline-to-crossflow frequency ratios and half-moon trajectories previously highlighted. This has not been seen for the upstream cylinder and is mathematically traced back to δy in the wake flow modelling, Equations (3-3), (3-5), and (3-6). In fact, there are trace frequencies following the black Strouhal line ($St_1 = St_2 = 0.2$) for the lowest reduced velocities that can be associated to f_{y1}/f_n . This feature indicates that as the downstream cylinder vibrates transversally within the disturbed wake flow, the wake-induced drag and lift forces are significantly affected for most of the reduced velocities studied for $d = 4$.

Furthermore, the upper branch of higher frequencies can be seen mostly following the doubled wake reduced Strouhal line ($2\chi St$), as expected from the model definitions and the previously explained 2:1 drag-lift hydrodynamic frequency ratio. Similar to what has been seen for f_{y2}/f_n , a frequency step synchronisation is observed at approximately $6 < U_r < 12$ for both of the two main inline oscillation frequency branches. Lastly, frequencies close to the green line (representing the doubled undisturbed Strouhal law) are shown for limited points at the lowest reduced velocities. These are related to f_{x1}/f_n and are a consequence of the influence of δx in the wake flow modelling derivation.

The f_{x2}/f_n experimental results of Assi [23] have been added to Figure 3-17 for reference. It can be seen that experimental oscillation frequencies in the inline direction transition from the green original ($2St$) line to the light-blue disturbed ($2\chi St$) line. This implies that the downstream cylinder transitions from an undisturbed regime, where VIV is likely to be the dominant excitation mechanism to a regime where wake flow effects from the upstream wake start to be relevant. This observation corresponds to the features seen from the modelling perspective.

A fact that draws attention when comparing model and experimental results for f_{x2}/f_n is that experimental measurements show only a single frequency. It is

unfortunately unclear whether this is due either to a lack of relevant secondary frequencies for a given U_r or if it is a choice of the researchers to only present the dominant frequencies. For instance, observation of time series of x_2 in Armin *et al.* [25] suggests a multifrequency response. However, there is nothing more that can be ascertained from this from the current point of view as their f_{x2}/f_n frequencies are not directly comparable to the present study. Having said that, in general, f_{x2}/f_n model predictions compare well to the reference measurements for $d = 4$, even in the presence of fundamental differences between the studies, for example Assi [23] has considered a fixed upstream cylinder, with different mass and damping ratios and designed the system to have a natural frequency in the x direction twice the magnitude of that in the y direction.

Finally, for the analysis of the $d = 4$ system, it is observed that wake-induced force coefficient frequencies are mostly related to the frequencies of the cylinder displacements, x_1 , y_1 , x_2 and y_2 . This is due to the high dependency that the wake induced steady drag and lift coefficients, C_{D12} and C_{L12} , have on the relative local wake position of the downstream cylinder. These hydrodynamic force coefficients vary respectively symmetrically and anti-symmetrically across the wake as well as decaying along the wake. Therefore, C_{D12} and C_{L12} fluctuations are direct results of the pair of cylinders' relative x - y oscillations and this association is reflected in Figure 3-17.

An investigation of the effect of the cylinder initial spacing on these observations and findings is now conducted. The cases of $d = 8$ and 20 are shown in Figure 3-18 and Figure 3-19 respectively. Frequencies of oscillation related to the upstream cylinder have been omitted from these figures since its response is assumed not to be affected by the initial spacing between the cylinders within the co-shedding regime.

Whilst increasing the initial spacing between the pair of cylinders to $d = 8$ and then to $d = 20$ does not affect f_{y2}/f_n significantly for both model and experimental results, f_{x2}/f_n , on the other hand, as mentioned previously presents two main branches of frequencies. The lower f_{x2}/f_n frequency branch has been attributed to f_{y2}/f_n as a direct result of the dependency of wake-induced forces on the transverse displacement of the downstream cylinder (y_2), mathematically through δy in the model equations. Hence, since f_{y2}/f_n does not vary significantly with increase of d , then neither does the f_{x2}/f_n lower branch of frequencies.

Having said that, observation of the f_{x2}/f_n upper branch of frequencies for $d = 8$ shows that frequencies are seen following the light-blue doubled wake reduced

Strouhal line for the majority of reduced velocities. Once approximately $U_r > 12$ is reached, frequencies visibly tune to a different mechanism. One may observe that the f_{x2}/f_n upper branch of frequencies becomes effectively parallel to the f_{x2}/f_n lower branch of frequencies. Indeed, the upper branch of frequencies for $U_r > 12$ seems to be a doubled projection of the lower branch of frequencies, which is not true for lower reduced velocities. With that in mind, a second analysis of f_{x2}/f_n for $d = 4$ (Figure 3-17) illustrates the same feature – the upper branch of inline oscillation frequencies is merely a projection of the lower branch of frequencies with twice its magnitude.

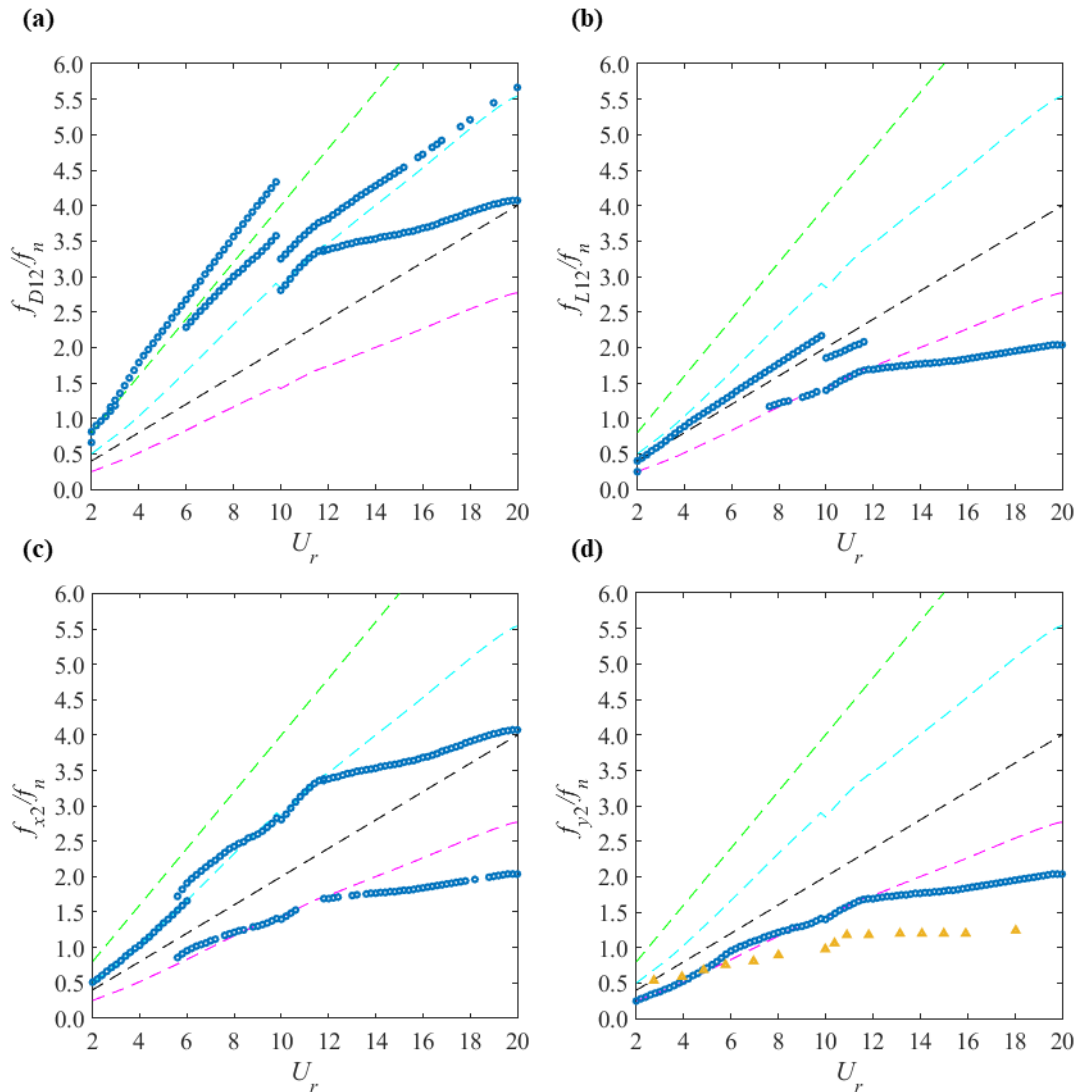


Figure 3-18: Variation of frequencies of oscillations of the pair of cylinders and wake-induced forces with U_r for $d = 8$. Legend: --- St law; --- χSt rule; --- 2St rule; --- $2\chi St$ rule; • Model results; • Armin et al. [25].

This observation implies that: a) there are no significant differences in the rear cylinder oscillation frequencies nor excitation mechanisms with increment of d for $U_r < 12$; this reinforces the concept of the first VIV regime and agrees with literature studies [11, 12, 23, 62]; b) For $U_r > 12$, the lower f_{x2}/f_n branch of frequencies has been

associated with f_{y2}/f_n . Since a relationship between the upper branch of frequencies and the lower f_{x2}/f_n branch of frequencies has been identified, it is possible to infer that both the f_{x2}/f_n branches of frequencies are related to f_{y2}/f_n . In other words, there is a clear transition of inline oscillation frequencies to a different excitation mechanism for $U_r > 12$ approximately for $d = 4$ and 8 . This observation supports the idea that there is a VIV-WIV mechanism transition since f_{x2}/f_n stops following the 2χ St line - a known feature of VIV wake oscillator modelling - and as it has been suggested from previous oscillation amplitude investigations (Figure 3-12).

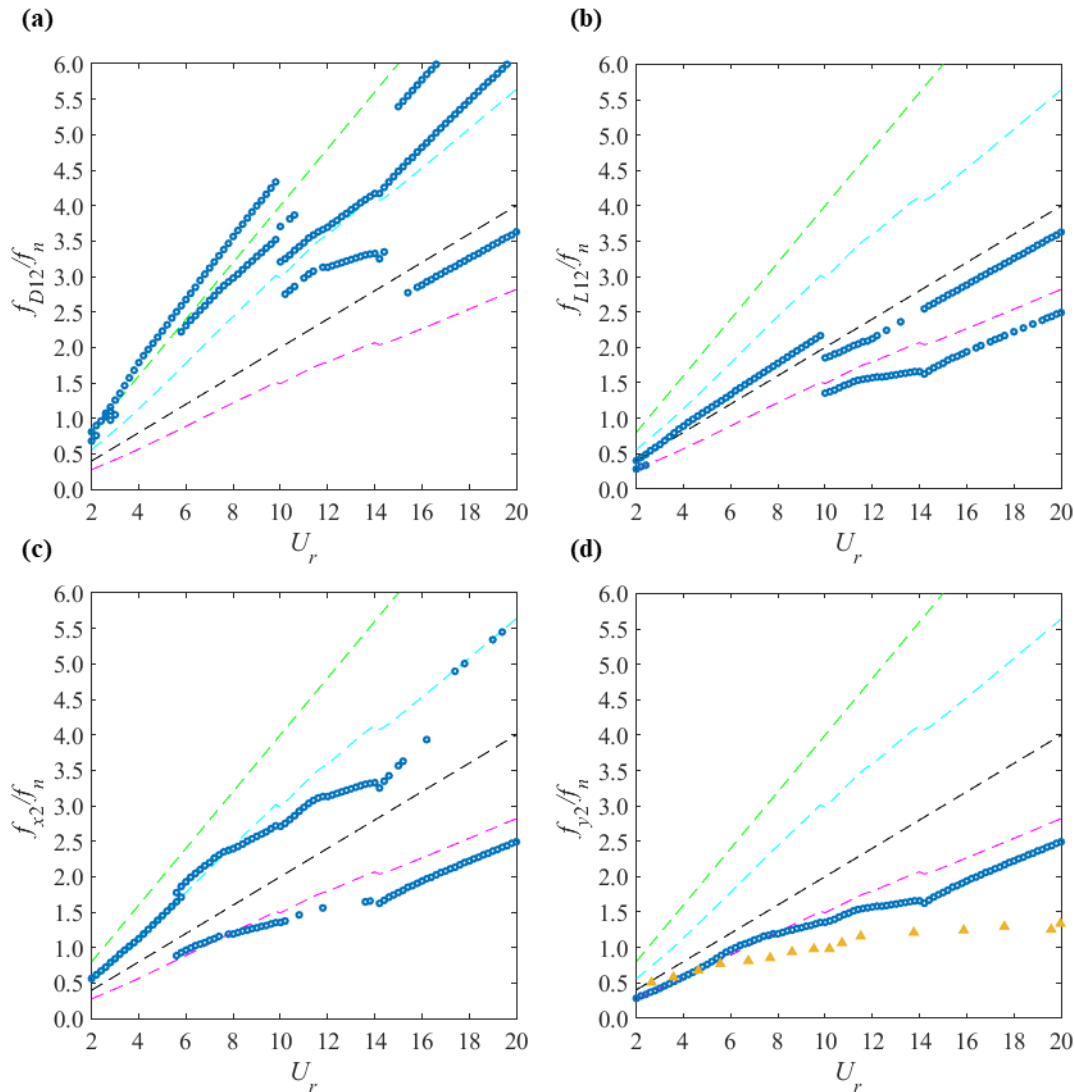


Figure 3-19: Variation of frequencies of oscillations of the pair of cylinders and wake-induced forces with U_r for $d = 20$. Legend: -- St law; - - χ St rule; - - 2St rule; - - 2χ St rule; • Model results; ▲ Armin et al. [25].

Nevertheless, for the case of $d = 20$, the upper branch of f_{x2}/f_n starts a switch from the 2χ St line for $U_r > 12$, but it is never completed as frequencies return to follow the doubled wake reduced Strouhal law. This indicates that the mechanism of WIV is never dominant due to the large initial spacing between the cylinders. In fact, the

vibration amplitude studies have shown that the second cylinder returns to behave similarly to a single cylinder under classical VIV for a sufficiently large spacing of $d = 20$.

3.4. Chapter Summary

This chapter has presented a reduced-order model to predict the problem of fluid-structure interaction of a pair of identical elastically mounted rigid cylinders allowed degree-of-freedom in both inline and crossflow directions. The flow regime around the two tandem cylinders is assumed to be fully developed and turbulent, i.e., the binary vortex shedding regime in the sense of each of the cylinders or the co-shedding regime is the focus of the present study. Therefore, a minimum initial separation distance greater than the critical spacing as defined in the literature [7], herein equal to or greater than 4 diameters measured from the centres of cylinders, has been prioritised.

Since vortex shedding occurs and the wake flow is well developed behind both cylinders, the main modelling assumption for the downstream cylinder is that of a combined effect of the phenomena VIV and WIV, the former associated with vortex shedding from the downstream itself whilst the latter with the disturbed incoming wake flow and vortex shedding from the upstream cylinder. This key assumption allowed for an independent modelling approach, where: a) van der Pol wake oscillators have been proposed to represent the fluctuating components of the drag and lift forces as has been widely employed for single cylinder VIV modelling studies [45]; b) wake flow deficit and wake-induced forces that contribute to the WIV of the second cylinder can be independently modelled through the boundary layer theory [33-35, 43].

The proposed model is an extended version strongly inspired by the 1DOF model in the previous chapter, hence many of the analyses and results have been compared to Chapter 2. However, one of the main fundamental differences is that the 2DOF study has accounted for geometric nonlinearities in the structural terms representation. This is justified by literature evidence that geometric nonlinearities may improve the prediction of the lower branch of amplitudes and figure-of-8 trajectories for 2DOF VIV of single cylinder systems [63].

The proposed model has empirical input parameters associated with both wake oscillator and wake flow theories and these have been calibrated and optimised based on reference experimental literature studies.

The model proposed has then been computationally solved for a broad range of parametric studies. Results have shown that the model is able to capture the important

features of VIV and WIV of the two tandem cylinders. Moreover, model outputs agree quantitatively and qualitatively with experimental results with reasonable precision for most of the cases studied. The main findings are summarised in the following:

- The upstream cylinder behaves as a single cylinder, hence there is no feedback from the second cylinder to the first. This is supported by literature observations within the co-shedding regime. Amplitudes of vibration and frequencies have been compared satisfactorily against experimental studies. The upstream cylinder mostly vibrates in a figure-of-8 pattern with inline-to-crossflow frequency ratio of 2:1.
- The downstream cylinder behaves as a single cylinder for low reduced velocity for all initial spacings (first VIV regime). Once U_r is increased, the response of the rear cylinder is highly dependent on d .
- For low initial spacings, the response is dominated by the WIV excitation mechanism, i.e., by the interaction of the downstream cylinder with the upstream wake flow and vortex shedding from the first cylinder. This type of response is characterised by progressive enlargement of amplitudes of vibration when U_r is increased, and not limited to a resonance range such as in single cylinder studies.
- Despite the fact that larger amplitudes of vibration are not restricted to the lock-in condition, whilst WIV of the downstream cylinder does indeed lead to a greater absolute maximum A_{y2}/D , the greatest change comes to A_{x2}/D , which may be more than doubled for flow-induced vibrations of two cylinders, when compared to flow-induced vibrations of an isolated cylinder with similar mass and damping properties.
- Several features of the 1DOF model of Chapter 2 have been also found for the present 2DOF model. However, the inline displacement of the downstream cylinder can lead to critical complications. Therefore, comparison between 1DOF and 2DOF systems must be carefully analysed.
- A build-up of amplitudes of vibration characterised by a WIV-dominated response has been observed for initial spacings as large as $d = 8$ in the present study. This observation contrasts with previous 1DOF studies [11] and Chapter 2, that have shown that the second cylinder would start to behave in a combined WIV-VIV for $d = 8$, resulting in a plateau of amplitudes of vibrations with increase of U_r . This is due to the dynamic relative spacing between the cylinders.

Therefore, a two-cylinder scheme with an initial $d = 8$ may in reality be vibrating a lot closer to each other.

- The dynamic relative spacing is a combination of three factors: i) the initial centre-to-centre separation between the cylinders in the streamwise direction, ii) the instantaneous relative difference between mean drifts of both cylinders caused by the mean hydrodynamic drag forces and iii) the instantaneous relative difference of vibration amplitudes of both cylinders in the inline direction. Therefore, all these factors may strongly influence the behaviour regime of the rear cylinder and may lead to the greater degree of disorder of the responses in the same way, by varying the downstream gap between the two cylinders which affects wake dynamics. Factors i), ii), and iii) above have been arranged in governing order, since, as discussed anteriorly, for i), this is at minimum a distance of 4 diameters, for ii) this can reach distances of up to 2 diameters, and for iii) difference in vibrations may reach 1 diameter as seen in the comparison of Figure 3-3 against Figure 3-12 for example.
- The possibility of having dynamic relative distances as close as 1.3 diameters has been analysed for $d = 4$. This increases the risk of collision of cylinders should instabilities arise and may increase the problem complexity with exposure to near wake phenomena. Moreover, it increases the effect of WIV mechanisms even for larger spacings, leading to greater oscillation amplitudes.
- In general terms, it has been demonstrated that the inline response of the downstream cylinder may be more irregular than its respective transverse displacement, since the response of x_2 is highly sensitive to the wake-induced forces, relative displacement between the cylinders in the streamwise direction, but also in the transverse direction.
- From the plane trajectories of the rear cylinder for $d = 4$, an unrepeated figure-of-8 pattern has been observed for $U_r = 5$ near the first VIV regime. Further increments of reduced velocity turn the cylinder's orbit into a shape that resembles a half-moon, hence with an inline-to-transverse oscillation frequency ratio more closely associated to a 1:1 ratio than to a 2:1 ratio. Nevertheless, cylinder trajectories return to figures-of-8 for $U_r > 20$.
- In association with the greater irregularity of x_2 , additional frequencies have been seen for the downstream cylinder oscillation frequencies in the inline

direction, whereas transverse frequencies of vibration are mostly dominated by a single frequency content.

- Two main frequency branches have been discovered for f_{x2}/f_n – an upper and a lower frequency branch.
- The lower f_{x2}/f_n frequency branch is related to f_{y2}/f_n for $U_r > 6$ for low initial spacings. Thus, it is concluded that the inline unsteady displacement of the downstream cylinder is directly affected by the transverse oscillation, which is a possible explanation for the 1:1 inline-to-crossflow frequency ratios and half-moon trajectories previously highlighted. This has not been seen for the upstream cylinder and is mathematically traced back to δy in the wake flow modelling.
- Whilst increasing the initial spacing between the pair of cylinders to $d = 8$ and then to $d = 20$ does not affect f_{y2}/f_n significantly for both model and experimental results, f_{x2}/f_n , on the other hand, as mentioned previously presents two main branches of frequencies. The lower f_{x2}/f_n frequency branch has been attributed to f_{y2}/f_n as a direct result of the dependency of wake-induced forces on the transverse displacement of the downstream cylinder (y_2), mathematically through δy in the model equations in Chapter 2. Hence, since f_{y2}/f_n does not vary significantly with increase of d , then neither does the f_{x2}/f_n lower branch of frequencies.
- The upper branch of frequencies for $U_r > 12$ has been understood as a projection of the lower branch of frequencies with twice its magnitude. This is explained by the excitation frequency of the drag force being double the corresponding lift.

Additional experimental studies with similar properties would be beneficial in validating the findings that could not be supported by literature studies due to scarcity of literature data, namely the multifrequency response of x_2 and oscillation trajectories of the downstream cylinder and this need has motivated the laboratory experiments conducted presently and that will be discussed in the next chapter.

CHAPTER 4. EXPERIMENTAL SETUP AND SINGLE CYLINDER TESTS

The scarcity of studies on WIV of a pair of tandem and/or staggered cylinders has been highlighted especially in the previous modelling studies in Chapter 2 and Chapter 3. Further complication arises when it is considered that whilst VIV studies of a single cylinder have relatively few control parameters (e.g., Re , mass and damping ratios) and may be correlated easily, WIV studies depend on the same parameters and more (e.g. number of cylinders, configuration, spacing range, whether they are fixed-free or free-free, amongst others). All these control parameters make correlation between studies challenging and require a greater number of studies to be conducted than the current stage of the topic does not offer.

Therefore, a comprehensive 2DOF experimental investigation of combined vortex- and wake-induced vibrations of a pair of cylinders is proposed to cover some of these aspects, provide reference data, and validate the present modelling theory. The tests were planned and conducted in the Wind, Wave and Current Tank at Newcastle University's Hydrodynamics Laboratory, a world-class facility that can simulate combinations of wind, wave and current loadings on marine/offshore structure models for renewable energy or oil and gas research. A detailed description of this tank and its specifications will be discussed in the next section.

4.1. Wind, Wave and Current Tank

The Wind, Wave and Current Tank (WWCT) was established in 2003 in Newcastle University's Hydrodynamics Laboratory. The tank is comprised of recirculating water and wind sections that allow investigations of academic projects especially related to marine, offshore, and subsea engineering. In the present study, wind loading analysis has not been considered but the WWCT is versatile enough that the wind compartment hinged hatches can be easily removed. Thus, the WWCT has effectively been employed as an open water tank in the present research.

The recirculating water channel current is provided by a four-bladed, 0.78m diameter impeller. Wave generators are also installed at the entry point of the tank's test section. The wave makers have three paddles and are of displacement piston type, they are capable of simulating different wave spectra, such as P-M, JONSWAP, Bretschneider, and Neumann. Furthermore, a honeycomb wave absorption beach system is located at the end of the testing section [68].

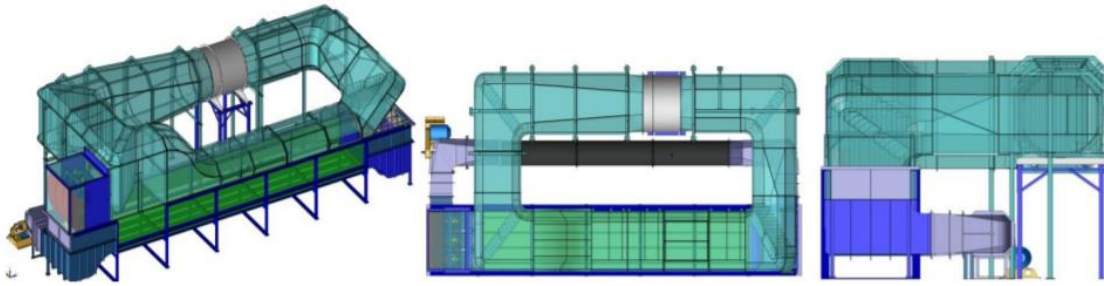


Figure 4-1: Technical drawing of Newcastle University Wind, Water and Current tank: Isometric view (left-hand side); top view (middle); and rear view (right-hand side). Adapted from [68].

4.2. Experimental Rig and Pendulum System

A system was designed to mount the pair of cylinders and springs to the tank allowing for effective frictionless movement in the inline and crossflow directions. The pendulum systems were chosen based on: i) previous experience of colleagues and technicians; ii) lab structure where a beam crosses roughly the centre of the tank test section, on which the pendulum system can be conveniently fixed; and iii) the height of the lab and the beam permitted use of a high aspect ratio pendulum system. This last point is important for reducing differences between cylinder linear displacements (variables of interest of the study) and the actual pendulum orbit to negligible amounts.

In the double pendulum system, each cylinder was connected at the top to a universal joint of a needle roller bearing type, allowing nearly frictionless rotation in all directions. The two lubricated universal joints were made of carbon steel, had a bore diameter of 25 mm, length of 108 mm, maximum working angle of 45° and maximum speed of 4000 rpm. Each universal joint was connected with bolts to the associated cylinder carbon fibre shaft on the bottom end and fixed from the top end to a purpose-made mounting sliding system directly attached to the laboratory beam.

The sliding carriage structure, seen in Figure 4-2, was designed and fabricated in the Hydrodynamics Laboratory. The double sliding mounting carriages allowed the cylinders' initial position to change either along the length of the tank in the streamwise direction (upstream cylinder) or across the tank in the crossflow direction (downstream cylinder). Therefore, d was controlled by moving the upstream cylinder and T was controlled by moving the downstream cylinder. Each sliding carriage was measured and marked in diameters to be easily moved and fixed to the desired position with the hand adjustment of four bolts. This convenient interchangeability was achieved with the use of Bosch Rexroth aluminium grooved struts as seen in Figure 4-3.



Figure 4-2: Attachment of pendulum systems to a beam over the Hydrodynamics Laboratory. View of the universal joints and mounting carriage system. Sliding carriage structure's greater length is aligned with the flow and WWCT tank. Photo taken at the single cylinder flow measurement phase with the downstream cylinder's carbon fibre tube in place.

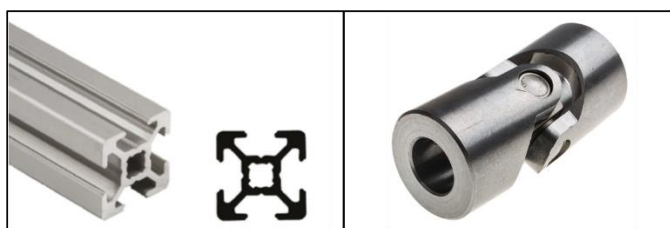


Figure 4-3: Catalogue view of the (a) Bosch Rexroth grooved strut and (b) universal joint used for the cylinders' mounting systems.

It is important to highlight that the hanging weights of both cylinder systems were relatively small, and the sliding carriage mounting structure was specifically designed and eight-point fixed to the laboratory beam to provide high system stiffness so that the mounting system would not vibrate at any point and transmit these vibrations to the pair of cylinders.

4.3. Cylinder-Springs Connection Planning

Linear extension springs were required to provide the elastic restoration force to the dynamic system of each of the cylinders. Attachment of rigid cylinders to springs has long been employed in academic research to study vibrations and simulate real life offshore-inspired structural stiffness properties [11, 15, 24, 25].

Having said that, the two-cylinder configuration has proven to be extremely challenging with respect to the position of the spring attachment. This is due to the minimum initial spacing between cylinders considered in the present study being as small as 90 mm (120 mm centre-to-centre) and possibly lower during tests. The eight springs required to stabilise the two cylinders should ideally be identical and attached to a frame on the tank.

Conventionally in VIV experiments of a single cylinder, four springs are normally attached to the cylinder on the front, back, left- and right-hand side to the streamwise direction, each phased 90° from the adjacent springs. Clearly, with the inclusion of a second tandem downstream cylinder, the rear spring for the first cylinder and the front spring for the second cylinder are compromised for this kind of scheme.

Therefore, during project planning and design discussions in the laboratory, several potential alternatives were proposed and discussed. Some of the discussed options were using compression leaf (curved) springs; using one spring per direction per cylinder; reducing the length of springs considerably and extending a metal plate from the tank to the space between the cylinders; modifying the once straight profile of the carbon fibre tube of Figure 4-2. However, the agreed idea was to rotate the system by 45° from the conventional spring scheme.

Therefore, the springs were attached diagonally to the cylinders with respect to the flow direction. The advantages of following this method were: a) the simplicity of the scheme, b) the allowance of small separations of the cylinders. On the other hand, the disadvantages were: i) the need to design new tank frames, ii) potential complications for the post processing of force measurements; and iii) nonlinear spring elongation effects. The first and second disadvantages were accounted for and solved, whilst the latter was considered to be negligible within the studied cylinder displacement limits which did not exceed five diameters.

As mentioned above, a tank frame was designed to accommodate the diagonal springs. In fact, this consisted of two frames complementing each other and made of aluminium. These were designed and built in Newcastle University's Hydrodynamics Laboratory and can be seen in Figure 4-4.

As shown in Figure 4-4, the two square frames have an open side each – the back side to the oncoming flow for the upstream cylinder frame and the front side to the oncoming flow for the downstream counterpart – and the downstream frame rests on top of the upstream frame. Thus, the frames can be manually displaced and fixed

in position with clamps. For convenience, measures in units of cylinder diameters were marked on the tank for correlation with the study.

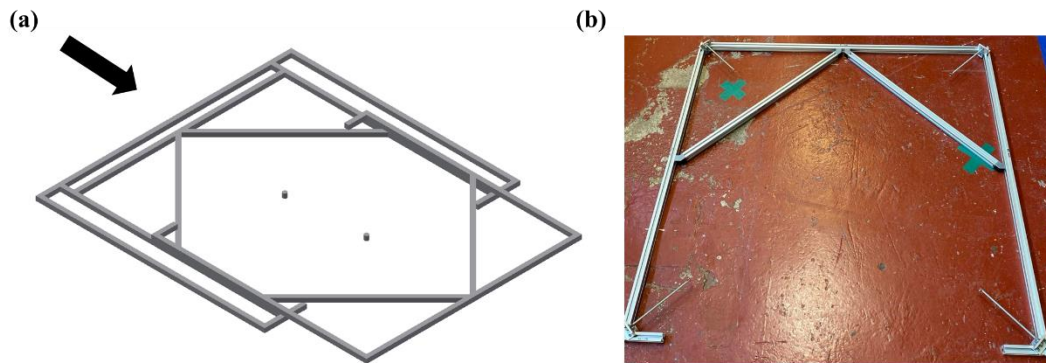


Figure 4-4: Double frames system of the pair of cylinders (on centre). Flow direction is demarked. Downstream cylinder frame rests on top of the upstream cylinder frame. (a) CAD drawing courtesy of the Hydrodynamics Laboratory; (b) Photo of the downstream cylinder frame with spring corner mounting studs.

Each frame had “V”-shaped braces added to provide greater stability. The springs were attached to the eight frames corners with the downstream cylinder springs 10 cm higher than the upstream cylinder set of springs.

The process for changing the cylinders’ initial position was to initially move the carriage mounting system on the ceiling of the laboratory and then move the associated frame the same distance in the same direction so that the cylinders were vertical and the eight springs returned to their initial tension. Moreover, according to Figure 4-2, whilst the initial tandem spacing, d , would be changed by moving the upstream cylinder along the tank, the staggered initial spacing, T , would be modified by sliding the downstream cylinder across the tank. This means that the two-frame system should account for the same relative motion. Hence, as seen in Figure 4-3, the two frames would form an elongated rectangle with increase of d by moving the bottom, upstream frame or would be offset a certain lateral distance with variation of T by moving the top, downstream frame over the wider bottom frame.

4.4. WWCT Current Flow Measurements

Even though the tank specifications indicate a maximum current velocity of 1 m/s, that value is nominal and does not account for real condition energy losses nor a later modification made to the tank, when optimal flow conditioners such as guide vanes were installed [68]. In fact, the real tank flow velocity varies with the depth (z) within the measuring section, although the variation is assumed to be minimal in the streamwise and crossflow directions within the central section of the tank considered

in the present study. Therefore, a series of flow measurement tests at different depths was conducted before any other experimental investigations were carried out.

The power intensity of the tank impeller is controlled by a dedicated computer and software in terms of percentages of Current Power Generation (CPG). The equipment allowed for one decimal place CPG percentage resolution. The temperature of the water in the tank was monitored and was at or very close to 15 °C on every testing day for the entire project, thus changes in water viscosity were negligible and no additional mention of the water temperature will be made in the following sections.

Current flow measurements were performed within the central tank volume where all tests have been conducted, more specifically at the position that the upstream cylinder was to be placed for $d = 4$, i.e., approximately 6.5 meters downstream from the wave makers and at the centre of the tank. A Nortek Vectrino, 3D high-resolution acoustic water velocity sensor, was used to measure flow velocity. This acoustic Doppler velocimeter has one transmission transducer and four receiving transducers that are placed equidistant to the Vectrino's main casing and components. This can be observed in Figure 4-5. An acoustic pulse is sent from the central transmission probe and echoes back to the four receiving units, being processed and compared against the speed of sound in the liquid. This way, the sampling volume is actually located 5 cm below the bottom of the instrument to reduce any possible disturbance from introducing the sensor into the flow.

The Vectrino velocimeter was clamped to a mounting structure secured to the tank walls, which was designed and built in the Hydrodynamics Laboratory, to make modifications of depths and planar positions easier and quicker. Marks for the desired measuring positions were added. For these initial depth investigations, four points were proposed: 10 cm below the water surface, 25 cm, 50 cm, and 85 cm. These were defined to map the flow profile based on the water depth of the tank, 1 m, and the 80 cm immersion height of the cylinders to be added later.

For each of these 4 depth points, 17 flow velocities were tested, for a CPG of 5% up to 85% in 5% increments, totalling 68 measurement points for this initial flow measurement campaign and multiple readings were taken for each point to test for successful effective repeatability.



Figure 4-5: Nortek's Vectrino 3D acoustic velocimeter and mounting system. WWCT central tank current flow measurements at different depths.

The results are presented in Figure 4-6. It can be seen from Figure 4-6a that the flow velocity closer to the surface is greater than at the largest depths for the lowest CPG's. At a CPG of 15%, the flow velocity is almost constant through the water column and for greater CPG's the previous pattern is reversed, where flow velocities at greater depths in the flume are higher than near the water surface. One can also observe that irregularities of flow velocities through the depth of the tank increase for higher CPG's and most importantly that the scale of the WWCT impeller power intensity to the free stream velocity is not 1:1, as it is possible to observe that the maximum $U_{\infty} = 0.7$ m/s approximately, whilst the maximum CPG is 85%. Clearly, this means that the maximum flow velocity at the central testing zone is not 1 m/s as in the nominal flow velocity of the tank specifications.

Moreover, Figure 4-6b shows how irregular the flow can be depending on the depth considered. For measurements at a depth of 85 cm below the water surface, the flow velocity increase with impeller power is nonlinear and irregular. Looking at the other 3 depths studied, 10 cm, 25 cm, and 50 cm, it is seen that they are similar for low to mid CPG's or flow velocities. It is only for CPG's greater than 50% that differences start to build up significantly. The mean curve obtained from the four depth points was calculated and it was found that flow velocities at 25 cm below the water surface are comparable to the average of the full flume depth and, therefore, this position has been considered for all the following tests to be discussed.

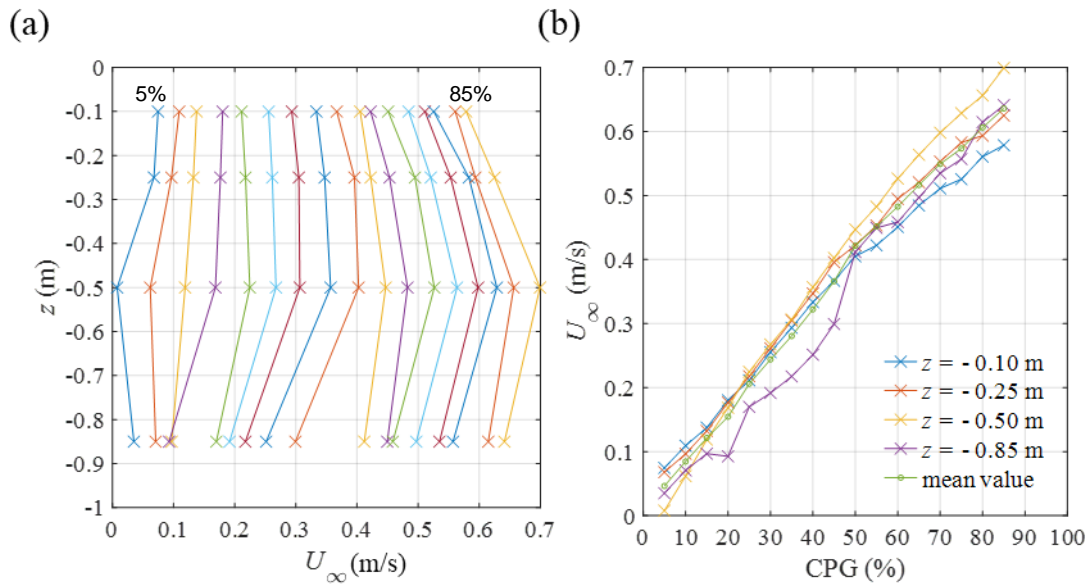


Figure 4-6: WWCT current flow measurements at different depths. (a) varying impeller's power intensity from left to right, CPG = 5%, 10%, ..., 85%; (b) Mean value of flow velocities for the 4 depth points studied.

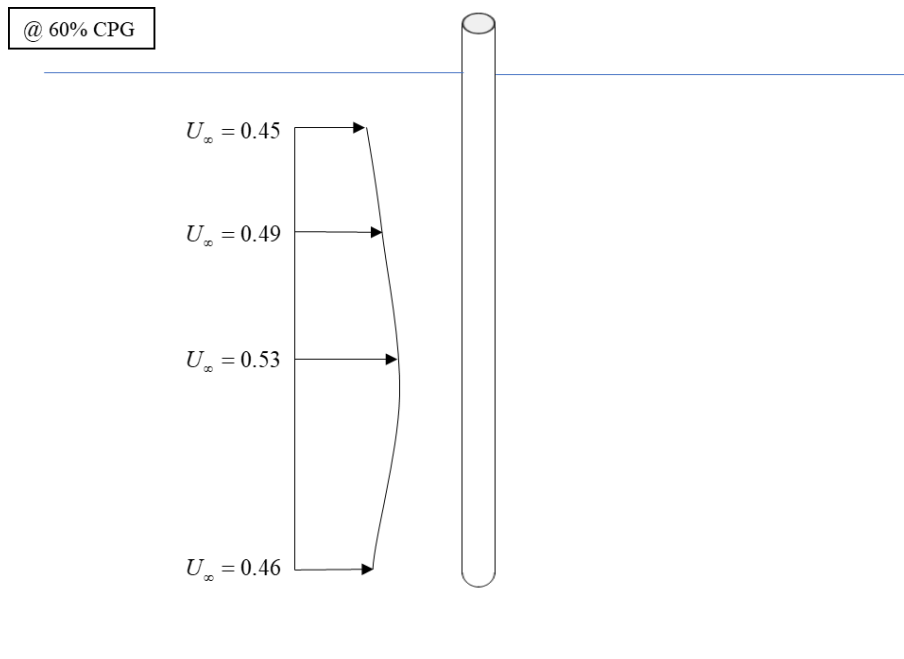


Figure 4-7: Flume free stream velocity (m/s) depth variation (10, 25, 50, and 85 cm below water surface) at the upstream cylinder's position at $d = 4$ and CPG = 60%.

The flume current flow velocity variation with depth in the tank is illustrated Figure 4-7. The aim of the study is to investigate fluid-structure interactions that occur for several different positions and configurations for both cylinders. The additional effect of variation with depth was not included and would be cumbersome to study. Thus, from this primary study of flume flow velocity along its depth, it has been concluded that the current velocity at 25 cm below the water surface is similar to the mean value of flow velocities and this depth has been established as the point of interest in the z

dimension for all succeeding tests. Another important observation is that this dependence of the tank's flow velocity on the depth is minimal for impeller power intensities less than approximately 50%. As it will be discussed in the following tests, this threshold will be taken in consideration to minimise flow irregularities along the depth of the tank and turbulence. Lastly, it is observed from Figure 4-6b that the increasing flow velocity profile at 25 cm depth is approximately linear, hence linear regression has been used to interpolate values and attribute CPG percentages to free stream velocities.

4.5. Free Decay Tests and Spring Selection

Once the framing system had been defined and maximum real velocity estimated, the next step was to select the spring model to be tested. As explained in the previous section, the maximum tank current velocity considered in the present study has been estimated to not exceed 0.5 m/s, despite the WWCT allowing for greater flow currents. This maximum velocity was implemented to limit turbulence to a minimum and reduced flume flow velocity variation over the depth of the tank. Thus, the reduced velocity (or Re) is the controlled parameter of the tests and is dimensionless as discussed in Section 1.1.

The diameter of the identical acrylic cylinders was 30 mm and so the maximum reduced velocity that can be achieved for the study is based on the system natural frequency. According to Zanganeh [69], the pendulum natural frequency is a function of several parameters, including the total oscillating mass, spring stiffness, the length of the pendulum, the length of the springs and connection heights. Most of these parameters are totally or partially constrained, but specific attention was given to selecting the spring stiffness as a key parameter to reduce the system natural frequency and consequently increase the maximum achievable reduced velocity.

Different spring models, dimensions and types were considered before the final definition of the new model of extension spring that had an outside diameter of 6.40 mm, free length of 101.60 mm at an initial tension of 0.92 N, extended length up to 444.90 mm, $k = 20$ N/m and a mass of 5.31 grams per spring.

The springs were mounted to the frame and each of the cylinders and free decay tests were conducted for each as a single cylinder system in both water and air. For the latter case, the WWCT tank was totally drained. It is important to stress that each cylinder was studied for free decay with the same frame, springs and components as in the succeeding tests. The whole system of one cylinder was completely removed for

the free decay tests of the other cylinder system. Also, even though there was no interest in force measurements at this project stage, load cells and their connection rings and studs were mounted to each frame in order to mimic real operation.

Free decay tests were conducted from an initial displacement of approximately 2 diameters or 60 mm from the central equilibrium position of each cylinder. This was achieved by marking this distance on a string, manually pulling this controlled distance and releasing the test subject. This was repeated five times per direction, namely inline or x direction, crossflow or y , and the fourth quadrant diagonal ($x > 0, y < 0$) for each of the cylinders. The diagonal direction was examined to validate the other two directions and to infer whether the diagonal springs could nonlinearly affect this axis.

The controlled initial displacement of each cylinder and its free vibration back to equilibrium were recorded in 6DOF by high-resolution Qualisys optical tracking acquisition cameras. The recorded free vibrations of the cylinders were then plotted against the elapsed time and fundamental calculations of logarithmic decrement, damping ratio and natural frequency were performed for both air and water and are presented in

Table 4-1.

The conclusion from the free decay results is that the two cylinders systems are effectively isotropic with negligible property differences in all directions. They are also equivalent to each other, reinforcing the idea of identical cylinders, with small differences amongst measured quantities apart from the damping ratio in air, which is normally very small (an order of magnitude of four decimal places) and could be related to experimental uncertainties, since other properties are comparable. No significant differences were observed between the free decay tests from the diagonal and the other directions, which validates the assumption of negligible spring nonlinear effects for the cylinder displacements.

With the definition of $f_n = 0.75$ Hz it is possible to compute the reduced velocity from its definition. For a lower limit of $CPG = 5\%$, the free stream velocity has been previously measured as 0.046 m/s, which is converted to a minimum reduced velocity, $U_r = 2$. The maximum planned $U_r = 20$ is achieved for a free stream of approximately 0.45 m/s and $CPG = 57.3\%$. This is within the ideal tank flow velocity range that minimises flow velocity depth variation and turbulence as mentioned previously. Moreover, 49 reduced velocity points were proposed for the VIV and WIV cylinders tests.

Table 4-1: Summary of free decay tests.

Upstream cylinder system						
	Air			Water		
	x	y	xy	x	y	xy
Natural frequency (f_n)	1.01 Hz	1.03 Hz	1.01 Hz	0.75 Hz	0.78 Hz	0.77 Hz
Damping ratio (ζ)	0.35%	0.35%	0.37%	5.5%	5.7%	5.5%
Downstream cylinder system						
	Air			Water		
	x	y	xy	x	y	xy
Natural frequency (f_n)	0.99 Hz	0.99 Hz	0.99 Hz	0.74 Hz	0.75 Hz	0.75 Hz
Damping ratio (ζ)	0.57%	0.52%	0.6%	5.8%	6.0%	6.0%

Representative values for the two cylinders are then considered as $\zeta_{air} = 0.45\%$, $f_n^{air} = 1$ Hz, $\zeta_{water} = \zeta = 5.5\%$, $f_n^{water} = f_n = 0.75$ Hz. The present study was conducted in a water flume and the properties in water shall be used primarily unless explicitly mentioned for direct comparison with literature studies.

4.6. Wake Deficit Flow Profile Measurements

Having validated the relationship between flow velocity and the user interface control parameters of the WWCT and defined the optimal depth of interest, for the remaining tests, the focus was on measuring the disturbed wake flow velocity behind an upstream cylinder that is either fixed in place or spring-mounted and allowed to vibrate.

The wake flow after a cylinder is normally turbulent even for previously laminar flows. This is due to wake shielding, i.e., the cylinder shields the flow, decelerating flow particles that come into the vicinity of the cylinder, and which are then accelerated along the surface curvature of the cylinder. Thus, abrupt variation of flow velocity and consequently pressure fields may culminate in a sequence of events of an adverse pressure gradient, boundary layer separation and vortex shedding. The thickened and separated boundary layer flow along with outer flow particles that may entrain this disturbed flow constitute the wake flow past a circular cylinder.

Despite the time-dependent flow velocity fluctuations caused by vortex shedding and turbulence, the disturbed wake flow profile downstream of a cylinder is governed by a deficit law. The cross-wake flow profile is a minimum at the wake centreline, close to the cylinder, and laterally symmetric up to the wake edges when flow velocity tends to the undisturbed magnitude [10, 11, 33, 36, 52]. One of the many wake flow or boundary layer thickness definitions is that it ends when $u > 99\%$ of U_∞ [32].

Nevertheless, a vibrating upstream cylinder is expected to affect its neighbouring flow and its immediate wake flow differently to an upstream cylinder that is held fixed. Blevins and Saint-Marcoux [36] studied the wake flow past a cylinder experimentally with controlled oscillations of $1.25 D$ in the transverse direction and concluded that its wake flow is flatter and wider than for a similar static cylinder.

Hence, an investigation of the wake flow deficit after a cylinder that is spring-mounted and allowed to oscillate in 2DOF, which to the author's knowledge has not been done in previous literature studies, became necessary to understand the flow behaviour. Most importantly, this would allow correlation of wake flow velocity findings with the dynamic response of a downstream cylinder as will be discussed in Chapter 5 and Chapter 6. The Vectrino acoustic velocimeter was mounted again to take flow velocity readings. As discussed, this stage of tests has been planned for the wake deficit past a stationary and a 2DOF upstream cylinder. The static upstream cylinder with 1 metre length, 30 mm diameter and made of standard carbon steel was machined and polished in the Hydrodynamics Laboratory. Therefore, for the fixed-free setup, the upstream cylinder is made of steel whilst the downstream cylinder is made of acrylic. A rigid frame of aluminium was also manufactured and fitted to the tank. Additional mechanical clamping points increased the stiffness of the mounting system. The immersed length of the metallic tube was 80 cm. This configuration can be seen in Figure 4-8.

The wake velocity profile matrix of tests for both the fixed and free cylinders is illustrated in Figure 4-9. For the static upstream cylinder, the Vectrino velocimeter was placed at 3 distances downstream, namely 4, 10, and 20 diameters. On the other hand, the velocity sensor could only be placed at 10 and 20 diameters downstream of the 2DOF upstream cylinder, since at closer separation, the cylinder and the probe would physically interfere with each other due to the mean displacement of the upstream cylinder, caused by the mean drag force, and its vibrations in the inline direction.

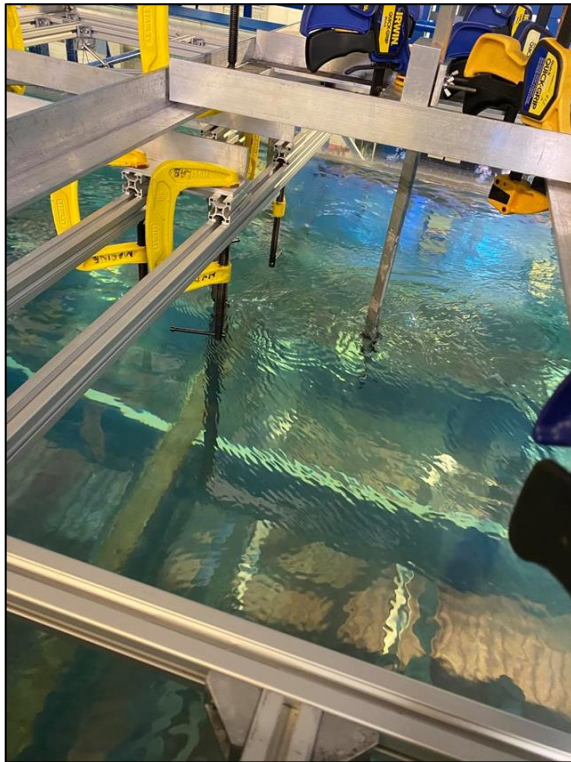


Figure 4-8: Wake deficit measurements for the flow past an upstream static cylinder at $d = 10$. Orientation of the flow is from left to right. The two immersed components are: metal stationary cylinder (upstream) and Vectrino acoustic velocimeter (downstream).

This way, for each of these 5 downstream distances, the probe was moved laterally and fixed in place at the desired position to measure the complete wake profile behind the cylinder. In total, 13 lateral positions have been investigated. For each of these locations, 6 different flow velocities were investigated. All the lateral locations and flow velocities were consistent for the fixed and the 2DOF upstream cylinder.

This is a total of 390 tests which highlights the importance of having defined a single depth position that satisfactorily represents the average of the current of the flume, otherwise the number of tests would be greatly increased. A waiting time of a minimum of 3 minutes was allowed for each flow velocity so that the flow would fully develop before data acquisition, which was recorded for an additional 2 minutes at a frequency of 200 Hz. Thereafter, the flow velocity in the streamwise direction was averaged for every test case, whilst velocities in the other two directions were negligible over the duration of the measurements.

The measured flow velocities behind the static upstream cylinder for $d = 4, 10,$ and 20 are shown in Figure 4-10.

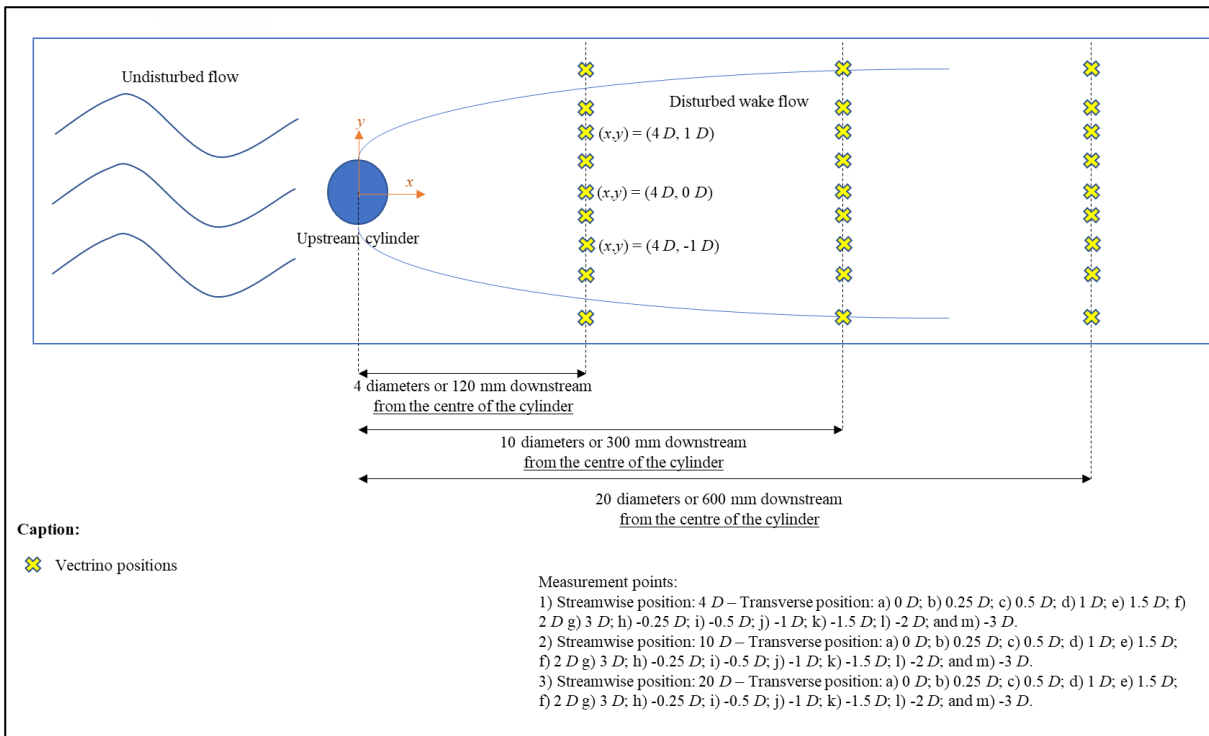


Figure 4-9: Simplified diagram of wake flow velocity measurements behind a fixed or a 2DOF cylinder. Graphic Vetrino quantity and location of tests are merely a schematic representation and not accurate.

The 6 velocities were controlled from the WWCT dedicated computer based on the tank's impeller power intensity, $CPG = 10\%$, 20% , ..., 50% , 55% . The maximum CPG of 55% was used because this was estimated to yield a reduced velocity very close to 20, which is the maximum U_r that will be considered in the vibration tests discussed in Chapter 4, Chapter 5, and Chapter 6.

The flow velocity profile across the wake behind the stationary cylinder is shown in Figure 4-10. As expected, the disturbed flow velocity is minimum at the wake centreline, where it is immediately shadowed by the upstream cylinder. Increasing the lateral distance from the wake centreline results in an increment of the flow velocity up to the wake edges (at approximately 2 diameters from the wake centreline), when the flow velocity stabilises at the free stream velocity. This wake deficit effect reduces for greater initial longitudinal spacings. In fact, the velocity profiles become almost flat, i.e., back to free stream undisturbed flow conditions, for $d = 20$ as seen in Figure 4-10.

A different aspect that can be investigated is that the flow velocity reduction that occurs, especially close to the wake centreline, is more evident for the higher free stream flow velocities and Reynolds numbers. This is clearly observed especially for $d = 4$, but also for the higher $d = 10$, and 20 . Despite this apparent greater variation of u for higher initial flume velocities, this is perhaps given in vast majority because of the

greater free stream velocity. In other words, proportionally speaking, the non-dimensional wake deficit ($\chi = u/U_\infty$) is effectively comparable amongst all free stream velocity cases, apart from the minimum $U_\infty = 0.08$ m/s setup which did not produce meaningful χ results and has been removed from the following analyses, due to the fact that it does not follow the same features and patterns as the other flow velocities and could not be analysed, perhaps due to being more susceptible to experimental uncertainties.

The insignificant dependence of the wake deficit, χ , on the free-stream velocity and consequently Reynolds number for the flow after a static cylinder is a positive observation for the modelling work conducted in Chapter 2 and Chapter 3. The wake deficit theory developed based on the boundary layer theory does not directly account for Reynolds number dependence, apart from any indirect contribution that could be analysed in terms of the input empirical parameters, α , β , μ , drag and lift coefficients. However, all of these parameters were previously considered as constants with respect to the Reynolds number. Thus, the present findings validate the previous modelling assumption of neglecting an insignificant dependence of Reynolds number on the wake deficit theory, at least for a fixed upstream cylinder and within the Reynolds number range studied herein. The question remains whether this also happens for the wake flow behind a 2DOF cylinder and that will be investigated below.

The wake velocity profile results after a static upstream cylinder have then been compared against the study of Blevins [33] and are shown in Figure 4-10. It is important to highlight that Blevins [33] has not considered initial inline spacings of $d = 10$, and 20, but rather 12, and 24 were the closest matches. Another difference between the studies is the Reynolds number, which is 100,000 for the mentioned study, but 13,500 for the present study. Nevertheless, the results in Figure 4-10 are comparable between the studies, especially for the case where the spacings are equal, $d = 4$ (Figure 4-10a). This agreement between the studies could also strengthen the argument that the wake deficit is approximately independent of the Reynolds number for the flow behind a fixed cylinder for a greater Re range, justified by the higher order of magnitude of the Reynolds number of the reference study of Blevins [33].

To analyse the wake flow profile past a cylinder that is free to vibrate in the inline and crossflow directions, an acrylic upstream cylinder was mounted to the frame and secured with the four diagonal springs previously discussed. This hollow cylinder had the same dimensions as the solid metal cylinder, i.e., $D = 30$ mm, length = 1 m, and

immersed length of 80 cm. Location, quantities and details of the tests were consistent with the stationary cylinder case, except for the initial inline spacing, $d = 4$, which as discussed previously was not possible due to the mean drag displacement of the upstream cylinder which led to physical interference between the cylinder, springs and the flow velocimeter.

Therefore, the results of the vibrating upstream cylinder study for $d = 10$, and $d = 20$ are presented in Figure 4-11. One may immediately notice that the lowest flow velocity profile, CPG = 10%, is different from the remaining 5 flow velocity profiles. The lowest flow velocity profile is flat, i.e., the wake deficit is minimal and comparable to the flow behind a fixed cylinder for a similar d , as previously seen from Figure 4-10. From observation of the experimental tests in the WWCT it became clear that this similarity between the two studies is associated with the low flow velocity, specifically $U_r < 4$ for a CPG = 10% and, therefore, as it will be discussed in the single cylinder VIV section to follow, this means that this low flow velocity is unable to excite the spring-mounted upstream cylinder. In other words, for the lowest velocity profile shown in Figure 4-11a- b, the 2DOF upstream cylinder is barely oscillating. For this reason, the first flow velocity profile does not follow the same trend as the other velocity profiles and for the same reason has been removed from the wake deficit analysis of Figure 4-11c-d.

Moreover, in the comparison in Figure 4-11, it becomes evident that the flow profile is indeed wider for the flow after the 2DOF upstream cylinder as opposed to a stationary upstream cylinder, as remarked by Blevins and Saint-Marcoux [36]. This can be directly related to the movement of the flow perturbation source, namely the upstream cylinder, which sheds vortices and disturbs the downstream flow at greater and time-dependent lateral positions. Attributed to this same reason, an interesting aspect can be brought up from observation of the wake deficit function profiles downstream of a leading 2DOF cylinder for $d = 10$: there is a considerable dependence on the current flow velocity that is not seen for either of the remaining cases studied. As discussed, this is a direct consequence of the excitation of the upstream cylinder into VIV, which is a complex nonlinear phenomenon. Under these conditions, the front cylinder undergoes a resonant-like behaviour in VIV that causes significant variation of its vortex shedding frequency and wake modes, as widely cited in single cylinder VIV studies [70] and which will be discussed in future sections. Therefore, the upstream cylinder's response is highly dependent on the flow velocity within the studied range

and consequently this is reflected on the downstream wake deficit profile as indicated by [43].

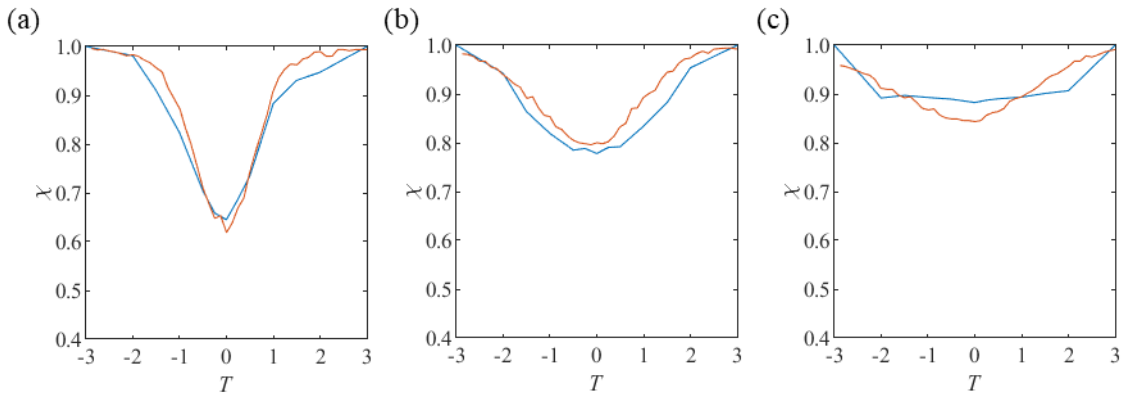


Figure 4-10: Comparison of wake flow velocity profiles behind a stationary cylinder. Legend:
 (a) — present study for $d = 4$ at $Re = 13500$; — Blevins [33] for $d = 4$ at $Re = 100000$;
 (b) — present study for $d = 10$ at $Re = 13500$; — Blevins [33] for $d = 12$ at $Re = 100000$;
 (c) — present study for $d = 20$ at $Re = 13500$; — Blevins [33] for $d = 24$ at $Re = 100000$.

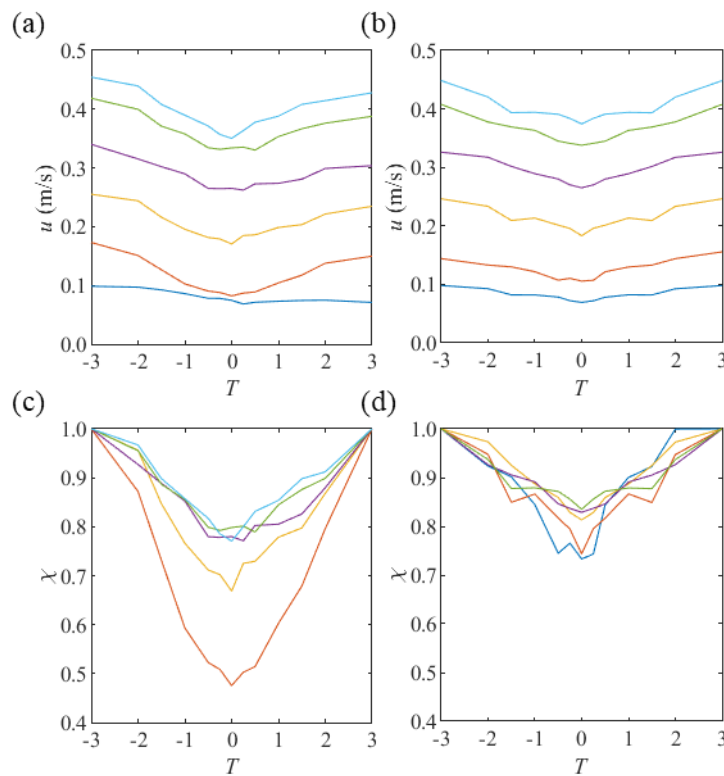


Figure 4-11: Tank cross sectional wake flow velocity measurements. Flow profile after a 2DOF acrylic upstream cylinder at: (a) $d = 10$; and (b) $d = 20$. Legend: — : CPG = 55%, $U_\infty = 0.45$ m/s, $Re = 13500$; — : CPG = 50%, $U_\infty = 0.4$ m/s, $Re = 12000$; — : CPG = 40%, $U_\infty = 0.32$ m/s, $Re = 9600$; — : CPG = 30%, $U_\infty = 0.25$ m/s, $Re = 7500$; — : CPG = 20%, $U_\infty = 0.17$ m/s, $Re = 5100$; — : CPG = 10%, $U_\infty = 0.08$ m/s, $Re = 2400$.

Apart from that, one may also observe that wake flow effects and wake depression at the wake centreline are still seen for the greatest inline separation of cylinders studied

herein, $d = 20$, for the wake flow behind a 2DOF cylinder. This contrasts with what has been previously investigated for the flow behind a restricted upstream cylinder, where the flow profiles are almost completely flat for $d = 20$. In other words, the wake deficit and wake effects linger for higher initial cylinder spacings for an oscillating upstream cylinder.

4.7. Single Cylinder Vortex-Induced Vibrations

Having mapped the WWCT flume flow profile and investigated the wake disturbed flow downstream of the leading cylinder, the focus is now given to the fluid-structure interaction of an isolated cylinder mounted with four diagonal springs as seen in the setup of Figure 4-12.

The upstream cylinder's set of components was used for the present single cylinder tests. The time-dependent displacement of the cylinder was captured by the high-resolution Qualisys infrared camera acquisition system, as detailed previously. The pair of Qualisys Oqus 300 high-speed cameras work by constantly keeping track of three infrared reflector spheres. The two Qualisys cameras need to be placed on the same side of the tank so they were placed on the starboard side of the WWCT flume for convenience of access. The three infrared reflector marking spheres were secured to a grey lightweight polystyrene collar which was attached to the cylinder model just above the spring connection level, as illustrated in Figure 4-12. A 2 cm separation between the marker collar and the spring collar was preserved to avoid any undesired interference, however unlikely, between the two collars.

The Qualisys acquisition system tracks the three infrared reflector markers in 6DOF, but as a single body. This means that the centre of the tracking imaginary body composed by the three marker spheres is located at the geometric centre of the spheres, which is clearly not concentric to the cylinder model. Therefore, all data related to the response of the cylinders and acquired by the Qualisys tracking system were post-processed to be corrected for the centre of the respective cylinder and projected to the bottom of the metre-long acrylic cylinder model for the maximum displacement of the pendulum system in question.

The reduced velocity based on a natural frequency in water was varied from $U_r = 2 - 20$ (CPG = 3.9% - 57.3%) with increments of $U_r = 0.25$ or 0.5 depending on the relevance and level of response complexity expected for the given excitation regime.

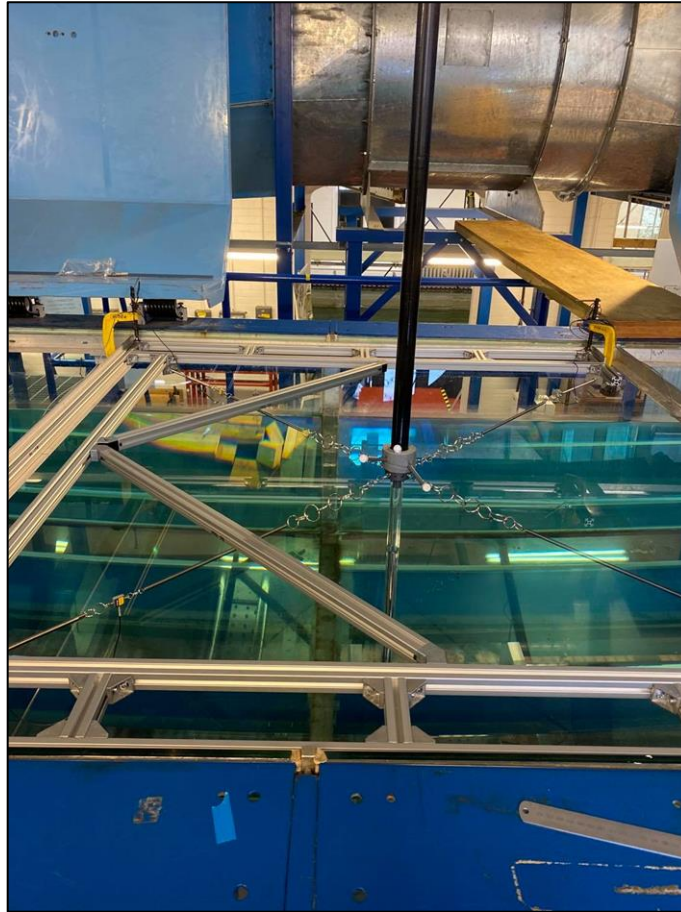


Figure 4-12: Setup of VIV tests of a single cylinder. Upstream cylinder's equipment set, mounting system and location used.

Consequently, the Reynolds number was varied within a range of approximately 1350 – 13500. The damping ratio as previously established from the free decay tests in water is $\zeta = 0.055$ and the mass ratio, $m^* = 3.75$, calculated as the total oscillating mass per equivalent mass of displaced fluid. The detailed description of the computation of the total oscillating mass, mass of displaced fluid, and finally the mass ratio is shown in Table 4-2. Note that the mass of the load cells and Qualisys polystyrene collar and markers are negligible.

The next step was to physically conduct the tank tests and measure the response of the isolated cylinder. The acquisition frequency was set as 200 Hz and the cameras were calibrated at the initial cylinder position, but only once for the full flow velocity variation range. The flow velocity was firstly increased and then decreased for the 49 flow velocity points.

Table 4-2: Description of oscillating pendulum components and their individual masses contributing to the total oscillating mass, computation of equivalent mass of displaced fluid for an immersed length of 0.8 m of the acrylic cylinder and resulting system mass ratio.

Component	Mass
Carbon fibre tube (2.5 m)	0.750 kg
Collar for connection with springs	0.084 kg
Acrylic cylinder model (1 m)	0.463 kg
Lower half of the universal joint	0.600 kg
4 sets of rings for connection with springs	0.200 kg
4 extension springs	0.020 kg
Total oscillating mass	2.117 kg
Displaced mass of fluid (0.8 m of submerged cylinder length)	0.564 kg
Resulting mass ratio	$m^* = 3.75$

The behaviour of the 2DOF cylinder differed between the transverse and streamwise directions. Whilst the cylinder displacement in the transverse direction was seemingly harmonic and well organised, its inline direction counterpart was more complex and required post-processing, i.e., a high-pass filter was used to filter out signal noise at very low frequencies that was unrelated to the vibrations of the cylinder.

Amplitudes of vibration were calculated as the *rms* of the displacements of the cylinder multiplied by $\sqrt{2}$ for consistency and direct comparison with literature studies. The results for increasing and decreasing U_r are presented side-by-side in Figure 4-13.

The only noticeable difference in the VIV behaviour of the single cylinder when increasing or decreasing the reduced velocity occurs at the transition from the upper branch to the lower branch of responses. This hysteretic behaviour, first reported by Feng [71], is a well-known feature of VIV of a single cylinder and has been widely reported in the literature. Despite still not being fully explained, the hysteresis effect has been attributed to nonlinearities in the hydrodynamic force coefficients, as mentioned by Bearman [70] and several studies have characterised this small hysteretic range, here approximately $10 \leq U_r \leq 12$, with a jump in phase angles between

the hydrodynamic force and the displacement of the cylinder and wake mode transitions [60].

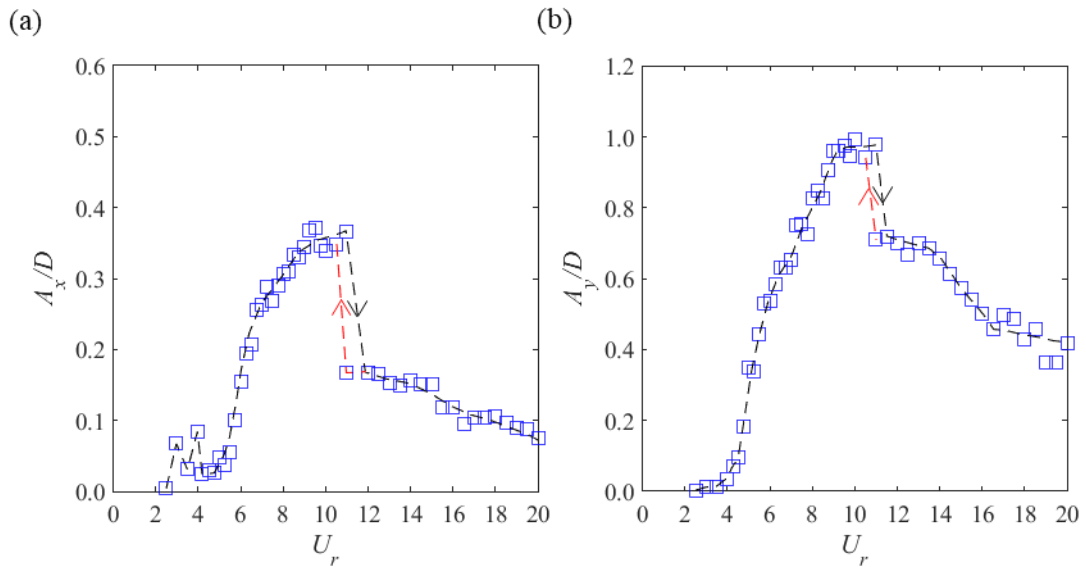


Figure 4-13: Dependence of the amplitudes of vibrations of a single cylinder on the increasing (black dashed line) or decreasing (red dashed line) reduced velocity for $m^* = 3.75$ and $\zeta = 0.055$ (damping ratio in water). (a) Inline oscillations; (b) Crossflow oscillations.

The present results show that the amplitudes of vibration in both directions are larger when the reduced velocities are varied in progression (black dashed line) rather than in retrogression (red dashed line), as initially observed by Feng [71].

Having discussed the differences between increasing or decreasing the flume velocity, the branches of responses and general behaviour of the cylinder will now be analysed in detail. Starting with the inline response seen in Figure 4-13a, it is possible to notice a couple of A_{x2}/D peaks for the lowest reduced velocities. Similar peaks have also been observed by Jauvtis and Williamson [15] for their inline oscillation amplitudes and have been associated with the inline vortex modes, namely the streamwise antisymmetric (AS) and the streamwise symmetric (SS) modes.

According to Jauvtis and Williamson [15], when excited by the AS mode, the cylinder undergoes a figure-of-eight trajectory with comparable inline and crossflow amplitudes. For each cylinder's streamwise cycle a vortex is shed into the trailing wake. In contrast, during the SS mode, a pair of symmetric vortices is shed for each cycle of cylinder oscillation which excites the body in purely streamwise motion.

Although the displacement time series and trajectories of motion will be thoroughly analysed later to validate the following observation, results of Figure 4-13 indicate that the first inline peak at approximately $U_r = 3$ is associated with the SS streamwise mode as transverse oscillations of the cylinder (Figure 4-13b) at the same

U_r are negligible, which suggests that the cylinder motion is purely in the inline direction.

Comparison of XY vibration amplitudes of Figure 4-13 for the second inline peak at approximately $U_r = 4$ shows that the dynamic motion amplitudes in the inline and crossflow directions are comparable with magnitudes of approximately 0.08 diameters for both. As mentioned previously, this is a feature of the AS inline wake mode, which is also characterised by figure-of-eight trajectories of displacement. The figure-of-8 trajectory feature requires that the inline-to-crossflow ratio of oscillation frequencies of the cylinder obeys a 2:1 ratio. Displacement time series, XY trajectories of oscillation and vibration frequencies will be investigated to ascertain whether this is true, but it is anticipated that the conclusion is that this is indeed the case. In conclusion, the first inline and the second inline peaks are in fact related to the SS and AS wake modes respectively. This observation agrees with the classical experimental study of Jauvtis and Williamson [15] for low mass ratio systems.

Furthermore, a wake mode transition happens from the inline vortex modes to the transverse wake modes for higher reduced velocities for both streamwise and crossflow response behaviours, specifically from the AS wake mode to the initial branch of response amplitudes, estimated to be within approximately $4 \leq U_r \leq 6.5$. It is worth mentioning that inline and transverse vortex modes may be observed for the X and Y amplitudes of vibrations of the cylinder due to the coupling of the system, hence inline or transverse vortex modes are characterised as such because of vortex formation and shedding mechanisms rather than feature appearances for a given direction of cylinder response amplitudes.

The initial branch, at approximately $4 \leq U_r \leq 6.5$, has been classified as a 2S wake regime as in the wake pattern map of Williamson and Roshko [72], i.e., two single vortices are shed per cycle of the cylinder's transverse oscillation. The initial branch has been associated with the classical von Kármán vortex street by Govardhan and Williamson [73] in their 1DOF transverse-only study and later investigated by Jauvtis and Williamson [15] for a 2DOF system. Even though the present study has not employed flow visualisation techniques, this classical vortex street is quite clearly seen on a video frame shown in Figure 4-14 at $U_r = 5.5$.

The initial branch denotes the onset of the VIV lock-in and the oscillation amplitudes rise gradually reaching approximately $A_{x2}/D = 0.23$ and $A_{y2}/D = 0.65$ around $U_r = 6.5$ for the present results, where there is a jump of amplitudes in the transition to

the upper response branch for $U_r > 6.5$. Govardhan and Williamson [73] state that the maximum total transverse force occurs at the initial to upper branch transition and the authors have remarked that there is also a jump in the phase angle between the vortex lift force and the transverse displacement of the cylinder in the initial to upper branch transition or super-upper branch, as defined by Jauvtis and Williamson [15] for a very low mass ratio 2DOF system.

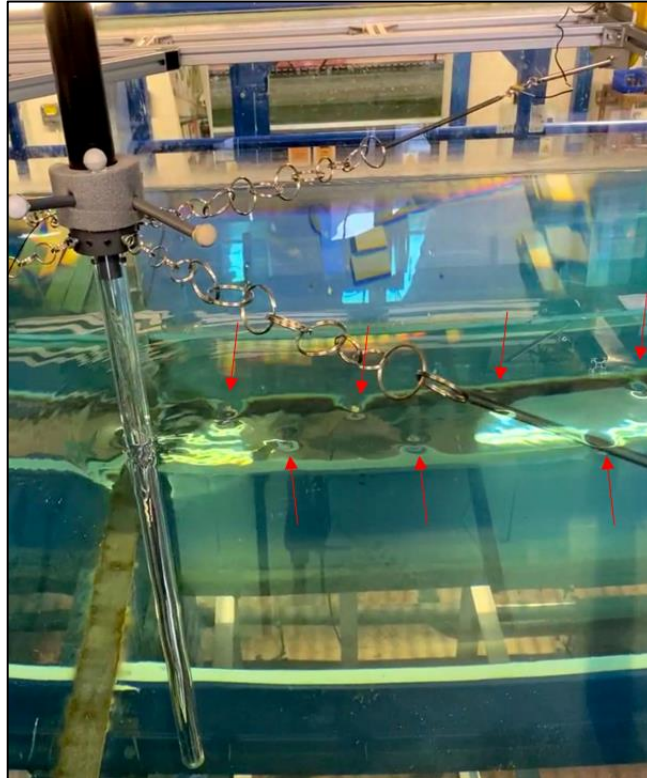


Figure 4-14: Selected frame of a video recording showing the classical von Kármán alternate vortices (highlighted by red arrows) street for the 2S initial branch wake mode at $U_r = 5.5$.

The upper branch features a $2P$ wake pattern, which means that two pairs of vortices are shed per cycle of cylinder oscillation in the crossflow direction, whilst the second vortex of each pair is notably weaker and rapidly decays downstream in the wake [72]. This upper branch wake mode regime is seen in Figure 4-13 between approximately $6.5 \leq U_r \leq 11$ and is responsible for the largest amplitudes of vibration for the present experiments, circa $A_{x2}/D = 0.38$ and $A_{y2}/D = 1$. This branch of largest responses is perhaps the most notable branch of amplitudes of the VIV lock-in of a single cylinder and it is characterised by the synchronisation of the cylinder's transverse oscillation frequency and vortex shedding frequency to its corresponding natural frequency. Trajectories of oscillations within this regime reportedly follow a crescent shape rather than a well-developed figure-of-8, as mentioned by Govardhan and Williamson [73].

A final wake pattern transition from upper to lower branch occurs for $U_r > 11$ approximately for the tested model. Unlike other wake mode transitions, there is no further change in wake characterisation in the lower branch, as it exhibits a $2P$ configuration with, once again, 2 pairs of vortices shed per cylinder transverse oscillation cycle, although the second vortex of each pair is considerably stronger than for the upper branch [73].

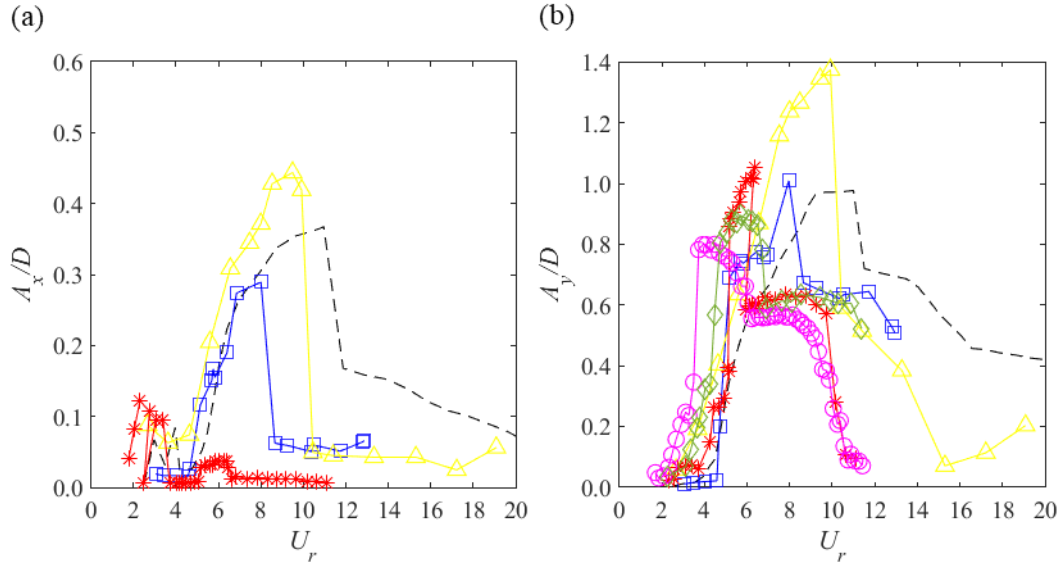


Figure 4-15: Comparison of amplitudes of vibrations with literature studies in (a) inline direction; (b) crossflow direction. Legend: - - : Present 2DOF study for $m^* = 3.75$ and $\zeta = 0.055$ (in water); -■- : Pereira *et al.* [24] 2DOF study with $m^* = 2.92$ and $\zeta = 0.025$ (assumed in water); -▲- : Armin *et al.* [25] 2DOF study with $m^* = 2.36$ and $\zeta = 0.015$ (in water); -*- : Jauvtis & Williamson [15] 2DOF study with $m^* = 6.9$ and $\zeta = 0.0015$ (assumed in air); -○- : Assi *et al.* [11] 1DOF study with $m^* = 2.6$ and $\zeta = 0.007$ (in air); -◇- : Khalak & Williamson [74] 1DOF study with $m^* = 2.4$ and $\zeta = 0.0059$ (assumed in air).

Even though the oscillation amplitudes plunge in the upper to lower branch transition, they are still considerable within the lower branch, $U_r > 11$, but gradually decrease for larger reduced velocities with wake-cylinder desynchronisation of the system out of the resonant condition.

It was important to validate the present results with reference literature studies and the comparison is presented in Figure 4-15. It is important to stress that the comparisons of Figure 4-15 should be made keeping in mind the fact that not all parameters are directly consistent. For instance, the studies considered differ in degrees-of-freedom, mass and damping ratios, method of calculation of amplitudes, method of computation of U_r – i.e., whether the natural frequency is measured in water or air –, and Reynolds number ranges. Nonetheless, the qualitative behaviour and features of VIV of single cylinders are expected to be comparable for low mass and damping ratio systems and this is reflected in Figure 4-15. The present tests exhibit

the most important VIV features and qualitative behaviour also observed for the reference studies.

Overall, the present results appear shifted to the right when compared to the other studies. In other words, the onset of the lock-in with large oscillations or the initial branch occurs for relatively higher reduced velocities for the present results. This is evident especially for the transverse response of the cylinder. The studies of Pereira *et al.* [24] and Armin *et al.* [25] are the ones that most resemble the present study in terms of the commencement of the initial branch. These studies performed free decay tests in water and have presented their results in terms of U_r based on a natural frequency in water as has also been done in the present study.

In fact, given that the natural frequency measured in water is normally lower than in air, as in the current example where $f_n^{water} = 0.75$ Hz and $f_n^{air} = 1$ Hz, the reduced velocity associated with triggering the lock-in for the initial branch amongst the studies would be expected to collapse or at least become closer. In that case, the 1DOF results of Assi [11] and Khalak and Williamson [74] may perhaps be the closest in comparison in terms of upper and lower branch extension, and overall transverse behaviour.

Regarding streamwise vibration amplitudes of response, it is observed that the first double inline peaks, happening approximately within $2 < U_r < 4$, are seen for almost every reference study as well as the present study. As mentioned previously, they are related to the SS and AS inline vortex modes. The starting U_r point of the initial branch achieving large inline oscillation amplitudes is relatively similar amongst the studies. On the other hand, the lateral extension of the lock-in regime for the present investigation is significantly larger than for other studies. Khalak and Williamson [60] have investigated that the mass ratio can largely affect this range of synchronisation for the single cylinder under VIV and Govardhan and Williamson [73] have cited that the combined mass-damping parameter, rather than just the mass ratio, should be considered for comparison amongst systems and studies. Therefore, the difference in these two parameters from the present experiments to the two mentioned sets of reference data are understood to affect the range of synchronisation and could be the cause of the discrepancies observed in lock-in extension for not only the inline amplitudes of vibrations but also for the transverse component as well.

It is now important to analyse these results with respect to the time evolution of parameters, oscillation trajectories and vibration frequencies. Therefore, the time series of the 2DOF vibration of the single cylinder under VIV were studied and are

presented in Figure 4-16. Time series have been selected for the final 20 seconds of testing of each U_r case, i.e. $t = 100-120$. This normally is translated to less than 40 cycles of oscillations presented, whilst the frequency in the x direction is known to be higher than that in the y direction. Overall, it is shown that the displacements of the cylinder can become quite complex with variation of reduced velocity, especially for its response in the longitudinal direction.

Figure 4-16a-d has been plotted with the same limits for the y axis for direct comparison between the inline and crossflow responses. Real-time tracking of the cylinder for $U_r = 3$ shows that, despite the visibly disorganised motion, magnitudes of vibrations highlight that the oscillations in the inline direction, of up to nearly 0.1 diameters, are considerably greater than the negligible amplitude values in the transverse direction. Therefore, this reflects that the cylinder mostly oscillates in the streamwise direction, which is a distinguishing feature of the SS inline wake mode.

Alternatively, results for $U_r = 4$ show that magnitudes of vibration of approximately 0.1 diameters are relatively comparable between the inline and crossflow motions. This is a notable feature of the AS inline wake mode and agrees with previous analyses. On the other hand, when the reduced velocity is increased to $U_r = 6$, this has been previously associated with the initial branch transverse wake mode. It is possible to observe from Figure 4-16e-f that the displacements of the cylinder are more organised and undergo a jump up in maximum magnitudes from previous reduced velocity cases to approximately $x = 0.15 D$ and $y = 0.6 D$. This observation is also compatible with initial branch regime features previously discussed.

Moreover, the time series for a reduced velocity, $U_r = 10$, for which approximately the largest amplitudes of vibrations have been noted on Figure 4-13, are plotted in Figure 4-16g-h. This regime is well characterised within the upper branch transverse wake mode regime. It leads to the largest oscillation amplitudes in both directions for a single cylinder subjected to VIV, namely a maximum of close to $x = 0.4 D$ and $y = 1 D$. Interestingly, it is the case that exhibits perhaps the most regular and organised XY responses, i.e., the streamwise response shows amplitude modulation but apparently is not disorderly, whilst the transverse response reflects a nearly harmonic behaviour with spiralling traces. Indeed, this relatively organised behaviour has also been commented on in the literature and is associated with figure-of-8 trajectories for the initial/upper branches.

Furthermore, a similar behaviour is seen between the two largest selected reduced velocity cases of Figure 4-16, $U_r = 15, 20$. From analysis of Figure 4-13, $U_r = 15$ and 20 are apparently located in separate branches of response, the lower branch and the desynchronisation regime. This is indicated especially for the transverse amplitudes of vibration. However, time series of Figure 4-16 show that the cylinder response amplitudes are remarkably similar in the two directions, although slightly larger for $U_r = 15$. The maximum amplitude viewed for $U_r = 15$ is nearly $x = 0.2 D$ and $y = 0.5 D$, whereas for $U_r = 20$, these values are slightly lower especially for x , whilst maximum y values remain similar.

Finally, it is important to stress that the maximum values of x and y seen in Figure 4-16 are different from A_{x2}/D and A_{y2}/D values reported for Figure 4-13 and Figure 4-15 that are calculated as *rms* of the full window of responses, $t = 0-120$ s. Nevertheless, time series results have proved relevant for a more detailed investigation of the specific behaviour of the cylinder, in a given direction, for selected key reduced velocities associated with different wake mode regimes and complement the holistic investigation of VIV of a single cylinder.

However, the motion of the single cylinder clearly is coupled in the two directions. Therefore, it is important to examine the integrated oscillation trajectories and these results are presented in Figure 4-17. The same 6 U_r cases are studied for consistency, these are: $U_r = 3, 4, 6, 10, 15,$ and 20 . The axis limits of the Lissajous figures are square for all cases and they have been set equally for a comparison in proportion to the initial $(x,y) = (0,0)$ position.

Starting off with the case of $U_r = 3$, in Figure 4-17a, trajectories of the cylinder are seen to be in line with what has been previously discussed, i.e., that this cylinder behaviour is characterised by a pure motion in the streamwise direction as it is associated with the SS inline wake mode. In fact, this trajectory is similar to what is seen in the study of Jauvtis and Williamson [15] for a comparable reduced velocity and related to the SS vortex regime.

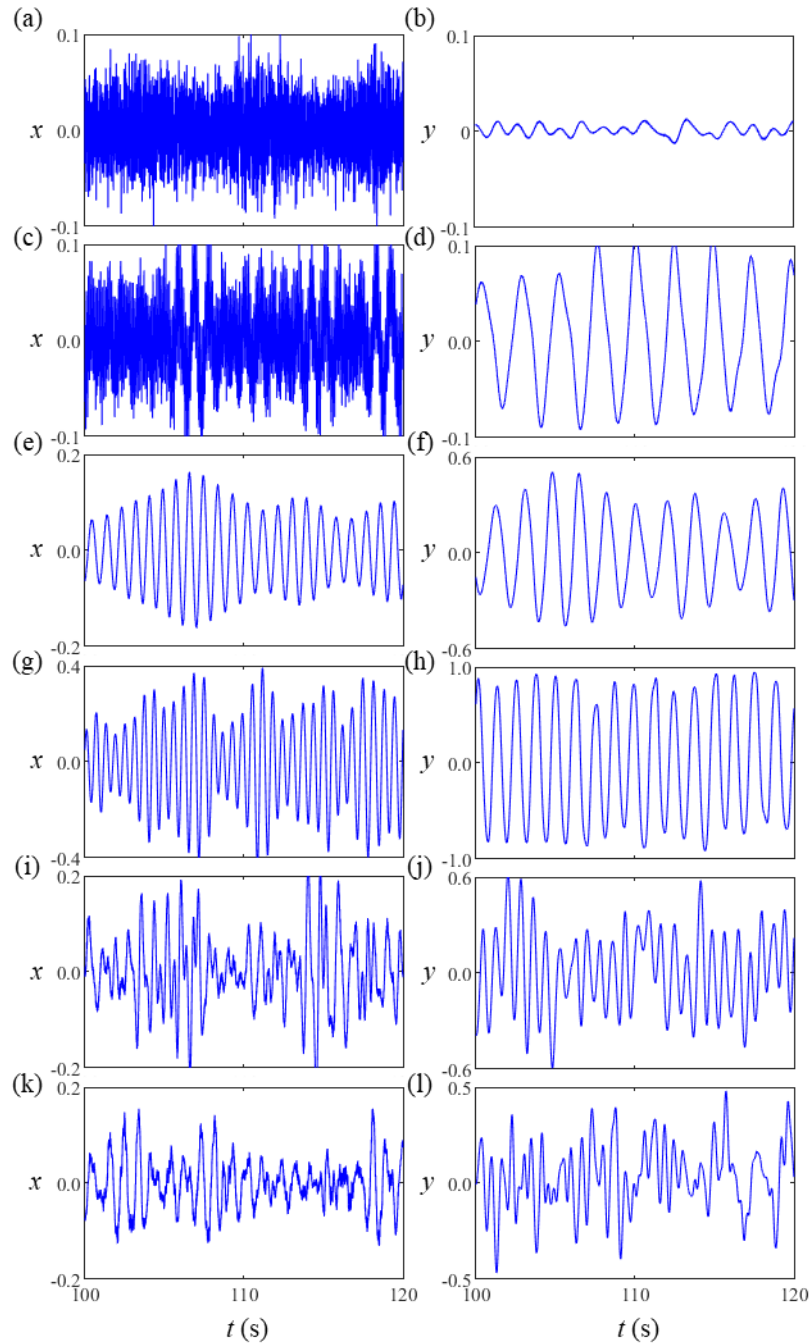


Figure 4-16: Time evolution of displacements of the single cylinder in the streamwise direction (left-hand side column), and transverse direction (right-hand side column). $U_r = 3$: first row of subfigures; $U_r = 4$: second row of subfigures; $U_r = 6$: third row of subfigures; $U_r = 10$: fourth row of subfigures; $U_r = 15$: fifth row of subfigures; and $U_r = 20$: sixth row of subfigures.

Although the $U_r = 3$ reduced velocity is very small, the trajectory shape is already visibly dislocated to the right-hand side of the figure, where $x > 0$. This mean displacement of the cylinder is a direct consequence on the oncoming flow loading the cylinder due to the mean drag force component.

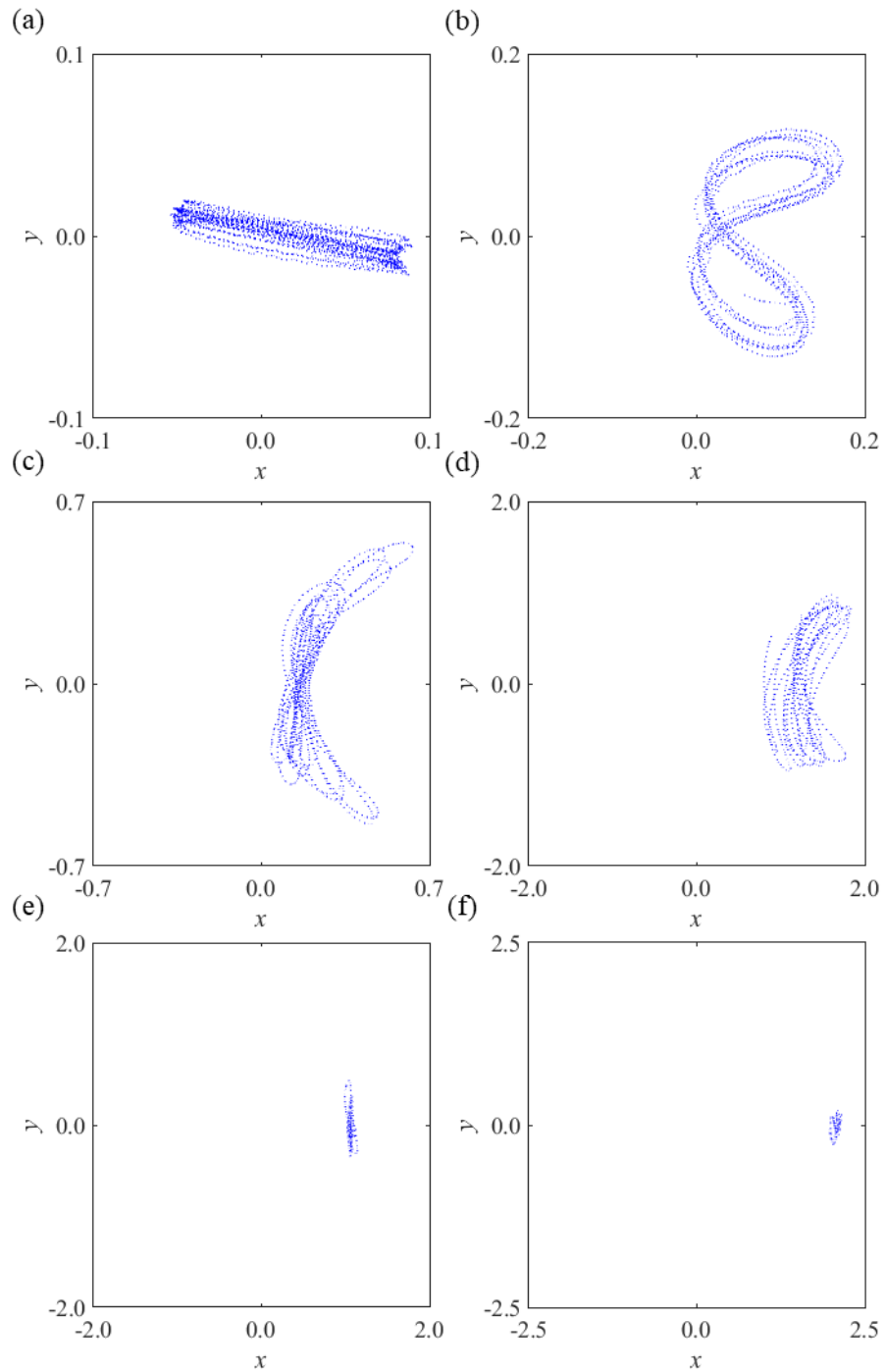


Figure 4-17: 2DOF trajectories of a single cylinder undergoing VIV for (a) $U_r = 3$; (b) $U_r = 4$; (c) $U_r = 6$; (d) $U_r = 10$; (e) $U_r = 15$; and (f) $U_r = 20$.

For the case previously identified as an example of the AS inline wake mode, $U_r = 4$, the trajectory shape of the single cylinder resembles a figure-of-8. This figure-of-8 motion highlights that the oscillation frequencies in the streamwise direction are twice the vibration frequencies in the transverse direction, as the cylinder undergoes 2 cycles of inline oscillations for each full cycle of transverse oscillations. Thus, the inline-to-transverse frequency ratio is 2:1 and, even though the figure-of-8 may be observed for other response branches and U_r cases, the trajectories associated with the AS inline

wake mode are the clearest and widest figures-of-8. This is a direct consequence of a distinguishing feature of the AS vortex mode whereby vibration amplitude magnitudes are relatively comparable between the displacements in the two directions, x and y . Regarding the time-independent dislocation of the cylinder, one may notice the mean loading on the cylinder is now sufficient to drag it to a position where the cylinder purely vibrates in the positive x direction. As it will be discussed later, this mean drift will be shown to have repercussions for the study of pairs of cylinders.

With the increase of reduced velocity to values previously characterised in the initial branch domain, presently $U_r = 6$, the transverse response, y , of the cylinder takes over and reaches magnitudes more than double that of x . This was also confirmed by Figure 4-13. In other words, even though the inline-to-transverse frequency ratio of 2:1 remains apparently unaltered, the jump of amplitudes that occurs at the initial branch and for this specific $U_r = 6$ is considerably greater for the transverse than for the inline response. This leads to the respective figures-of-8 becoming elongated and slender shapes as in Figure 4-17c.

Another striking feature of the trajectories of the cylinder for $U_r = 6$ is that different figure-of-8 shapes compose its Lissajous figure. This feature indicates amplitude modulations and can be related to the displacement time series of Figure 4-16. Clearly, besides the primary higher frequency oscillations, there is also a lower frequency component and the response is modulating in both directions leading to the different figure-of-8 shapes seen in Figure 4-17c depending on the response modulation stage. Finally, the mean drift of the cylinder for $U_r = 6$ is shown to have been augmented, as expected due to the increase of flow current velocity, to approximately 20% - 40% of a cylinder diameter.

For a higher reduced velocity associated with the upper branch, $U_r = 10$, the recorded trajectories for 20 s of oscillations in Figure 4-17d show a similar trait to the case discussed above, where different figures-of-8 are observed. The figures-of-8 associated with the upper branch are elongated reflecting the notably larger transverse amplitudes of oscillation as similarly demonstrated by the study of Jauvtis and Williamson [15]. There is, however, a notable difference between the x - y motion cases of $U_r = 6$ and 10: although the difference in axis limits between the two subfigures needs to be taken in consideration, the figures-of-8 appear to vary considerably in the x -axis direction, but not in the y -axis direction for the higher U_r case, whereas

significant variations in the y -axis direction were previously seen for the lower reduced velocity.

These different figures-of-8 of the excursion of the single cylinder have been associated with the amplitude modulation and oscillating mean values observed in the time series of Figure 4-16. For $U_r = 6$, it has been discussed above that amplitude modulations and response envelope spiralling occurred for both directions, however, for $U_r = 10$, whilst this is still clear for Figure 4-17g-h for the streamwise vibrations of the cylinder, the transverse oscillations of the cylinder, on the other hand, exhibit a nearly harmonic behaviour especially in comparison with Figure 4-17f. Therefore, the response of the cylinder for $U_r = 10$ shows greater variability for the x -axis response and organisation than for the y -axis response, whilst maintaining similar dominant frequency ratios that lead to the different figures-of-8 plotted on Figure 4-17d.

Another characteristic of the motion trajectories is the substantial rise of the mean drift from Figure 4-17c-d, where with the increment of 4 dimensionless units of reduced velocity or approximately 0.1 m/s from $U_r = 6$ to $U_r = 10$, the steady displacement of the cylinder, associated with the mean drag force, grows from approximately 20% - 40% of its diameter to 150% - 200% of a cylinder diameter.

Although specific laboratory tests have not been conducted to determine the reason for this abrupt leap in mean displacements, this is theoretically understood to be an outcome of the following two aspects:

i) the hydrodynamic forces acting on the cylinder, as in the steady drag force component, are nonlinear with respect to the flow velocity [62, 75]. More specifically, the steady drag force component increases quadratically with flow velocity governed by the following equation:

$$\bar{F}_D = (1/2)\rho D L \bar{C}_D U^2$$

Hence, considering that the cylinder springs are linear and no other relevant time-averaged factor acts on the system, the cylinder is expected to be displaced nonlinearly with the flow velocity according to the steady drag force;

ii) the mean drag coefficient, \bar{C}_D , as highlighted in the equation of mean drag force above, is widely reported in the literature to suffer amplification within the VIV lock-in of large transverse oscillation amplitudes [2, 66, 76, 77]. Blevins [66] describes that the average drag on a cylinder that vibrates at or near the vortex shedding frequency, i.e. lock-in regime, is a function of transverse vibration amplitude and the author reviews a number of semi-empirical models that relate the mean drag coefficient

and the transverse vibration amplitude. In fact, different studies and authors consider that the mean drag coefficient may nearly double or even triple within the lock-in regime [36, 45, 46, 62, 64].

Therefore, given that the cylinder springs are considered linear, then in the absence of other significant time-invariant phenomena, the static equilibrium location of the cylinder is expected to drift by a similar proportion.

In summary, the mean drift of the cylinder may increase with flow velocity and VIV lock-in regime given the nonlinear behaviour of the mean drag force with variation of the flow velocity and the VIV mean drag amplification. For the present study this is observed especially for the upper branch of response amplitudes illustrated by $U_r = 10$ in Figure 4-17d, for which the cylinder may have drifted downstream a distance equal to nearly 2 diameters. For the study of a pair of cylinders that will be discussed in Chapter 5 and Chapter 6 such a mean drift will make the two cylinders substantially closer which may be critical.

Moving on to analyse the trajectories of the lower branch of response in $U_r = 15$, the jump down in amplitude of vibrations from the upper, $U_r = 10$, to the lower branch, $U_r = 15$, becomes evident as the subfigures have the same axis limits. Regarding the motion shapes themselves, despite some traits of disorganisation, the cylinder still moves respecting a figure-of-8 orbit. However, this figure-of-8 is now nearly flat and almost a purely transverse side-to-side straight movement, although a figure-of-8 trajectory shape may still be observed if Figure 4-17e is carefully analysed. This observation agrees with the findings of Jauvtis and Williamson [15] in their Figure 8 for a U_r case within the lower branch of response, for which they present a flat figure-of-8 with almost negligible x -axis dynamic displacement.

The justification for this flat figure-of-8 profile for $U_r = 15$ may be traced back to oscillation amplitudes of Figure 4-13. Whilst amplitudes of vibration are still relatively large for $U_r = 15$, reaching *rms* amplitudes of approximately $A_y/D = 0.6 D$, *rms* response amplitudes in the x -axis direction are only approximately one-fifth of this magnitude, vibrating with approximately $A_x/D = 0.12 D$ and resulting in the flat figure-of-8 discussed.

Interestingly, when motion paths are investigated between $U_r = 10$ (Figure 4-17d) and $U_r = 15$ (Figure 4-17e), the dynamic equilibrium position distance to the initial position, $(x,y) = (0,0)$, due to the mean drift of the cylinder is about 100% - 150% of a cylinder diameter, which is either lower or nearly equal between these two reduced

velocity cases, despite the considerable difference of 5 in U_r . A question can then be asked as to why the mean drift of the single cylinder does not appear to increase in the same proportion from $U_r = 10$ to $U_r = 15$, given its previous escalation from $U_r = 6$ to $U_r = 10$?

Theoretically, this question can be answered based on the two contributing factors previously discussed to increase the mean drift of a cylinder in the present study:

i) the mean drag force component increases quadratically with the flow velocity; and

ii) the mean drag amplification attributed to VIV lock-in, i.e., the mean drag coefficient depends on the transverse amplitude of the cylinder [2].

Therefore, whilst the reduced velocity rises by 5 dimensionless units or approximately 0.1125 m/s from $U_r = 10$ to 15, the transverse amplitude of the cylinder has been demonstrated in Figure 4-13 to decrease as the response regime transitions from the upper to the lower branch. Blevins [66] proposed the drag coefficient amplification relationship with the transverse amplitude of vibrations at lock-in may be nonlinear. The words “at lock-in” are key in the sense that a high reduced velocity such as $U_r = 15$ might be a case near desynchronisation of the cylinder from its vortex shedding frequency so it may be unclear whether the drag coefficient is still even amplified. Thus, the rise in flow velocity would normally cause the mean drift of the cylinder to increase, however, the drop in magnitude of the mean drag coefficient seems to compensate for that and the resulting mean drift is roughly unchanged between $U_r = 10$ to $U_r = 15$ in Figure 4-17.

The highest U_r has also been selected and corresponding cylinder trajectories plotted in Figure 4-17f. It is possible to observe that the cylinder no longer vibrates in figures-of-8 and cylinder trajectories are disordered in both directions, as similarly discussed for the time series results of Figure 4-17. Indeed, Jauvtis and Williamson [15] concluded that body motions can be quite different from a figure-of-eight in given circumstances. Moreover, the mean drift of the cylinder can be seen to increase to close to a distance equal to 2.5 diameters for the highest reduced velocity studied herein. The disorganised character of cylinder trajectories for $U_r = 20$ may be related to turbulence of the flow surrounding the cylinder and in the near wake flow. Freire [78] discusses that turbulent flow is inherently transient and fluctuates in space and time. According to the author, a turbulent flow is rich in time and space scales, from the

largest scales with dimensions comparable to the flow field all the way to the smallest scales in which dissipative processes occur. Furthermore, the VIV phenomenon is a resonant mechanism [11], hence it inputs large energy to the system within the resonance zone, but with an increment of reduced velocity out of the resonant regime (desynchronisation), the VIV mechanism becomes negligible and other excitation sources may start to interact with the system.

Finally, the recorded vibration results of the single cylinder are now analysed in the frequency domain. Based on the camera acquisition sampling frequency of 200 Hz, and length of recording, the time series results have been converted using the discrete Fourier Transform in-built Matlab function based on the widely published FFT algorithm [79][80]. Application of the FFT algorithm to the measured data allowed it to be seen in terms of frequencies. Subsequently, the dominant frequencies have been determined for each reduced velocity case, normalised by the natural frequency of the system, and plotted in Figure 4-18 for the cylinder oscillations in both directions.

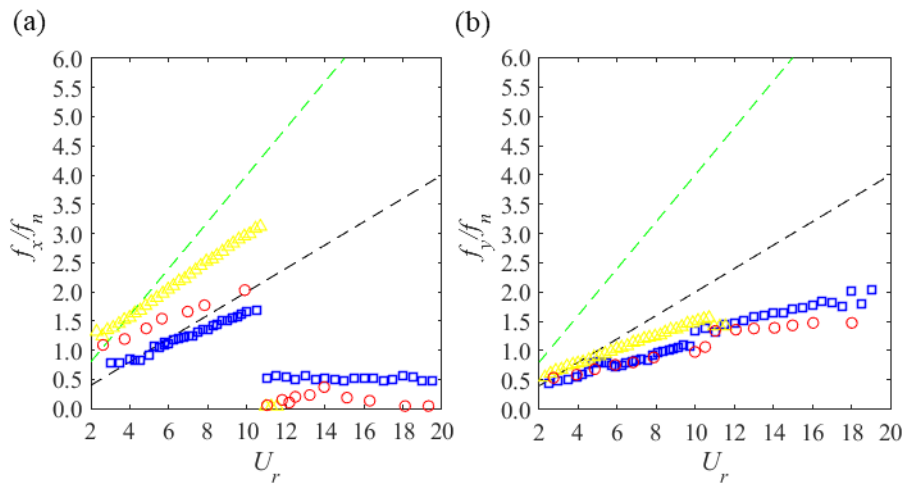


Figure 4-18: Dominant normalised frequencies of oscillations varying with the reduced velocity for the VIV of a single cylinder in a flume in the: (a) streamwise direction; (b) crossflow direction. Legend: - - : Strouhal law ($St = 0.2$); - - : Doubled Strouhal law ($2St = 0.4$); \square : Present 2DOF study for $m^* = 3.75$ and $\zeta = 0.055$ (in water); \triangle : Assi [23] $m^* = 1.6$ and $\zeta = 0.003$ (in air); and \circ : Armin *et al.* [25] $m^* = 2.36$ and $\zeta = 0.015$ (in water).

The frequency results from the present experiments are observed to follow the black-dashed Strouhal line for the transverse oscillation outputs and the double Strouhal green-dashed line for streamwise oscillation measurements for the lowest reduced velocities analysed. This is a well-known feature of VIV prior to synchronisation [66], when the cylinder vibrates in the transverse direction at its vortex shedding frequency governed by the classical Strouhal law. It is also a known fact of VIV that the response frequency of the cylinder in the inline direction is mostly twice

the corresponding frequency in the crossflow direction, which is the reason for comparing f_x/f_n with the doubled Strouhal line as previously done in Chapter 2.

The Strouhal lines of Figure 4-18 have been plotted considering a rounded and widely accepted value for the Strouhal number in the literature [45, 66, 75], i.e., $St = 0.2$, $2St = 0.4$. This, however, may not be entirely accurate for the present study as similarly found in the literature, where variations of the order of $St = 0.18 - 0.22$ may be encountered [46]. From observation of Figure 4-18, it is clear that the oscillation frequencies of the present laboratory model increase at a gradient lower than $St = 0.2$ as both f_x/f_n and f_y/f_n are below the respective doubled and original Strouhal lines. These discrepancies are more evident for f_x/f_n since the frequencies and consequently the discrepancies are doubled. In fact, it is thus possible to estimate that the present Strouhal number is more in line with the following values of $St = 0.18$, and $2St = 0.36$. Whether the black-dashed and green-dashed lines of Figure 4-18 are corrected to reflect $St = 0.18$, optimal congruency may be seen between the experimental results and the $St = 0.18$, $2St = 0.36$ lines for the lowest reduced velocities as expected from literature. Nevertheless, the two reference Strouhal lines have been chosen to remain with the typical value of $St = 0.2$ for Figure 4-18 for direct correlation with the modelling section conducted in Chapter 3.

Experimental frequencies of vibration increase similarly to the vortex shedding frequency and the Strouhal law with reduced velocity for approximately $U_r < 4$. As the reduced velocity is further increased, the cylinder enters lock-in and synchronises with the natural frequency as it is perhaps more clearly seen for the transverse response of the cylinder that sustains values close to $f_y/f_n = 1$. The inline frequencies of vibration appear to undergo a similar feature as the gradient of f_x/f_n against U_r changes at approximately $f_x/f_n = 2$ within a similar reduced velocity range, however, it is not as evident as the completely separated lock-in branch of frequencies shown in Figure 4-18b. This is expected as it is understood from literature that the lock-in regime is the resonant regime of the transverse response and it is associated with transverse wake modes as discussed previously and in the studies of Khalak and Williamson [60] and Jauvtis and Williamson [15]. It is the only VIV regime capable of re-organising vortex shedding and the trailing wake and it affects indirectly, but considerably, the cylinder response in the inline direction. This indirect coupled contribution from the transverse to the streamwise cylinder response is the reason for the angle difference in inline frequency branches of response at roughly $f_x/f_n = 2$.

Therefore, no greater difference is observed for the f_x/f_n in the transverse lock-in regime of intermediary reduced velocities, approximately $4 < U_r < 10$ for the present study. This more discrete variation of f_x/f_n when compared to f_y/f_n could also be related to why the previously discussed body motion trajectories transition from clear figures-of-8 to more disassociated figures-of-8 or unrecognised shapes as the cylinder's inline-to-crossflow frequency ratio might not be perfectly 2:1. Furthermore, even though f_x/f_n appears relatively unfazed within $4 < U_r < 10$, the inline amplitudes of vibration of the cylinder have been shown to rise substantially and there is also the mean drag amplification that occurs during lock-in as discussed.

What happens during the resonance of $f_y/f_n = 1$ (and consequently $f_x/f_n = 2$) has been investigated but no clear feature can be distinguished from Figure 4-18 for the inline resonance of the system, $f_x/f_n = 1$. It is possible, however, to correlate the frequency results with the amplitude results previously presented to compare that $f_x/f_n = 1$ occurs at approximately $U_r = 3 - 4$, for which peaks of inline oscillation amplitudes have been identified in Figure 4-13 and related to the inline AS and SS wake modes.

On the other hand, the transition from upper to lower branches of response that occurs near $U_r = 10$ is noticeable for both f_x/f_n and f_y/f_n results of Figure 4-18. The dominant inline oscillation frequencies drop to the lowest normalised frequencies near $f_x/f_n = 0$ or 0.1. These agree with literature and seem to be related to the DC frequency component associated with the mean signal value. In fact, it has been shown that the dynamic inline response of the cylinder is greatly reduced to nearly negligible magnitudes, whilst the cylinder mostly drifted downstream with the flow due to the mean drag force. In contrast, transverse frequency outputs de-synchronise from $f_y/f_n = 1$ to a different response frequency branch unrelated to either the Strouhal law or $f_y/f_n = 1$. These observations agree with the experimental results shown.

The present results have been validated with the experimental measurements of Assi [23] and Armin *et al.* [25]. The current study highlights the main features of VIV of an isolated cylinder as compared with the two reference literature investigations. Slight discrepancies are observed in Figure 4-18 for the Strouhal number (initial frequency branch gradient), extension of VIV lock-in regime, and position of the transition of upper to lower branches of responses. Nevertheless, these slight discrepancies must take into consideration that: i) literature results of Figure 4-18 have been normalised and plotted against U_r each calculated from their respective and unreported natural frequencies – obtained differently from water and air free decay tests; ii) mass and

damping ratio differences; iii) Reynolds number variations; iv) different experimental setups, for instance, Assi [23] removed the cylinder's mean drag steady displacement. Having said that, the agreement of responses and features is satisfactory, contributes to the understanding of the phenomena involved and will be important for the WIV study of pair of cylinders to be discussed in Chapter 5 and Chapter 6.

4.8. Chapter Summary

- The experimental rigs and supporting systems for the two cylinders have been designed and built in-house at Newcastle University's WWCT.
- Four springs were attached to each cylinder for 2DOF vibrations. Because of the required centre-to-centre spacings between cylinders required to investigate the most critical WIV cases, $d = 4D = 120$ mm, or a surface-to-surface distance of 90 mm, not to mention the lateral separation between the cylinders, the standard spring fixing was not feasible. Therefore, springs were diagonally fixed to the cylinders.
- Free decay tests have been conducted and the conclusion is that the damping ratio in water is $\zeta = 0.055$, mass ratio, $m^* = 3.75$, and natural frequency $f_n^{water} = f_n = 0.75$ Hz for the identical double cylinders systems.
- Wake flow measurements have been conducted after a stationary cylinder and a single cylinder undergoing VIV. Results have shown that the wake depression is largest (wake flow velocity is minimum) at the centre of the wake behind a stationary cylinder than for a vibrating cylinder. This is expected as the vibrating cylinder is not always blocking the flow at the same position, but, as it will be seen, this observation will be helpful to analyse features of WIV in the next chapters.
- Tests on the vibration of a single cylinder have also been done and compared against literature studies. The present experimental study single cylinder system has shown clear VIV features, including an initial branch of responses, upper and lower/desynchronisation response. Lock-in regime was observed as well as figure-of-8 plane motion trajectories and a hysteresis phenomenon between increasing and decreasing U_r tests.

CHAPTER 5. COMBINED VIV AND WIV OF A PAIR OF CYLINDERS FOR A STATIONARY UPSTREAM CYLINDER (“FIXED-FREE” CASE)

The experimental study and conclusions of VIV of an isolated cylinder have contributed to the understanding of the phenomenon and the behaviour of the cylinder body with the given mass and damping ratio properties and specific to the conditions of the WWCT tank. This study has also been important to serve as a benchmark for the succeeding and now focused analyses of a pair of cylinders, which is the main motivation of the present PhD thesis.

As described previously, the external flow of a fluid, water for the study in question, against and surrounding multiple cylinders in relative proximity may trigger a series of complex phenomena and the resulting turbulent wake flow trailing each cylinder and vortex shedding may lead to a combined effect of VIV and WIV. This has already been comprehensively analysed theoretically in Chapter 2 and Chapter 3 and a computer efficient reduced order model has been formulated and proposed to investigate the behaviour of the cylinders. Insights and conclusions from this study have helped in the understanding of this problem which may happen in practical applications, especially in subsea engineering.

Apart from the specific and technical conclusions of the modelling study, it has also been identified that higher fidelity experimental research of the flow induced vibrations of a pair of cylinders, when they are both free to vibrate in two directions, was lacking and was needed to address open questions, corroborate findings, and to be used as a reference for future modelling.

Therefore, experiments involving the external flow and behaviour of two cylinders in tandem and staggered configurations have been conducted and are presented for two cases namely for a static upstream cylinder (“fixed-free” case) in this chapter and for a 2DOF upstream cylinder (“free-free” case) in Chapter 6.

The study of the combined VIV and WIV of a pair of cylinders is especially relevant for parametric studies which are important for the fundamental understanding of the subject. A greater number of literature studies is available for the numerical and experimental analysis of VIV and WIV of groups of cylinders in fixed-free schemes. Hence, the proposed fixed-free setup and experimental measurements have been inspired and are validated with reference literature studies.

5.1. Fixed-Free Experimental Setup Details

The experiments were conducted in the WWCT tank, where the carbon fibre tube and acrylic cylinder pendulum system with the four spring sets described in Section 4.7 were removed and replaced by the static metallic cylinder and its supporting rig. The metallic cylinder was again fixed at its base in a cantilever to its supporting frame at a height of 20 cm above the WWCT tank water level. The static metallic cylinder has been placed at the same location as the upstream pendulum and held vertically down the tank with an immersed depth of 80 cm.

As mentioned in Section 4.1, the total length of the solid metallic cylinder is 1 m, thus, the gap between the bottom of the cylinder and the tank floor is 20 cm. The effect of the gap flow near the tank floor has been considered to negligibly affect the measurements and no end plate or fitting has been deemed necessary.

A picture of the upstream static cylinder system can be seen on Figure 5-1. The frame was mounted against the tank's lateral L-shaped brackets with a smooth surface that functioned as rails so that the entire frame and cylinder could be easily moved and fixed either upstream or downstream the WWCT tank. More details about the static upstream cylinder setup can be found in Section 4.1.

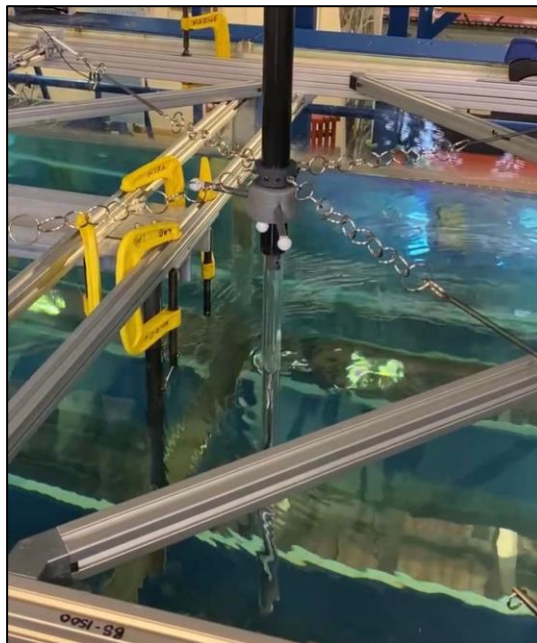


Figure 5-1: Combined VIV and WIV tests of a 2DOF cylinder (on the right-hand side) downstream of a metallic cantilevered cylinder (on the left-hand side). The upstream metallic fixed cylinder is allowed to have its initial position varied along the tank length, increasing the tandem distance between the cylinders, whilst the downstream acrylic cylinder is moved transversally for staggered studies.

The experimental campaign for the fixed-free pair of cylinders was conducted over approximately 20 working days. The tests were divided into tandem, for the initial gap

separations of $(d, T) = (3,0), (4,0), (6,0), (8,0), (10,0)$, and $(20,0)$ and later into staggered tests with initial spacings of $(d, T) = (4,1), (4,2), (4,3), (4,4), (10,1), (10,2), (10,3)$.

An observation that has not been considered to affect the measured quantities, but is recorded here for the information of the reader, is that the metallic upstream cylinder had built up a thin layer of superficial rust towards the end of this experimental phase. This happened because the static upstream cylinder was made of untreated carbon steel and had been kept immersed for 80% of its length during the greater part of the 20 days that the measurements lasted for. This superficial thin layer of rust was then cleaned without further complications and the surface of the metallic cylinder was inspected visually and manually for severe changes in diameter, cross-section, and roughness, which were not detected.

In conclusion, whilst the metallic upstream cylinder was not completely ideal for underwater tests, use of one of the two identical acrylic cylinder models was ruled out of the fixed-free WIV tests since the risk of bending and/or damaging the acrylic cylinder due to the hydrodynamic loading was considered too great.

Therefore, it was a question of using an upstream cylinder made of different material with different roughness and superficial corrosion, or the acrylic stationary upstream cylinder that could be damaged by the flow or on connection to the fixed cylinder rig. The superficial thin layer of rust and the roughness difference between the carbon steel cylinder and the acrylic cylinder has been concluded to minimally affect the experiments as it will be made clear in the validation with reference experimental studies in future sections.

5.2. “Fixed-Free” WIV amplitudes of vibrations

The WIV fixed-free tests followed the same logical order and procedures as for the single cylinder measurements in terms of U_r variation. However, this time the proposed investigation of dependence of the behaviour of the downstream cylinder on the initial gap spacing meant that the complete set of flow velocity tests had to be repeated 13 times, which is the number of tandem and staggered spacings studied. In other words, the flow velocity in the WWCT tank could be controlled in terms of CPG and translated to U_r , which then would be varied across $U_r = 2 - 20$ with different increments as discussed in Section 4.1, for a given initial position of the fixed-free pair of cylinders. Once U_r variation was over and results were checked, the position of the cylinders was changed.

The results from the WIV of a 2DOF cylinder downstream of a stationary identical cylinder are now presented. Amplitudes of vibration of the downstream cylinder for the inline and crossflow directions, A_{x2}/D and A_{y2}/D , have been calculated and are presented in Figure 5-2.

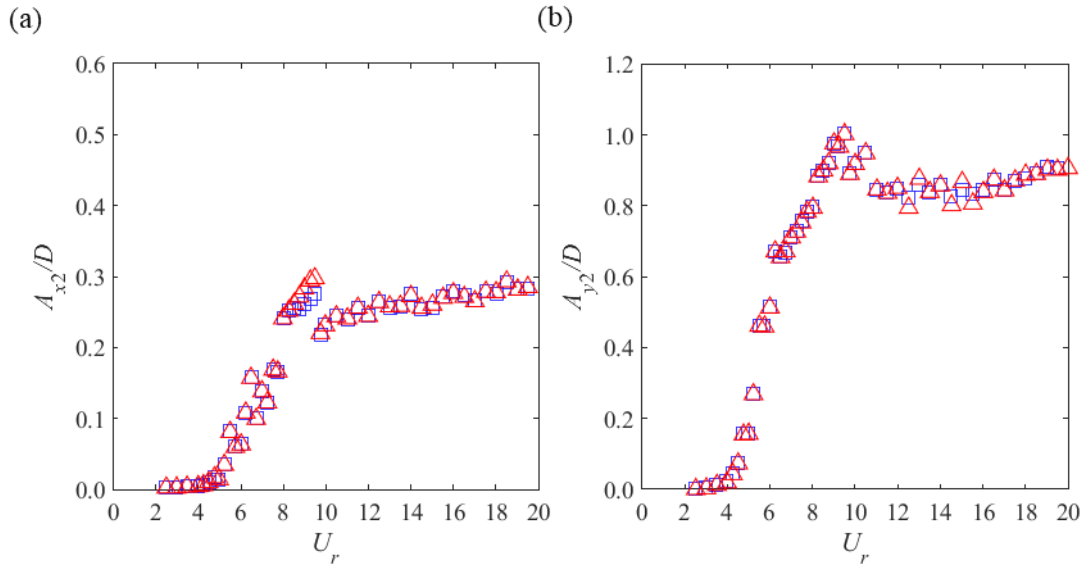


Figure 5-2: Dependence of normalised amplitudes of vibrations on the reduced velocity for a 2DOF downstream cylinder behind a static cylinder at initial spacing, $d = 4$. Caption: \triangle : increasing U_r ; \square : decreasing U_r .

As for the study of a single cylinder under VIV, the flow velocity was increased from $U_r = 2 - 20$ and later decreased within the same range for a pair of fixed-free cylinders. This was done to understand whether features such as VIV hysteresis for single cylinders would repeat themselves for WIV of groups of cylinders. Figure 5-2 shows that the response of a pair of fixed-free cylinders is not hysteretic for the given properties and conditions of the present experiments. Indeed, no or negligible differences are observed in the comparison of cylinder responses when the reduced velocity is successively increased against when U_r is sequentially decreased.

This observation agrees with the study of Brika and Laneville [13] who reported that the response of the downstream cylinder after a stationary cylinder is no longer hysteretic. On the other hand, the researchers have observed hysteretic behaviour for other setups of pair of cylinders, however, correlation is difficult as their study had fundamental differences to the present study, e.g., flexible cylinders immersed in air rather than water, extremely large mass ratios ($m^* = 821$), extremely low damping ratios $\zeta = 0.068$, and the investigation of different cylinder couplings.

Other studies have mentioned hysteretic behaviour with respect to the variation of initial spacing, d [19], but there have been no significant observations of hysteretic

behaviour with variation of reduced velocity in studies with comparable conditions to date.

As discussed previously, the VIV hysteresis of a single cylinder is a feature associated with the transition of wake modes. The same wake modes are still expected to be present for a given system at a certain U_r when an identical cylinder is placed downstream of the first one if the initial inline separation between them is large enough. This minimum distance between the cylinders is usually considered greater than the critical spacing [7], normally approximately $d > 3.5$, which is one of the assumptions of this project.

Therefore, there remains a question - why does the same wake mode switching occur for an upstream cylinder, but hysteresis is not seen for the downstream cylinder? This question can only be answered by using flow visualisation devices for wake mode mapping, which unfortunately were not available for this research. However, hypothetically it could be associated with the convergence and mixing of upstream and downstream wakes and vortices. Whilst the flow velocity exerted on the upstream cylinder is the free stream velocity, the flow velocity on the downstream cylinder is reduced due to wake shielding. Thereafter, they could be excited and behave differently and with different vortex patterns and wake modes. Once the disturbed flow from the upstream cylinder reaches the downstream cylinder, the flow merges and this could explain why VIV features such as hysteresis are not observed.

In summary, it is clear from Figure 5-2 that the measurements of the downstream cylinder when the reduced velocity is successively increased or decreased have no change. Based on this observation, from this point onwards the tests will not be repeated for a decreasing set of reduced velocities. This will allow the study to focus on other aspects such as the detailed study of initial spacing variation for systems of twin cylinders.

5.3. Tandem cylinders

Initially, the two cylinders were locked inline in a tandem configuration and had only the streamwise position varied. As mentioned in Section 4.1 this was done through fixing of the upstream stationary cylinder for each of the 6 spacings considered, whilst the downstream cylinder remained in place.

Amplitudes of vibration of the downstream cylinder in 2DOF for $d = 4, 6, 8, 10,$ and 20 are collectively plotted in Figure 5-3.

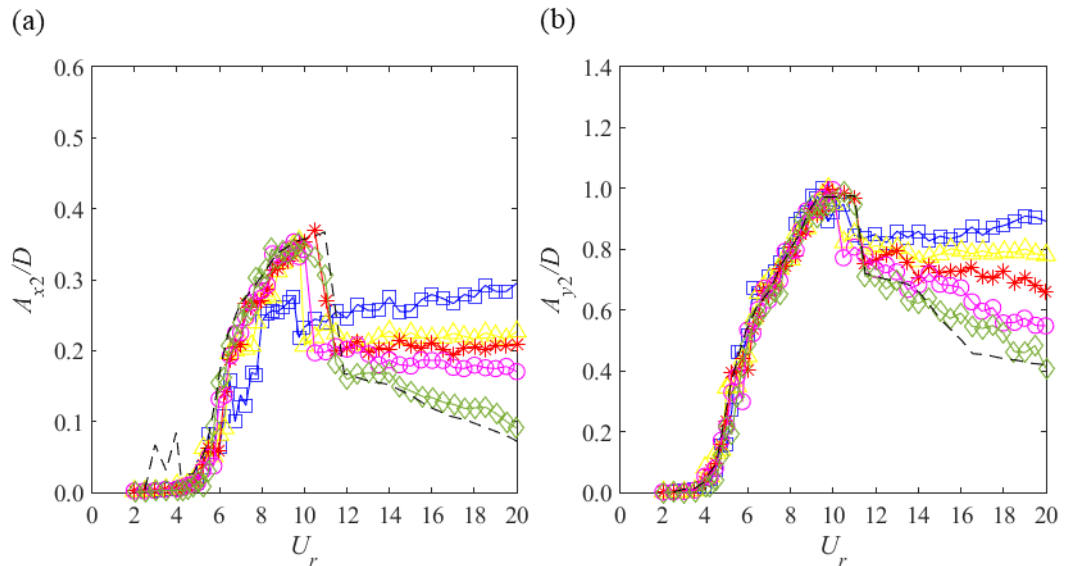


Figure 5-3: Dependence of normalised oscillation amplitudes of the downstream cylinder on the initial tandem spacing between the two cylinders for a fixed-free system in the (a) in-line direction and (b) crossflow direction. Caption: $- -$: single cylinder; \square : $d = 4$; \triangle : $d = 6$; $*$: $d = 8$; \circ : $d = 10$; and \diamond : $d = 20$.

It is shown that the response of the downstream cylinder of a fixed-free pair in both directions, at least in terms of amplitudes of vibrations, is roughly independent on the initial tandem spacing between the cylinders for low-intermediary reduced velocities, which were previously associated with the initial and upper branches of response of a single cylinder in the discussion of Figure 4-13.

Exceptions to this almost total d independence for lower-medium reduced velocities are especially observed for the streamwise cylinder behaviour, A_{x2}/D . More specifically for the two initial in-line peaks associated with the SS and AS wake regimes, for $U_r = 3$ and 4, as previously commented for the single cylinder tests, which are apparently absent from the response of the downstream cylinder with negligible vibration amplitudes for all spacings at low reduced velocities. This is understood to be related to the lower flow velocity ($U_r \chi$), as seen in Figure 4-10, acting on the downstream cylinder due to the wake flow deficit when compared to a single cylinder (U_r) and to the higher degree of turbulence and mixing that certainly affects the vortex shedding and wake modes that may impede the occurrence of the SS and AS in-line amplitude peaks.

Another exception, although almost imperceptible, is that the build-up of oscillation amplitudes observed for the transition of initial-upper branches, approximately for $6 \leq U_r \leq 8$, seems to be delayed to slightly higher reduced velocities and not only that, but the maximum A_{x2}/D peak is slightly lower around $U_r = 10$. These features are also

understood to be related to the wake flow deficit at the downstream cylinder's location. As observed in earlier sections for the wake flow velocity measurements, e.g., Figure 4-10, the wake flow velocity is lower the closer the cylinders are and especially at the wake centreline, $T = 0$, for tandem cylinders. This explains why the amplitude curve for $d = 4$ is the most affected configuration for the points under discussion and when d is increased, the response amplitudes gradually start to match more closely those of a single cylinder.

These exceptions are relatively insignificant nevertheless, and, in general the oscillation amplitudes of the downstream cylinder in both directions are considered independent of the initial spacing between the cylinder couple up to a critical intermediary U_r . This critical U_r seems to coincide with the upper to lower transition of response branches of a single cylinder and is observed to depend on the initial tandem spacing, as well as certainly on the Reynolds number, mass and damping ratios, even though these latter influences are out of the present scope and not explored in this study.

However, for reduced velocities higher than the critical U_r , Figure 5-3 shows that the amplitude response of the downstream body of a fixed-free pair of cylinders is extremely dependent on the initial streamwise separation between them, d .

This dependence may be described as follows: when the cylinders are closer together, i.e., lower d , the downstream cylinder is investigated to continue to be excited into considerably larger 2DOF oscillations for the remaining reduced velocities than those of classical VIV of one cylinder. In other words, WIV does not appear to show resonance features in the sense that amplitudes of vibrations would reduce past a certain U_r range of synchronisation. Instead, amplitudes are sustained when the flow velocity is increased to $U_r = 20$. This has been referred to in the past as a galloping behaviour in literature studies [14, 39], although more recently Assi *et al.* [11] have advocated against the potential confusion of using this term since the authors have demonstrated the fundamental differences between the mechanisms of WIV of multiple circular cylinders and classical galloping phenomenon.

Moreover, as the spacing between the cylinders rises, clearly A_{y2}/D gradually decreases for $U_r > 10$ and tends to return to single cylinder behaviour. This feature highlights that the mechanism of WIV tends to disappear when $d \rightarrow \infty$ and two cylinders with sufficient spacing between them effectively behave as two isolated cylinders. This is perhaps intuitive as once farther away from the perturbation source (upstream

cylinder), wake flow effects and upstream vortices tend to disappear. This tendency is explained by the energy dissipation of the disturbed wake flow that is constantly exchanging energy with the free stream flow being pumped downstream by the tank. This could be clearly observed at the WWCT, where the flow visibly was indistinguishable at the inlet and outlet sections of the laboratory tank, for example. This dissipation of wake flow effects is widely reported in the literature and is reported in pioneer studies of fluid dynamics past a circular cylinder, such as the studies of Schlichting [32], Abramovich [34] and Blevins [35], to name a few.

Having said that, Figure 5-3 illustrates that wake flow and WIV effects are still marginally seen in the amplitudes of vibration of the fixed-free downstream cylinder for the highest spacing considered in the present study, $d = 20$. This affirmation is based on: (i) the (small) difference between A_{y2}/D for $d = 20$ and A_y/D (single cylinder); (ii) non-existence of the initial A_{x2}/D double peaks, SS and AS, for $U_r = 3$ and 4; (iii) the discrepancies between A_{x2}/D for $d = 20$ and A_x/D (single cylinder); (iv) as well as on the wake flow profile for $d = 20$ previously shown in Figure 4-10.

In fact, point (iii) above is an interesting observation that has not been identified in the literature review because of the lack of 2DOF fixed-free studies that consider variation of d . In contrast to A_{y2}/D , streamwise oscillation amplitudes A_{x2}/D are shown in Figure 5-3 to be more disorganised with respect to the dependence on d . In summary, amplitudes A_{x2}/D are the largest for $d = 4$ and 6 as similarly demonstrated by A_{y2}/D . However, the increase of d to higher degrees lead to lower vibration amplitudes for the downstream cylinder than for a single cylinder. The fact that A_{x2}/D is qualitatively similar to A_x/D for $d = 20$ and $U_r > 12$ is considered to be an indication that this lower-amplitude behaviour is also related to the wake-reduced flow velocity that the downstream cylinder is subjected to due to wake shielding. Therefore, it appears that A_{x2}/D is more sensitive to the wake deficit flow velocity reduction than A_{y2}/D for large spacings and reduced velocities, but this needs to be further investigated with the analyses of time series and trajectories of the cylinder.

However, before moving on to those studies, validation of present experimental oscillation amplitudes results against reference literature studies is presented in Figure 5-4.

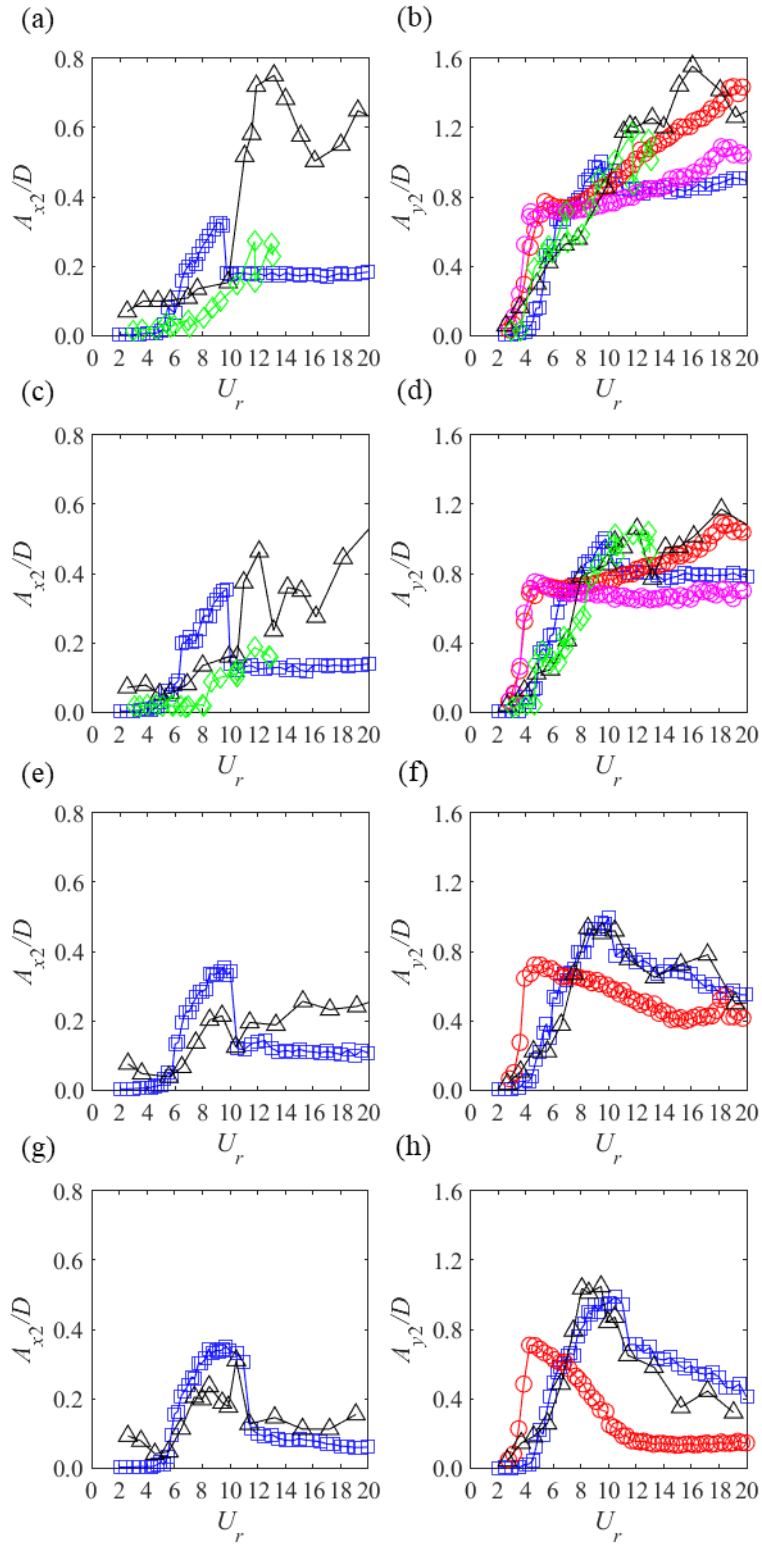


Figure 5-4: Comparison of normalised oscillation amplitudes of the downstream cylinder of fixed-free twin cylinders with reference literature studies. (a) A_{x2}/D at $d = 4$; (b) A_{y2}/D at $d = 4$; (c) A_{x2}/D at $d = 6$; (d) A_{y2}/D at $d = 6$; (e) A_{x2}/D at $d = 10$; (f) A_{y2}/D at $d = 10$; (g) A_{x2}/D at $d = 20$; (h) A_{y2}/D at $d = 20$. Caption: \square : Present results; \ominus : Assi *et al.* [11] with same d ; \oplus : Assi *et al.* [11] with $d_{\text{Assi}} = d + 2$; \triangle : Armin *et al.* [25]; \diamond : Pereira *et al.* [24].

A limited number of comparison data sets are available in literature studies. Indeed, this emphasises the need for the current experimental study for the

understanding and validation of the modelling theory developed in Chapter 2 and Chapter 3. The reference studies that have been considered as the most relevant for validation purposes of the current experiments of 2DOF fixed-free twin cylinders are the works of Assi *et al.* [11], Armin *et al.* [25], and Pereira *et al.* [24] despite the first being a 1DOF transversal oscillations study, whilst the second and third are free-free research papers.

Unfortunately, reference data from a fixed-free point of view for the inline oscillation amplitudes of the downstream cylinder at similar spacing and Reynolds number ranges is lacking. The present study fills this gap but cannot be compared with other fixed-free studies.

Because of this, the comparison for A_{x2}/D in Figure 5-4 for $d = 4, 6, 10,$ and 20 is not relevant especially for the lower spacings, $d = 4$ and 6 , for which A_{x2}/D is especially sensitive to whether the upstream cylinder is static or dynamic. There is also the question of how the studies have been post-processed as this information is at times undisclosed. For instance, it is unclear if the lower frequency mean component of inline oscillation of the downstream cylinder has been considered in the A_{x2}/D results of Armin *et al.* [25] once their amplitudes of vibration are significant even for the lowest reduced velocities such as $U_r = 2$ ($A_{x2}/D > 0.1$ approximately). This is not seen in the present study or in Pereira *et al.* [24].

However, the present A_{x2}/D results qualitatively agree with literature results for the pair of cylinders at $d = 10$ and 20 . On the other hand, a similar spacing dependence trend can be observed for A_{x2}/D for the 3 studies in question for spacings considered in Figure 5-4, where the amplitudes are the largest for $d = 4$ and progressively decrease with distancing of the cylinders.

Thereafter, oscillation amplitude results of the fixed-free downstream cylinder in the crossflow direction, A_{y2}/D , can be more easily correlated to available studies due to the existence of reference data from the Assi *et al.* [11] 1DOF fixed-free experiments. Moreover, the transversal response of a downstream cylinder of a pair appears to be less sensitive to the differences between a stationary or dynamic upstream cylinder since there is greater agreement to free-free studies shown in Figure 5-4.

Two A_{y2}/D amplitude curves of Assi *et al.* [11] have been plotted in Figure 5-4 where this data was available (Figure 5-4b & d), one for double cylinders with similar spacing to the present study (red circles), and the other (magenta circles) for a system with a spacing 2 diameter units higher than the present study. In other words, red

circles symbolise $d = 4$ and magenta circles $d = 6$ for Figure 5-4b, and red circles represent $d = 6$ whilst magenta circles are $d = 8$ in Figure 5-4d. This apparently brings unnecessary confusion to the comparison; however, this has been done in an attempt to correct or to minimise the effect of the mean streamwise displacement of the downstream cylinder caused by the mean drag force on the cylinder. Since the study of Assi *et al.* [11] is 1DOF, basically their initial longitudinal spacing, d , would be a constant for the duration of their experiments. The same is not true for this project where the cylinders are given the second degree-of-freedom in the inline direction. As it will be discussed later in investigations of measured temporal displacements of the downstream cylinder, this mean drift of the cylinder is not a constant but can reach values higher than 2 diameters depending on the steady drag force acting on the cylinder, which in turn is directly and nonlinearly proportional to the flow velocity.

Nonetheless, it is observed that this mean cylinder drift correction is useful even if it does not account for the flow velocity dependence, as the present measured amplitudes of vibrations, A_{y2}/D , more closely agree with the reference data represented by magenta circles. The results obtained show good agreement to the fixed-free 1DOF measurements of Assi *et al.* [11], apart from the onset of the initial branch of amplitudes. This was similarly observed in the single cylinder VIV section and it was possibly associated with the difference in mass and damping ratios. Comparison with the free-free studies of Armin *et al.* [25] and Pereira *et al.* [24] also show a good agreement for A_{y2}/D , apart from $d = 4$.

In summary, amplitudes of vibration of a fixed-free downstream cylinder obtained for the actual experiments are considered to represent the main features of WIV with respect to the dependence on the initial streamwise distancing between the two cylinders. Comparison with the single cylinder VIV tests presented in Chapter 4 show that oscillation amplitudes of the downstream cylinder is initially independent of d for low-intermediary reduced velocities. Once a certain critical intermediary U_r is achieved and exceeded, the response of the downstream cylinder is heavily dependent on d . This behaviour agrees with well-known literature information on the WIV of a downstream cylinder of a pair. Assi *et al.* [11] named this initial single-cylinder type behaviour as the first VIV peak. This has also been observed and extensively discussed in the modelling results in Chapter 2 and Chapter 3.

Although only a few spacings could be validated with high fidelity experimental results from literature sources due to the limited number of these studies, the overall

picture of what occurs to the response of the cylinder in the two directions when d is varied matches those of the present study.

5.3.1. Time Series of the Displacements of the Downstream Cylinder

Even though the analysis of amplitudes of vibration allowed for observation of important features of WIV in the results of this study, the temporal behaviour of the fixed-free downstream cylinder is now investigated to address previous observations from a more detailed point of view of the behaviour of the downstream cylinder. Time evolution of x_2 and y_2 have been selected and plotted using the same methodology as for the single cylinder already discussed in Chapter 4. Thus, time series for vibrations of a fixed-free downstream cylinder are presented in Figure 5-5, Figure 5-6, and Figure 5-7 for $d = 4, 10,$ and 20 respectively. Mainly, the time range considered spanned from 100-120 s, the number of cycles is not fixed and depends on the oscillation frequency, selected reduced velocities are $U_r = 3, 4, 6, 10, 15,$ and $20,$ and, lastly, the y -axis limits where possible have been kept the same as in Figure 4-16 for direct correlation.

Starting with the discussion of the time histories of x_2 and y_2 for $d = 4$ as seen in Figure 5-5 for low reduced velocities, $U_r = 3$ and $4,$ one may notice that the magnitudes of vibrations in both directions are reduced for the downstream cylinder when compared with a single cylinder under VIV as in Figure 4-16. The inline response of the fixed-free downstream cylinder is especially reduced for $U_r = 3$ and $4.$ This reinforces the previous conclusion from the oscillation amplitude study that the response peak associated with the SS and AS wake modes are attributed to the inline dynamics of the cylinder. The meaning is that the SS and AS initial inline peaks are not removed from Figure 5-3, for instance, because of *rms* calculations as done for $A_{x2}/D,$ but rather are not present in the response of the downstream cylinder, not even partially nor traces of response.

The crossflow response of the fixed-free downstream cylinder is also reduced for the same reduced velocities, especially for $U_r = 4,$ for which classical VIV of an isolated cylinder would start to show a build-up of amplitudes of vibrations in the initial branch of responses (Figure 4-13). This lower x_2 and y_2 response of the downstream cylinder for low reduced velocities has been linked to the lower flow velocity due to the wake deficit and, therefore, lower hydrodynamic forces acting on the downstream cylinder as previously discussed.

In contrast to that, the behaviour of the downstream cylinder in both directions for $U_r = 6$ is comparable to the single cylinder outputs in terms of both magnitudes – even

though still slightly reduced for the downstream of a pair of cylinders – and overall dynamic behaviour with clear modulation of amplitudes.

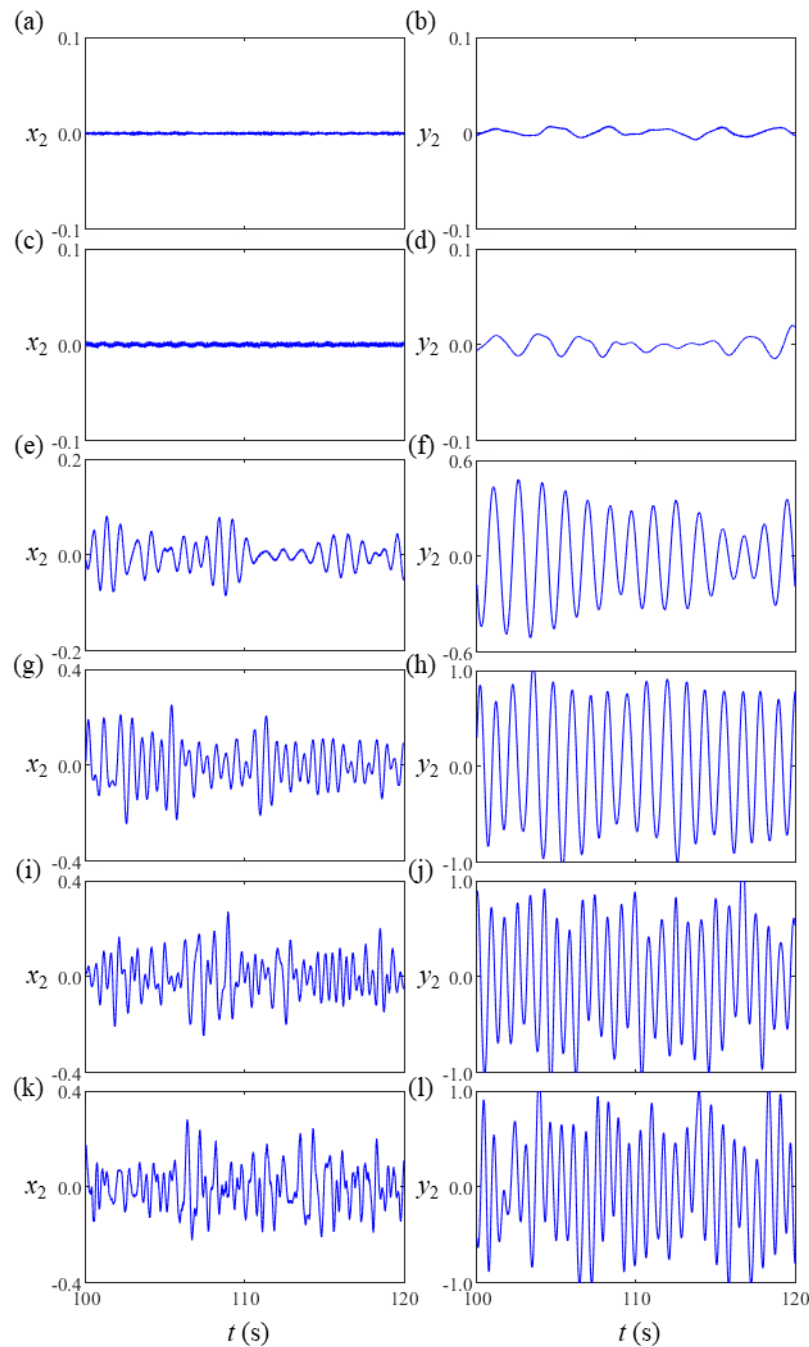


Figure 5-5: Temporal displacements of the downstream of a fixed-free pair of cylinders for $d = 4$. (a) x_2 at $U_r = 3$; (b) y_2 at $U_r = 3$; (c) x_2 at $U_r = 4$; (d) y_2 at $U_r = 4$; (e) x_2 at $U_r = 6$; (f) y_2 at $U_r = 6$; (g) x_2 at $U_r = 10$; (h) y_2 at $U_r = 10$; (i) x_2 at $U_r = 15$; (j) y_2 at $U_r = 15$; (k) x_2 at $U_r = 20$; and (l) y_2 at $U_r = 20$.

So far, considering the amplitudes of vibration for $U_r = 3$ and 4 are minimal, the displacements of the downstream cylinder for low-intermediary reduced velocities correspond to the concept of a first VIV peak where the downstream cylinder of a pair roughly behaves as a single cylinder under typical VIV, as previously discussed.

However, it has been discussed that the downstream cylinder may behave completely differently under WIV compared to a single cylinder under VIV, depending on the initial spacing d once a critical U_r (approximately $U_r = 10$ for the present study) is reached and exceeded. This critical U_r has been found to not be a constant, but to depend on d amongst other factors, such as mass and damping ratios. For $d = 4$ and $U_r = 10$, the time series of the downstream cylinder in Figure 5-5 indicates that the behaviour is still similar to the classical VIV results of Figure 4-16. It is, nevertheless, for $U_r = 15$ and 20 that x_2 and y_2 are observed to continue to be excited into significantly larger oscillations than x and y .

Due to the first VIV peak, the time series of the downstream cylinder for $d = 10$ and 20, Figure 5-6 and Figure 5-7, are also only considerably different from those of $d = 4$ and of a single cylinder for $U_r \geq 10$. The instantaneous dynamic response of the second cylinder for $d = 10$ and 20 at $U_r = 10$ exhibits larger magnitudes of vibration than for $d = 4$. This initially seems to be a contrast to well-known WIV features, however, it is related to the critical U_r for $d = 10$ and 20 being slightly higher than 10 as also seen in Figure 5-3. Therefore, the response of the rear cylinder for $d = 10$ and 20 is still in the classical VIV upper branch regime, whilst for $d = 4$ a leap-down discontinuity of oscillation magnitudes is already observed for $d = 4$.

Finally, x_2 and y_2 for $d = 10$ and 20 as well as $d = 4$, plus x and y at $U_r = 15$ and 20 are then totally different regarding oscillation magnitudes due to the great dependence on the initial inline spacing d of the response of the downstream cylinder for intermediary-high reduced velocities. The 2DOF displacements of the downstream cylinder for $d = 20$ are already observed to closely match the displacements of the single cylinder.

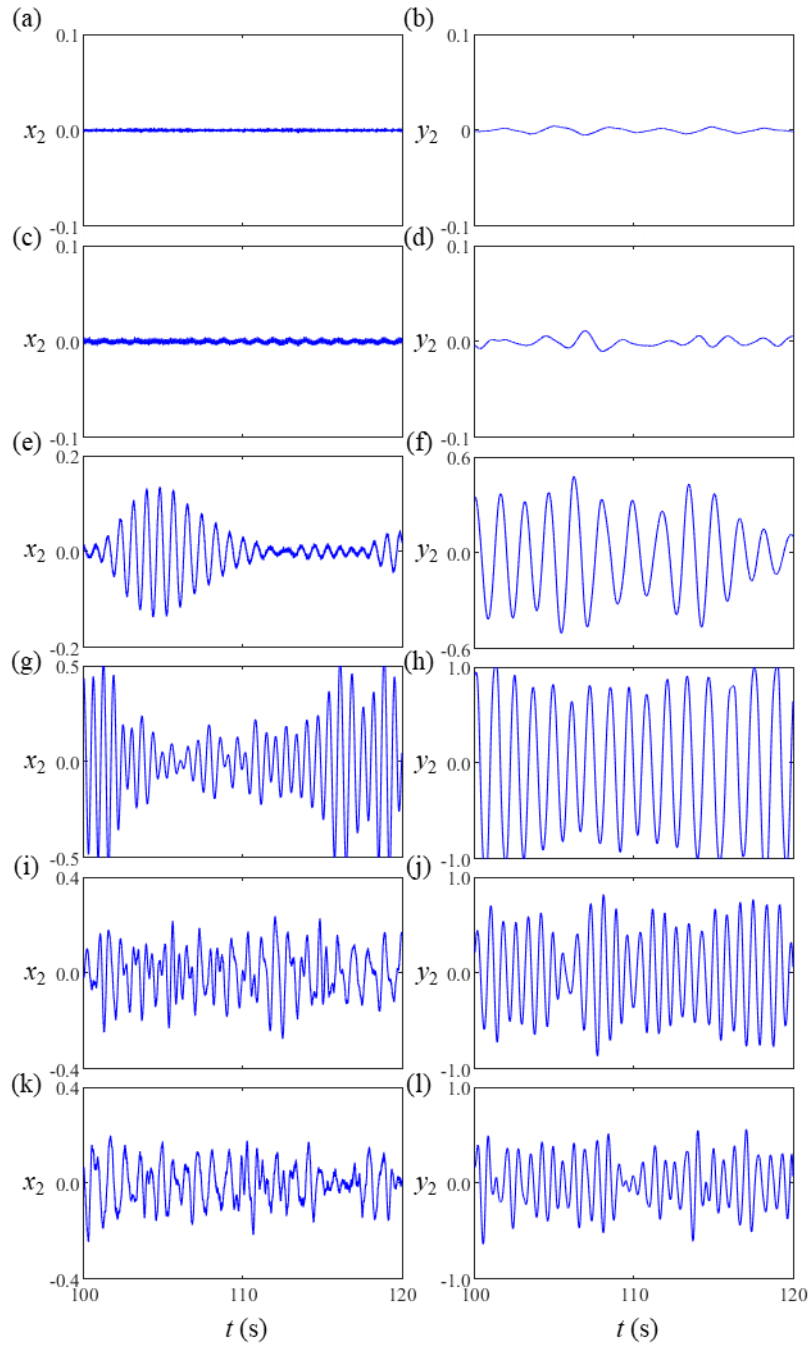


Figure 5-6: Temporal displacements of the downstream of a fixed-free pair of cylinders for $d = 10$. (a) x_2 at $U_r = 3$; (b) y_2 at $U_r = 3$; (c) x_2 at $U_r = 4$; (d) y_2 at $U_r = 4$; (e) x_2 at $U_r = 6$; (f) y_2 at $U_r = 6$; (g) x_2 at $U_r = 10$; (h) y_2 at $U_r = 10$; (i) x_2 at $U_r = 15$; (j) y_2 at $U_r = 15$; (k) x_2 at $U_r = 20$; and (l) y_2 at $U_r = 20$.

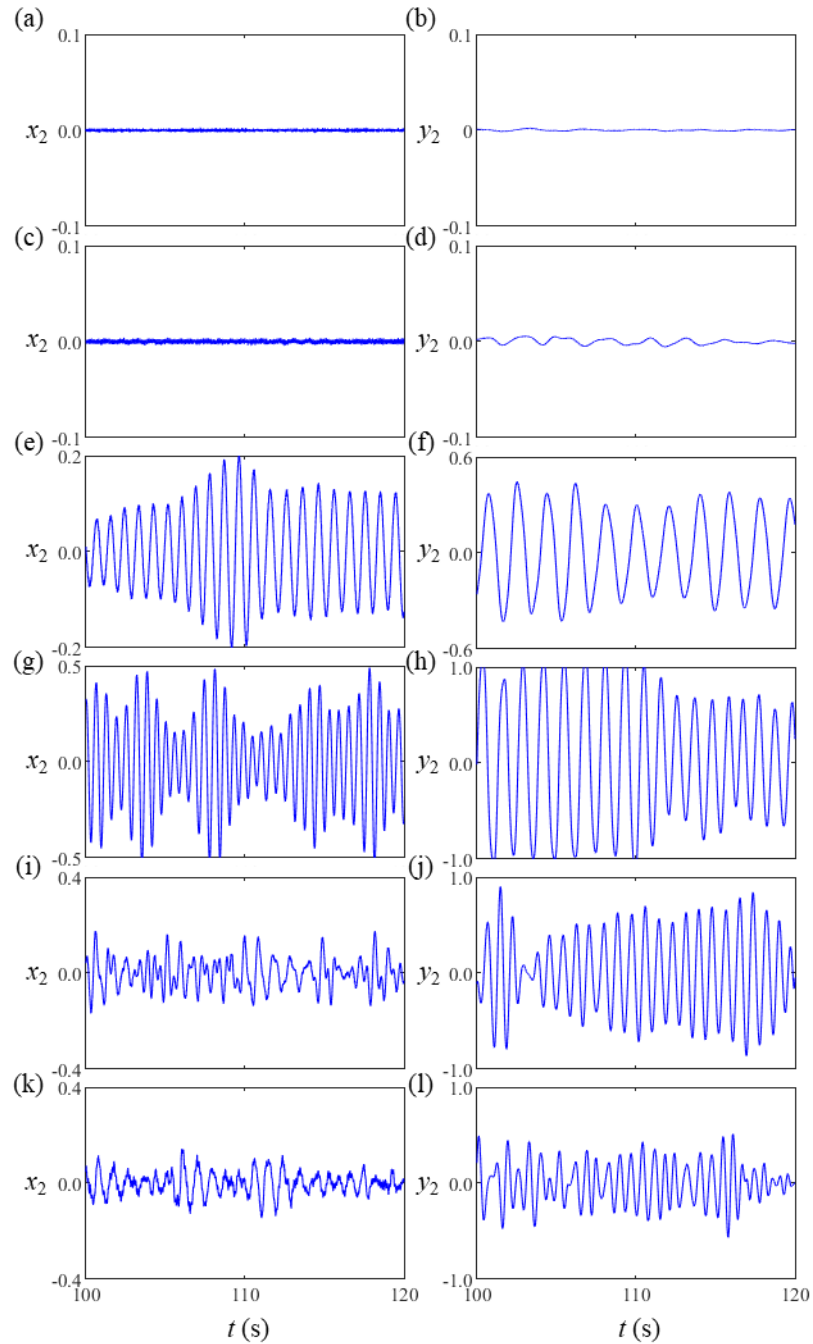


Figure 5-7: Temporal displacements of the downstream of a fixed-free pair of cylinders for $d = 20$. (a) x_2 at $U_r = 3$; (b) y_2 at $U_r = 3$; (c) x_2 at $U_r = 4$; (d) y_2 at $U_r = 4$; (e) x_2 at $U_r = 6$; (f) y_2 at $U_r = 6$; (g) x_2 at $U_r = 10$; (h) y_2 at $U_r = 10$; (i) x_2 at $U_r = 15$; (j) y_2 at $U_r = 15$; (k) x_2 at $U_r = 20$; and (l) y_2 at $U_r = 20$.

5.3.2. Plane Oscillation Trajectories of the Fixed-Free Second Cylinder

After analysing the real time-varying displacements separately, it is equally important to examine how the fixed-free downstream cylinder vibrates in 2DOF by plotting the real-time oscillation trajectories of the cylinder and comparing to the previous tests with a single cylinder. These are presented in Figure 5-8, Figure 5-9,

and Figure 5-10 for the same spacings and reduced velocity points as before, namely $U_r = 3, 4, 6, 10, 15,$ and 20 ; $d = 4, 10,$ and 20 .

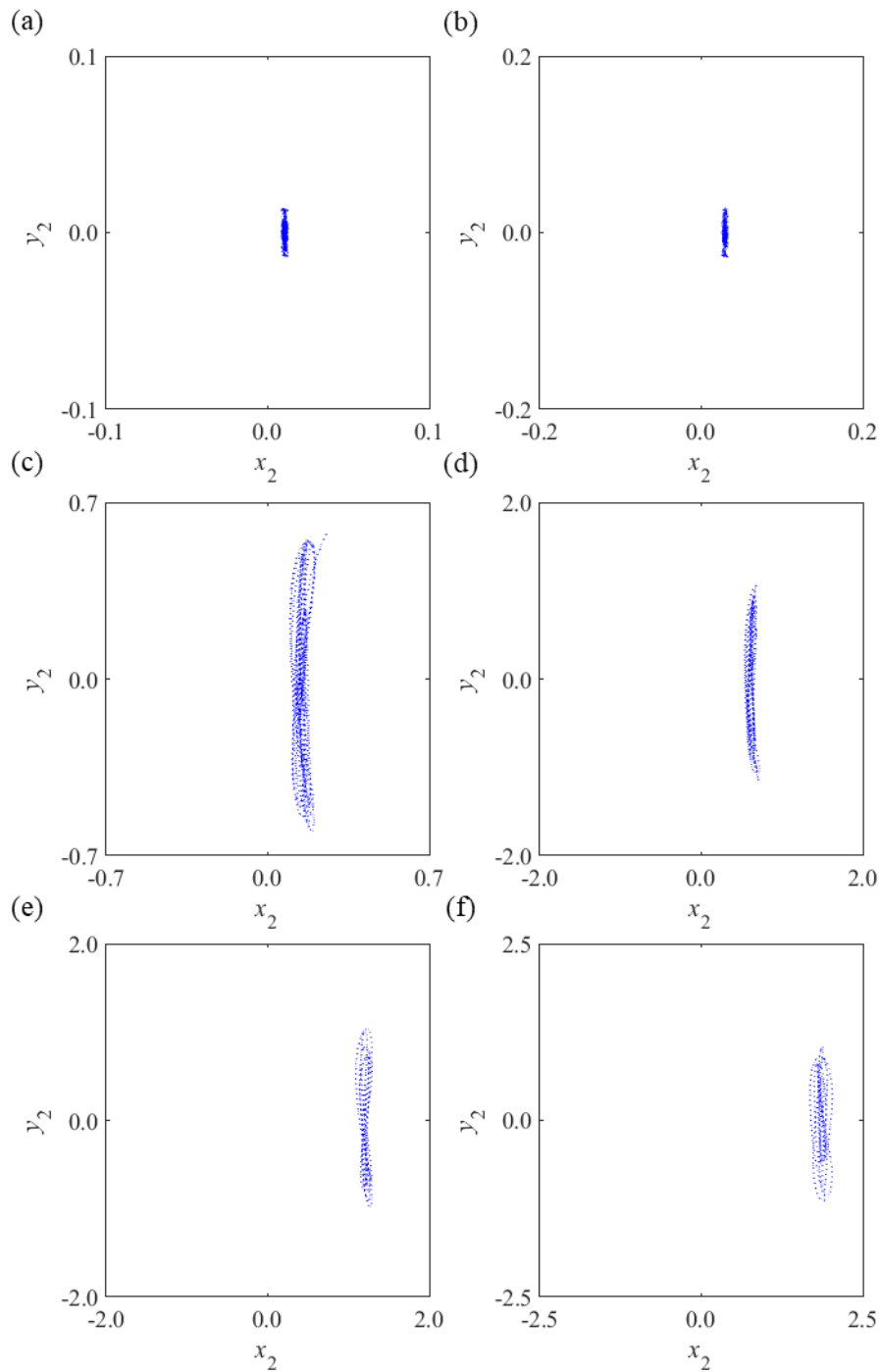


Figure 5-8: 2DOF trajectories of the downstream of a fixed-free twin bundle of cylinders undergoing WIV for $d = 4$. (a) $U_r = 3$; (b) $U_r = 4$; (a) $U_r = 6$; (a) $U_r = 10$; (a) $U_r = 15$; and (a) $U_r = 20$.

Figure 5-8, Figure 5-9, and Figure 5-10 illustrate the results of measurements for the fixed-free downstream cylinder and the reader is also referred to Figure 4-17 for the following comparison analysis between the tests of a single cylinder and pair of fixed-free cylinders.

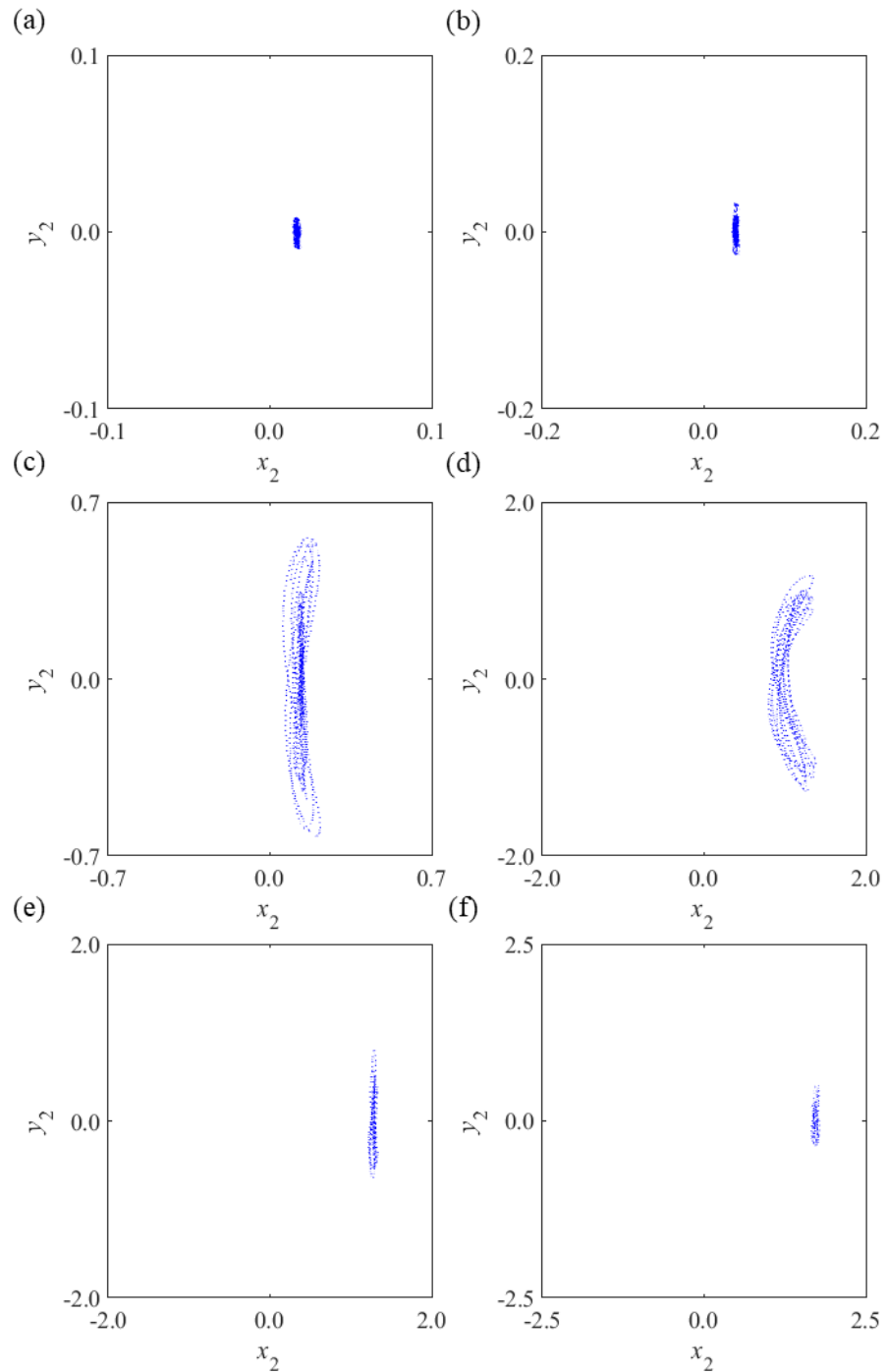


Figure 5-9: 2DOF trajectories of the downstream of a fixed-free twin bundle of cylinders undergoing WIV for $d = 10$. (a) $U_r = 3$; (b) $U_r = 4$; (c) $U_r = 6$; (d) $U_r = 10$; (e) $U_r = 15$; and (f) $U_r = 20$.

Consideration of plane trajectories of the rear cylinder for all 3 spacings reflects how the trailing cylinder barely vibrates and how the AS and SS wake modes are absent for $U_r = 3$ and 4 respectively. However organised trajectories have been observed for the single cylinder system (Figure 4-17) including a figure-of-8 shape ($U_r = 4$) as previously discussed.

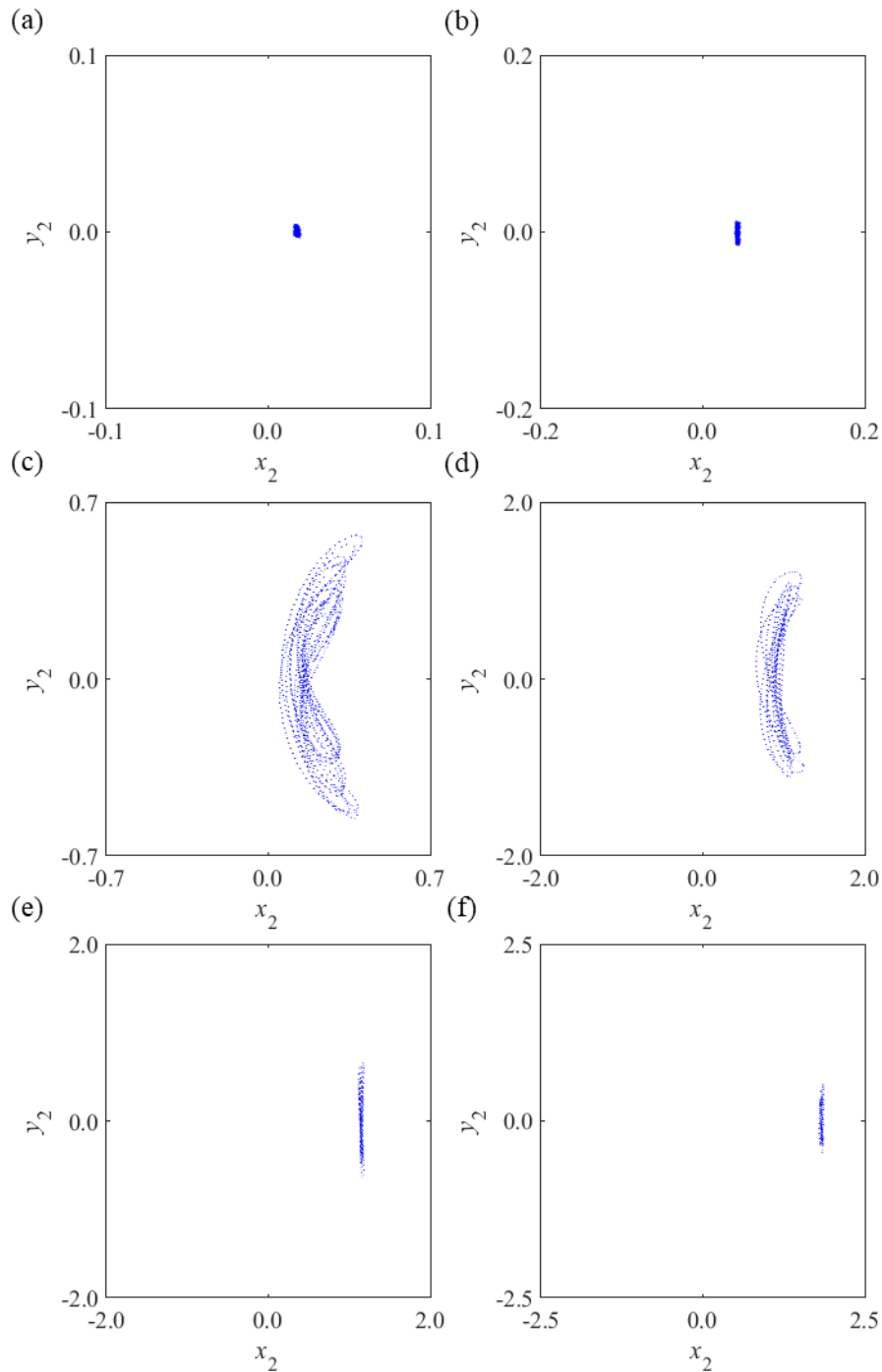


Figure 5-10: 2DOF trajectories of the downstream of a fixed-free twin bundle of cylinders undergoing WIV for $d = 20$. (a) $U_r = 3$; (b) $U_r = 4$; (c) $U_r = 6$; (d) $U_r = 10$; (e) $U_r = 15$; and (f) $U_r = 20$.

The comparison of oscillation orbits for $U_r = 6$ shows figure-of-8 profiles for the one-cylinder setup as well as the double-cylinder setups with every spacing shown in Figure 5-8, Figure 5-9, and Figure 5-10. Interestingly, the trajectories for $d = 4$ and 10 show flatter figure-of-8 profiles which are the consequence of reduced x_2 amplitudes thought to be associated with the previously mentioned greater sensitivity of the inline degree-of-freedom to the wake-reduced flow velocity that acts on the downstream

cylinder. On the other hand, response trajectories for the downstream cylinder at $d = 20$ (Figure 5-10) are remarkably similar to the trajectories of a single cylinder (Figure 4-17).

Similar to the initial VIV tests of a single cylinder, vibration trajectories for a fixed-free downstream cylinder follow figure-of-8 trends for the remaining and larger reduced velocities plotted in the figures. Figure-of-8 patterns, as commented before, are the result of an inline-to-crossflow degree-of-freedom frequency ratio of 2:1. The present experiments reveal that this feature is also present for a fixed-free pair of cylinders with natural frequencies that are equal in the two directions. Assi [23] has shown similar features but for a system with $d = 4$ and $f_{nx}/f_{ny} = 2$.

The agreement of characteristics seen for the analyses of amplitudes of vibration, time series, and 2DOF trajectories of the downstream cylinder suggests that the *rms* is a suitable representation of the cylinder amplitude response.

Finally, Figure 5-8, Figure 5-9, and Figure 5-10 can also be compared to Figure 4-17 in terms of the mean inline displacement of the cylinder systems in question. As a general rule, the mean inline position of the cylinder rises with the flow velocity and is still considerably large for the maximum $U_r = 20$, even for the downstream of a twin cylinder setup, with mean drifts just over 2 diameters for $d = 4$ and 10, whilst for the single cylinder system and for the downstream cylinder of a pair at $d = 20$, the mean inline drift reaches slightly higher values closer to 2.5 diameters. This difference is due to the wake flow deficit, and these magnitudes of mean inline displacement of the 2DOF cylinder systems considered herein justify the previous comparison attempted with a fixed-free 1DOF system that had a larger initial separation (2 diameters larger) as in Figure 5-4.

5.3.3. Oscillation Frequencies of a Fixed-Free Downstream Cylinder

The studies of time series and oscillation trajectories have shown that the response of the rear cylinder of a pair may be complex for some U_r and d cases, whilst it has also been shown capable of obeying well-known figure-of-8 trajectories of movement. Hence, the analysis of the response of the fixed-free downstream cylinder in the frequency domain is proposed to investigate such observations and the detailed behaviour of the body.

Transformation of the temporal x_2 and y_2 has been done from the computation of the FFT as done for the single cylinder tests and previously explained. The main points are that the sampling frequency from the Qualisys acquisition system is 200 Hz, and

the response envelope window considered is the same as for Figure 5-5, Figure 5-6, and Figure 5-7, i.e. $t = 100-120$ s. This way the response is ensured to be the steady state response of the cylinder. More details are found in Section 4.7.

The dominant oscillation frequency of the downstream cylinder for each U_r has been plotted, as was done in Figure 4-18, and for direct comparison with literature studies. These are presented in Figure 5-11 and Figure 5-12 for f_{x2}/f_n and f_{y2}/f_n respectively.

Initially, dominant vibration frequencies of the rear cylinder are displayed for all 5 tandem spacings considered, $d = 4, 6, 8, 10, 20$, in Figure 5-11a and Figure 5-12a. Despite occasional fluctuations, the oscillation frequencies of the downstream cylinder are relatively unchanged with variation of d . This agrees with the study of a 1DOF fixed-free downstream cylinder in Assi *et al.* [12].

Dominant frequencies of vibration of the fixed-free second cylinder have been compared with dominant oscillation frequencies of the previous single cylinder tests and to literature data. Validation of the present experiments is sought once again with the 1DOF fixed-free downstream cylinder study of Assi *et al.* [12] and the 2DOF free-free rear cylinder investigation of Armin *et al.* [25], which are considered to be the two closest studies to the present tests, despite the fundamental differences already explained in the previous vibration amplitude discussions.

The initial focus is placed on the analysis of f_{x2}/f_n . As in previous observations, the response of the cylinder and consequently its oscillation frequencies do not vary considerably with d nor do they deviate considerably from single cylinder results within the first VIV regime, i.e. $U_r < 10$ approximately for the current study. For the lowest reduced velocities, frequencies of vibration of the downstream cylinder are complex and perhaps chaotic. These frequencies ($U_r < 5$) have been removed from the graphs as they have been considered to be residual frequencies without apparent physical meaning. They are possibly a consequence of the negligible x_2 amplitudes of vibration seen in the time series.

Vibration frequencies for reduced velocities immediately larger show that the experimental downstream cylinder is seen to vibrate with a dominant frequency which is close to the green dashed line of the doubled Strouhal law, but the frequencies are lower by a certain amount. In fact, the downstream cylinder frequency branch agrees with frequencies of the single cylinder that have been previously associated with the

doubled wake-reduced Strouhal law ($2\chi St$), which accounts for the wake-reduced U_r acting on the second cylinder.

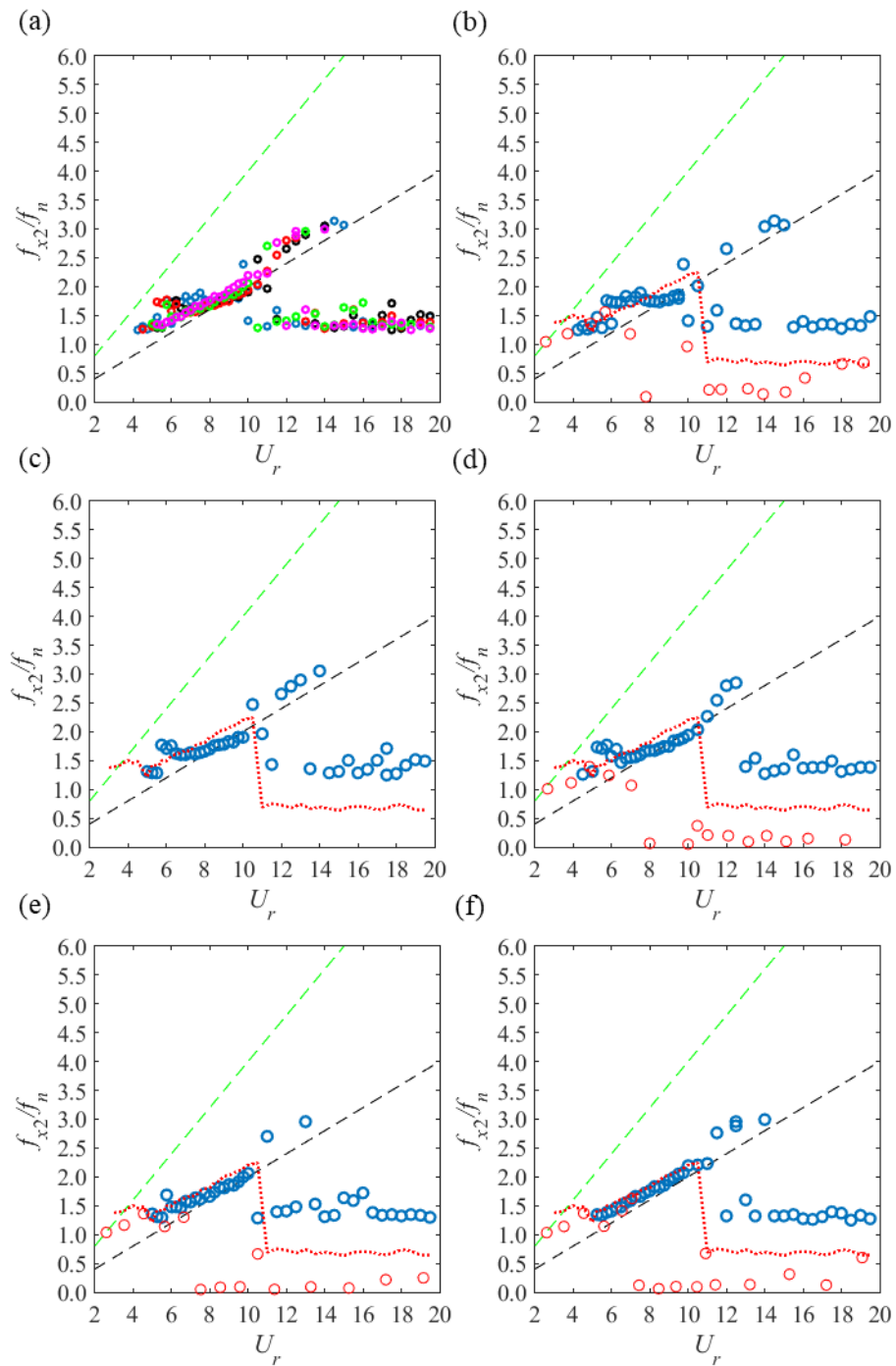


Figure 5-11: Initial tandem spacing dependence of the dominant normalised frequencies of oscillations for the WIV of the downstream of a pair of cylinders in a flume in the streamwise direction. Validation with reference literature studies. (a) Present results for all d ; (b) $d = 4$; (c) $d = 6$; (d) $d = 8$; (e) $d = 10$; (f) $d = 20$. Legend: $- -$: Strouhal law ($St = 0.2$); $- -$: Doubled Strouhal law ($2St = 0.4$); \circ : Present 2DOF study for $m^* = 3.75$ and $\zeta = 0.055$ (in water); \cdots : Present results for a single cylinder; \triangle : Assi [12] $m^* = 2.6$ and $\zeta = 0.007$ (in air); and \circ : Armin *et al.* [25] $m^* = 2.36$ and $\zeta = 0.015$ (in water).

Increasing the reduced velocity, $6 < U_r < 10$ (roughly), seems to lock normalised frequencies f_{x2}/f_n to the classical Strouhal law black dashed line. This is also observed for the 2DOF free-free study of Armin *et al.* [25].

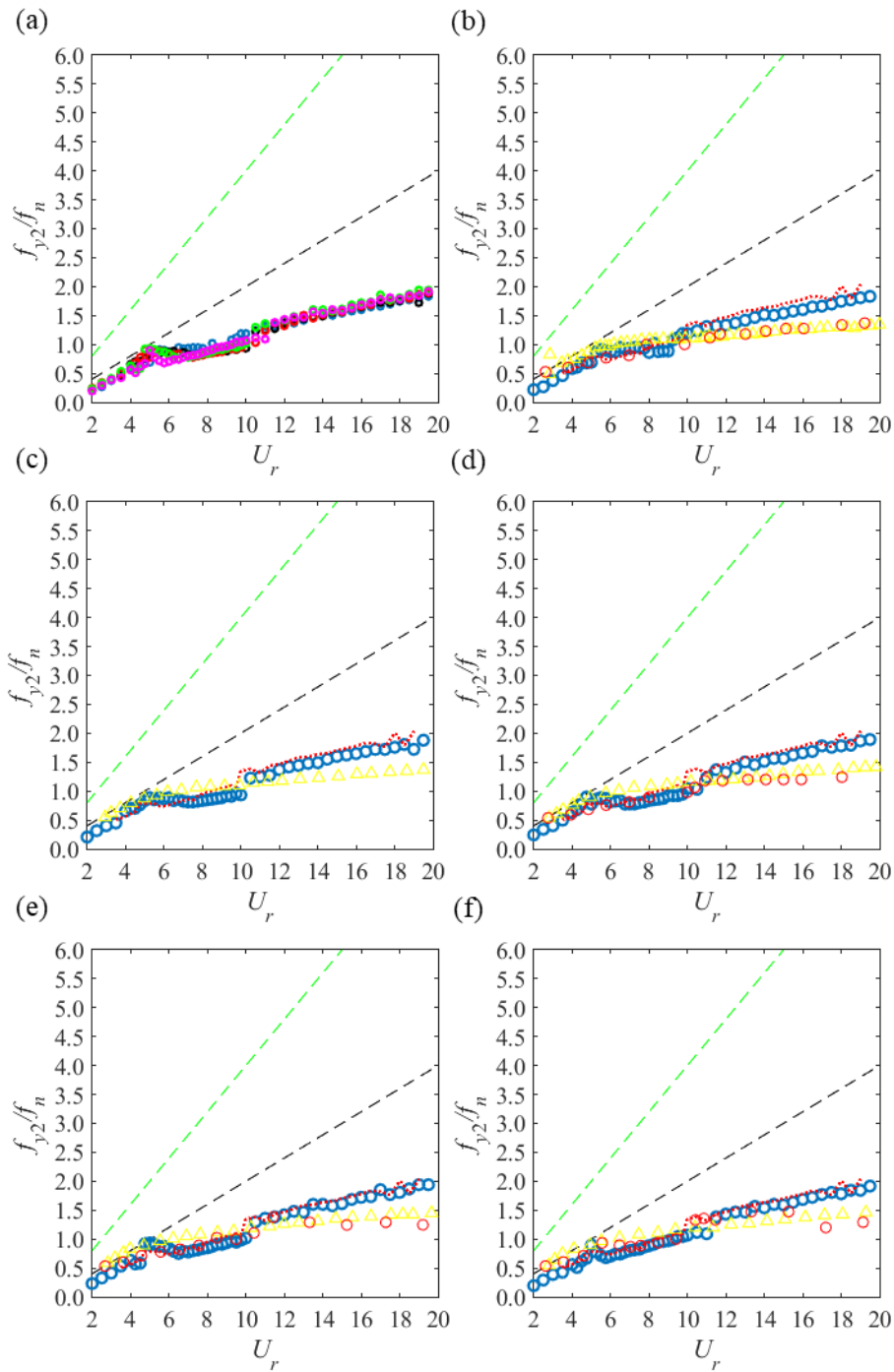


Figure 5-12: Initial tandem spacing dependence of the dominant normalised frequencies of oscillations for the WIV of the downstream of a pair of cylinders in a flume in the crossflow direction. Validation with reference literature studies. (a) Present results for all d ; (b) $d = 4$; (c) $d = 6$; (d) $d = 8$; (e) $d = 10$; (f) $d = 20$. Legend: — — : Strouhal law ($St = 0.2$); — — : Doubled Strouhal law ($2St = 0.4$); \circ : Present 2DOF study for $m^* = 3.75$ and $\zeta = 0.055$ (in water); \bullet : Present results for a single cylinder; \triangle : Assi [12] $m^* = 2.6$ and $\zeta = 0.007$ (in air); and \circ : Armin *et al.* [25] $m^* = 2.36$ and $\zeta = 0.015$ (in water).

The Strouhal law is well known to describe vortex shedding frequencies behind a stationary cylinder and the fact that f_{x2}/f_n locks to the St line and not to $2St$, χSt , $2\chi St$, or any other frequency, may be seen as strong evidence that the inline degree-of-freedom of the downstream cylinder is highly sensitive to the upstream cylinder behaviour as it is mainly excited by its vortex shedding. This corroborates previous observations and discussions that have raised the possibility of a greater sensitivity of the inline degree-of-freedom of the downstream cylinder to the static upstream cylinder when compared to its respective crossflow response. This reduced velocity range of approximately $6 < U_r < 10$ coincides with the upper branch and the first VIV amplitude peak of responses shown in Figure 5-3.

Moreover, dominant f_{x2}/f_n oscillation frequencies become more complex for $U_r > 10$ when it appears to alternate between a frequency branch close to the Strouhal line and is thus associated with the upstream vortex shedding and another lower frequency branch that is close to $f_{x2}/f_n = 1$ and to f_{y2}/f_n within a similar U_r range, as it will be shown from the discussion of Figure 5-12. Thus, this lower frequency branch could be related to the coupling with the transverse oscillation of the downstream cylinder.

A greater distancing of the cylinders (increased d) shows a greater similarity with the frequencies of a single cylinder. However, it is clear from Figure 5-11 that oscillation frequencies for the fixed-free downstream cylinder at $d = 20$ are still different from the oscillation frequencies of an isolated cylinder. This has also been commented on before in the analysis of amplitudes of vibration, suggesting that the downstream cylinder still experiences disturbance effects from the upstream cylinder even for a large $d = 20$, although these are now small. The expectation is that further increase of spacing (possible $d = 30$) would then cause the downstream cylinder's behaviour to resemble that of an isolated cylinder.

Frequencies of transverse oscillations of the fixed-free downstream cylinder are seen to be more organised and without significant differences from the single cylinder results. For the lowest reduced velocities, f_{y2}/f_n follows a frequency slightly lower than the Strouhal law. This frequency branch has been observed to be related to the wake-reduced velocity of the cylinder and can be modelled by a corrected wake deficit Strouhal law, χSt .

Thereafter, f_{y2} locks to the natural frequency ($f_{y2}/f_n = 1$) for approximately $6 < U_r < 10$. For a single cylinder this would represent the lock-in regime observed for the upper branch of responses and that leads to the largest amplitudes of vibration for VIV of a

single cylinder. This finding would agree with the idea of a first VIV regime. Once $U_r > 10$, the branch of f_{y2}/f_n frequencies switch to a different frequency gradient for the remaining reduced velocities.

The behaviour of the $f_{y2}/f_n \times U_r$ curve of the present laboratory tests correlate well to the literature studies used for validation, despite the difference in system properties amongst studies. The similarity between the present results for a single cylinder and fixed-free downstream cylinder has also been reported in these studies.

5.4. Staggered Cylinders

Even though it has been demonstrated that the wake deficit is greater in the wake centreline for the critical configuration of tandem cylinders, in real operations tandem cylinders are rarely observed as it is difficult to control the alignment of adjacent structures in offshore installations, plus the sea current direction varies with time and space. Staggered structures are therefore the more typical configuration observed in practical applications and this present section reports on an experimental investigation for fixed-free staggered systems.

As explained previously, the experimental rig was designed and mounted to easily accommodate changes to the initial cylinder separation, whether in the downstream or crossflow directions. For staggered cylinders, this was done by unclamping the downstream cylinder, moving it across the tank within the marked positions, securely fixing it to the tank and moving the overhead pendulum system by the same distance. A picture of the experimental model of staggered cylinders is seen in Figure 5-13.

The problem of WIV of staggered cylinders is expected to share many similarities with the previously discussed WIV of tandem cylinders as the WWCT tank, flow parameters and methodology have been kept the same. Another possible contributor to the common features that tandem and staggered cylinders share is that, whether the cylinders are initially arranged in tandem or staggered configurations, once transverse vibration starts, initially tandem cylinders will definitely find themselves in staggered positions and initially staggered cylinders will likely find themselves in tandem positions respectively. However, the different initial or equilibrium position locations between the two arrangements expose the cylinders to different wake stiffness and wake flow velocity magnitudes which cause a few key differences between the two studies. Therefore, for conciseness the focus of this section is only on the points that differ between tandem and staggered fixed-free cylinders in terms of oscillation amplitudes and frequencies, as well as instantaneous response variations.



Figure 5-13: Photograph of staggered WIV tests for a flexibly mounted cylinder behind a stationary upstream cylinder.

5.4.1. Amplitudes of Vibrations of the Downstream Cylinder

As for the results of the experimental tests of tandem cylinders, *rms* oscillation amplitudes have been computed and the effect of staggered spacing is shown for the displacements in both directions in Figure 5-14.

The dependence of the downstream cylinder on the initial staggered spacings, T , for $d = 4$, reveals a trend that is somewhat similar to the dependence of the behaviour of the second cylinder on the initial tandem spacing ($d = 4, 6, \dots, 20$) as seen in Figure 5-3, i.e., the increase of T generally leads to lower vibration amplitudes and a response that resembles more classical VIV of single cylinders if T is large enough, meaning that the downstream cylinder is positioned at the edges of the disturbed wake flow.

For comparison purposes, the response amplitudes of the single cylinder (black dashed line) and of the downstream cylinder of a fixed-free tandem pair at $d = 4$ (green dashed line) have been plotted in Figure 5-14.

It has been said that the increase of T generally, but not always, leads to lower vibration amplitudes. This is because whilst this is always the case for the transverse response, A_{y2}/D , it is not always the case for the inline response, A_{x2}/D as shown by Figure 5-14a. Interestingly, inline oscillations of the downstream staggered cylinder rise with T within the first VIV regime, $U_r < 12$ approximately. Within the first VIV regime, A_{x2}/D is seen not only to be larger than the green dashed line representing a tandem cylinder, but even larger than the black dashed line representing the single cylinder case.

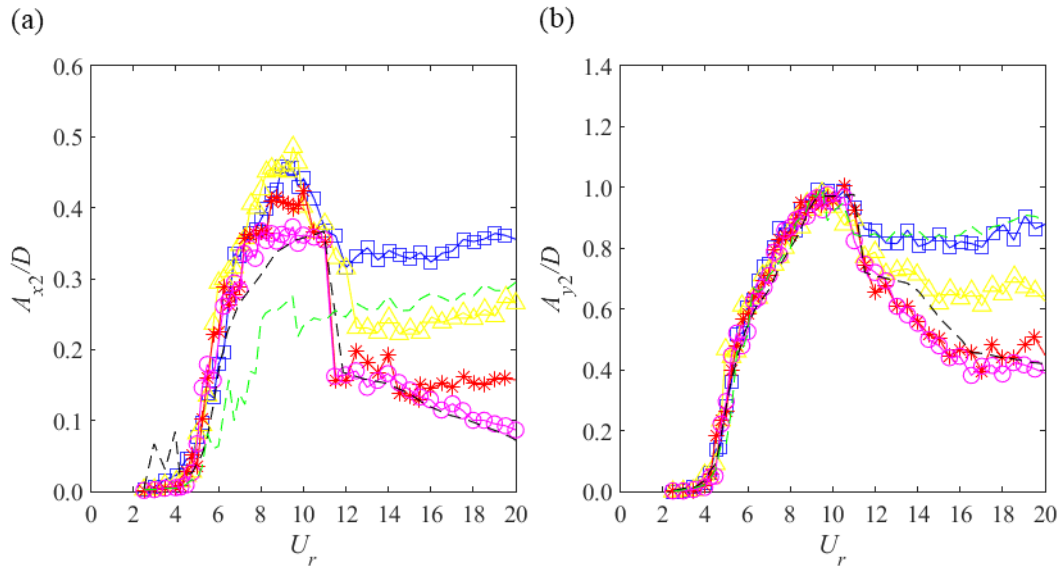


Figure 5-14: Dependence of normalised oscillation amplitudes of the downstream cylinder on the initial staggered spacing between the two cylinders for a fixed-free system with $d = 4$ in the (a) inline direction and (b) crossflow direction. Caption: - - : single cylinder; - - : tandem fixed-free cylinders at $d = 4$; \square : $d = 4, T = 1$; \triangle : $d = 4, T = 2$; $*$: $d = 4, T = 3$; \ominus : $d = 4, T = 4$; and \diamond : $d = 20$.

On the one hand, it is straightforward to understand the reason for a reduction in oscillation amplitude magnitude when the offset between the cylinders is increased ($T \uparrow$), as the downstream cylinder is increasingly far from the wake centreline and closer to the wake flow edges and undisturbed flow with greater flow velocity. Hence, the tendency of the downstream cylinder response is to return to classical isolated cylinder VIV when $T \rightarrow \infty$, similar to what has been concluded for tandem cylinders (or any other configuration) when $d \rightarrow \infty$.

On the other hand, it is not as straightforward to understand why the downstream cylinder may present larger amplitudes of vibration in the streamwise direction for staggered cylinders.

To explain this, the greater dependence of the cylinder's displacements in the x direction is recalled in which the inline degree of freedom is more sensitive to the flow velocity and its fluctuations as the relative flow and body motion are aligned, whereas for the transverse degree of freedom, the relative flow and motion are obviously orthogonal. The excitation mechanisms differ fundamentally in hydrodynamic "dragging" and a pressure differential lift due to vortex shedding, respectively.

Revisiting Figure 4-10 and Figure 4-11 for the wake flow measurements after a stationary and a vibrating upstream cylinder, it was concluded that the wake deficit is maximum, and consequently the flow velocity is minimum, at the wake centreline

(tandem cylinders). This means that the wake flow velocity is greater for staggered cylinders than for tandem cylinders. Therefore, a greater flow velocity directly translates to a greater hydrodynamic drag which leads to larger A_{x2}/D for staggered cylinders when compared to tandem cylinders.

However, the issue remains to explain why the first VIV peak is higher for staggered cylinders than for single cylinders, which in theory are positioned in the undisturbed zone and largest flow velocity profile of the WWCT tank. The only plausible explanation for this is that this is directly related to WIV and the upcoming vortex street. From the experimental system shown in Figure 5-13, where the flow comes from the left to the right-hand side, it is proposed that whilst the incoming flow is perturbed to a lesser degree when the downstream cylinder is offset, and not aligned with the upstream cylinder, the alternate vortices being shed from the front cylinder are still expected to affect the rear cylinder. In fact, the vortices formed from the upstream cylinder are shed not at the wake centreline but at given curvatures on both sides of the cylinder in a von Karman vortex street and travel at an angle downstream of the wake (wake widening). This is, for example, very clear for the vorticity structure study of Alam *et al.* [81] for their triple-cylinder system, although it would be the same for two cylinders as considered presently since only the vortices shed from the upstream cylinder are discussed.

For staggered cylinders with magnitudes of transverse oscillation, as seen in Figure 5-14b, this means that the downstream cylinder will most, or all of the time be vibrating unilaterally within the wake flow. Depending on the instantaneous position of the downstream cylinder, it may be impacted, whether fully or partially, by only one side of the alternate vortex street. The unsteady nature of the vortices is proposed to contribute to the larger A_{x2}/D that is observed in Figure 5-14a for staggered cylinders when compared to either tandem cylinders or a single cylinder.

For reduced velocities larger than the first VIV regime (approximately $U_r > 12$), A_{x2}/D is observed to decrease with T as expected. For $d = 4$ and $T = 1$, inline amplitudes of vibration are still larger than for tandem cylinders for the highest U_r studied. The other staggered cases do not exceed the tandem cylinder case for larger reduced velocities.

The amplitudes of vibration of staggered fixed-free cylinders are validated against the experiments of Assi [23] in Figure 5-15. However, it is important to highlight the fundamental differences between the study of Assi [23] and the present study: i) the

literature study has enforced an inline-to-transverse natural frequency ratio of 2:1, whilst the cylinder-spring system is homogeneous, i.e., an inline-to-transverse natural frequency ratio or 1:1 herein; ii) reduced velocities from both studies vary with natural frequency but here they have been considered as nominal values for simplicity; iii) different mass and damping ratios as well as Reynolds numbers.

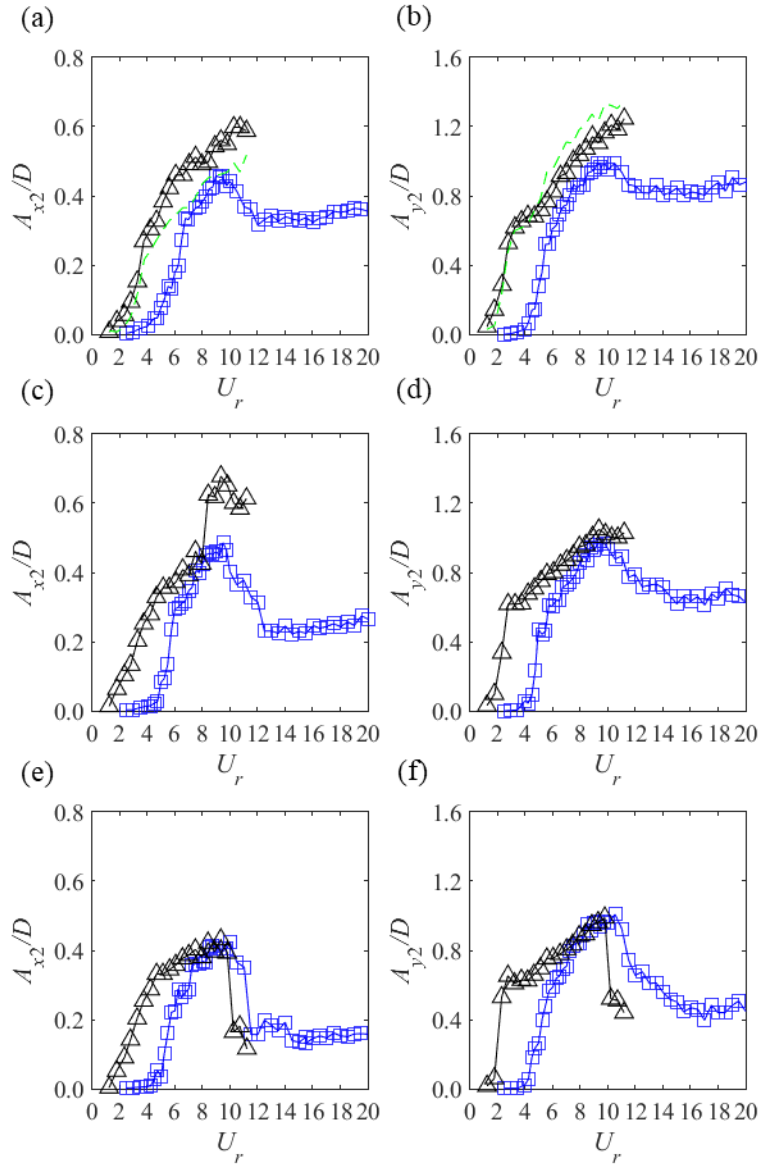


Figure 5-15: Comparison of normalised oscillation amplitudes of the downstream cylinder of fixed-free staggered twin cylinders with reference literature studies. (a) A_{x2}/D at $d = 4$, $T = 1$; (b) A_{y2}/D at $d = 4$, $T = 1$; (c) A_{x2}/D at $d = 4$, $T = 2$; (d) A_{y2}/D at $d = 4$, $T = 2$; (e) A_{x2}/D at $d = 4$, $T = 3$; (f) A_{y2}/D at $d = 4$, $T = 3$. Caption: \square : Present results; \triangle : Assi [23]; $- -$: Assi [23] tandem cylinders ($d = 4$, $T = 0$).

Overall, the present results agree with the results of Assi [23] within reasonable limits considering the above-mentioned differences between studies. Unfortunately, there is a limited range of reduced velocities available from the literature study to be used as comparison. Assi's [23] measurements for the tandem cylinder have been

added for correlation to Figure 5-15a-b and are represented by the green dashed lines. It is clear that A_{x2}/D is larger for the staggered cylinder than for the tandem cylinder also for the literature study even though this has not been highlighted or discussed.

Despite these differences, the two studies agree in the most important features, namely a similar dependence on the increase of T such as a larger A_{x2}/D for staggered cylinders than for tandem cylinders, and a return to VIV-type response with increase of T out of the wake flow.

The staggered cylinders in the WWCT tank were then repositioned to $d = 10$ and results are presented in Figure 5-16.

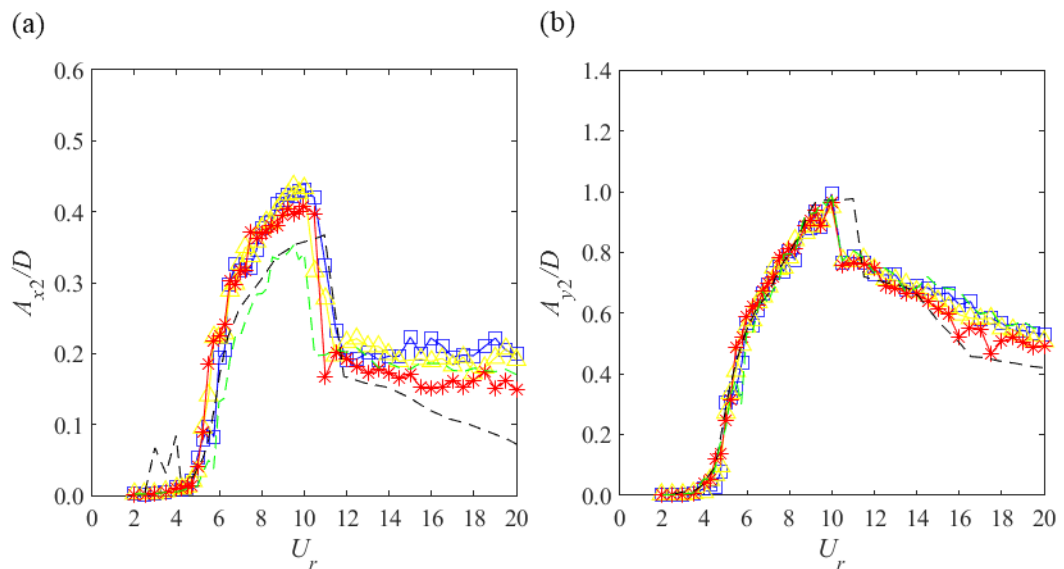


Figure 5-16: Dependence of normalised oscillation amplitudes of the downstream cylinder on the initial staggered spacing between the two cylinders for a fixed-free system with $d = 10$ in the (a) inline direction and (b) crossflow direction. Caption: — — : single cylinder; — — : tandem fixed-free cylinders at $d = 10$; \square : $d = 10$, $T = 1$; \triangle : $d = 10$, $T = 2$; $*$: $d = 10$, $T = 3$.

The results highlight that the increase of downstream spacing to $d = 10$ does not seem to alter the dependence of the behaviour of the rear cylinder on the staggered position, T , as similar features are observed. Even for a large spacing such as $d = 10$, staggered cylinders still produce generally larger vibrations in the inline direction, whilst the transverse oscillation amplitudes are effectively similar except for a slight deviation in the upper-to-lower regime transition that occurs approximately at $10 < U_r < 12$.

5.5. Displacement Time Series and Oscillation Trajectories

Following what was done for the single cylinder and for the fixed-free tandem cylinders experimental analyses, the time series of inline and transverse displacements of the downstream cylinder, as well as their trajectory behaviour, are now investigated and presented for the configurations of $(d = 4, T = 1)$, $(d = 4, T = 4)$,

and ($d = 10$, $T = 1$) in Figure 5-17, Figure 5-18, and Figure 5-19 respectively, for a more detailed description of the response of staggered cylinders.

For the investigation of the staggered cylinder behaviour, the y-axis limits, where possible, have been kept consistent with the axis of Figure 5-5, which illustrates the time series of tandem cylinders for $d = 4$.

Although the vibrations in both x and y directions are slightly larger at $U_r = 3$ and 4 for the staggered pair ($d = 4$, $T = 1$), they are still negligible.

In the tandem vs staggered comparison of Figure 5-5 and Figure 5-17, the noticeable differences only start to be observed for $U_r = 6$ and higher, especially for the temporal downstream cylinder responses in the inline direction. Such a feature has been previously observed in the study of *rms* amplitudes of vibration of staggered cylinders in Figure 5-14, where the inline behaviour of the downstream cylinder has been highlighted to undergo considerable changes, whereas the difference was small for the transverse response.

Normally the total x_2 motion is asymmetric towards the flow direction due to the large mean cylinder drift caused by the mean hydrodynamic drag force. Herein, the x_2 time series have been post-processed to disregard the mean drift oscillation as this is typically how x_2 time series are presented in related studies. Nevertheless, inline oscillations have been seen to be symmetric so far considering the studies of VIV of a single cylinder and WIV of a fixed-free tandem pair. On the other hand, offsetting the cylinders in the staggered case has been observed to result in asymmetric x_2 responses for some reduced velocity cases for ($d = 4$, $T = 1$), where $U_r > 4$. When that is the case, the x_2 response is larger towards the positive axis, i.e. the flow direction, as expected. As discussed previously, at an initial offset of $T = 1$, the downstream cylinder could be directly affected by unilateral vortex shedding from the upstream cylinder which could be the onset of this larger positive oscillation for x_2 .

In general, when comparing the fixed-free tandem couple at $d = 4$ against the staggered pair of cylinders at ($d = 4$, $T = 1$), the x_2 responses are different in behaviour and normally larger for the staggered cylinder couple, whereas the y_2 behaviours are comparable between the two cases both quantitatively and qualitatively.

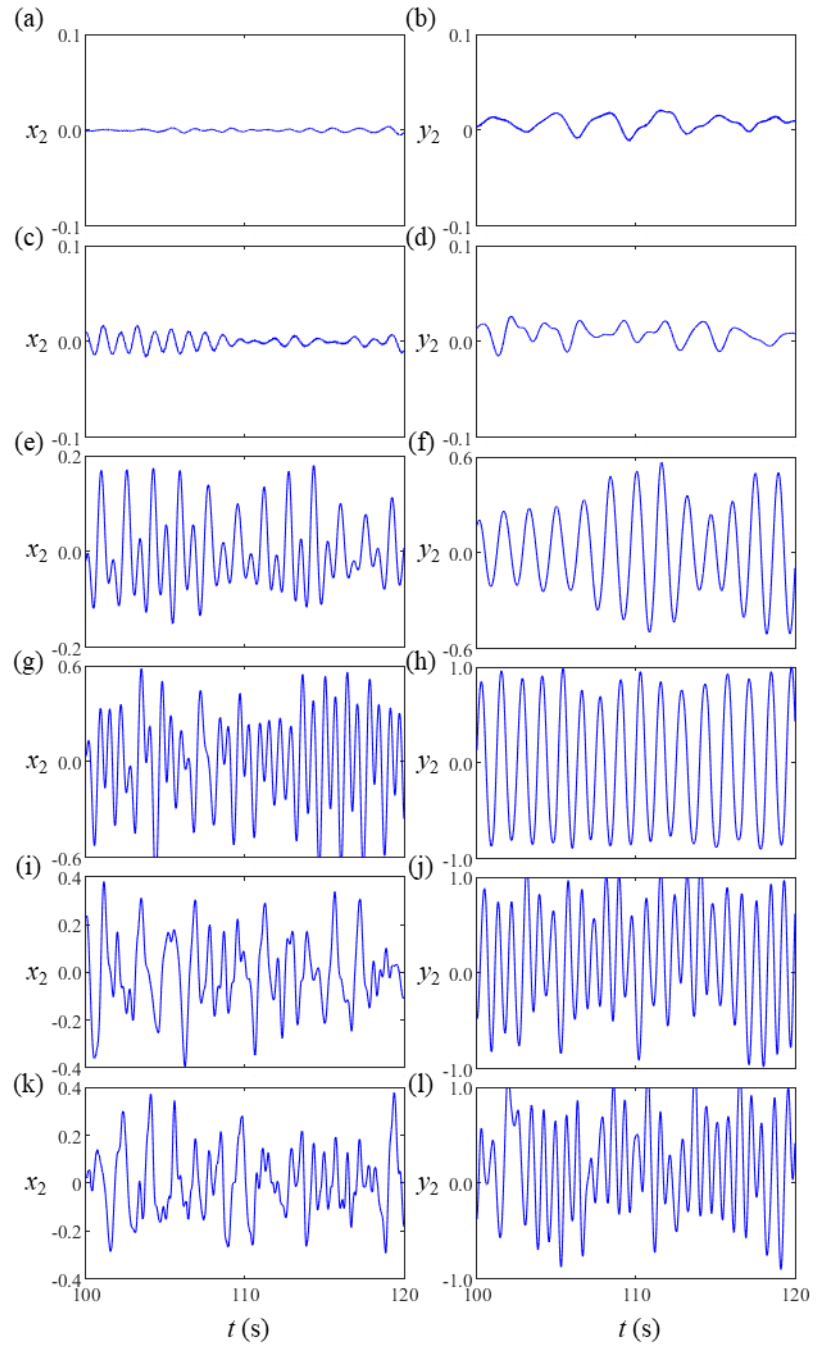


Figure 5-17: Time series of displacements of the downstream of a fixed-free pair of cylinders for $d = 4$, $T = 1$. (a) x_2 at $U_r = 3$; (b) y_2 at $U_r = 3$; (c) x_2 at $U_r = 4$; (d) y_2 at $U_r = 4$; (e) x_2 at $U_r = 6$; (f) y_2 at $U_r = 6$; (g) x_2 at $U_r = 10$; (h) y_2 at $U_r = 10$; (i) x_2 at $U_r = 15$; (j) y_2 at $U_r = 15$; (k) x_2 at $U_r = 20$; and (l) y_2 at $U_r = 20$.

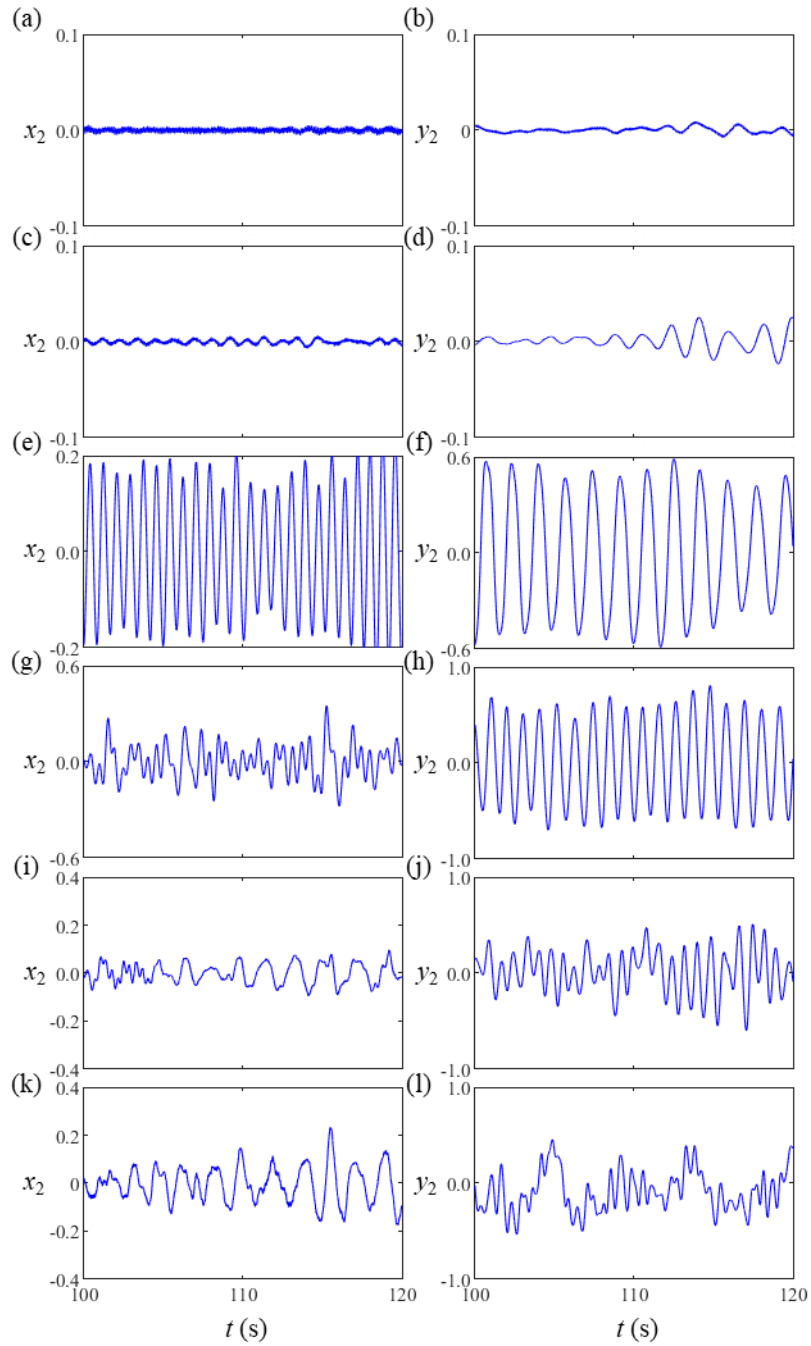


Figure 5-18: Time series of displacements of the downstream of a fixed-free pair of cylinders for $d = 4$, $T = 4$. (a) x_2 at $U_r = 3$; (b) y_2 at $U_r = 3$; (c) x_2 at $U_r = 4$; (d) y_2 at $U_r = 4$; (e) x_2 at $U_r = 6$; (f) y_2 at $U_r = 6$; (g) x_2 at $U_r = 10$; (h) y_2 at $U_r = 10$; (i) x_2 at $U_r = 15$; (j) y_2 at $U_r = 15$; (k) x_2 at $U_r = 20$; and (l) y_2 at $U_r = 20$.

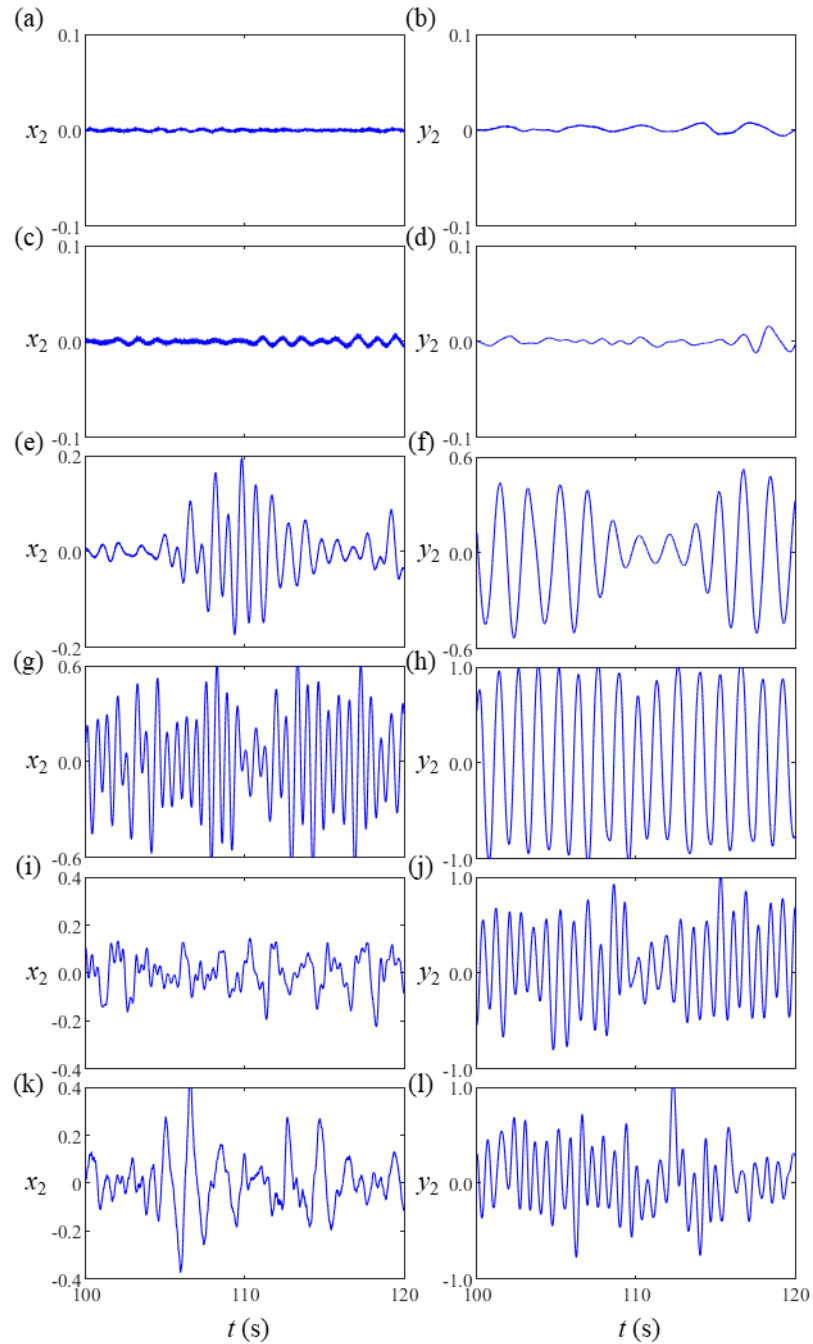


Figure 5-19: Time series of displacements of the downstream of a fixed-free pair of cylinders for $d = 10$, $T = 1$. (a) x_2 at $U_r = 3$; (b) y_2 at $U_r = 3$; (c) x_2 at $U_r = 4$; (d) y_2 at $U_r = 4$; (e) x_2 at $U_r = 6$; (f) y_2 at $U_r = 6$; (g) x_2 at $U_r = 10$; (h) y_2 at $U_r = 10$; (i) x_2 at $U_r = 15$; (j) y_2 at $U_r = 15$; (k) x_2 at $U_r = 20$; and (l) y_2 at $U_r = 20$.

For the staggered twin cylinders of ($d = 4$, $T = 4$), the x_2 oscillations return a symmetric response, however, discrepancies are still observed in the comparison of streamwise responses with the tandem cylinder, suggesting that wake effects may still be observed for lateral distances as far as four diameters. This observation goes against the measurements of the wake deficit of Figure 4-10. However, the transverse vibrations of the two cylinders which are likely to be non-synchronised may instead be

reducing this original lateral distance from 4 diameters to a relative lateral distance that could be within the wake interaction zone, as reflected by the results obtained. The y_2 behaviour is once again seen to be comparable between tandem and staggered cylinders.

The behaviour of staggered cylinders further downstream from each other ($d = 10$, $T = 1$) has also been studied with respect to the time series of x_2 and y_2 oscillations and is presented in Figure 5-18 for comparison against a similar tandem cylinder system in Figure 5-6. Overall, although the time-dependent responses seem to have a greater degree of disorder for the staggered cylinders, they are mostly comparable qualitatively for the vibrations in both directions and quantitatively for y_2 , whereas the x_2 oscillations for the staggered cylinders are still larger than for the tandem cylinders, although less so than for the previous cases.

In terms of bidimensional oscillation trajectories, the results for the fixed-free downstream cylinder of a staggered couple are presented in Figure 5-20, Figure 5-21, and Figure 5-22 for initial spacings of ($d = 4$, $T = 1$), ($d = 4$, $T = 4$), and ($d = 10$, $T = 1$). The comparison with the respective trajectories of a tandem fixed-free downstream cylinder is possible through Figure 5-8, Figure 5-9, and Figure 5-10, namely for initial configurations of ($d = 4$, $T = 0$), ($d = 10$, $T = 0$), and ($d = 20$, $T = 0$).

Overall, in the comparison of vibration motions for a system with ($d = 4$, $T = 1$) against ($d = 4$, $T = 0$) above a minimum threshold ($U_r > 4$), figure-of-8 oscillation shapes are also observed for the downstream cylinder of a staggered system, indicating an inline-to-transverse oscillation frequency of approximately a 2:1 ratio as was also the case for the studies of VIV of a single cylinder and fixed-free pair of tandem cylinders. However, the figures-of-8 for the fixed-free staggered system are wider, highlighting a greater dynamic response of x_2 as commented on before, and may also be asymmetric for both x_2 and y_2 depending on U_r . On the other hand, with respect to the mean inline drift of the downstream cylinder, the differences between tandem and staggered fixed-free downstream cylinders are shown to be negligible, with magnitudes reaching almost 2.5 diameters for $U_r = 20$ for any of the two systems.

The trajectories of a cylinder initially positioned at ($d = 4$, $T = 4$) are not directly comparable to its closest tandem counterpart at ($d = 4$, $T = 0$), as expected from the large initial offset. It has been previously discussed that wake interaction effects are non-existent for such a large initial lateral distance from the wake centreline, approximately $T > 3$ for the present study, as shown by the wake flow velocity

measurements of Figure 4-10, so it might be expected that the downstream cylinder of such a system would respond as a single cylinder under classical VIV. Instead, the transverse vibration of the downstream cylinder when directed back towards the wake flow results in a different behaviour.

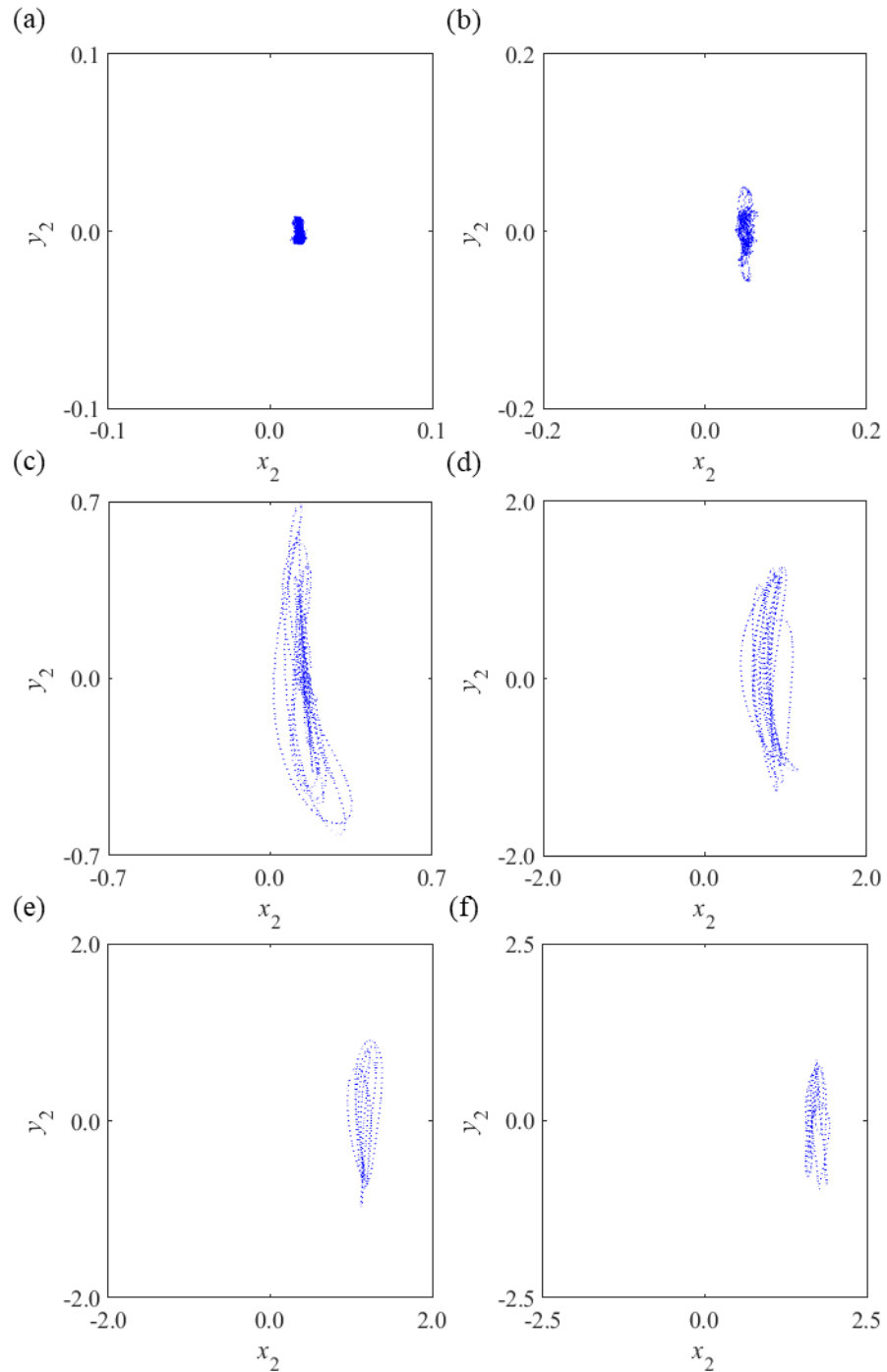


Figure 5-20: 2DOF trajectories of the downstream of a fixed-free staggered twin bundle of cylinders undergoing WIV for $d = 4$, $T = 1$. (a) $U_r = 3$; (b) $U_r = 4$; (c) $U_r = 6$; (d) $U_r = 10$; (e) $U_r = 15$; and (f) $U_r = 20$.

This becomes clear from the analysis of Figure 5-17, which shows that features that have been observed for $(d = 4, T = 1)$ are also observed and even amplified for $(d$

= 4, $T = 4$) for $U_r \leq 10$, namely wider figure-of-8 trajectory shapes with considerable x_2 motion. Interestingly, this U_r range, more specifically around $6 \leq U_r \leq 10$, is exactly the U_r range for which the largest transverse vibration amplitudes are seen in Figure 5-14. Those large oscillations when directed towards the wake centreline work to reduce the instantaneous lateral distance between the cylinders and immerse the cylinder back into the wake interaction zone, resulting in the figure-of-8 trajectories.

When U_r is increased to $U_r = 10$, transverse amplitudes of vibration decrease and the downstream cylinder's trajectories for $U_r = 15$ and 20 are comparable to what is shown for the tandem system at ($d = 20$, $T = 0$), which is a VIV-like response. Therefore, the staggered rear cylinder at ($d = 4$, $T = 4$) shows traits of WIV or VIV depending on the U_r considered.

Finally, oscillation trajectories of a downstream fixed-free staggered cylinder at ($d = 10$, $T = 1$) are reasonably similar to its tandem counterpart ($d = 10$, $T = 0$) which suggests that the WIV features of staggered cylinders are more sensitive to the energy dissipation that occurs with distance downstream of the upstream cylinder.

As previously, the investigation of the dominant oscillation frequencies for the downstream cylinder will be considered in the following section in order to further discuss the issues raised from the time series and oscillation trajectory results.

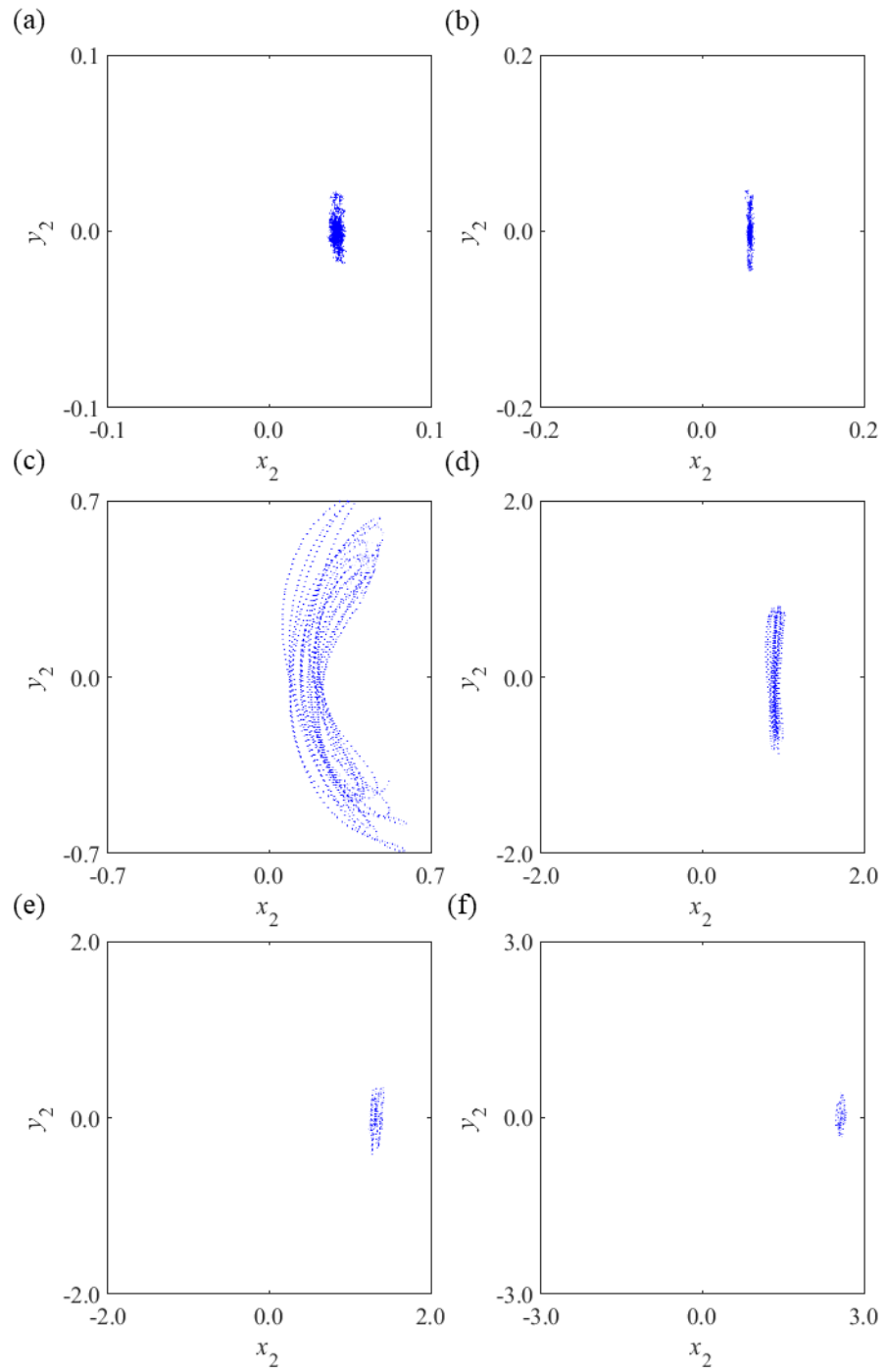


Figure 5-21: 2DOF trajectories of the downstream of a fixed-free staggered twin bundle of cylinders undergoing WIV for $d = 4$, $T = 4$. (a) $U_r = 3$; (b) $U_r = 4$; (c) $U_r = 6$; (d) $U_r = 10$; (e) $U_r = 15$; and (f) $U_r = 20$.

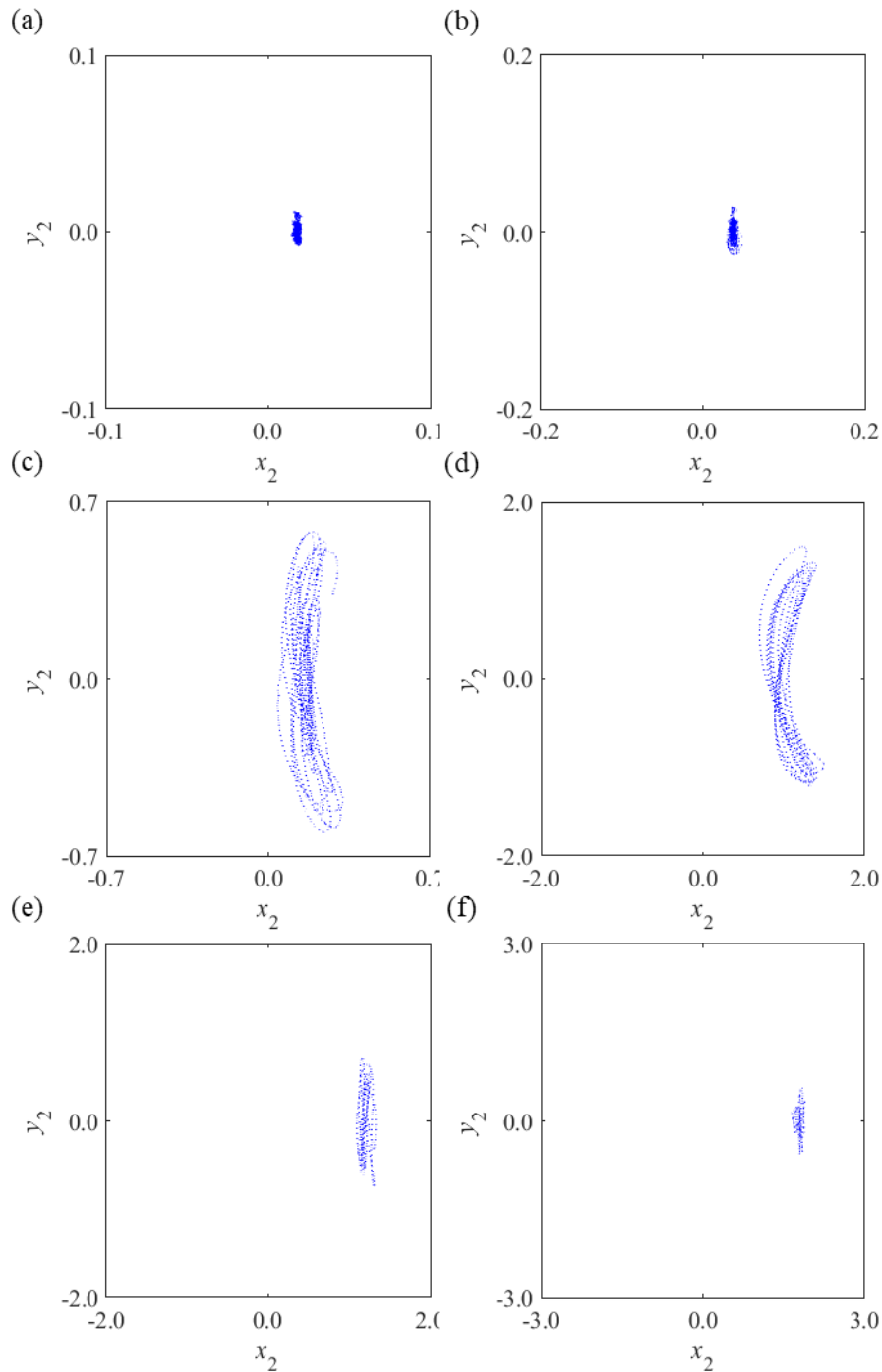


Figure 5-22: 2DOF trajectories of the downstream of a fixed-free staggered twin bundle of cylinders undergoing WIV for $d = 10$, $T = 1$. (a) $U_r = 3$; (b) $U_r = 4$; (c) $U_r = 6$; (d) $U_r = 10$; (e) $U_r = 15$; and (f) $U_r = 20$.

5.5.1. Dominant Oscillation Frequencies

The PSD of the oscillations of the cylinder downstream of a cylinder fixed and unable to vibrate, for every staggered configuration considered herein, namely ($d = 4$, $T = 1$), ($d = 4$, $T = 2$), ($d = 4$, $T = 3$), ($d = 4$, $T = 4$), ($d = 10$, $T = 1$), ($d = 10$, $T = 2$), and ($d = 10$, $T = 3$), have been computed as explained before and compared to the single cylinder VIV study, and the pair of tandem fixed-free cylinders. The effect of variation

of U_r in the predominant frequencies of vibrations of the cylinder systems is presented in Figure 5-23.

Overall, it is possible to conclude that the dominant oscillation frequencies of the downstream cylinder are not particularly sensitive to the variation of initial spacings and cylinder position, where results obtained in the present study for the fixed-free staggered pair of cylinders mostly collapse, one over the other, for both oscillation directions. In fact, the same feature has been observed for the dependence of initial spacing, d , for tandem cylinders, as exhibited in Figure 5-11 and Figure 5-12 and, not only that, but tandem frequencies have been previously discussed to be similar to the frequencies of single-cylinder VIV. Therefore, it is possible to conclude that frequencies of vibration for systems with two, and possibly more cylinders, where the upstream cylinder is stationary, are not significantly different from a system with only one cylinder under VIV, even though amplitudes of vibration, time histories and oscillation trajectories show significant differences between single and multiple cylinders cases.

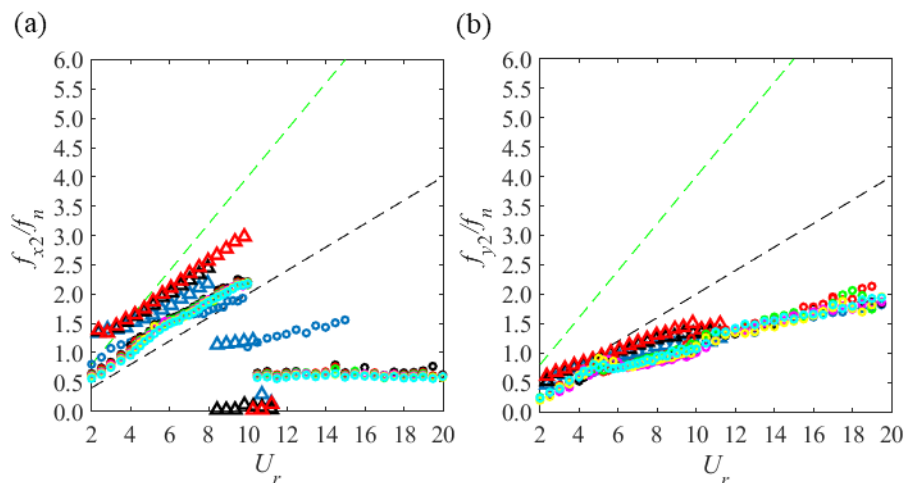


Figure 5-23: Initial staggered spacing dependence of the dominant normalised frequencies of oscillations for the WIV of the downstream of a fixed-free pair of cylinders in a flume.

Validation with reference literature studies. (a) Inline and (b) crossflow oscillation frequencies. Legend: - - : Strouhal law ($St = 0.2$); - · - : Doubled Strouhal law ($2St = 0.4$); Circles: Present 2DOF study for $m^* = 3.75$ and $\zeta = 0.055$ (in water) – blue: ($d = 4, T = 1$), black: ($d = 4, T = 2$), red: ($d = 4, T = 3$), green: ($d = 4, T = 4$), pink: ($d = 10, T = 1$), yellow: ($d = 10, T = 2$), cyan: ($d = 10, T = 3$); Triangles: Assi [23] $m^* = 1.6$ and $\zeta = 0.003$ (in air) – blue: ($d = 4, T = 1$), black: ($d = 4, T = 2$), red: ($d = 4, T = 3$).

Nevertheless, the only significant difference seen occurs for f_{x2}/f_n in the lower branch of responses, approximately for $U_r > 10$ when the initial staggered position in the gap between the fixed-free cylinders is changed. Whilst every staggered configuration, with the exception of ($d = 4, T = 1$), oscillates at an inline frequency approximately half the natural frequency of the system, which is comparable to the single-cylinder case as seen in Figure 4-18, the downstream cylinder at ($d = 4, T = 1$)

vibrates at a frequency that matches or nearly surpasses the natural frequency of the system. This inline lower branch resonance state, which had not been identified previously, is likely an important contributing factor to the largest inline vibration amplitudes occurring for ($d = 4$, $T = 1$).

Even though, the studies are dissimilar, the results of Assi [23] have been included for validation of the present experiments. Despite the lack of exact agreement between the reference data and that of the present study already discussed, the differences are reasonable and most importantly the trend and general behaviour of oscillation frequencies agree between the two studies.

The question now is whether the same observed characteristics of WIV of a pair of fixed-free cylinders would be repeated or how would they differ for a more general configuration where the upstream cylinder is also free to vibrate. This will be discussed in the following chapter.

5.6. Chapter Summary

This chapter has been dedicated to the experimental tests of a 2DOF cylinder that is free to vibrate downstream of a fixed cantilever vertical metal cylinder. Thus, the downstream cylinder is elastically supported by four springs that have been fitted diagonally. Tandem and staggered tests have been conducted for several spacing and reduced velocity combinations. Results have been analysed in terms of temporal domain, amplitudes of vibrations, planar oscillation trajectories, and dominant frequencies of vibrations.

The main discussion points for tandem cylinders are:

- Vibrations have been analysed for $d = 4, 6, 8, 10$, and 20 from $U_r = 2 - 20$.
- When comparing the present WIV results of the second cylinder against the single cylinder tests previously run, it is seen that the build-up of oscillation amplitudes observed for the transition of initial-upper branches, approximately for $6 \leq U_r \leq 8$, seems to be delayed to slightly higher reduced velocities and not only that, but the maximum vibration amplitude peak is slightly lower around $U_r = 10$. These features are understood to be related to the wake flow deficit at the downstream cylinder's location, or in other words, related to the fact that the wake flow velocity acting on the downstream cylinder is lower than the free stream flow velocity acting on the upstream cylinder.

- One point that is implicit in the above remark is that the mechanism of WIV is negligible for lower reduced velocities. Herein this is approximately $U_r < 10$. Therefore, the cylinder has been observed to be responding with similar trends as a single cylinder but subjected to a wake-reduced flow velocity. This is observed for all spacings studied, i.e. the response is independent of d for lower reduced velocities.
- The response of the downstream cylinder of a system of fixed-free cylinders is not hysteretic for the given properties and conditions of the present experiments. No significant differences have been observed in the comparison of cylinder responses when the reduced velocity has been successively increased against when U_r has been sequentially decreased.
- For reduced velocities greater than a given critical U_r , here approximately $U_r > 10$, the response of the downstream cylinder can be described as follows:
 1. Low spacings – when the cylinders are closer together, i.e., lower d , the downstream cylinder is investigated to continue to be excited into considerably larger 2DOF oscillations for the remaining reduced velocities than those of classical VIV of one cylinder. In other words, WIV does not appear to show resonance features in the sense that amplitudes of vibrations would reduce past a certain U_r range of synchronisation. Instead, amplitudes are sustained when the flow velocity is increased to $U_r = 20$.
 2. Large spacings – as the spacing between the cylinders rises, clearly vibration amplitudes gradually decreases for $U_r > 10$ and tends to return to single cylinder behaviour. This feature highlights that the mechanism of WIV tends to disappear when $d \rightarrow \infty$ and two cylinders with sufficient spacing between them effectively behave as two isolated cylinders. This is perhaps intuitive as once farther away from the perturbation source (upstream cylinder), wake flow effects and upstream vortices tend to disappear.
 3. Intermediary spacings – The behaviour of the cylinder is a combination between regimes 1) and 2), i.e., a combination or transition between VIV and WIV.

Alternatively, the main discussion points for the staggered cylinders have been:

- There is a reduction in oscillation amplitude magnitude when the offset between the cylinders is increased ($T \uparrow$), as the downstream cylinder is increasingly far from the wake centreline and closer to the wake flow edges and undisturbed flow with greater flow velocity. Hence, the tendency of the downstream cylinder response is to return to classical isolated cylinder VIV when $T \rightarrow \infty$, similarly to what has been observed for tandem cylinders (or any other configuration) when $d \rightarrow \infty$.
- Despite the observation above, the downstream cylinder may present larger amplitudes of vibration in the streamwise direction for staggered cylinders especially for low d . Wake flow measurements after a stationary and a vibrating upstream cylinder have demonstrated that the wake deficit is maximum, and consequently the flow velocity is minimum, at the wake centreline (tandem cylinders). This means that the wake flow velocity is greater for staggered cylinders than for tandem cylinders. Therefore, a greater flow velocity directly translates to a greater hydrodynamic drag which leads to larger A_{x2}/D for staggered cylinders when compared to tandem cylinders.

CHAPTER 6. COMBINED VIV AND WIV OF A PAIR OF CYLINDERS FOR A DYNAMIC UPSTREAM CYLINDER (“FREE-FREE” CASE)

Having studied the behaviour of a single cylinder and a fixed-free pair of cylinders, the final laboratory investigation is to release the 2-degrees-of-freedom of the upstream cylinder. Therefore, the metallic stationary upstream cylinder and frame system were replaced by a pendulum-spring system identical to the downstream cylinder, as shown in Figure 6-1, allowing the two cylinders to dynamically respond to the hydrodynamic excitations. This final configuration has been referred to as the “free-free” case for simplicity.



Figure 6-1: Photograph of the free-free pair of tandem identical cylinders, frame and pendulum systems.

The presence of four springs per cylinder is justified to provide the restoring force necessary to sustain vibrations that are the focus of this study. In practical subsea engineering applications, the restoring force is provided by the structural connections, moorings, joints and vessel connections, this is simulated here by the springs. As it is observed from Figure 6-1, the proximity of the cylinders, springs and frames increases the complexity of the experimental setup for the free-free case. The space between the cylinders, accounting for the dynamic motion of both cylinders, was cluttered and limited for the closest initial spacings. Measures were put in place to mitigate the risk of collision between cylinders or interference with the springs including, the installation

of diagonal springs instead of conventional springs (inline and transversal to the flow) and the integrated cylinder-frame-pendulum movement, i.e. the entire frame and pendulum of a given cylinder could be displaced for the variation of initial spacings, as discussed in Chapter 4. As for the fixed-free setup, the upstream cylinder system controlled the tandem spacings, whereas the downstream cylinder allowed for variation of staggered spacings.

The free-free analysis conducted in this project generally follows the same script as for the single cylinder and the fixed-free experimental models, where the downstream cylinder for the tandem and staggered systems is studied for amplitudes of vibration, displacement time histories, trajectory and frequencies of oscillation.

6.1. Tandem Cylinders

6.1.1. Free-Free Tandem Downstream Cylinder Amplitudes of Vibration

For the purposes of validation and comparison with previous studies, the Qualisys motion acquisition system was initially attached to the upstream cylinder and tests for tandem cylinders at $d = 4$ were performed. The conclusion, which agrees with many literature sources [12, 18, 23-25], is that the upstream cylinder behaves exactly as a single cylinder, even for the minimum initial spacings considered in this study ($d = 4$) and considering oscillations in the inline direction of both cylinders. Therefore, there is no reason to believe that the upstream cylinder would behave differently for the other initial spacing cases considered. This way, the dynamic response of the downstream cylinder is the sole subject of interest of the present study and the Qualisys motion tracker camera was therefore set up and calibrated to measure only the downstream cylinder for the remaining tests. A standard high-definition camera was also positioned underneath the tank to simultaneously record the behaviour of the upstream cylinder if required.

From the analysis of the *rms* amplitudes of vibration of the free-free downstream cylinder shown in Figure 6-2, it is possible to observe that oscillation amplitudes progressively build-up in both directions with the increase of U_r up to the largest reduced velocity. This feature has been previously referred to as galloping, but Assi [11] has argued against the use of this terminology due to the potential of confusion with the different, but similarly named phenomenon that occurs for the flow past square cylinders.

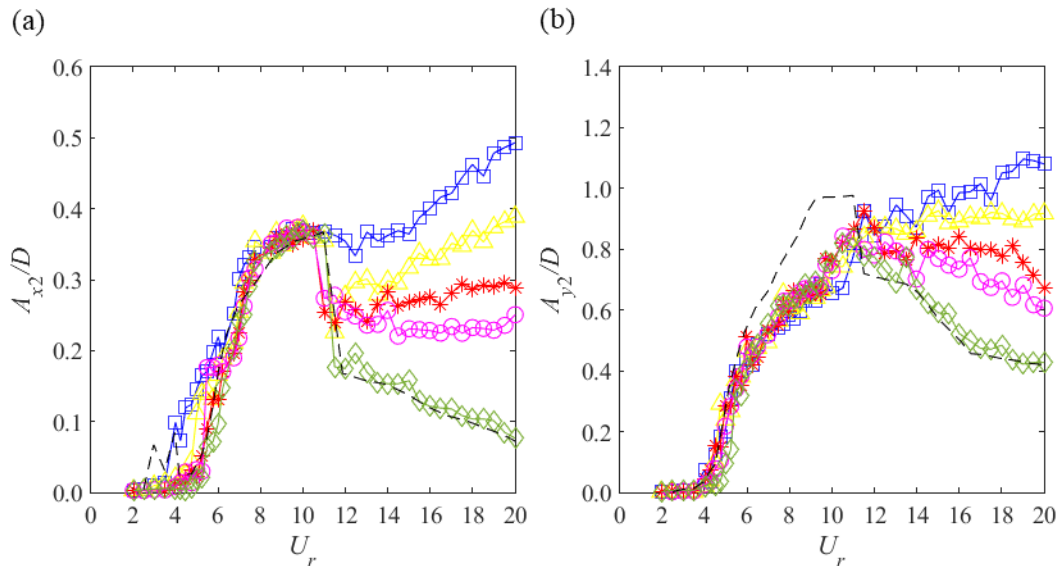


Figure 6-2: Dependence of normalised oscillation amplitudes of the downstream cylinder on the initial tandem spacing between the two cylinders for a free-free system in the (a) inline direction and (b) crossflow direction. Caption: - - : single cylinder; free-free cylinders at \square : $d = 4$; \triangle : $d = 6$; $*$: $d = 8$; \circ : $d = 10$; and \diamond : $d = 20$.

As demonstrated previously, this amplitude build-up does not occur for the fixed-free downstream cylinder and it has been discussed that a possible reason for that is associated with the instantaneous spacing between the fixed-free cylinders, where most of the time they were up to 2.5 diameters further than the initial tandem spacing prescribed. On the other hand, the free-free cylinders do not suffer from the same problem as both the upstream and the downstream cylinders are allowed to move in the streamwise direction and are, therefore, expected to have a mean drift caused by the mean hydrodynamic drag force. Hence, for free-free cylinders, one may expect that the instantaneous or real spacing between the cylinders approximately matches the initial tandem spacing, causing wake interaction effects to be stronger for the smallest distances between cylinders.

Moreover, it becomes clear that amplitudes of vibration are inversely proportional to the increase of d , with the $d = 4$ case leading to the largest downstream cylinder vibrations in both directions. Interestingly, whilst the A_{x2}/D results show a well-defined first VIV peak within approximately $4 \leq U_r \leq 12$, the response of the downstream cylinder in the transverse direction does not exhibit such a clear first VIV regime. Assi [23] has shown that the first VIV regime may not be so clear for both A_{x2}/D and A_{y2}/D , but here this is not the case for A_{x2}/D . Also, the response of a free-free downstream cylinder seems less organised and shows more amplitude fluctuations than for the respective fixed-free results.

6.1.2. Free-Free Tandem Downstream Cylinder Time Series and Oscillation Trajectories

For further comparison against the fixed-free tandem pair of cylinders, the time series of the bidimensional motion of the downstream cylinder of the free-free tandem couple has also been studied. These are plotted in Figure 6-3, Figure 6-4, and Figure 6-5.

In the comparison with the fixed-free downstream cylinder at $d = 4$, Figure 5-5, it is possible to observe that the y_2 response is relatively comparable between fixed-free and free-free cases, especially for $U_r \leq 6$, but it is also similar for the higher reduced velocities. However, the x_2 amplitudes of vibration are clearly larger for the free-free configuration for almost every reduced velocity considered.

The comparison of the systems with $d = 10$, Figure 5-6 and Figure 6-4, show a smaller difference between the two cases. Nevertheless, oscillation amplitudes for the free-free case are still noticeably larger. These larger amplitudes have previously been associated with the greater proximity of the cylinders and consequently greater wake interaction/WIV due to the mean drift of the upstream cylinder in the streamwise direction.

The trend continues to repeat itself for the largest initial spacings, namely $d = 20$, where it is seen that the downstream cylinder is able to sustain larger vibrations at higher reduced velocities, which suggests that WIV may still excite the cylinder even for $d = 20$. Overall, the time series of x_2 and y_2 are observed to present a greater degree of irregularity and fluctuations. This is expected due to the greater complexity that the system is subjected to with the vibrations of the upstream cylinder which generates the upstream wake flow.

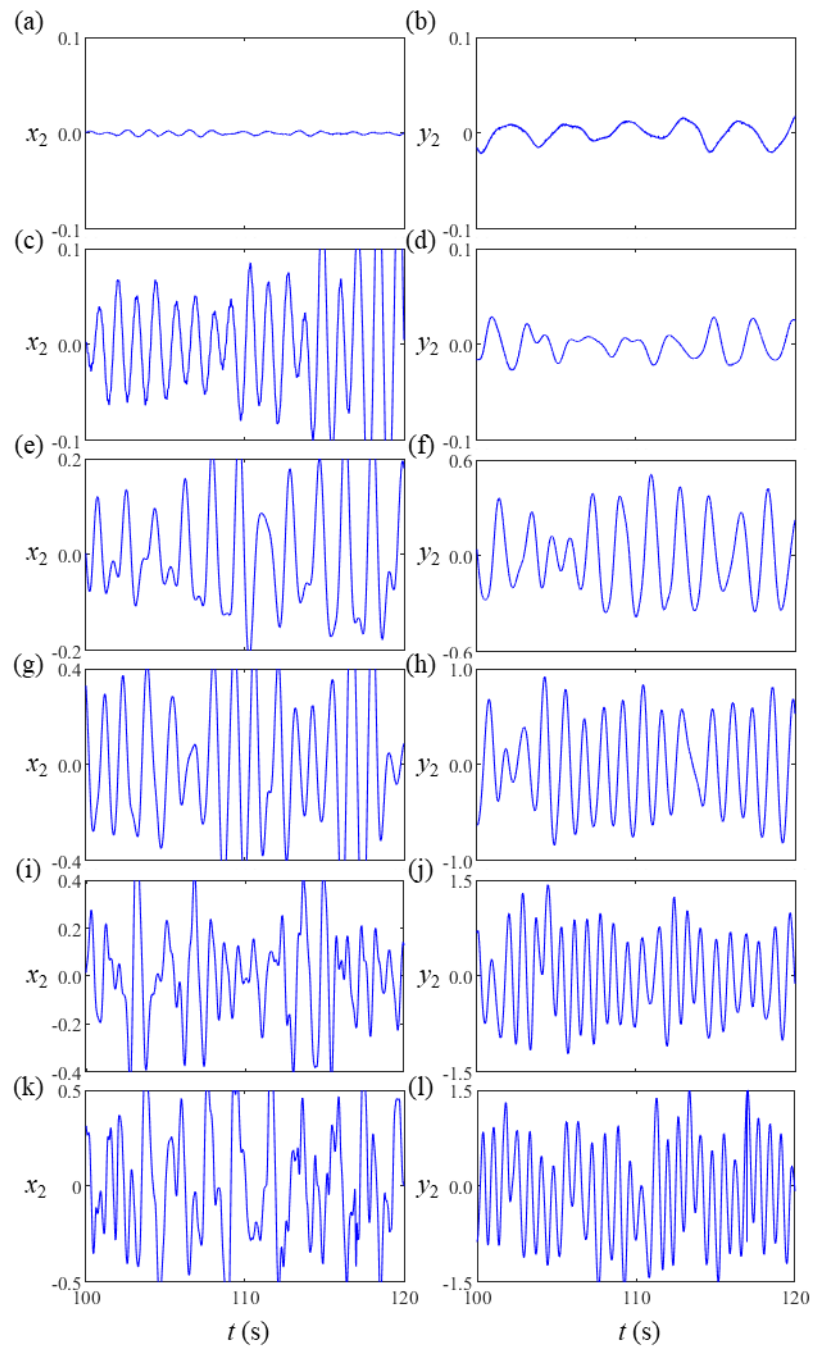


Figure 6-3: Time series of displacements of the downstream of a free-free pair of cylinders for $d = 4$. (a) x_2 at $U_r = 3$; (b) y_2 at $U_r = 3$; (c) x_2 at $U_r = 4$; (d) y_2 at $U_r = 4$; (e) x_2 at $U_r = 6$; (f) y_2 at $U_r = 6$; (g) x_2 at $U_r = 10$; (h) y_2 at $U_r = 10$; (i) x_2 at $U_r = 15$; (j) y_2 at $U_r = 15$; (k) x_2 at $U_r = 20$; and (l) y_2 at $U_r = 20$.

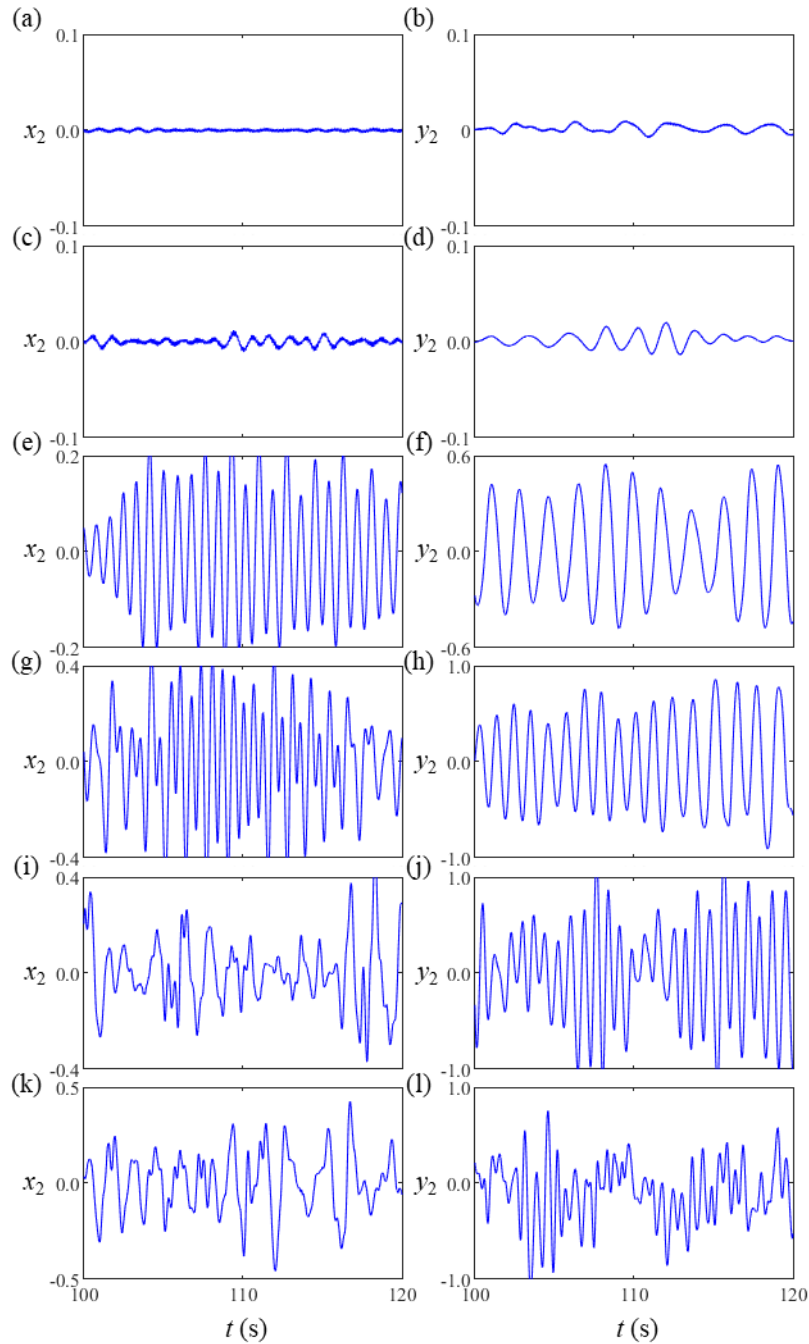


Figure 6-4: Time series of displacements of the downstream of a free-free pair of cylinders for $d = 10$. (a) x_2 at $U_r = 3$; (b) y_2 at $U_r = 3$; (c) x_2 at $U_r = 4$; (d) y_2 at $U_r = 4$; (e) x_2 at $U_r = 6$; (f) y_2 at $U_r = 6$; (g) x_2 at $U_r = 10$; (h) y_2 at $U_r = 10$; (i) x_2 at $U_r = 15$; (j) y_2 at $U_r = 15$; (k) x_2 at $U_r = 20$; and (l) y_2 at $U_r = 20$.

The analysis of oscillation trajectories is shown in Figure 6-6, Figure 6-7, and Figure 6-8. In general terms, the features observed in the 2DOF motion of the downstream one of a free-free tandem pair of cylinders are somewhat similar to the fixed-free counterparts for all spacings studied. It is important to note that figure-of-8 trajectory shapes, indicating 2:1 inline-to-transverse frequency ratios are also observed for the free-free cases.

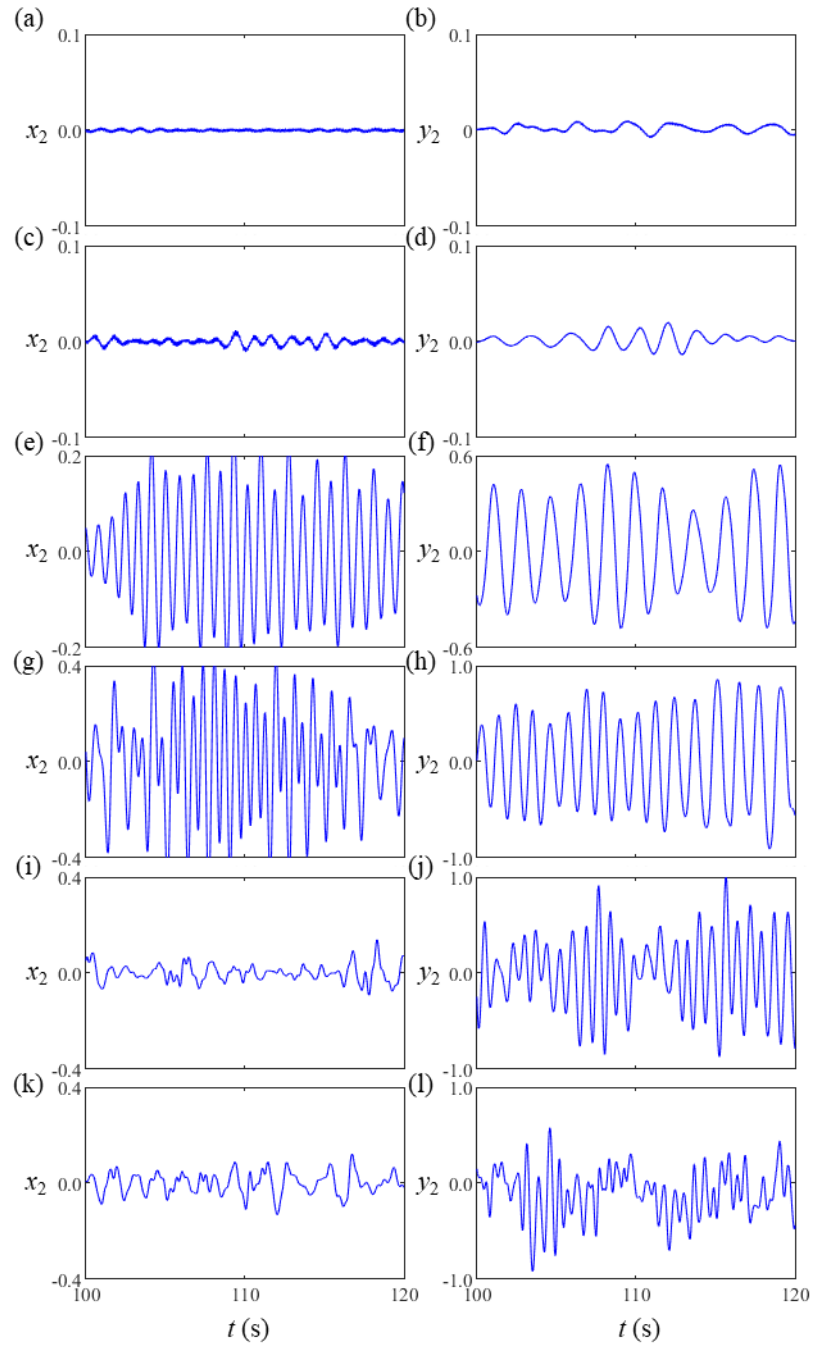


Figure 6-5: Time series of displacements of the downstream of a free-free pair of cylinders for $d = 20$. (a) x_2 at $U_r = 3$; (b) y_2 at $U_r = 3$; (c) x_2 at $U_r = 4$; (d) y_2 at $U_r = 4$; (e) x_2 at $U_r = 6$; (f) y_2 at $U_r = 6$; (g) x_2 at $U_r = 10$; (h) y_2 at $U_r = 10$; (i) x_2 at $U_r = 15$; (j) y_2 at $U_r = 15$; (k) x_2 at $U_r = 20$; and (l) y_2 at $U_r = 20$.

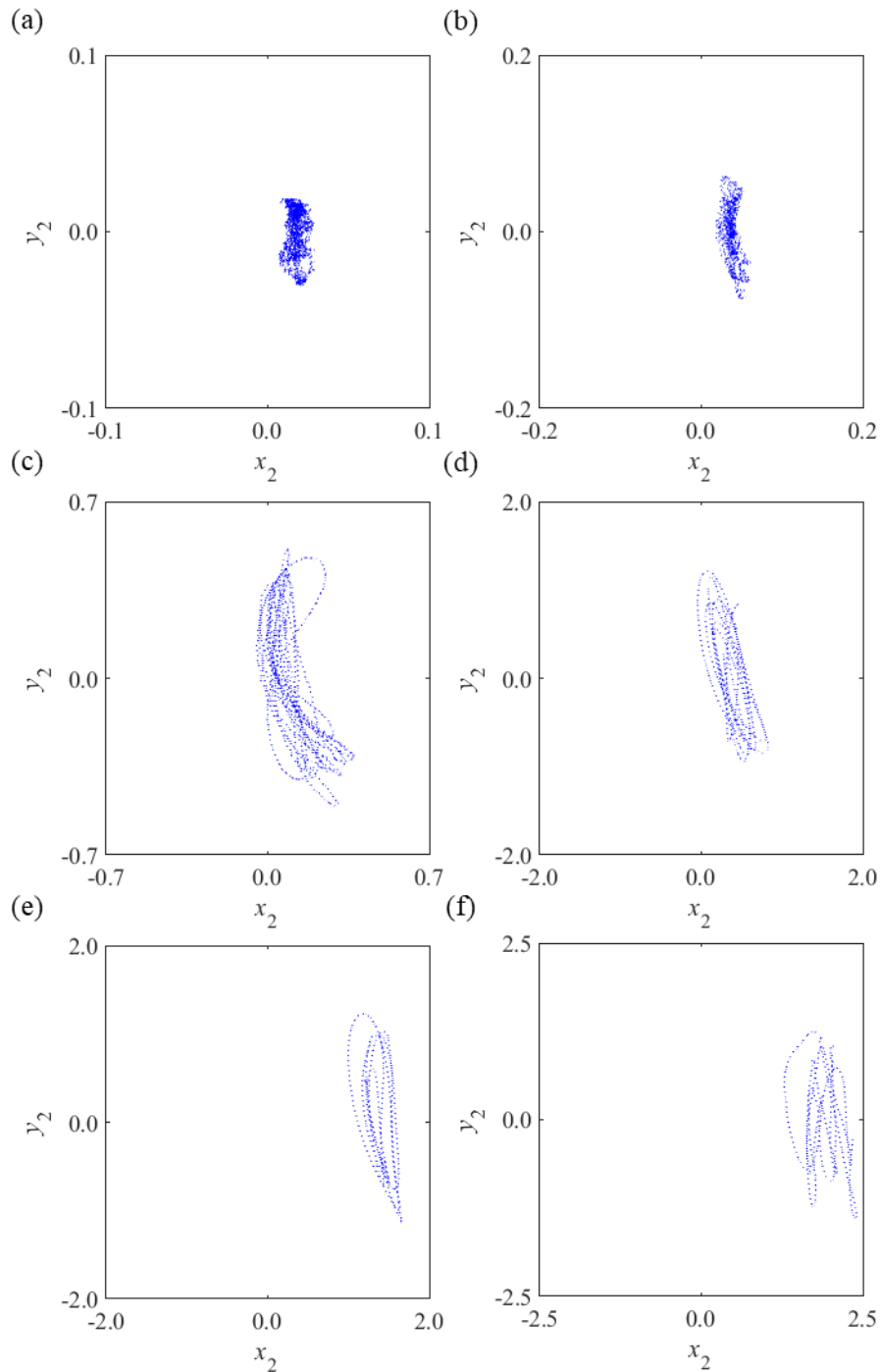


Figure 6-6: 2DOF trajectories of the downstream of a free-free tandem twin bundle of cylinders undergoing WIV for $d = 4$. (a) $U_r = 3$; (b) $U_r = 4$; (c) $U_r = 6$; (d) $U_r = 10$; (e) $U_r = 15$; and (f) $U_r = 20$.

Overall, the free-free response is more complex and less organised than the fixed-free case as expected and discussed previously. As the spacing is increased, the free-free tandem downstream cylinder gradually returns to single-cylinder behaviour, but this is seen to occur at slightly higher spacings for the free-free case than for the fixed-free case.

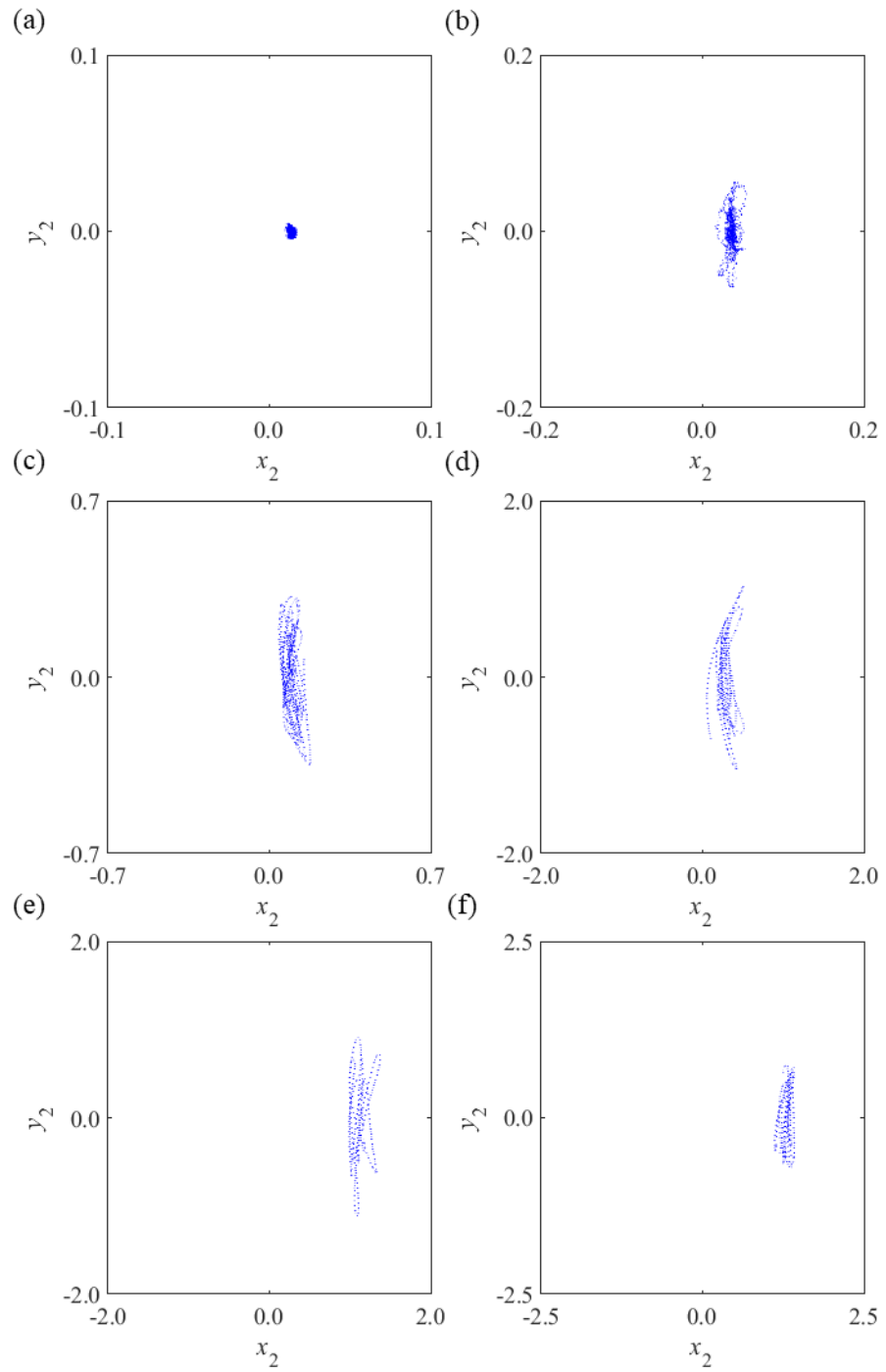


Figure 6-7: 2DOF trajectories of the downstream of a free-free tandem twin bundle of cylinders undergoing WIV for $d = 10$. (a) $U_r = 3$; (b) $U_r = 4$; (c) $U_r = 6$; (d) $U_r = 10$; (e) $U_r = 15$; and (f) $U_r = 20$.

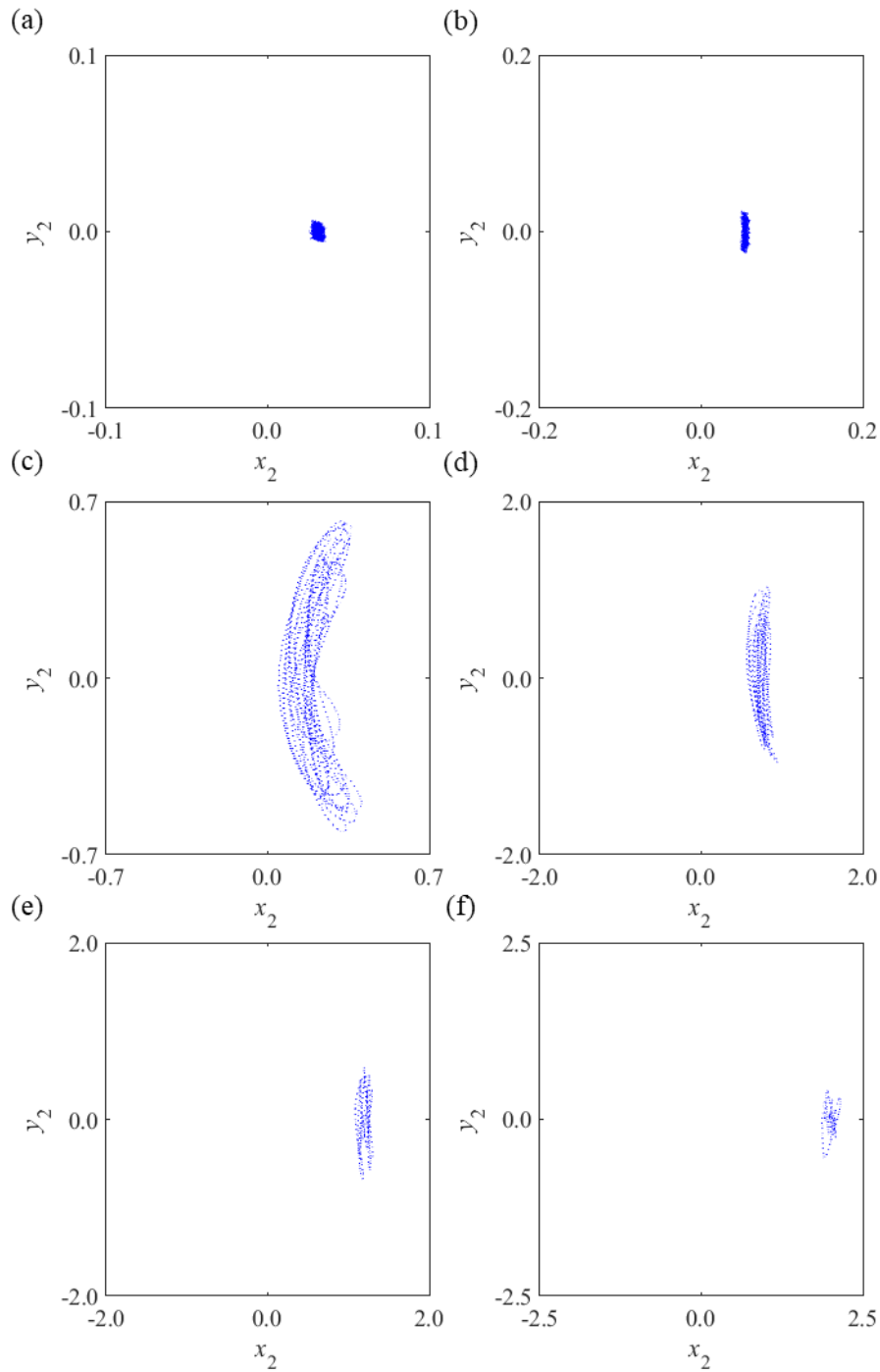


Figure 6-8: 2DOF trajectories of the downstream of a free-free tandem twin bundle of cylinders undergoing WIV for $d = 20$. (a) $U_r = 3$; (b) $U_r = 4$; (c) $U_r = 6$; (d) $U_r = 10$; (e) $U_r = 15$; and (f) $U_r = 20$.

6.1.3. Frequencies of Oscillations of the Downstream Free-Free Tandem Cylinder

As for the study of VIV of a single cylinder and WIV of a fixed-free downstream cylinder, dominant frequencies of oscillation of the downstream cylinder of a tandem free-free couple have been computed and presented in Figure 6-9 and Figure 6-10.

The analysis of these oscillation frequencies in comparison with the fixed-free system (Figure 5-11 and Figure 5-12) is discussed below.

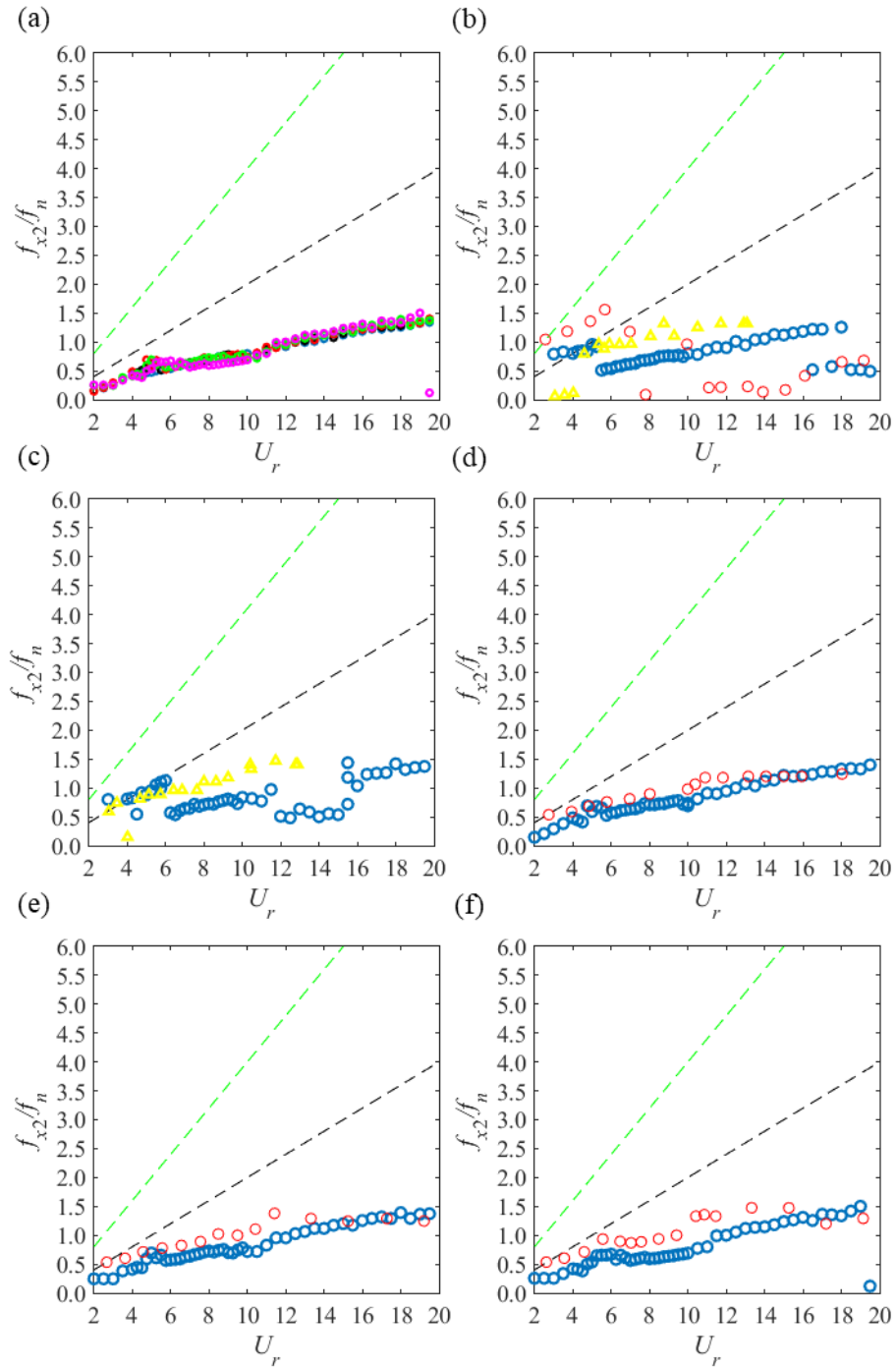


Figure 6-9: Initial tandem spacing dependence of the dominant normalised frequencies of inline oscillations for the WIV of the downstream of a free-free pair of cylinders in a flume in the crossflow direction. Validation with reference literature studies. (a) Present results for all d ; (b) $d=4$; (c) $d=6$; (d) $d=8$; (e) $d=10$; (f) $d=20$. Legend: $- -$: Strouhal law ($St = 0.2$); $- -$ (green): Doubled Strouhal law ($2St = 0.4$); \circ : Present 2DOF study for $m^* = 3.75$ and $\zeta = 0.055$ (in water); \circ (red): Armin *et al.* [25] $m^* = 2.36$ and $\zeta = 0.015$ (in water); and \triangle : Pereira *et al.* [24] 2DOF study with $m^* = 2.92$ and $\zeta = 0.025$ (assumed in water).

Initially, it is possible to conclude that vibration frequencies of the downstream cylinder of a tandem free-free cylinder pair are not sensitive to the variation of d since

the results from $d = 4, 6, 8, 10,$ and 20 seem to remain unchanged with variation of d for the two oscillation directions. This feature has also been observed in the previous cases studied, where frequencies of vibration of the downstream cylinder of a tandem or staggered fixed-free pair of cylinders showed similar behaviour. In fact, these frequencies of the downstream cylinder have been shown to be effectively identical to the oscillation frequencies of a single cylinder under classical VIV.

Overall, the normalised oscillation frequencies in the inline direction, f_{x2}/f_n , are almost identical to the transverse vibration frequencies, f_{y2}/f_n , with the exception that the $f_{x2}/f_n \times U_r$ curve appears relatively more irregular and less controlled. Therefore, this strong x - y coupling may suggest that the response in one of the directions is influencing and dictating the behaviour in the other direction. In the comparison with other experimental cases that did not show such a feature, such as either the single cylinder VIV or the fixed-free tests, it is possible to infer from these lower frequencies that the response of the cylinder in the transverse direction is dominating and influencing the response in the inline direction. A similar characteristic has been observed in the results from the 2DOF numerical modelling presented in Chapter 3.

In the frequency comparison against the fixed-free tandem pair of cylinders, one may notice that the release of the upstream cylinder and its consequent vibrations lead to the disappearance of the frequency contents near the black-dashed Strouhal line for the free-free case. This observation is in agreement with the oscillation amplitude study presented in Section 6.1.1, in that the first VIV peak regime, within approximately $6 < U_r < 10$, is not clearly evident for the free-free system when compared to the fixed-free twin cylinders.

Therefore, from the study of the free-free tandem system, the main observations identified are: i) amplitude build-up regime for low d is observed leading to the largest responses observed so far; ii) free-free cylinders vibrate with lower instantaneous spacings due to the mean drift of both cylinders and wake interaction or WIV effects are observed for higher spacings than for the fixed-free case; iii) the x_2 response is strongly coupled to the y_2 response for the free-free cylinders, with oscillation frequencies almost identical; iv) the vibration of the upstream cylinder causes the first VIV regime, if not to disappear then at least to become more moderate and less evident. It is now important to study the response of free-free cylinders with staggered configurations with the aim to establish if these observations are also seen for staggered cylinders and if any other interesting features arise.

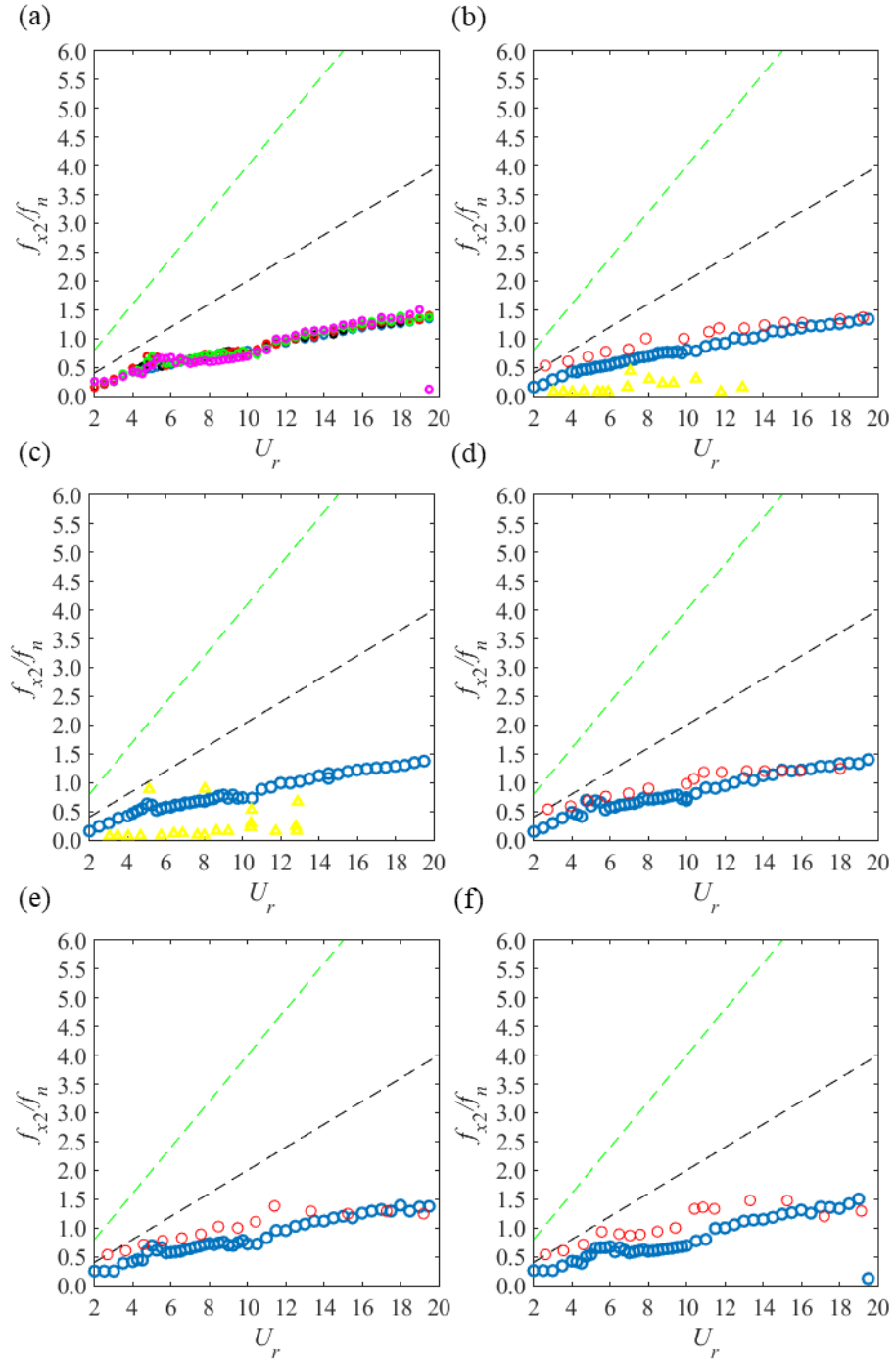


Figure 6-10: Initial tandem spacing dependence of the dominant normalised frequencies of transverse oscillations for the WIV of the downstream of a free-free pair of cylinders in a flume in the crossflow direction. Validation with reference literature studies. (a) Present results for all d ; (b) $d = 4$; (c) $d = 6$; (d) $d = 8$; (e) $d = 10$; (f) $d = 20$. Legend: $- -$: Strouhal law ($St = 0.2$); $- -$: Doubled Strouhal law ($2St = 0.4$); \circ : Present 2DOF study for $m^* = 3.75$ and $\zeta = 0.055$ (in water); \circ : Armin *et al.* [25] $m^* = 2.36$ and $\zeta = 0.015$ (in water); and \triangle : Pereira *et al.* [24] 2DOF study with $m^* = 2.92$ and $\zeta = 0.025$ (assumed in water).

6.2. Staggered Cylinders

In the final stage of the laboratory tests, the spring-supported identical cylinders were offset to consider staggered positions from $T = 0 - 4$ diameters as previously

done for the fixed-free study. The setup remained unchanged from the fixed-free study, where the downstream cylinder was initially displaced across the tank before each test for a given staggered configuration and this setup can be seen in Figure 6-11.

As it can be observed from Figure 6-11, the clearance between the springs, cylinders and connections was extremely limited for the staggered free-free setup. This slightly limited the spacings that could be studied; however, the main comparison cases were tested. Whenever there was a clearance spacing limitation or collision between the two cylinder systems, this will be mentioned in the following.

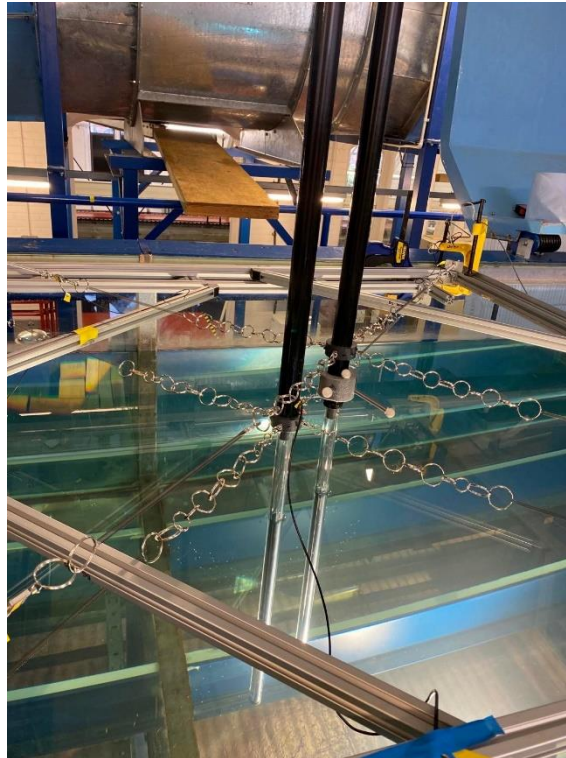


Figure 6-11: Photograph of the free-free pair of staggered identical cylinders, frame and pendulum systems.

The investigation of the dynamics of the downstream cylinder for the free-free staggered pair of cylinders was conducted similarly to the previous systems, where amplitudes of vibration are initially analysed against reduced velocities and variation of initial spacings, followed by a study of time-varying cylinder responses and frequencies of oscillation.

6.2.1. Amplitudes of Vibration of the Downstream Cylinder

As previously, initial tests were carried out for the case with initial spacing ($d = 4$, $T = 1$) (expected to be the most critical case) for which the Qualisys motion tracking system was set up and calibrated to measure the response of the upstream cylinder initially. This was done to investigate whether previous observations, both from this

study as well as literature (on tandem cylinders or fixed-free staggered cylinders), affirming that the upstream cylinder effectively behaves as a single cylinder undergoing classical VIV and being unaffected by wake interaction and wake deficit effects, would be repeated for the free-free staggered cylinders.

The experimental study of free-free staggered cylinders is one of the novel contributions of this study as there were no previous reports in the literature for wake interaction and WIV spacing regimes to the best of the author's knowledge. It was therefore important to determine whether the first cylinder behaves as a single cylinder. The observations and data from these initial measurements confirmed that the upstream cylinder is also unaffected by any sort of downstream or proximity interference from the second cylinder for free-free staggered cylinders, considering the present Re , d , T and system properties. Hereafter, the focus of the present subsection is to investigate the downstream cylinder of the pair, and all subsequent laboratory tests were completed with the Qualisys motion tracking system set up and calibrated for the rear cylinder.

Unfortunately, the nature of the experimental setup is such that the line of vision of the Qualisys imaging system of the infrared markers mounted on the downstream cylinder could be blocked at certain instances for the free-free cylinder system at $d = 4$ and offset initial spacings larger than $T = 1$. This is a limitation of the present laboratory setup.

Figure 6-11 does not show the dual acquisition cameras of the Qualisys system, but these are mounted on the tank walls approximately in the direction of the bottom left- and right-hand sides of the photograph. Thus, as the downstream cylinder had varied staggered initial positions and was displaced to the farthest side of the tank, the upstream cylinder, or its support system would block the line of sight of the cameras. The clearance spacing between cylinders and springs are critical and even if the staggered distances had been towards the closest side of the tank, staggered positions any larger than $T = 1$ would not have been possible to study for $d = 4$ as clashing would occur. Additionally, $d = 6$ was attempted but for approximately $T \geq 3$, the cylinders would collide with the springs.

Therefore, the minimum downstream initial spacing able to account for all staggered spacings intended to be investigated ($T = 0 - 4$) without physical interference between the upstream and downstream cylinders' systems was concluded

to be $d = 8$. The amplitudes of vibration for these configurations are plotted in Figure 6-12.

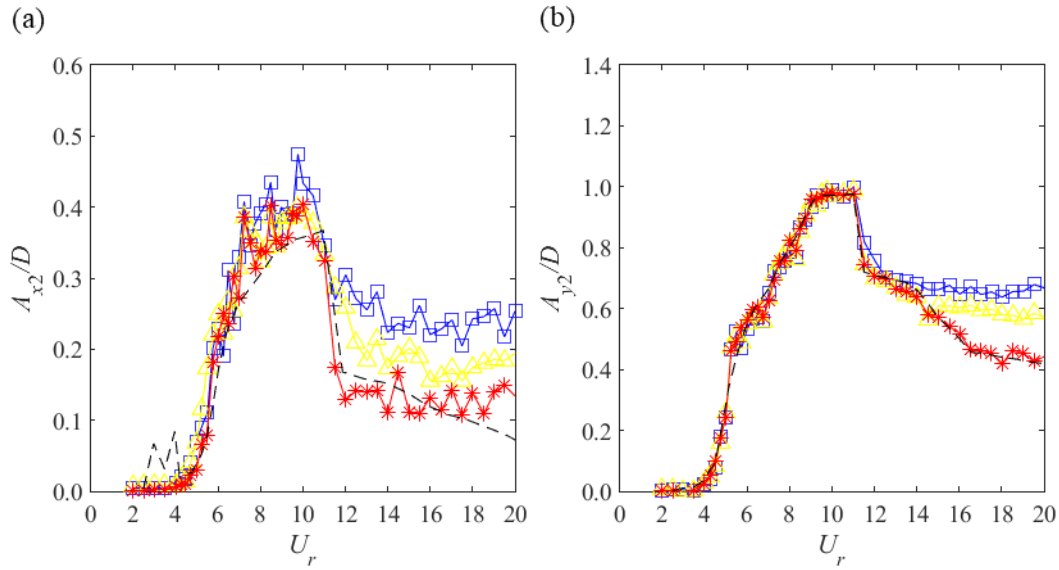


Figure 6-12: Dependence of normalised oscillation amplitudes of the downstream cylinder on the initial staggered spacing between the two cylinders for a free-free system in the (a) inline direction and (b) crossflow direction. Caption: - - : single cylinder; free-free cylinders at \square : $d = 8, T = 1$; \triangle : $d = 8, T = 2$; and $*$: $d = 8, T = 3$.

It is seen that the amplitudes of vibration are disorganised and fluctuate significantly with variation of U_r for the free-free staggered downstream cylinder of a pair, especially for A_{x2}/D . Also, the first VIV peak regime is well-developed and clear, as can be seen in Figure 6-12. Nevertheless, the magnitudes of oscillation are reduced in comparison with the free-free tandem cylinder system at $d = 8, T = 0$.

It is observed that whilst the cases for $(d = 8, T = 1)$ and $(d = 8, T = 2)$ still show amplitudes of vibration that are different from the single cylinder reference case (even though this difference is small), the case at $(d = 8, T = 3)$ is shown to be effectively behaving as a single cylinder, subjected to the VIV excitation phenomenon only. Finally, as both cylinders are allowed 2DOF, the upstream and the downstream cylinders are expected to exhibit a mean drift movement in the streamwise direction due to the mean drag force acting on the cylinders. For the downstream cylinder, it has been shown that this mean drag force and consequently the mean drift is reduced when compared to the upstream cylinder.

In conclusion, once the tests start, the free-free cylinders are expected to be displaced with slightly different mean drift, but with same order of magnitude, and in reality to be closer to each other, increasing wake effects, when compared to a fixed upstream cylinder and a 2DOF downstream cylinder that distances itself in the

streamwise direction from the leading cylinder once the tests start. Therefore, for free-free cylinders, a spacing of $d = 8$, could be compared to perhaps a spacing of $d = 6$ for fixed-free systems.

For the transverse mean position, both cylinders are normally located on the wake centreline, since there is not a counterpart of the mean drag force in terms of lift force. However, for free-free staggered cylinders, the range of δy is greater and the cylinders vibrate across a larger proportion of the disturbed wake flow. This could be one of the reasons associated with the large amplitude of vibration fluctuations seen in Figure 6-12.

Given the mentioned approximation of the pair of cylinders for the free-free system, an additional set of staggered spacings with varying d and T but keeping the same proportion have been investigated. These are: ($d = 4, T = 1$), ($d = 8, T = 2$), ($d = 12, T = 3$), and ($d = 16, T = 4$) and are seen in Figure 6-13.

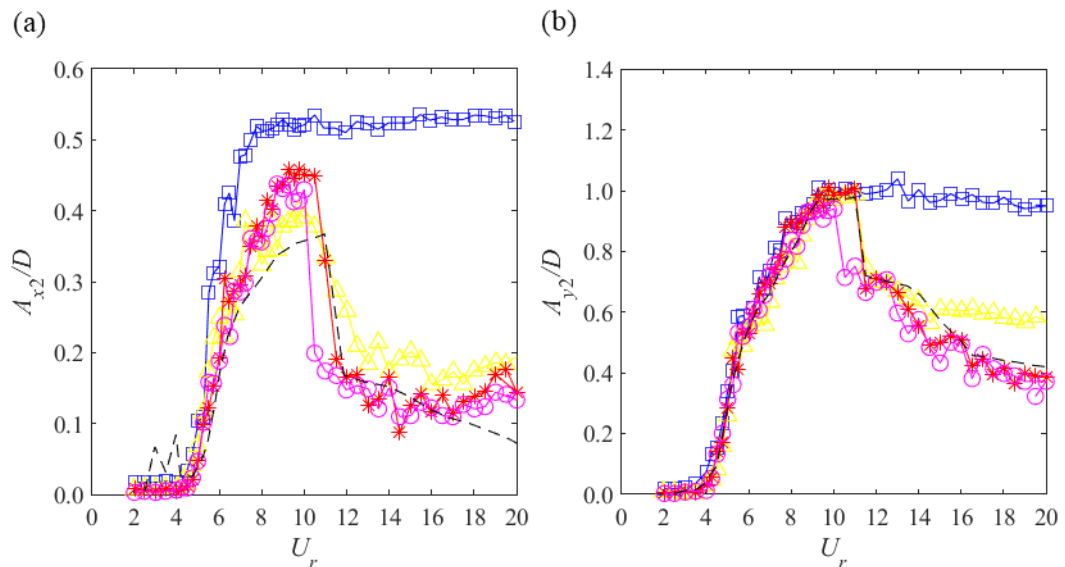


Figure 6-13: Dependence of normalised oscillation amplitudes of the downstream cylinder on the initial staggered spacing between the two cylinders for a free-free system in the (a) inline direction and (b) crossflow direction. Caption: - - : single cylinder; free-free cylinders at \square : $d = 4, T = 1$; \triangle : $d = 8, T = 2$; $*$: $d = 12, T = 3$, and \ominus : $d = 16, T = 4$.

The features observed draw attention, especially for the largest amplitudes of vibration in the inline direction seen for the present study across all systems and configurations. These occur for $d = 4, T = 1$, following a trend also seen for the fixed-free cylinders, where staggered cylinders yield the greatest inline oscillation amplitudes. This has previously been proposed to be associated with the skewed position of the downstream cylinder in one of the sides of the wake, where the alternate vortices shed from the upstream cylinder could impinge on the structure and excite the

inline degree-of-freedom which is more sensitive to flow velocity fluctuations (directly proportional to the drag force).

Amplitudes of vibration for the cases of $(d = 12, T = 3)$, and $(d = 16, T = 4)$ are nominally the same as the reference response of a single cylinder with some staggered amplitudes of vibration shown to be even lower than the single cylinder case. This can possibly be explained by the wake deficit profile and the consequent reduced flow velocity that the cylinder is subjected to. As the cylinders are too distant from the upstream cylinder and wake flow, WIV is no longer significant, but the lower flow velocity could be exciting the downstream cylinder in a form of reduced-velocity VIV.

6.2.2. Time Series of Displacements and Oscillation Trajectories

The study of instantaneous motions of the downstream cylinder of a free-free staggered couple is presented in the time series in Figure 6-14, Figure 6-15, and Figure 6-16 for specific configurations of $(d = 4, T = 1)$, $(d = 8, T = 2)$, $(d = 12, T = 3)$.

In general terms, the time series results show that the behaviour of a free-free staggered downstream cylinder may be complex, in fact perhaps the most complex system presently studied, with non-repeatable fluctuations and disorganised traces of amplitude modulations. This is especially the case for the inline degree-of-freedom and increasingly so for the most critical staggered case of $(d = 4, T = 1)$.

Additionally, asymmetric inline responses are observed for the same critical staggered configuration at $(d = 4, T = 1)$. The cylinder vibrates asymmetrically with larger magnitudes towards the positive x_2 , as expected, due to the direction of the flow. This asymmetric behaviour observed for the downstream staggered cylinder has also been reported in the experiments with fixed-free staggered cylinders as well as for the 2DOF model results for staggered cylinders discussed in Chapter 3.

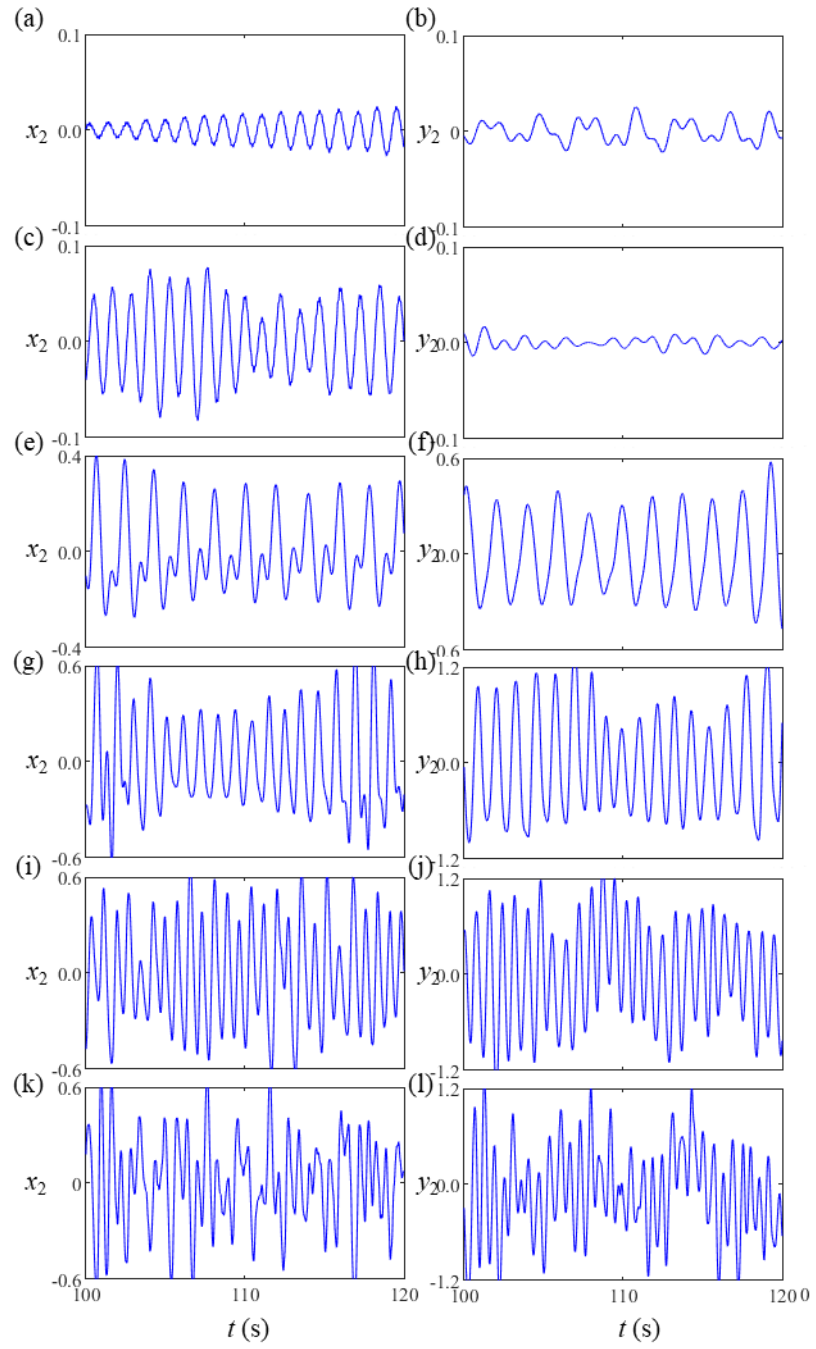


Figure 6-14: Time series of displacements of the downstream of a free-free pair of cylinders for $d = 4$, $T = 1$. (a) x_2 at $U_r = 3$; (b) y_2 at $U_r = 3$; (c) x_2 at $U_r = 4$; (d) y_2 at $U_r = 4$; (e) x_2 at $U_r = 6$; (f) y_2 at $U_r = 6$; (g) x_2 at $U_r = 10$; (h) y_2 at $U_r = 10$; (i) x_2 at $U_r = 15$; (j) y_2 at $U_r = 15$; (k) x_2 at $U_r = 20$; and (l) y_2 at $U_r = 20$.

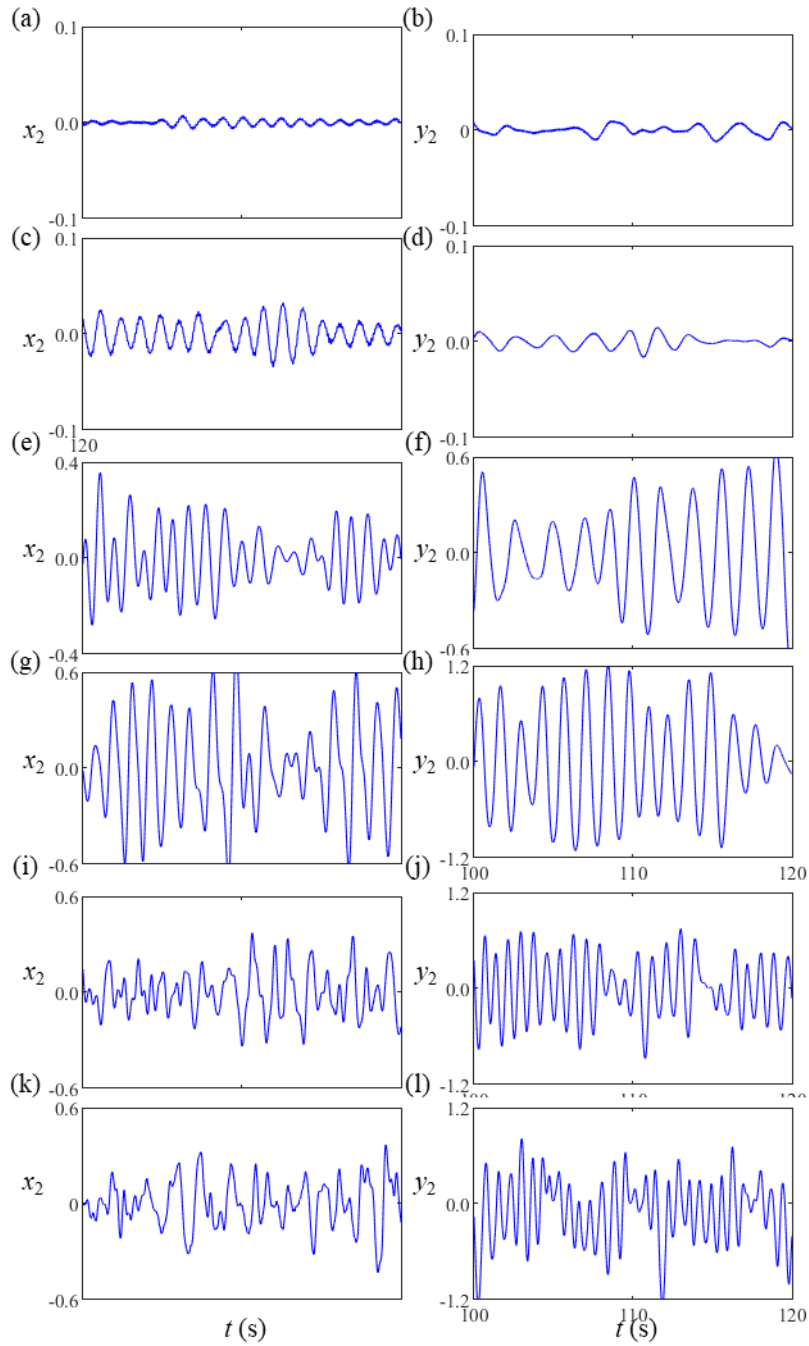


Figure 6-15: Time series of displacements of the downstream of a free-free pair of cylinders for $d = 8$, $T = 2$. (a) x_2 at $U_r = 3$; (b) y_2 at $U_r = 3$; (c) x_2 at $U_r = 4$; (d) y_2 at $U_r = 4$; (e) x_2 at $U_r = 6$; (f) y_2 at $U_r = 6$; (g) x_2 at $U_r = 10$; (h) y_2 at $U_r = 10$; (i) x_2 at $U_r = 15$; (j) y_2 at $U_r = 15$; (k) x_2 at $U_r = 20$; and (l) y_2 at $U_r = 20$.

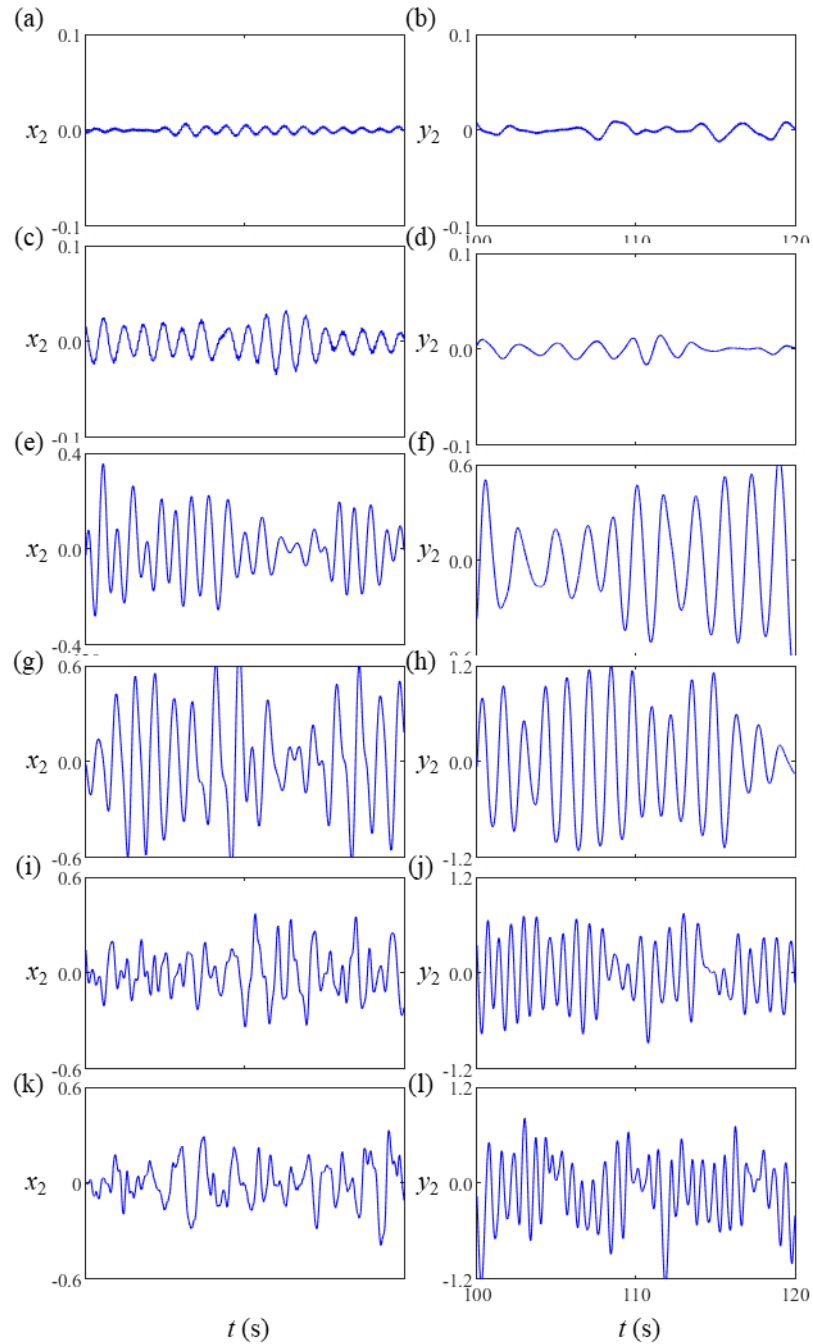


Figure 6-16: Time series of displacements of the downstream of a free-free pair of cylinders for $d = 12$, $T = 3$. (a) x_2 at $U_r = 3$; (b) y_2 at $U_r = 3$; (c) x_2 at $U_r = 4$; (d) y_2 at $U_r = 4$; (e) x_2 at $U_r = 6$; (f) y_2 at $U_r = 6$; (g) x_2 at $U_r = 10$; (h) y_2 at $U_r = 10$; (i) x_2 at $U_r = 15$; (j) y_2 at $U_r = 15$; (k) x_2 at $U_r = 20$; and (l) y_2 at $U_r = 20$.

The asymmetric response may be associated with the wake deficit, more specifically the variation of the wake-induced drag force profile across the wake. For instance, if Figure 6-14e-f are analysed together, one may observe that as the downstream cylinder vibrates laterally to $0 > y_2 > y_{2\max}$ ($= 0.5$ approximately) positions, the cylinder is in reality further distancing itself from the wake centreline during this positive half-cycle as the initial lateral spacing is $T = 1$. Hence, the cylinder is oscillating

from $\delta y = 1$ to approximately $\delta y = 1.5$. Recalling Figure 2-5 and literature studies [5, 11, 33, 49], such an oscillation means that the wake-induced drag acting on the downstream cylinder increases to magnitudes near the free-stream C_{D02} , which consequently is expected to lead to larger x_2 vibrations.

On the other hand, an opposite effect is seen during the remaining transverse half-cycle of the downstream cylinder, $0 < y_2 < y_{2min}$, where the cylinder is approaching the wake centreline, which is well-known for the occurrence of the minimum wake-induced drag, consequently leading to smaller inline vibrations.

The question that can be asked then is: why the asymmetric behaviour is only observed for some reduced velocities and not every U_r for staggered cylinders? To answer this, it is important to highlight that this variation in the wake-induced drag force and subsequent asymmetry in the inline direction is a consequence of the transverse oscillation of the cylinder. Thus, in order for this interaction to be significant, it is necessary that the cylinder's oscillation frequencies in the two directions are approximately matching. Also, once the reduced velocity is increased, other excitation mechanisms may interfere and take over. For instance, it is well-known from classical VIV of one cylinder, and it has also been commented herein for the double cylinder 2DOF systems, that the inline degree-of-freedom is coupled and sensitive to the at times dominant transverse degree-of-freedom.

For the other staggered cases, the explanation may be sought from the fact that the wake deficit is lower further from the upstream cylinder and consequently there is a smaller variation of the wake-induced drag for larger spacings.

The motion orbits in Figure 6-17, Figure 6-18, and Figure 6-19 highlight the complexity and asymmetry of some staggered cases, especially for $(d = 4, T = 1)$ as previously discussed.

All three staggered cases show figure-of-8 oscillation trajectories, indicating components of 2:1 inline-to-transverse frequency responses. The most complex vibration trajectories are those of $(d = 4, T = 1)$ and as the downstream cylinder is distanced both along and across the wake, it slowly returns to behave similarly to a single cylinder, for instance in comparison with Figure 4-17.

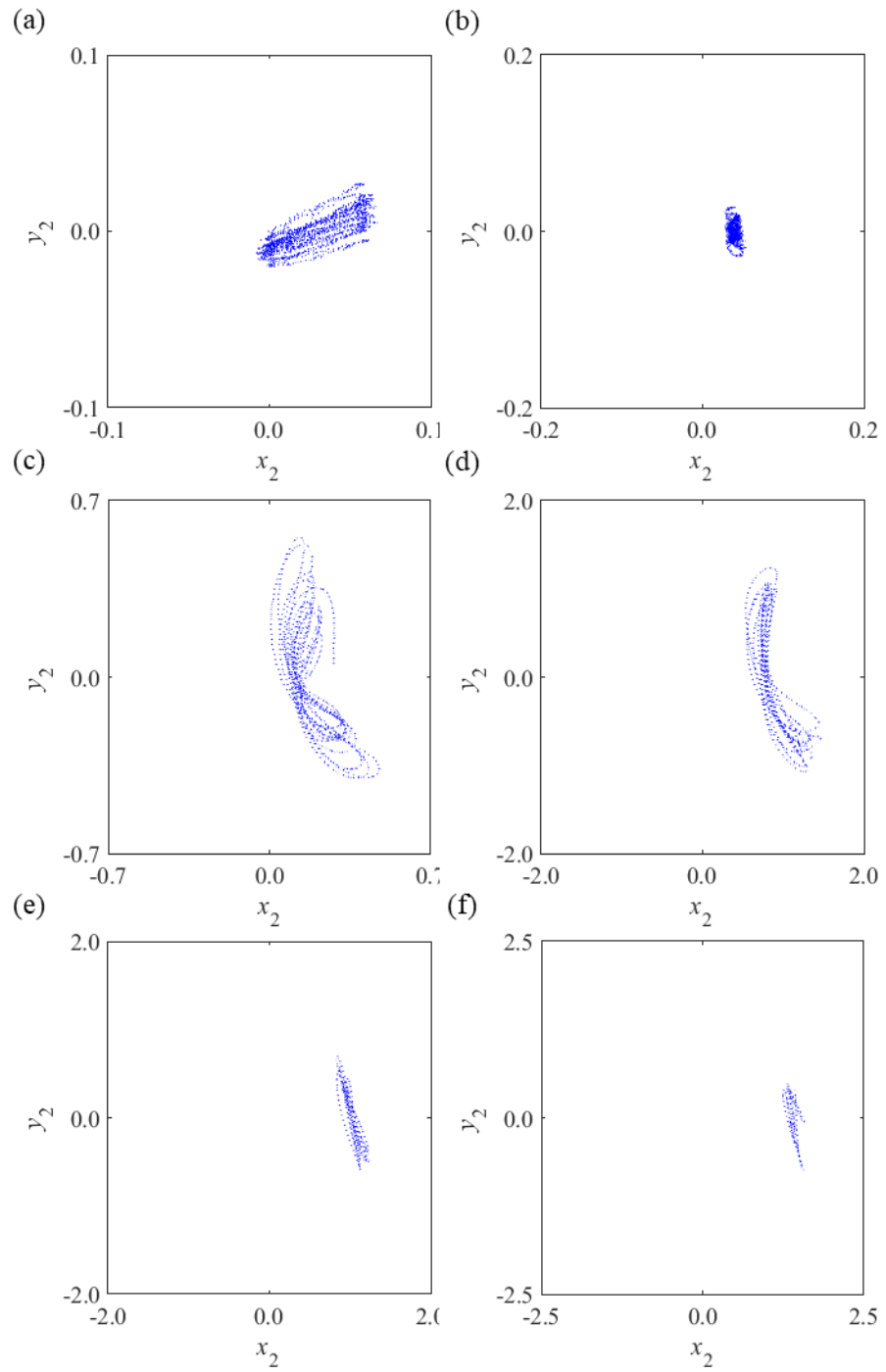


Figure 6-17: 2DOF trajectories of the downstream of a free-free staggered twin bundle of cylinders undergoing WIV for $d = 4$, $T = 1$. (a) $U_r = 3$; (b) $U_r = 4$; (c) $U_r = 6$; (d) $U_r = 10$; (e) $U_r = 15$; and (f) $U_r = 20$.

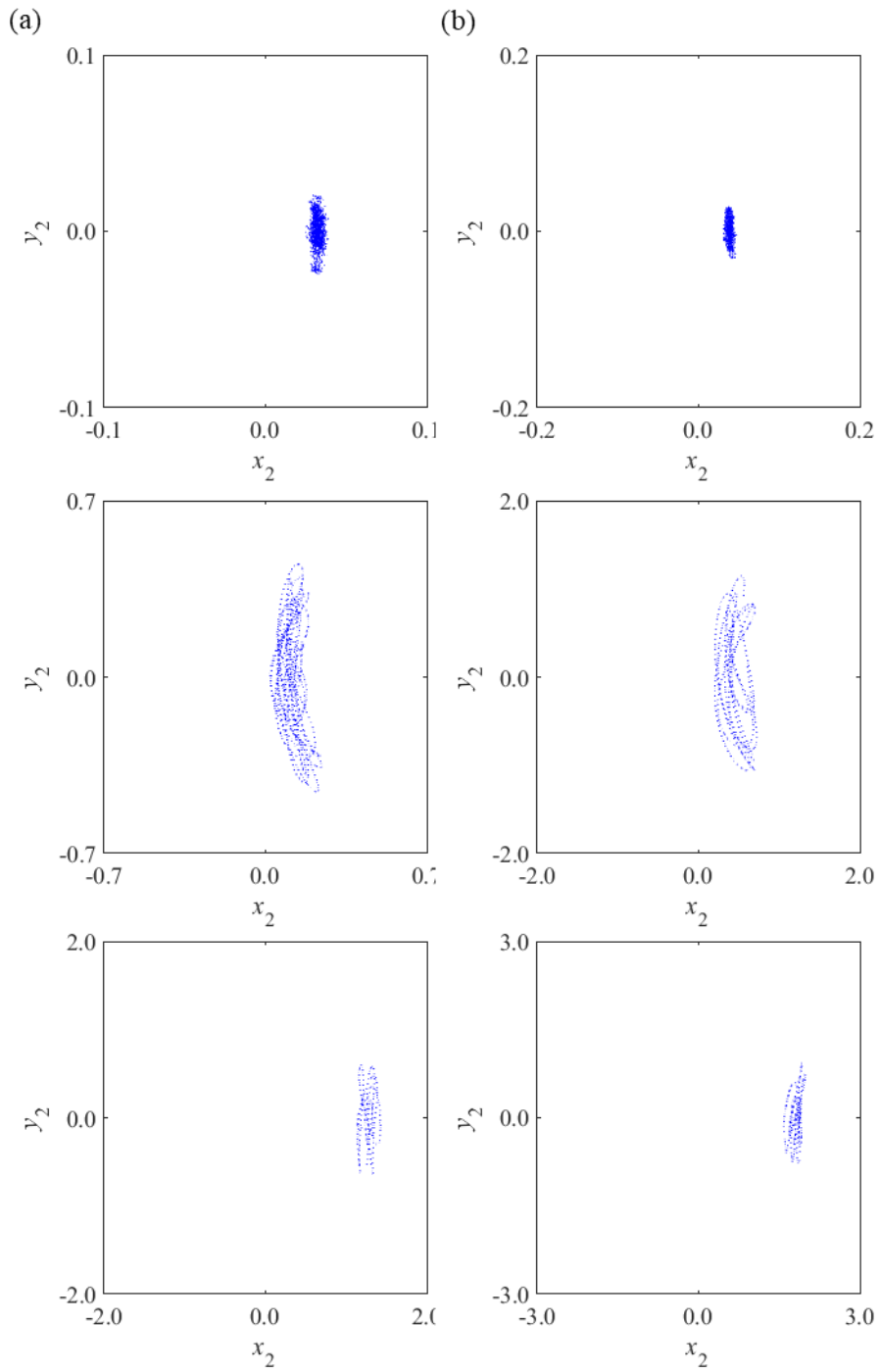


Figure 6-18: 2DOF trajectories of the downstream of a free-free staggered twin bundle of cylinders undergoing WIV for $d = 8$, $T = 2$. (a) $U_r = 3$; (b) $U_r = 4$; (a) $U_r = 6$; (a) $U_r = 10$; (a) $U_r = 15$; and (a) $U_r = 20$.

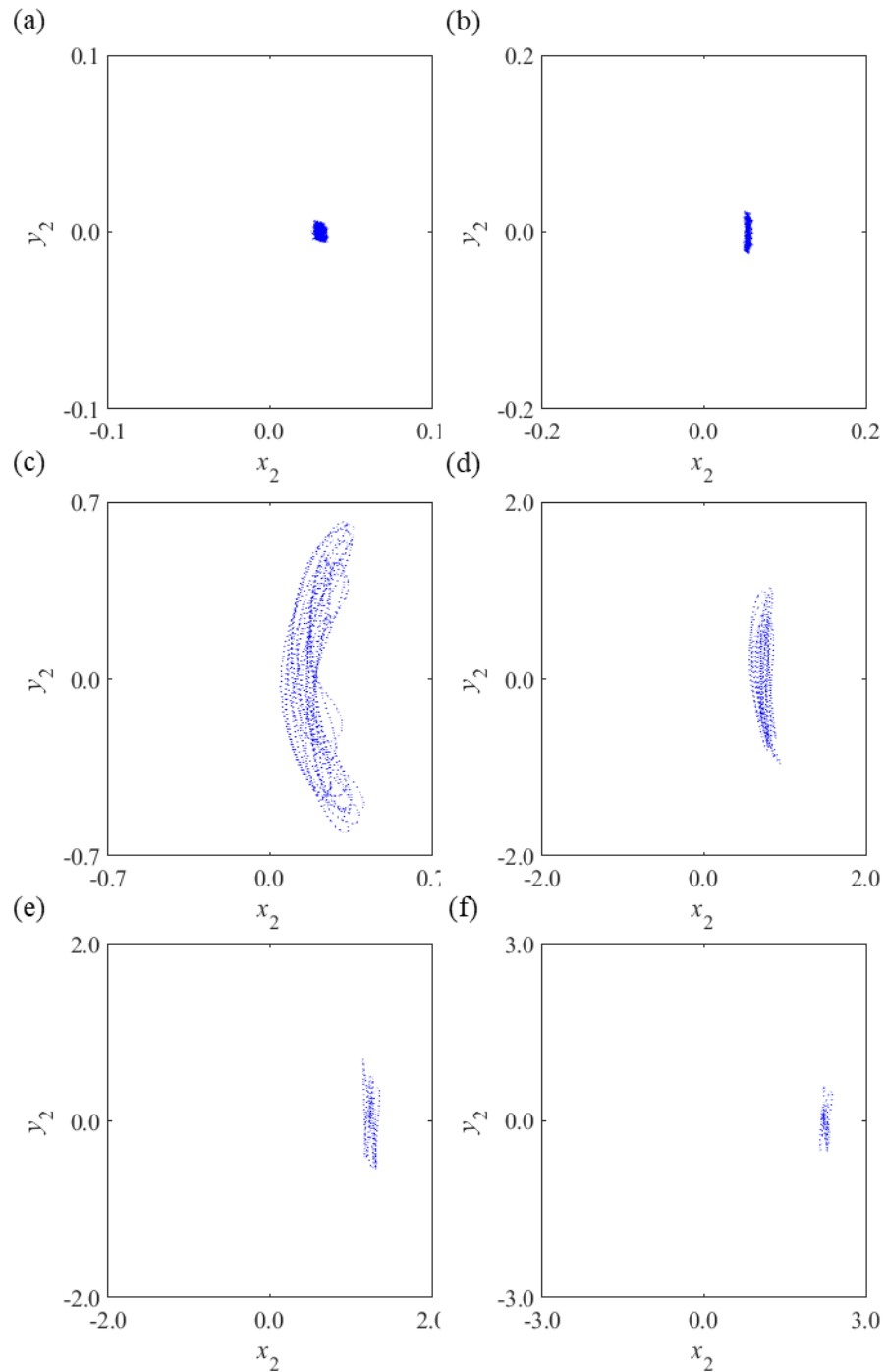


Figure 6-19: 2DOF trajectories of the downstream of a free-free staggered twin bundle of cylinders undergoing WIV for $d = 12$, $T = 3$. (a) $U_r = 3$; (b) $U_r = 4$; (c) $U_r = 6$; (d) $U_r = 10$; (e) $U_r = 15$; and (f) $U_r = 20$.

6.2.3. Dominant Frequencies of Oscillations

The dominant frequencies of oscillation of the free-free staggered cylinder were calculated as previously explained and normalised by the natural frequency of the system for each U_r – spacing combination. The results are presented in Figure 6-20.

The oscillation frequencies observed for the free-free staggered cylinders are mostly different from previous configurations. In other words, apart from some initial

correlation with the natural frequency, $f_{x2}/f_n = 1$ and $f_{y2}/f_n = 1$, and with the original $St = 0.2$ line, the downstream free-free staggered cylinder oscillates at frequencies distinguished from the other fixed-free and tandem free-free configurations.

It is observed that one of the frequency branches, perhaps the main one, for the inline response of the cylinder may be directly associated with the transverse oscillation frequencies. In fact, this strong xy coupling is well-known for VIV of single cylinders and has been observed for WIV of previous configurations in the present study.

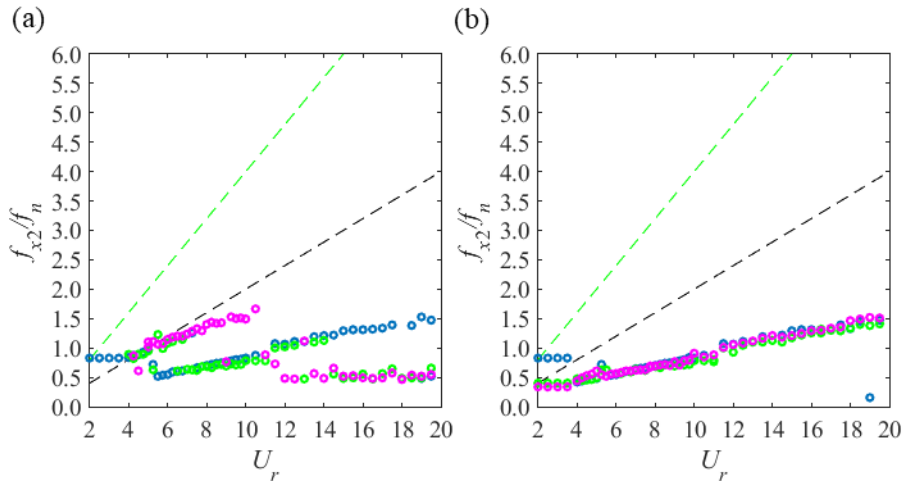


Figure 6-20: Initial staggered spacing dependence of the dominant normalised frequencies of oscillations for the WIV of the downstream of a free-free pair of cylinders in a flume in the crossflow direction. (a) Inline direction; (b) Crossflow direction. Legend: - - : Strouhal law ($St = 0.2$); - - : Doubled Strouhal law ($2St = 0.4$); \circ : $d = 4V$, $T = 1$; \circ : Armin *et al.* [25] $m^* = 2.36$ and $\zeta = 0.015$ (in water); and \triangle : Pereira *et al.* [24] 2DOF study with $m^* = 2.92$ and $\zeta = 0.025$ (assumed in water).

Moreover, the lower frequency branch observed for f_{x2}/f_n for approximately $U_r > 12$ may be directly correlated to the same frequency content exhibited for the fixed-free staggered system seen in Figure 5-20.

6.3. Validation of 2DOF Model with Experiments

The present study has been broadly divided into two parts: 1) numerical modelling and 2) experimental testing of the dynamics of two cylinders under combined VIV and WIV with several configurations. Therefore, it is now important to integrate both parts and compare how the predictions from the proposed mathematical model reproduce the features observed experimentally in the laboratory.

The 2DOF model has been calibrated and validated against literature experimental data in Chapter 3 with different Reynolds numbers, mass and damping ratios, as well as outputs of interest. However, instead of re-calibrating the model to account for the

new laboratory system properties, the previous function has been used since in the practical case, experimental data for every engineering problem is not available and at times it is unfeasible to obtain. Thus, it is perhaps more useful to compare and try to find a set of calibrated input parameters that could work for a wider range of cases. This has been attempted herein and the amplitude results from the 2DOF model based on the calibration and input parameters discussed in Chapter 3 are compared in Figure 6-21.

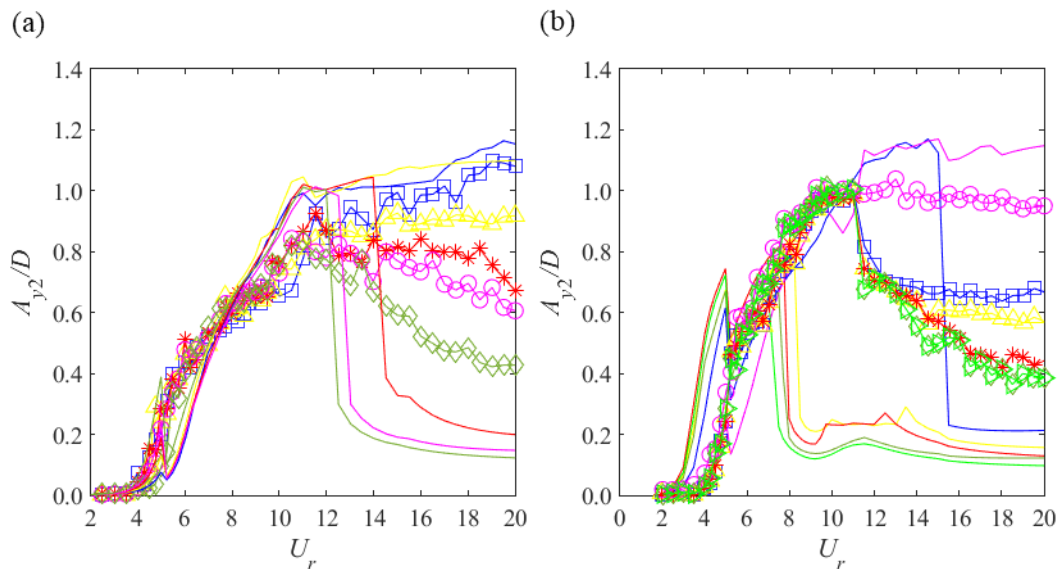


Figure 6-21: Comparison of transverse oscillation amplitudes of a free-free downstream cylinder for tandem and staggered cases between numerical and experimental results. (a) Tandem cylinders and (b) staggered cylinders. Caption: symbols – experimental results; lines – numerical results. (a) blue – $d = 4$, yellow – $d = 6$; red – $d = 8$; pink – $d = 10$; green – $d = 20$; (b) blue – $d = 8$, $T = 1$, yellow – $d = 8$, $T = 2$; red – $d = 8$, $T = 3$; pink – $d = 4$, $T = 1$; green – $d = 12$, $T = 3$.

Starting off with the tandem cylinder comparison for $d = 4, 6, 8, 10$, and 20 , Figure 6-21a, a good overall agreement is seen for the most critical cases that lead to the absolute maximum vibrations, namely $d = 4$ and 6 . The reduced velocity that is the onset of the initial branch (approximately $U_r = 5$), the first VIV peak regime, as well as the WIV amplitude responses are well represented for these spacings. This is an interesting observation that goes in favour of the model since its input parameters have been previously calibrated to a completely different system in Chapter 3.

However, when the axial spacing between tandem cylinders is increased to $d = 8, 10$, and 20 , it becomes clear that model results or more specifically the input parameters to the model have an upper boundary of validity at approximately $U_r = 12-14$. In other words, model predictions behave well in the first VIV regime and for

reduced velocities up to about $U_r = 12-14$. From that point onwards, any further increase of reduced velocity is not accurately captured by the model.

When the cylinders are offset in staggered arrangements as shown in Figure 6-21b, the overall picture is similar where the model is capable of accurately representing the most critical case, ($d = 4$, $T = 1$), which is responsible for the largest oscillation amplitudes. Nevertheless, once the inline spacing between the cylinders is increased, the accuracy and range of validity of the proposed model reduces. Unfortunately, the only experimental staggered case where $d \leq 6$ is ($d = 4$, $T = 1$), for which the model is able to accurately capture the behaviour of the downstream cylinder. However, it is then difficult to analyse how the calibrated parameters and model compare to the other staggered cylinder cases as the model has been shown to already have a limited range of validity for $d > 6$ for tandem cylinders.

The reason why only transverse oscillation amplitudes have been presented is because it has been found to be extremely difficult to determine what output could be directly compared between the experiments and the numerical results for the inline direction dynamics. For the transverse response, this is straightforwardly done in the form of amplitudes of vibration since usually the mean of the transverse response of the downstream cylinder is zero. For the inline response, on the other hand, the occurrence of mean drift and relatively low frequency mean oscillations makes it more difficult to compare both responses.

It is noteworthy to stress that in an ideal scenario, the experimental part of the Thesis should come first so that the mathematical modelling part would follow and have high fidelity data available for the calibration of the model and comparison against the experiments in the present study. However, this has not been possible, hence, literature data has been adopted as calibration data for the model. However, many of the studied system configurations were not available and interpolation/extrapolation was needed. Nevertheless, model results still show a good agreement with the response of the 2DOF downstream cylinder, whether in a tandem or staggered arrangement, for the spacings that are critical. These are the spacings for which the cylinders are closer ($d = 4$, for instance) and that have been shown to lead to the largest amplitudes of vibrations. The model has performed well and capture important features such as dominant oscillation frequencies and the wake stiffness mechanism for a series of different system properties and literature data.

More importantly, a novel modelling framework that is computationally efficient and could be applied in optimisation schemes (or machine learning scripts for example) due to the reduced computational effort required. Ultimately, with reasonable adjustments it could have applications in the industry of subsea engineering. Also, experimental results and investigations have been conducted in the present study for a wide range of configurations and parameters of interest, especially for staggered cylinders for the first time.

In conclusion, the input parameters obtained and proposed in the present study have been analysed to be versatile and represent a wide range of systems, properties, spacings, and reduced velocities. Also, the input parameters, especially Λ_{y2} , can always be re-calibrated to reference data with the use of the methodology proposed in Chapter 2 and Chapter 3, which is expected to improve the accuracy of the model and ranges of validity.

For information, dominant frequencies of oscillation have not been presented as it has been previously concluded in Chapters Chapter 5 and Chapter 6 that these frequencies do not vary considerably with d or T , which agrees with literature studies [11, 12].

6.4. Chapter Summary

This chapter has been dedicated to the experimental tests of two identical cylinders, both free to vibrate in 2 degrees-of-freedom (free-free) and diagonally supported by four springs (8 in total). It is well known and accepted that the response of the upstream cylinder within the co-shedding regime, i.e., when the minimum spacing between the cylinders is greater than the critical spacing, is similar to the response of a single cylinder under classical VIV. Thus, the focus is on the response of the downstream cylinder.

Tandem and staggered tests have been conducted for several spacing and reduced velocity combinations. Results have been analysed in terms of temporal domain, amplitudes of vibrations, planar oscillation trajectories, and dominant frequencies of vibrations.

The main discussion points for tandem cylinders are:

- Vibrations have been analysed for $d = 4, 6, 8, 10,$ and 20 from $U_r = 2 - 20$.
- From the analysis of the *rms* amplitudes of vibration of the free-free downstream cylinder, it is possible to observe that oscillation amplitudes

progressively build-up in both inline and transverse directions with the increase of U_r up to the largest reduced velocity.

- This amplitude build-up does not occur for the fixed-free downstream cylinder and it has been discussed that a possible reason for that is associated with the instantaneous spacing between the fixed-free cylinders, where most of the time they were up to 2.5 diameters further than the initial tandem spacing prescribed. On the other hand, the free-free cylinders do not suffer from the same problem as both the upstream and the downstream cylinders are allowed to move in the streamwise direction and are, therefore, expected to have a mean drift caused by the mean hydrodynamic drag force.
- Overall, the free-free response is more complex and less organised than the fixed-free case as expected and discussed previously. As the spacing is increased, the free-free tandem downstream cylinder gradually returns to single-cylinder behaviour, but this is seen to occur at slightly higher spacings for the free-free case than for the fixed-free case.
- Therefore, from the study of the free-free tandem system, the main observations identified are: i) amplitude build-up regime for low d is observed leading to the largest responses observed so far; ii) free-free cylinders vibrate with lower instantaneous spacings due to the mean drift of both cylinders and wake interaction or WIV effects are observed for higher spacings than for the fixed-free case; iii) the x_2 response is strongly coupled to the y_2 response for the free-free cylinders, with oscillation frequencies almost identical; iv) the vibration of the upstream cylinder causes the first VIV regime, if not to disappear then at least to become more moderate and less evident.

The main discussion points for staggered cylinders are:

- Vibrations have been analysed for $(d = 4 \ T = 1)$, $(d = 8 \ T = 2)$, $(d = 12 \ T = 3)$, $(d = 16 \ T = 4)$, $(d = 8 \ T = 1)$, $(d = 8 \ T = 2)$, $(d = 8 \ T = 3)$ and $(d = 8 \ T = 4)$ from $U_r = 2 - 20$.
- It is seen that the amplitudes of vibration are disorganised and fluctuate significantly with variation of U_r for the free-free staggered downstream cylinder of a pair, especially for Ax_2/D . Also, the first VIV peak regime is well-developed and clear. Nevertheless, the magnitudes of oscillation are

reduced in comparison with the free-free tandem cylinder system at $d = 8$, $T = 0$.

- It is observed that whilst the cases for $(d = 8, T = 1)$ and $(d = 8, T = 2)$ still show amplitudes of vibration that are different from the single cylinder reference case (even though this difference is small), the case at $(d = 8, T = 3)$ is shown to be effectively behaving as a single cylinder, subjected to the VIV excitation phenomenon only.
- For the downstream cylinder, it has been shown that this mean drag force and consequently the mean drift is reduced when compared to the upstream cylinder.
- For the transverse mean position, both cylinders are normally located on the wake centreline, since there is not a counterpart of the mean drag force in terms of lift force. However, for free-free staggered cylinders, the range of $\bar{\delta}y$ is greater and the cylinders vibrate across a larger proportion of the disturbed wake flow. This could be one of the reasons associated with the large amplitude of vibration fluctuations seen.
- All three staggered cases show figure-of-8 oscillation trajectories, indicating components of 2:1 inline-to-transverse frequency responses. The most complex vibration trajectories are those of $(d = 4, T = 1)$ and as the downstream cylinder is distanced both along and across the wake, it slowly returns to behave similarly to a single cylinder.

With the completion of the experiments and obtained measurements for different two-cylinder setups, it is now important to check and validate whether the modelling theory or more importantly the set of model empirical inputs proposed and discussed in Chapter 3 are also valid for the present experimental system with different system properties. This will be discussed in the following chapter.

CHAPTER 7. CONCLUSIONS AND RECOMMENDATIONS FOR FURTHER WORK

The present thesis has focused on the dynamic response of a pair of cylinders acted upon by an external water flow, more specifically the combined phenomena of VIV and WIV of two cylinders. The main outputs of this project are summarised in the following in terms of conclusions, the contribution of the work, and suggestions for future work.

7.1. Conclusions and Contribution of the Work

A research gap associated with the lack of a wake interaction model for engineering analysis of multiple subsea structures has been identified. Hence, the focus of this project has been on addressing the mathematical modelling theory that resulted in a computationally efficient model for the prediction of the response of the cylinders, as well as a corresponding experimental investigation. Several cases and setups have been studied, these are: a) 1DOF modelling of fixed-free and free-free pairs of tandem cylinders, b) 2DOF modelling of fixed-free and free tandem cylinders and fixed-free staggered cylinders, c) experiments on a single cylinder, d) experiments on fixed-free double cylinders for tandem and staggered configurations, and e) experiments with free-free double cylinders for tandem and staggered regimes.

The minimum inline spacing between the cylinders considered on this work is $d \geq 4$ and it has been concluded from the results of all the conducted experiments that the behaviour of the upstream cylinder is unaffected by the addition of a second cylinder. In other words, whilst there is a considerable interaction from the upstream on the second cylinder, the downstream cylinder does not affect the response of the leading cylinder significantly for the spacings and Reynolds number ranges considered in the present study. This conclusion agrees with literature data for the co-shedding regime [6], which $d \geq 4$ fits into, and confirmed one of the main assumptions of the present modelling theory that has not considered an interaction coupling from the rear to the front cylinder.

In general terms, a modelling framework based on boundary layer theory and the wake oscillator concept has been integrated and proposed for the first time. The model has been extensively tested and validated with previous and present experimental results.

Initially, the modelling theory was restricted to 1DOF transverse vibrations of a pair of cylinders for a fixed or free upstream cylinder for the verification and validation of

the most fundamental features of WIV. Tandem and staggered configurations have been investigated. Thereafter, the higher order solution of Blevins and Saint-Marcoux [36], discussed to account for the vibrations of the upstream cylinder in a free-free case, has been applied for the first time and validated for VIV/WIV.

The response of the downstream cylinder has been shown to be independent of the variation of d for the reduced velocity regime known as the first VIV regime; in the present study this is approximately $U_r \leq 5$, i.e. the second cylinder behaves as a single cylinder undergoing VIV. This is one of the main features of this study and has been observed for all configurations and systems tested, whether these are for a 1DOF or 2DOF, fixed-free or free-free, tandem or staggered arrangement and from experimental or numerical results

For $U_r > 5$, investigation of time series, amplitudes of vibration and oscillation frequencies led to the conclusion that, depending on d , the second cylinder could behave within three regimes: WIV, classical VIV or a transition from WIV to VIV.

Three distinct oscillation frequency branches have been observed in the 1DOF response of the second cylinder. These are associated with three different concepts: the first cylinder vortex shedding frequency through the free-stream Strouhal law; the wake stiffness equivalent natural frequencies [12]; a wake-reduced vortex shedding frequency based on the Strouhal law which is computed using the steady wake flow velocity. They have been correlated to the mechanisms of VIV of the upstream cylinder, WIV and VIV of the downstream cylinder respectively. However, these frequency branches, although still observed, are less evident when the cylinders are also allowed to vibrate in the inline direction, as for the 2DOF numerical or experimental results.

Frequency, time series and oscillation trajectory results demonstrated that the proposed model is able to capture the most important features of a pair of cylinders subjected to VIV and WIV, for instance, the wake stiffness concept has been modelled and validated with the data of Assi *et al.* [12]. This was important because it allowed for the association of one of the 3 previously mentioned frequency branches to the phenomenon of WIV.

As discussed in Chapter 1, the majority of WIV experimental studies concentrate on the response of a dynamic cylinder downstream of a stationary upstream cylinder. The reasoning for this is that a free-free system is considerably more complex to design and operate in a laboratory tank, but also because by fixing the first cylinder, it becomes easier to focus on certain features. However, the most common problem in

industry applications in the subsea engineering area is the more general case of two dynamic (free-free) cylinders. Thus, it is important to understand what the difference is between fixed-free and free-free systems, and this is has been studied in the present thesis.

Overall, it has been shown that there are key differences between these systems. Even if amplitudes of vibration between fixed-free and free-free are comparable for 1DOF systems, oscillation frequency results have been seen to vary significantly, being more complex and multi-frequency for the free-free cylinders. It has been discussed that the vibration of the upstream cylinder is reflected on the upstream gap that leads to WIV and consequently on the oscillation frequencies of the downstream cylinder.

Nevertheless, it is for 2DOF systems that the contrast becomes more evident. The difference then between the fixed-free cylinders and free-free cylinders is that for the latter, apart from oscillations, both cylinders are dragged in the streamwise direction and remain relatively within the original spacing between them. On the other hand, the upstream cylinder is not dragged, whilst the downstream drifts in the streamwise direction for the fixed-free system. This results in an increase in the spacing gap between the cylinders that under normal conditions causes a reduction in the response amplitudes of the upstream cylinder.

The allowance of an additional degree-of-freedom in the inline direction leads to similar effects as above, where the response of the downstream cylinder is more disorganised and starts to become dependent on the relative inline spacing between the cylinders. The inline vibration amplitudes of the downstream cylinder under WIV may be amplified and significantly larger than for a single cylinder, including an oscillation of the mean drift of the downstream cylinder, as observed in the experiments conducted in this study.

Furthermore, the study of staggered cylinders, especially for the experimental free-free setup which had not been done before, has highlighted that the transverse response of the downstream cylinder may be asymmetric due to the local asymmetry of the wake-induced lift force, even though this force is symmetric, globally speaking across the wake. Alternatively, the inline response of the rear staggered cylinder is greater than for tandem cylinders. This has been associated with the wake deficit and the reduced wake-induced drag that the offset second cylinder is facing.

7.2. Recommendations for Further Work

Following the present study, the investigation of combined VIV and WIV of flexible cylinders would be a topic that would be industrially relevant and is suggested for future studies. Moreover, the modelling of the influence of the second cylinder on the first cylinder would also be important to understand and predict the phenomena that occur in the near wake regime. Lastly, the inclusion of waves as well as current would be interesting and useful for the common understanding of the problem. Although it was not included in the scope of the present study, at the end of the current experiments, waves were also generated in the Wind, Wave, and Current tank. The response of the cylinder was not measured, but the visual observation of the cylinder highlighted that the inline vibration response of the cylinder was greatly increased and may become dominant over the transverse counterpart. More studies are needed in the future to confirm this and to examine this further.

Further work on the extension of this study to additional cylinders for both modelling and experimental parts are also highly important and recommended for investigating whether similar WIV and VIV features are observed and to establish whether the model is applicable to the more general form. It is currently believed that the present model and experimental observations would hold for a greater number of cylinders if the same study assumptions are respected, especially that they are in the co-shedding regime, i.e., the minimum axial spacing between the cylinders is greater than the critical spacing. On the present study this has been considered as $d \geq 4$. As previously mentioned, the interaction from the downstream cylinder on the upstream is negligible. Otherwise, this interaction needs to be modelled as it is also suggested as further work.

Another recommendation is that a study is conducted to calibrate the model with the comprehensive experimental data provided on this study for tandem, staggered, fixed-free and free-free cylinders. This would have been the ideal scenario for the present study but the laboratory was close due to COVID-19 and the experimental part of the study was then postponed.

A final recommendation is for the investigation on the potential for clean energy generation from systems of groups of structures under WIV. As it has been seen throughout this thesis, WIV causes larger vibrations and over wider ranges of excitations (not limited to resonance states).

REFERENCES

- [1] R. T. Hartlen and I. G. Currie, "Lift-oscillator model of vortex-induced vibration," *Journal of the Engineering Mechanics Division*, vol. 96, no. 5, pp. 577-591, 1970.
- [2] R. E. D. Bishop and A. Y. Hassan, "The lift and drag forces on a circular cylinder oscillating in a flowing fluid," *Proceedings of the Royal Society of London. Series A. Mathematical and Physical Sciences*, vol. 277, no. 1368, pp. 51-75, 1964, doi: doi:10.1098/rspa.1964.0005.
- [3] M. M. Zdravkovich, "The effects of interference between circular cylinders in cross flow," *Journal of Fluids and Structures*, pp. 239-261, 1987.
- [4] D. Sumner, "Two circular cylinders in cross-flow: a review," *Journal of Fluids and Structures*, vol. 26, no. 6, pp. 849-899, 2010/08/01/ 2010, doi: <https://doi.org/10.1016/j.jfluidstructs.2010.07.001>.
- [5] Y. Zhou and M. Alam, "Wake of two interacting circular cylinders: a review," *International Journal of Heat and Fluid Flow*, pp. 510-537, 2016, doi: 10.1016/j.ijheatfluidflow.2016.08.008.
- [6] T. Igarashi, "Characteristics of the flow around two circular cylinders arranged in tandem: 1st report," *Bulletin of JSME*, vol. 24, no. 188, pp. 323-331, 1981, doi: 10.1299/jsme1958.24.323.
- [7] B. S. Carmo, J. R. Meneghini, and S. J. Sherwin, "Secondary instabilities in the flow around two circular cylinders in tandem," *Journal of Fluid Mechanics*, vol. 644, pp. 395-431, 2010, doi: 10.1017/S0022112009992473.
- [8] T. Maekawa, "Study on wind pressure against ACSR double conductor," *Electrical Engineering in Japan*, vol. 84, 1964.
- [9] W. A. M. Mair, D. J., "Aerodynamic behaviour of bodies in the wakes of other bodies," *Philosophical Transactions of the Royal Society*, vol. 269, no. A, 1971.
- [10] S. J. Price, "The origin and nature of the lift force on the leeward of two bluff bodies," *Aeronautical Quarterly*, vol. 27, no. 2, pp. 154-168, 1976, doi: 10.1017/S0001925900007642.

- [11] G. R. S. Assi, P. W. Bearman, and J. R. Meneghini, "On the wake-induced vibration of tandem circular cylinders: the vortex interaction excitation mechanism," *Journal of Fluid Mechanics*, Article vol. 661, pp. 365-401, 2010, doi: 10.1017/S0022112010003095.
- [12] G. R. S. Assi, P. W. Bearman, B. S. Carmo, J. R. Meneghini, S. J. Sherwin, and R. H. J. Willden, "The role of wake stiffness on the wake-induced vibration of the downstream cylinder of a tandem pair," *Journal of Fluid Mechanics*, Article vol. 718, pp. 210-245, 2013, doi: 10.1017/jfm.2012.606.
- [13] A. Laneville and D. Brika, "The fluid and mechanical coupling between two circular cylinders in tandem arrangement," *Journal of Fluids and Structures*, vol. 13, no. 7, pp. 967-986, 1999/10/01 1999, doi: <https://doi.org/10.1006/jfls.1999.0245>.
- [14] F. S. Hover and M. S. Triantafyllou, "Galloping response of a cylinder with upstream wake interference," *Journal of Fluids and Structures*, vol. 15, no. 3, pp. 503-512, 2001/04/01 2001, doi: <https://doi.org/10.1006/jfls.2000.0364>.
- [15] N. Jauvtis and C. H. K. Williamson, "The effect of two degrees of freedom on vortex-induced vibration at low mass and damping," *Journal of Fluid Mechanics*, vol. 509, pp. 23-62, 2004, doi: 10.1017/S0022112004008778.
- [16] Y. Bao, C. Huang, D. Zhou, J. Tu, and Z. Han, "Two-degree-of-freedom flow-induced vibrations on isolated and tandem cylinders with varying natural frequency ratios," *Journal of Fluids and Structures*, vol. 35, pp. 50-75, 2012/11/01/ 2012, doi: <https://doi.org/10.1016/j.jfluidstructs.2012.08.002>.
- [17] K. R. Yu, S. Étienne, Y.-M. Scolan, A. Hay, E. Fontaine, and D. Pelletier, "Flow-induced vibrations of in-line cylinder arrangements at low Reynolds numbers," *Journal of Fluids and Structures*, vol. 60, pp. 37-61, 2016/01/01/ 2016, doi: <https://doi.org/10.1016/j.jfluidstructs.2015.10.005>.
- [18] Y. Gao, Y. Zhang, M. Zhao, and L. Wang, "Numerical investigation on two degree-of-freedom flow-induced vibration of three tandem cylinders," *Ocean Engineering*, vol. 201, p. 107059, 2020/04/01/ 2020, doi: <https://doi.org/10.1016/j.oceaneng.2020.107059>.

- [19] G. V. Papaioannou, D. K. P. Yue, M. S. Triantafyllou, and G. E. Karniadakis, "On the effect of spacing on the vortex-induced vibrations of two tandem cylinders," *Journal of Fluids and Structures*, vol. 24, no. 6, pp. 833-854, 2008/08/01/ 2008, doi: <https://doi.org/10.1016/j.jfluidstructs.2007.11.006>.
- [20] T. K. Prasanth and S. Mittal, "Flow-induced oscillation of two circular cylinders in tandem arrangement at low Re," *Journal of Fluids and Structures*, vol. 25, no. 6, pp. 1029-1048, 2009/08/01/ 2009, doi: <https://doi.org/10.1016/j.jfluidstructs.2009.04.001>.
- [21] A. Bokaian and F. Geoola, "Proximity-induced galloping of two interfering circular cylinders," *Journal of Fluid Mechanics*, vol. 146, pp. 417-449, 1984, doi: 10.1017/S0022112084001932.
- [22] S. P. Singh and S. Mittal, "Vortex-induced oscillations at low Reynolds numbers: Hysteresis and vortex-shedding modes," *Journal of Fluids and Structures*, vol. 20, no. 8, pp. 1085-1104, 2005/11/01/ 2005, doi: <https://doi.org/10.1016/j.jfluidstructs.2005.05.011>.
- [23] G. R. Assi, "Wake-induced vibration of tandem and staggered cylinders with two degrees of freedom," *Journal of Fluids and Structures*, vol. 50, pp. 340-357, 2014.
- [24] P. H. T. Pereira, F. Cenci, and A. L. C. Fajarra, "Transverse displacement phase analysis on 2DOF FIV of rigid cylinders in tandem configurations," *Journal of Marine Science and Technology*, vol. 25, no. 4, pp. 1217-1227, 2020/12/01 2020, doi: 10.1007/s00773-020-00710-z.
- [25] M. Armin, M. Khorasanchi, and S. Day, "Wake interference of two identical oscillating cylinders in tandem: An experimental study," *Ocean Engineering*, vol. 166, pp. 311-323, 2018/10/15/ 2018, doi: <https://doi.org/10.1016/j.oceaneng.2018.08.012>.
- [26] L. Y. Shiau, T. Y., "Two-cylinder model for wind vortex-induced vibration," *Journal of Engineering Mechanics*, vol. 113, pp. 780-789, 1987.
- [27] S. J. Price and M. P. Paidoussis, "An improved mathematical model for the stability of cylinder rows subject to cross-flow," *Journal of Sound and Vibration*, vol. 97, no. 4, pp. 615-640, 1984/12/22/ 1984, doi: [https://doi.org/10.1016/0022-460X\(84\)90512-1](https://doi.org/10.1016/0022-460X(84)90512-1).

- [28] M. L. Facchinetti, E. de Langre, E. Fontaine, P. A. Bonnet, F. Biolley, and S. Etienne, "VIV of two cylinders in tandem arrangement: analytical and numerical modeling," presented at the 12th ISOPE, Japan, 1/1/2002, 2002. [Online]. Available: <https://doi.org/>.
- [29] L. Shiau and T. Y. Yang, "Two-cylinder model for wind vortex-induced vibration," *Journal of Engineering Mechanics*, vol. 113, pp. 780-789, 1987.
- [30] W. Wu, S. Huang, and N. Barltrop, "Current induced instability of two circular cylinders," *Applied Ocean Research*, vol. 24, no. 5, pp. 287-297, 2002/10/01/ 2002, doi: [https://doi.org/10.1016/S0141-1187\(03\)00003-8](https://doi.org/10.1016/S0141-1187(03)00003-8).
- [31] E. Huse, "Interaction in deep-sea riser arrays," presented at the OTC, Houston, 1993, 1993. [Online]. Available: <https://doi.org/10.4043/7237-MS>.
- [32] H. Schlichting, *Boundary-layer theory*, 7th ed. New York: McGraw-Hill, 1979.
- [33] R. D. Blevins, "Forces on and stability of a cylinder in a wake," *Journal of Offshore Mechanics and Arctic Engineering*, vol. 127, no. 1, pp. 39-45, 2005, doi: 10.1115/1.1854697.
- [34] G. N. Abramovich, *Theory of turbulent jets*. Cambridge, MA: MIT Press, 1963.
- [35] R. D. Blevins, *Applied fluid dynamics handbook*. Malabar Florida: Krieger Publishing, 1984.
- [36] R. D. Blevins and J.-F. Saint-Marcoux, "Wake of a vibrating cylinder at $Re = 10^5$," in *ASME 2011 30th OMAE*, Rotterdam, June 19-24 2011, no. 44397, pp. 97-103, doi: 10.1115/OMAE2011-49075. [Online]. Available: <http://dx.doi.org/10.1115/OMAE2011-49075>
- [37] I. Borazjani and F. Sotiropoulos, "Vortex-induced vibrations of two cylinders in tandem arrangement in the proximity-wake interference region," *Journal of Fluid Mechanics*, vol. 621, pp. 321-364, 2009, doi: 10.1017/S0022112008004850.
- [38] D. W. Allen and D. L. Henning, "Vortex-induced vibration current tank tests of two equal-diameter cylinders in tandem," *Journal of Fluids and Structures*, vol. 17, no.

6, pp. 767-781, 2003/05/01/ 2003, doi: [https://doi.org/10.1016/S0889-9746\(03\)00019-7](https://doi.org/10.1016/S0889-9746(03)00019-7).

[39] A. Bokaian and F. Geoola, "Wake-induced galloping of two interfering circular cylinders," *Journal of Fluid Mechanics*, vol. 146, pp. 383-415, 1984, doi: 10.1017/S0022112084001920.

[40] A. Cigada, G. Diana, M. Falco, F. Fossati, and A. Manenti, "Vortex shedding and wake-induced vibrations in single and bundle cables," *Journal of Wind Engineering and Industrial Aerodynamics*, vol. 72, pp. 253-263, 1997/11/01/ 1997, doi: [https://doi.org/10.1016/S0167-6105\(97\)00247-X](https://doi.org/10.1016/S0167-6105(97)00247-X).

[41] M. M. Zdravkovich, "Review of Flow Interference Between Two Circular Cylinders in Various Arrangements," *Journal of Fluids Engineering*, vol. 99, no. 4, pp. 618-633, 1977, doi: 10.1115/1.3448871.

[42] H. Schlichting and K. Gersten, *Boundary-layer theory*, 9th ed. Springer-Verlag Berlin Heidelberg, 2017.

[43] J.-F. Saint-Marcoux and R. D. Blevins, "Wake induced riser interference under VIV at 10^5 Reynolds," presented at the The Twenty-second International Offshore and Polar Engineering Conference, Rhodes, Greece, 1/1/2012, 2012. [Online]. Available: <https://doi.org/>.

[44] M. P. Paidoussis, S. J. Price, and E. de Langre, *Fluid-structure interactions: cross-flow-induced instabilities*. Cambridge: Cambridge University Press, 2010.

[45] M. L. Facchinetti, E. de Langre, and F. Biolley, "Coupling of structure and wake oscillators in vortex-induced vibrations," *Journal of Fluids and Structures*, vol. 19, no. 2, pp. 123-140, 2004/02/01/ 2004, doi: <https://doi.org/10.1016/j.jfluidstructs.2003.12.004>.

[46] N. Srinil, P.-A. Opinel, and F. Tagliaferri, "Empirical sensitivity of two-dimensional nonlinear wake-cylinder oscillators in cross-flow/in-line vortex-induced vibrations," *Journal of Fluids and Structures*, vol. 83, pp. 310-338, 2018/11/01/ 2018, doi: <https://doi.org/10.1016/j.jfluidstructs.2018.08.002>.

- [47] F. S. Lawrence and W. R. Mark, "The MATLAB ODE suite," *SIAM Journal on Scientific Computing*, vol. 18, no. 1, pp. 1-22, 1997, doi: 10.1137/s1064827594276424.
- [48] G. Xu and Y. Zhou, "Strouhal numbers in the wake of two inline cylinders," *Experiments in Fluids*, vol. 37, no. 2, pp. 248-256, 2004/08/01 2004, doi: 10.1007/s00348-004-0808-0.
- [49] M. M. Alam, M. Moriya, K. Takai, and H. Sakamoto, "Fluctuating fluid forces acting on two circular cylinders in a tandem arrangement at a subcritical Reynolds number," *Journal of Wind Engineering and Industrial Aerodynamics*, vol. 91, no. 1, pp. 139-154, 2003/01/01/ 2003, doi: [https://doi.org/10.1016/S0167-6105\(02\)00341-0](https://doi.org/10.1016/S0167-6105(02)00341-0).
- [50] E. Huse, "Experimental investigation of deep sea riser interaction," presented at the Offshore Technology Conference, Houston, Texas, 1996, 1996. [Online]. Available: <https://doi.org/10.4043/8070-MS>.
- [51] R. D. Blevins and C. S. Coughran, "Experimental Investigation of Vortex-Induced Vibration in One and Two Dimensions With Variable Mass, Damping, and Reynolds Number," *Journal of Fluids Engineering*, vol. 131, no. 10, 2009, doi: 10.1115/1.3222904.
- [52] K. R. Cooper, "Wind tunnel measurements of the steady aerodynamics forces on a smooth circular cylinder immersed in the wake of an identical cylinder," *National Research Council of Canada LTR-LA-119*, 1974.
- [53] R. D. Blevins, J.-F. Saint-Marcoux, and M. Wu, "Experimental investigation of two dimensional motion of an elastically supported cylinder in a wake," *Journal of Offshore Mechanics and Arctic Engineering*, vol. 130, no. 4, pp. 044502-044502-4, 2008, doi: 10.1115/1.2948958.
- [54] J.-F. Saint-Marcoux, R. D. Blevins, and M. Wu, "An engineering approach to VIV for riser interference," presented at the The Nineteenth International Offshore and Polar Engineering Conference, Osaka, Japan, 2009, 2009. [Online]. Available: <https://doi.org/>.

- [55] I. Eames, C. Jonsson, and P. B. Johnson, "The growth of a cylinder wake in turbulent flow," *Journal of Turbulence*, 2011/01/01 2011, doi: 10.1080/14685248.2011.619985.
- [56] G. R. S. Assi, J. R. Meneghini, J. A. P. Aranha, P. W. Bearman, and E. Casaprima, "Experimental investigation of flow-induced vibration interference between two circular cylinders," *Journal of Fluids and Structures*, vol. 22, no. 6, pp. 819-827, 2006/08/01/ 2006, doi: <https://doi.org/10.1016/j.jfluidstructs.2006.04.013>.
- [57] J. C. Lagarias, J. A. Reeds, and M. H. W. Wright, P. E., "Convergence properties of the Nelder-Mead simplex method in low dimensions," *SIAM Journal of Optimization*, vol. 9, no. 1, pp. 112-147, 1998.
- [58] K. Lin, J. Wang, H. Zheng, and Y. Sun, "Numerical investigation of flow-induced vibrations of two cylinders in tandem arrangement with full wake interference," *Physics of Fluids*, vol. 32, no. 1, p. 015112, 2020/01/01 2020, doi: 10.1063/1.5134984.
- [59] G. Assi, "Experimental study of the interference effect on the flow around aligned circular cylinders. (In Portuguese: Estudo experimental do efeito de interferência no escoamento ao redor de cilindros alinhados)," 2005.
- [60] A. Khalak and C. H. K. Williamson, "Motions, forces and mode transitions in vortex-induced vibrations at low mass-damping motions," *Journal of Fluids and Structures*, vol. 13, no. 7, pp. 813-851, 1999/10/01/ 1999, doi: <https://doi.org/10.1006/jfls.1999.0236>.
- [61] W. Xu, C. Ji, H. Sun, W. Ding, and M. M. Bernitsas, "Flow-induced vibration of two elastically mounted tandem cylinders in cross-flow at subcritical Reynolds numbers," *Ocean Engineering*, vol. 173, pp. 375-387, 2019/02/01/ 2019, doi: <https://doi.org/10.1016/j.oceaneng.2019.01.016>.
- [62] B. Soares and N. Srinil, "Capturing Wake Stiffness in Wake-Induced Vibration of Tandem Cylinders," presented at the ASME 2020 39th International Conference on Ocean, Offshore and Arctic Engineering, Virtual, Online., August 3–7, 2020. [Online]. Available: <https://doi.org/10.1115/OMAE2020-18423>.

- [63] N. Srinil and H. Zanganeh, "Modelling of coupled cross-flow/in-line vortex-induced vibrations using double Duffing and van der Pol oscillators," *Ocean Engineering*, vol. 53, pp. 83-97, 2012/10/15/ 2012, doi: <https://doi.org/10.1016/j.oceaneng.2012.06.025>.
- [64] A. Postnikov, E. Pavlovskaja, and M. Wiercigroch, "2DOF CFD calibrated wake oscillator model to investigate vortex-induced vibrations," *International Journal of Mechanical Sciences*, vol. 127, pp. 176-190, 2017/07/01/ 2017, doi: <https://doi.org/10.1016/j.ijmecsci.2016.05.019>.
- [65] H. Zanganeh and N. Srinil, "Characterization of Variable Hydrodynamic Coefficients and Maximum Responses in Two-Dimensional Vortex-Induced Vibrations With Dual Resonances," *Journal of Vibration and Acoustics*, vol. 136, no. 5, 2014, doi: 10.1115/1.4027805.
- [66] R. D. Blevins, *Flow-Induced Vibration*, Second Edition ed. Van Nostrand Reinhold International, 1990.
- [67] C. Norberg, "Fluctuating lift on a circular cylinder: review and new measurements," *Journal of Fluids and Structures*, vol. 17, no. 1, pp. 57-96, 2003/01/01/ 2003, doi: [https://doi.org/10.1016/S0889-9746\(02\)00099-3](https://doi.org/10.1016/S0889-9746(02)00099-3).
- [68] M. Atlar, "Recent upgrading of marine testing facilities at Newcastle University," *Proceedings of the Second International Conference on Advanced Model Measurement Technology for the EU Maritime Industry. AMT'11*, pp. 4-6, 01/01 2011.
- [69] H. Zanganeh, "Modelling and analysis of vortex-induced vibrations of rigid and flexible cylinders," Department of Naval Architecture, Ocean and Marine Engineering, University of Strathclyde, 2015.
- [70] P. W. Bearman, "Vortex Shedding From Oscillating Bluff-Bodies," *Annual Review of Fluid Mechanics*, vol. 16, pp. 195-222, // 1984, doi: 10.1146/annurev.fl.16.010184.001211.
- [71] C. C. Feng, "The Measurement of Vortex Induced Effects in Flow Past Stationary and Oscillating Circular and D-Section Cylinders," Text, 1968.

- [72] C. H. K. Williamson and A. Roshko, "Vortex formation in the wake of an oscillating cylinder," *Journal of Fluids and Structures*, vol. 2, no. 4, pp. 355-381, 1988/07/01/ 1988, doi: [https://doi.org/10.1016/S0889-9746\(88\)90058-8](https://doi.org/10.1016/S0889-9746(88)90058-8).
- [73] R. Govardhan and C. H. K. Williamson, "Modes of vortex formation and frequency response of a freely vibrating cylinder," *Journal of Fluid Mechanics*, vol. 420, pp. 85-130, 2000, doi: 10.1017/S0022112000001233.
- [74] A. Khalak and C. H. K. Williamson, "FLUID FORCES AND DYNAMICS OF A HYDROELASTIC STRUCTURE WITH VERY LOW MASS AND DAMPING," *Journal of Fluids and Structures*, vol. 11, no. 8, pp. 973-982, 1997/11/01/ 1997, doi: <https://doi.org/10.1006/jfls.1997.0110>.
- [75] B. Sumer and J. Fredsøe, *Hydrodynamics Around Cylindrical Structures* (Advanced Series on Ocean Engineering). 2006.
- [76] T. Sarpkaya, "Fluid forces on oscillating cylinders," *Journal of the Waterway Port, Coastal and Ocean Division*, vol. 104, pp. 275-290, August 01, 1978 1978. [Online]. Available: <https://ui.adsabs.harvard.edu/abs/1978STIA...7846523S>.
- [77] Y. Tanida, A. Okajima, and Y. Watanabe, "Stability of a circular cylinder oscillating in uniform flow or in a wake," *Journal of Fluid Mechanics*, vol. 61, no. 4, pp. 769-784, 1973, doi: 10.1017/S0022112073000935.
- [78] A. P. S. Freire. "Teoria de Camada Limite." UFRJ. <https://pantheon.ufrj.br/handle/11422/7857> (accessed 16/11/2021, 2021).
- [79] M. T. Heideman, D. H. Johnson, and C. S. Burrus, "Gauss and the history of the fast Fourier transform," *Archive for History of Exact Sciences*, vol. 34, no. 3, pp. 265-277, 1985/09/01 1985, doi: 10.1007/BF00348431.
- [80] E. G. Chu, A., *Inside the FFT Black Box: Serial and Parallel Fast Fourier Transform Algorithms (1st ed.)*: CRC Press, 1999.
- [81] M. M. Alam, Q. Zheng, J. F. Derakhshandeh, S. Rehman, C. Ji, and F. Zafar, "On forces and phase lags between vortex sheddings from three tandem cylinders," *International Journal of Heat and Fluid Flow*, vol. 69, pp. 117-135, 2018/02/01/ 2018, doi: <https://doi.org/10.1016/j.ijheatfluidflow.2017.12.012>.